Académie universitaire Wallonie-Europe
Université de Liège
Faculté des Sciences Appliquées
Département d'Electricité, Electronique
et Informatique (Institut Montefiore)

Local and centralized control of multi-terminal DC grids for secure operation of combined AC/DC systems

Lampros Papangelis

Liège, Belgium, October 2018

Submitted in partial fulfilment of the requirements for the degree of
Doctor of Philosophy (Ph.D.) in Engineering Sciences

Examining Committee

Professor (President of Jury), Cristophe Geuzaine, Université de Liège, Belgium

Professor Xavier Guillaud, Ecole Centrale de Lille, France

Patrick Panciatici, Scientific Advisor, R&D department, RTE, France

Professor Kai Strunz, Technical University of Berlin, Germany

Professor Patricia Rousseaux, Université de Liège, Belgium

Professor Louis Wehenkel, Université de Liège, Belgium

Professor Thierry Van Cutsem (Ph.D. advisor), FNRS and Université de Liège, Belgium

Abstract

High Voltage Direct Current (HVDC) transmission has become increasingly popular in the recent years, fueled by the shift to renewable energy sources and the gradual decommissioning of conventional power plants. The vast majority of HVDC connections in the world consists of point-to-point links. The next step envisaged is the extension to Multi-Terminal DC (MTDC) grids. However, several challenges have to be first addressed, one of which is the secure operation of the combined AC/DC systems that are going to arise. This thesis proposes local and centralized control schemes in order to improve the security and to enhance the dynamic behavior of such systems, by taking advantage of the flexibility of the AC/DC converters.

First, a hierarchical structure is proposed to control an MTDC grid, consisting of a primary, a secondary and a tertiary level. The primary level aims at adjusting the power of the Voltage Source Converters (VSC) connected to the MTDC grid in order to correct any power imbalances that might arise. The secondary level monitors the MTDC grid to alleviate system-wide violations and steer it towards a desired operating point. The role of the tertiary level is to minimize the losses in the MTDC grid and ensure its secure operation after the loss of any single component.

Next, the issue of frequency support among asynchronous AC systems is explored. Since more and more conventional power plants are decommissioned in favor of new power electronics-interfaced generation, AC frequency control may become critical in the future. Two decentralized control schemes are proposed in this thesis. The VSCs are equipped with the proposed controllers and react to important frequency deviation to either provide a pre-defined participation to frequency support or to keep frequency inside a desired range. In both cases, constraints imposed by the DC grid are respected.

Last but not least, a framework for the security assessment of combined AC/DC grid is outlined. The control flexibility offered by MTDC grids must be taken into consideration when investigating corrective control actions against a set of credible contingencies. The framework highlights the need for cooperation and exchange of relevant information between the TSOs connected to the same MTDC grid, in order to avoid conflicts between them and ensure the security of the combined AC/DC system.

Acknowledgements

I was always interested in reading the acknowledgements section of the theses that fell into my hands. Perhaps this interest stemmed from a need to learn something more about the author before diving into the technical content. Perhaps it was just an opportunity for me to daydream of the moment I would write my own acknowledgements. Now, almost five years after the beginning of my studies, it is my turn to devote some paragraphs to the people who helped, one way or another, in the realization of this thesis.

First and foremost, I wish to express my gratitude to my supervisor, Prof. Thierry Van Cutsem, for the opportunity he offered me to work with him during the last years. Throughout this period, he has generously devoted a significant part of his time to share his knowledge. His patience and attention to detail were an inspiration to me, that contributed not only to develop my research-related skills, but also to mature as a person. I am thankful to have been part of his unique research group; a group he leads with enthusiasm, good humor and mutual trust.

I would also like to thank each one of the members of the committee for devoting their time to assess this thesis. Special thanks to my diploma thesis supervisor in NTUA, Prof. Costas Vournas. It was thanks to him that this wonderful journey began in the first place.

Teaching activities can be an extremely rewarding aspect of academic life and an invaluable experience for young PhD students. Thus, I am grateful to Prof. Patricia Rousseaux for inviting me to teach a part of her course on HVDC grids.

During these years I had the fortune to collaborate and benefit from the interactions with many researchers from other institutions. This project was funded by RTE, the French Transmission System Operator. I would especially like to thank the people from the R&D department of RTE, Patrick Panciatici, Marie-Sophie Debry and Thibault Prevost, for their valuable feedback and excellent suggestions during our meetings. I also had the pleasure of enjoying a very fruitful collaboration with the research group of Prof. Xavier Guillaud in Ecole Centrale de Lille in France. I would like to thank him for his input and comments, as well as for his hospitality during my visits in Lille. I would like to extend my thanks to his researchers, Dr. Frederic Colas, Dr. Julian

Freytes, Dr. Moez Belhaouane, Quentin Cossart and Khaled Almaksour with whom we worked closely in the context of several projects.

It would be impossible to forget my colleagues and friends from University of Liège. Several insightful and very interesting discussions took place at the entrance of our building with Dr. Mevludin Glavic during our afternoon coffee breaks. I greatly appreciate his willingness and eagerness to give advice and share his experience, on technical and non-technical topics alike. I am thankful to Dr. Petros Aristidou, for his support during my first two years in Liège. I wish him and his family the best in all aspects of their life. My thanks to Dr. Frederic Plumier for his friendship and assistance with French during the first months in Liège. I started my PhD almost at the same time with my dearest friend, Dr. Hamid Soleimani Bidgoli, with whom we shared the same research environment for almost four memorable years. On the way back home or over a plate of delicious food, I learned a lot from him about the fascinating Persian culture and life. Special thanks to Dr. Tilman Weckesser for all the interesting conversations we had and the time we spent together during his stay in Liège. I would also like to thank Gilles Chaspierre, and wish him the best towards the accomplishment of his PhD studies.

I would like to extend my appreciation to all researchers who briefly joined our group and shared a cup of coffee with me: Dr. Boris Alcaide-Moreno, Dr. Theodoros Kyriakidis, Dr. Angel Perez, Dr. Lena Robitzky and Gustav Lammert.

A life without friends would be quite boring. So, I want to thank my old friends from Greece and the ones I met here in Liège for making my life more enjoyable. I will not cite them all here, but I am sure they can identify themselves along these lines.

It is difficult to find words to describe my gratitude to my family: my parents, Nikitas and Konstantina, for always being there for me and supporting my decisions; my brother, Kostas, his wife Maria and my nephew Achilleas, a source of energy and joy in our lives; my grandparents, who still brag about their “grandson who is studying abroad”. My last thanks and all my love go to Eleftheria for standing by my side in this adventure and lifting me up every time I was feeling down.

To my late grandfather, Kostas

Contents

Chapter 1

Introduction

1.1 AC vs DC: The "War of the Currents"

The power system industry is going through significant changes and faces multiple challenges. These include the shift to cleaner renewable sources of energy in order to reach the environmental targets, the decommissioning of conventional power plants along with the public opposition to the building of new facilities, and the liberalization of the power markets. As a result, power systems are pushed to operate closer to their limits with smaller security margin. In order to keep the reliability of their systems at the same high levels as before, the Transmission System Operators (TSO) have to resort to more efficient use of their assets and address the new technological challenges.

One of the technologies considered as key to reaching the aforementioned targets is the High Voltage Direct Current (HVDC) technology, which has gained popularity during the recent years. HVDC is considered as a competitive alternative to Alternative Current (AC) transmission in projects where long-distance transfer of bulk amounts of power is investigated.

This competition between AC and DC technologies is not something new in the power industry. In fact, it all started in the end of the 19th century, at the dawn of electricity, with a series of events and a conflict between two businessmen of that time, Thomas Edison and George Westinghouse[1], the main advocates for DC and AC transmission, respectively. This dispute has been recorded as the "War of the Currents", from which AC emerged as the superior transmission technology of the time. The "War of Currents" eventually ended with the widespread adoption of AC transmission, mainly due to the ability to use AC transformers to step-up voltages and efficiently transfer power over long distances. In contrast, efficient transformation of DC voltages was not yet accomplished

[1] who had bought the patents of Nikola Tesla

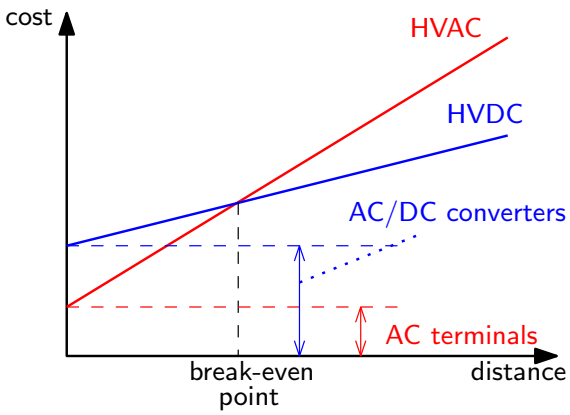

Figure 1.1: Comparison of cost over distance between HVDC and HVDC transmission

(something that would be achieved much later with the development of DC-DC converters) and the DC technology was limited to small-scale applications.

DC transmission was revived again during the 1950s, fueled by the developments in semiconductor technologies, which led to the development of AC/DC converters. Generating high DC voltages became a reality and led to efficient long-distance HVDC transmission.

As a matter of fact, as shown in Fig. 1.1, although an HVDC link requires a significant initial investment due to the large cost of AC/DC terminals, it eventually becomes cheaper for large distances. The break-even point is around 500 km for overhead lines, and 40 km for underground or submarine cables [Bah08]. A key factor to the increase of the HVAC cost is the need for substations every two or three hundred kilometers to provide reactive power compensation. This problem is especially evident in undersea/underground applications due to the large shunt capacitance of the cables.

The shift towards renewable sources is also one of the reasons that have attracted attention to HVDC connections. The main attribute of these sources is that they are usually located in remote distant areas, away from load centers. For example, the largest amounts of wind potential in Europe are located offshore or near the sea [VG10]. This requires the transmission of large amounts of power over long distances. Due to the strong public opposition against new overhead AC lines, underground (and/or submarine) cables have to be used, leaving HVDC transmission as the only feasible option. It should be also noted that, even in overhead line transmission, an HVDC corridor has smaller Right-of-Way compared to its AC counterpart.

Furthermore, as several blackouts have shown, large AC interconnections are exposed to stability issues and cascading outages with severe consequences on the security of power supply [ADF+05]. HVDC connections can contribute to improving the security and reliability of a power system since they act as a “firewall” by preventing propagation of a disturbance outside the area

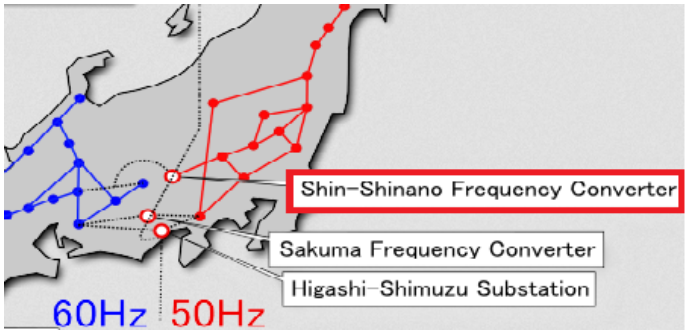

Figure 1.2: The Shin Shinano HVDC connection in Japan

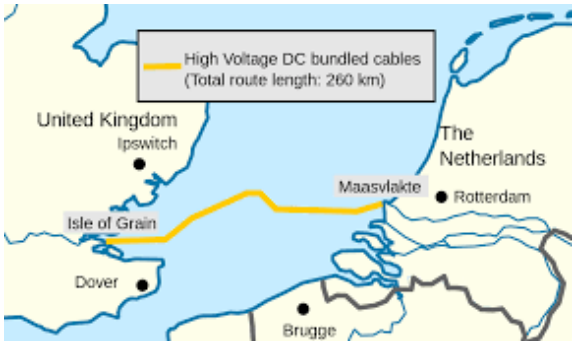

Figure 1.3: The BritNed HVDC connection between UK and the Netherlands

of the initiating event. A real-life case was observed during the Northeastern Blackout in 2003 in USA. Namely, the grid of Québec being connected to New England through an HVDC link, it helped to restrain the consequences of the disturbance on the USA side of the grid [BPR+04].

In addition, HVDC connections offer extremely high flexibility to TSOs. They can be used to interconnect two large asynchronous AC systems. Interconnection of such systems would be impractical with AC lines, either due to different nominal frequencies or due to stability issues arising from synchronization of two large systems. For example, the Shin Shinano HVDC link (shown in Fig. 1.2) is a back-to-back converter between the Western power grid of Japan (operating at 60 Hz) and the Eastern (operating at 50 Hz). Another example is the BritNed link [bri], a submarine HVDC connection between the Netherlands and UK (shown in Fig. 1.3), both operating at 50 Hz, but not synchronously.

Furthermore, embedded HVDC links can help to increase the maximum power transfer between two areas, for example, in the France-Spain HVDC link [CDBB13] (see Fig.1.4). In general, HVDC transmission offers several advantages compared to its AC counterpart, a non-exhaustive list of which includes [Rau14]:

- no reactive power transmission losses;

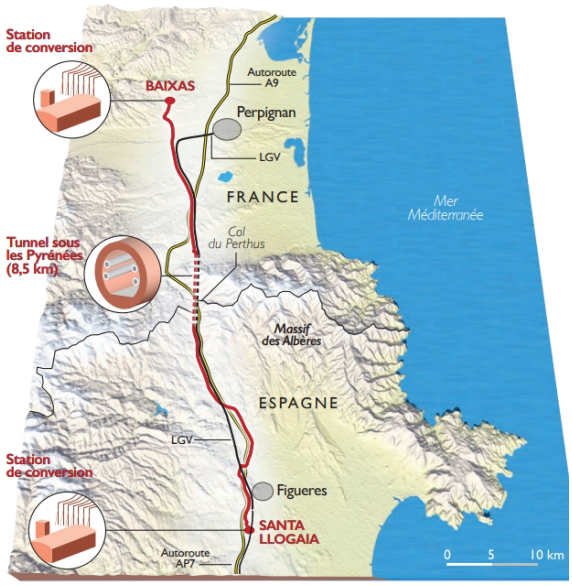

Figure 1.4: The INELFE HVDC connection between France and Spain. In order to cross the Pyrenees mountains, a tunnel had to be built, inside which the HVDC cable was placed.

- no stability limitation of transmission length;
- high controllability;
- interconnection of asynchronous areas;
- smaller right of way;
- reduced footprint;
- lower losses.

Obviously, this new competition between AC and DC is not a repetition of the first "War of Currents". Building a new grid based exclusively on DC technology is neither desired nor feasible. The power system infrastructure has been built relying on the AC technology, which will continue dominating the power supply and consumption. Instead, the target of several researchers, manufacturers and operators is to investigate methods to combine AC and DC transmission, thus creating mixed AC/DC systems, and taking advantage of their individual benefits.

1.2 Technologies of HVDC converters

The two dominant HVDC converter technologies in use presently are the Line Commutated Converter (LCC) and the Voltage Source Converter (VSC). Currently, most of the HVDC connections in operation worldwide use the LCC technology, which relies on thyristor semiconductor switches. Their power and voltage ratings have increased significantly through time reaching up to 800 kV

and 7200 MW in China, whereas a connection of 10 GW at a voltage level of 1100 KV is under construction [ABB17].

On the other hand, VSCs are the newest generation of converters and have gained momentum during the recent years. VSCs rely on Insulated Gate Bipolar Transistors (IGBT) for the conversion process, which allows to generate an independent AC voltage waveform. Depending on the topology of the VSC, the AC voltage waveform can include two or three levels. In order to decrease the total harmonic distortion of the generated voltage, techniques like Sinusoidal Pulse Width Modulation (SPWM) have been widely used. However, the relatively new technology of Modular Multilevel Converters (MMC) [LM03] allows to generate multiple voltage levels on the AC side, thus approaching a near-sinusoidal waveform and reducing the filtering requirements.

Although LCC technology is mature and has proven very reliable up to now, VSC technology offers several advantages, and draws continuously attention into more and more applications [RCGN12]. The main features are:

- Four-quadrant operation: LCCs consume large amounts of reactive power. In contrast, VSCs can absorb or consume reactive power depending on the system requirements, thus achieving independent active and reactive power control.
- Power reversal: VSCs can almost instantaneously change the power flow direction, whereas in LCC connections this requires shutting down the link and reversing the DC voltage polarity.
- Possibility to connect to weak AC grids: LCCs require a strong enough AC grid to operate correctly. VSCs do not necessarily face such a limitation.
- Grid forming and black-start capability: VSCs can generate a voltage output to which other devices can synchronize. This makes it extremely attractive for offshore applications.
- Fault-ride through capability: VSCs can ride through low AC voltages, whereas LCCs are prone to commutation failures.
- Harmonics: VSCs generate less harmonic content than LCCs. Therefore, the need for AC and DC filters is smaller.
- Footprint: VSC stations are generally less bulky than LCC stations of the same rating, mainly due to the smaller requirements for filters.
- Cheaper cables: VSCs can be connected with XLPE cables, instead of the oil-based (mass impregnated) cables required for LCC connections.

The VSC technology is still inferior to LCC on some aspects. Namely, VSCs have not yet reached the voltage and power levels of LCCs, they have limited overloading capability and higher switching losses. In addition, they exhibit poor performance during DC faults, for which reliable DC

breakers are still required to be developed and tested [VG10]. Nevertheless, these drawbacks are expected to be overcome in the future following the further development of MMC.

1.3 Hopes and challenges for MTDC grid

The vast majority of HVDC connections in the world consists of point-to-point links. The next step envisaged is the extension to Multi-Terminal DC (MTDC) grids. However, there is relatively little experience from the operation of MTDC grids. In fact, as of writing this thesis, only five MTDC grids are in operation. The first two were commissioned in Italy and Canada [JA15] and rely on the LCC technology. The remaining three use VSCs and have been very recently put into service. Two are located in China (Nan'ao-Shantou and Zhoushan) and the latest one in India (North-East Agra) [Akk16].

The VSC technology is considered the most appropriate for MTDC operation due to the capability of changing the power flow direction very quickly, without shutting down the whole connection temporarily. MTDC grids with LCCs have been already in operation for several years. However, even for small radial grids (like the SACOI link in Italy), their control is extremely complex. When meshed grids are considered, VSCs pose as the only solution. In addition, only VSCs can be used to connect passive or inertia-less networks (e.g. offshore wind farms) to an MTDC grid. For these reasons, it is expected that the vast majority of future MTDC grids will use the VSC technology.

Apart from encouraging the integration of more renewable sources, the introduction of MTDC grids is expected to deliver several more advantages to the future power systems. To begin with, they are expected to contribute to better asset utilization. For example, in the current situation, a remote offshore Wind Farm (WF) is connected to the main grid through a point-to-point HVDC link. The outage of a VSC or of the cable would automatically result in loss of revenue since, obviously, the WF power cannot be transferred. The extension to MTDC grids offers alternative paths for evacuation of the WF power, thus the loss of revenue is minimized. Furthermore, MTDC grids are expected to provide ancillary services to their adjacent AC systems. Network codes have already been drafted to the advantage of those services [EE14a]. This will lead to increased security and reliability of the power transfer. Another benefit consists of the possibility of connecting several asynchronous and/or distant AC areas, hence enhancing power trading, and providing better flexibility to the operators.

Most likely, such grids will not be built from scratch, but will result from the connection of multiple pre-existing point-to-point links. Therefore, the situation in the near future will most probably consist of MTDC grids with a small number of terminals (i.e. 3-10 VSCs) [Rau14]. Ambitious projects of MTDC supergrids spanning the whole European network have been proposed in the

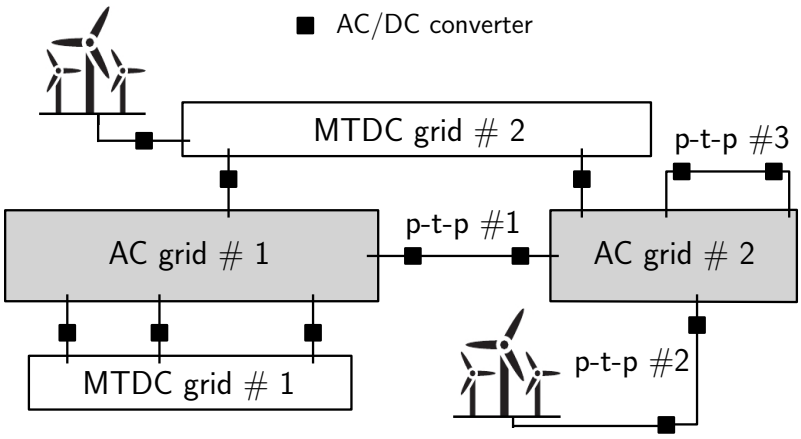

Figure 1.5: Illustrative example of combined AC/DC system

literature, such as the North Sea Super Grid [Vra13], the DESERTEC project [Tri06] and the European Supergrid [VG10]. The main idea behind these projects is to harvest the power from multiple renewable sources of energy, i.e. wind in the North Sea, solar in Southern Europe and Northern Africa and hydro in the Nordic countries. This would allow to partially deal with the uncertain nature of such sources, and encourage bulk power transfers and trades over long distance, e.g. by consuming in Belgium solar power produced in Greece. Even more ambitious proposals [CEA13] introduce the concept of a "Global Grid", realized by connecting the different continents with HVDC links and grids.

The above are expected to result in quite complex AC/DC network topologies. An illustrative example is sketched in Fig. 1.5, where AC grids are shown with gray boxes, and DC with white. The system includes three point-to-point HVDC links. Point-to-point link #1 is an asynchronous link allowing power exchange between the asynchronous AC systems #1 and #2. Link #2 is also an asynchronous connection between a wind park and AC system #2. Link #3 is embedded in AC grid #2. Such a link could be used to transfer power over long distances in order to improve system stability. Similarly, MTDC grid #1 is an embedded MTDC grid (also called overlay grid) and serves as a backbone reinforcing AC system #1 by offering an alternative path for power transfers between remote locations inside that system. MTDC grid #2 collects the energy produced by an off-shore wind park, but also allows power transfers between AC systems #1 and #2.

Nevertheless, several challenges have to be addressed before MTDC grids become more commercially and technically accessible. The work in [VG10] lists the most important as follows:

- standardization of the DC voltage ratings and interoperability between devices from different manufacturers should be established. Up to now, HVDC projects have been implemented on a case-by-case basis, with each project carried out usually by a single manufacturer,

and there are no "off-the-shelf" solutions. As with AC systems, MTDC grids should be expandable with new terminals and cables, and relying on a single manufacturer should be avoided. Appropriate generic models should be developed and provided to be able to test the behavior of the various components. This was the main subject of the Best Paths project [Fre17].

- the problems of DC fault clearing, protection and grounding have to be addressed. As far as protection is concerned, significant progress has been made with the development of the first DC circuit breakers and full-bridge MMCs with DC fault-blocking capability. Various DC fault clearing strategies (selective or not) have been proposed in [HL17].
- appropriate control schemes have to be developed. MTDC grids consist of very expensive equipment; hence, it should be ensured that all variables are controlled well-within limits. This would probably require to build the necessary communication infrastructure to exchange fast and reliable information and coordinate the various DC grid components. In addition, grid codes like [EE14a] should be drafted, to define the auxiliary services provided to the AC systems by the MTDC grids.
- an operation framework has to be established. Building an MTDC grid is a considerable investment, connecting multiple AC areas operated by different TSOs, with different objectives. MTDC grids are expected to provide high control flexibility to the TSOs, but increased coordination and information exchange between the TSOs is probably required to avoid undesired interactions and conflicts. In Europe, this need for coordination (of the AC grids) has resulted in the formation of Regional Security Coordinators (RSC) such as CORESO [ENT], intended to assist the TSOs in maintaining the operation security of the combined electricity system.

1.4 Motivation and Objectives of this thesis

Addressing some of the aforementioned challenges was the motivation behind the work presented in this thesis. To this purpose, advanced schemes are proposed in order to control the powers flowing in the AC/DC terminals embedded in an MTDC grid.

Focusing first on the MTDC grid, this work addresses the need to (i) first ensure its stable operation, then (ii) correct the power flows so that a desired schedule is satisfied, and finally (iii) secure the grid against plausible disturbances. Although the control principles for point-to-point links have been well tested in practical cases, the same methodologies cannot be applied to multi-terminal systems. Therefore, alternatives should be investigated. Inspired of the way frequency has been controlled for several decades in AC systems, this work proposes a similar hierarchical control structure for MTDC grids.

Next, the issue of auxiliary services to the AC systems is explored. Since more and more conventional power plants are decommissioned in favor of new power electronics-interfaced generation, AC frequency control may become critical in the future. By developing new control schemes for the VSCs, asynchronous areas interconnected through an MTDC grid can provide frequency support to each other. This mutual assistance can be continuous or activated in emergency cases. Two methods of the latter case have been developed and tested on various scenarios in the course of this work.

Last but not least, the reliable operation of mixed AC/DC systems requires running offline and online various contingency scenarios and assessing the system response as acceptable or unacceptable. In case of unacceptable response, corrective control actions have to be suggested. Adjusting the MTDC grid power flow could be a very effective means of corrective control and should be considered for the TSOs. However, the impact on the other AC systems connected to the same MTDC grid might be significant and undesirable. This thesis discusses a generic framework in order to assess the security of AC/DC systems and resolve conflicts that might arise between different TSOs with different objectives.

1.5 Thesis outline

The thesis is organized as follows:

Chapter 2. The phasor approximation has been adopted in this work to depict the average dynamic behavior of the various components of an HVDC grid and their impact on AC system stability. After a brief description of the phasor approximation for power system simulation studies, the models of converters and DC lines are presented based on various references in the literature. In particular, the average-value models of a typical 2-level VSC and of an MMC are given along with their controls. Then, two configurations are described: (i) a point-to-point HVDC link and (ii) an MTDC grid. The control strategies followed in each configuration, i.e. the Master-Slave control for a point-to-point link and the droop control for an MTDC grid, are elaborated.

Chapter 3. The impact of integrating HVDC grids into AC systems is demonstrated with illustrative examples using the models and the control strategies described in Chapter 2. Four cases are considered, each emphasizing a different aspect. The first two address the possibility to use the MTDC grid to provide support to the AC systems it is connected to. The third illustrates the impact of an AC/DC converter outage on the MTDC grid and on the adjacent AC systems. The fourth presents a case study of a new type of instability that might arise when a VSC is connected to a weak AC grid.

Chapter 4. This chapter details the proposed hierarchical scheme to control an MTDC grid. Starting from the droop control mentioned in Chapter 2, a secondary control scheme inspired of Model Predictive Control (MPC) is proposed. The objective and the various constraints of the controller are detailed. The hierarchical control structure is complemented by a tertiary level, whose target is to ensure that the MTDC grid can continue operating after the loss of any single component. The effectiveness of the proposed methods is demonstrated with simulation results on a test system consisting of multiple asynchronous AC areas connected through a five-terminal MTDC grid.

Chapter 5. Frequency support among asynchronous AC areas through MTDC grids is investigated. First, previous works on the subject are presented. Then, two methods are proposed, both resorting to MPC. Relying exclusively on local information, the proposed schemes are incorporated into the control structure of the VSCs and adjust their power setpoint to control the power they inject into their AC area. The objective and constraints of each strategy are detailed and their effectiveness is demonstrated through simulation results.

Chapter 6. A general framework is discussed in this chapter in order to enable the TSOs connected to an MTDC grid to perform security assessment of their system. The challenges and opportunities introduced by the interconnection of multiple asynchronous AC areas through an MTDC grid are highlighted. Through simple examples, possible conflicts are illustrated, which might arise when each TSO attempts to use the MTDC grid to its own benefit. A methodology to resolve such conflicts is outlined.

Chapter 7. The last chapter of the thesis summarizes the thesis achievements. Conclusions are provided and possible extensions for future investigation are listed.

1.6 Publication list

This thesis expands material that has been published in various journals and presented at various conferences:

[1] **L. Papangelis**, M.-S. Debry, T. Prevost, P. Panciatici, T. Van Cutsem. Decentralized Model Predictive Control of Voltage Source Converters for AC Frequency Containment. International Journal of Electrical Power Energy Systems, 2018 [PDP+18a].
Also available at http://hdl.handle.net/2268/217222.

[2] **L. Papangelis**, M.-S. Debry, P. Panciatici, T. Van Cutsem. Coordinated Supervisory Control of Multi-Terminal HVDC Grids: a Model Predictive Control Approach. IEEE Transactions

on Power Systems, 2017 [PDPV17b].
Also available at http://hdl.handle.net/2268/205528

[3] **L. Papangelis**, M.-S. Debry, P. Panciatici, T. Van Cutsem. A Receding Horizon Approach to Incorporate Frequency Support into the AC/DC Converters of a Multi-Terminal DC Grid. Electric Power Systems Research, 2017 [PDPV17a].
Also available at http://hdl.handle.net/2268/207952

[4] **L. Papangelis**, M.-S. Debry, T. Prevost, P. Panciatici, T. Van Cutsem. Stability of a Voltage Source Converter subject to Decrease of Short-Circuit Capacity: a Case Study. In proceedings of the 20th Power Systems Computations Conference (PSCC), Dublin, 2018 [PDP+18b].
Also available at http://hdl.handle.net/2268/221413

[5] **L. Papangelis**, M.-S. Debry, P. Panciatici, T. Van Cutsem. Local Control of AC/DC Converters for Frequency Support Between Asynchronous AC Areas. In proceedings of 2017 IEEE PES PowerTech conference, Manchester, 2017 [PDPV17c].
Also available at http://hdl.handle.net/2268/209421

[6] J. Freytes, **L. Papangelis**, H. Saad, P. Rault, T. Van Cutsem, X. Guillaud. On the modeling of MMC for use in large scale dynamic simulations. In proceedings of the 19th Power Systems Computations Conference (PSCC), Genova, 2016 [FPS+16].
Also available at http://hdl.handle.net/2268/194281

[7] **L. Papangelis**. Centralized Model Predictive Control of Multi-Terminal Direct Current Grids. In proceedings of the 8th IEEE Benelux Young Researchers Symposium, Eindhoven, 2016.

[8] P. Aristidou, **L. Papangelis**, X. Guillaud, T. Van Cutsem. Modular modelling of combined AC and DC systems in dynamic simulations. In proceedings of 2015 IEEE PES PowerTech conference, Eindhoven, 2015 [APGV15].
Also available at http://hdl.handle.net/2268/181310

[9] **L. Papangelis**, X. Guillaud, T. Van Cutsem. Frequency support among asynchronous AC systems through VSCs emulating power plants. In proceedings of 11th IET Conference on AC and DC Power Transmission, Birmingham, 2015 [PGV15].
Also available at http://hdl.handle.net/2268/176473

The following articles have been accepted for publication or are still under preparation:

[1] M. M. Belhaouane, K. Almaksour, **L. Papangelis**, F. Colas, T. Prevost, X. Guillaud, T. Van Cutsem. Experimental Validation of a Model Predictive Control Strategy on a Three-

terminal VSC-HVDC Mock-up. Accepted for presentation at the 11th IET Conference on AC and DC Power Transmission, Coventry, 2019.

[2] M. M. Belhaouane, K. Almaksour, **L. Papangelis**, F. Colas, T. Prevost, X. Guillaud, T. Van Cutsem. Implementation Process of an Advanced Control Strategy Based on Three-terminal VSC-HVDC Mock-up (provisional title). to be submitted in IEEE Transactions on Industry Applications.

The following works have been published by the author, albeit not in direct link to the subject of this thesis:

[1] J. Weckesser, **L. Papangelis**, C. Vournas, T. Van Cutsem. Local Identification of Voltage Instability from Load Tap Changer Response. Sustainable Energy, Grids and Networks, 2017.
Also available at http://hdl.handle.net/2268/205002

[2] **L. Papangelis**, P. Panciatici, M.-S. Debry, T. Van Cutsem. A dynamic simulation approach to identify additional reactive reserves against long-term voltage instability. In proceedings of 2015 IEEE PES PowerTech conference, Eindhoven, 2015.
Also available at http://hdl.handle.net/2268/180919

[3] IEEE PES Task Force. Test Systems for Voltage Stability Analysis and Security Assessment. Technical Report PES-TR19 [IEE15].
Also available at
http://resourcecenter.ieee-pes.org/pes/product/technical-publications/PESTR19

Chapter 2

Modeling and control of HVDC grid components

This chapter describes the modeling and control of the various HVDC grid components used extensively in this work under the phasor-mode (or quasi-sinusoidal) approximation [AFV14]. Section 2.1 recalls some basics of dynamic simulation under the phasor-mode approximation. Section 2.2 presents the generic models of the various converters used. Section 2.3 deals with the dynamics of the DC voltage in an HVDC network and provides an overview of the control schemes applied for a point-to-point link as well as for an MTDC grid. Section 2.4 summarizes the chapter.

2.1 Overview of models under the phasor-mode approximation

In the future, the need for dynamic simulation of combined AC and DC systems will keep increasing [BGG+14]. For instance, HVDC systems are expected to take a greater part in frequency and voltage control [EE14a]. Furthermore, the response of AC/DC converters to nearby faults in AC grids must be taken into account when assessing system security.

To reproduce the dynamics of AC/DC converters, Electro-Magnetic Transient (EMT) simulation remains the reference in terms of accuracy [ACJ+14]. However, the EMT models are not suited to the large-scale studies and long-term dynamics, mainly due to the small time step required, in the order of some hundreds of microseconds or even less. Simply stated, the phasor approximation consists of approximating network voltages and currents by sinusoidal functions of time with varying amplitudes and phase angles [KBL94]. It allows using time steps up to several tens of milliseconds, making it more suitable for large-scale studies.

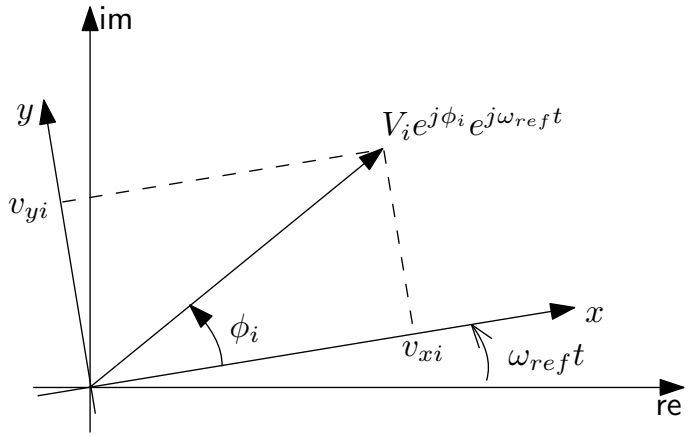

Figure 2.1: xy reference frame used in phasor-mode simulation

In the phasor-mode approximation, the fast dynamics of the network are neglected [KBL94]. Thus, the network is represented by the following algebraic equations:

$$\bar{\mathbf{I}} = \mathbf{Y}\bar{\mathbf{V}} \tag{2.1}$$

where $\bar{\mathbf{I}}$ the vector of complex currents injected into the network at the various nodes, $\bar{\mathbf{V}}$ the vector of complex voltages at the various buses, and $\mathbf{Y}$ the nodal admittance matrix. Matrix $\mathbf{Y}$ involves network impedances determined at fundamental frequency (or possibly updated with frequency when the latter significantly deviates from its nominal value).

Under the phasor approximation, the voltage at the i-th bus takes on the form:

$$\begin{aligned} v_i(t) =& \sqrt{2} V_i(t) \cos\left(\omega_{ref} t + \phi_i(t)\right) = \sqrt{2}\, re\left[V_i(t)\, e^{j\phi_i(t)}\, e^{j\omega_{ref}t}\right] \\ =& \sqrt{2}\, re\left[\left(v_{xi}(t) + j v_{yi}(t)\right) e^{j\omega_{ref}t}\right] \end{aligned} \tag{2.2}$$

where $V_i(t)$, $\phi_i(t)$ are the magnitude and phase angle of the voltage at time t, respectively, and ω_{ref} is the reference angular frequency of the system. $v_{xi}(t) + j v_{yi}(t)$ is the voltage phasor, in rectangular coordinates, expressed with respect to (x, y) axes rotating at the angular speed ω_{ref}, as shown in Fig. 2.1.

On the other hand, the various power system components are modeled by a set of nonlinear Differential Algebraic Equations (DAE) assuming three-phase balanced network. A general modeling of the network and the various components has been presented in [APGV15] and is briefly described in the following. For further details regarding the algorithmic techniques used to solve the resulting set of DAEs, the reader is referred to [Ari15, APGV15].

2.1.1 AC and DC transmission sub-networks

To preserve modeling flexibility a modular approach is desirable, allowing to simulate an arbitrary combination of (disjoint) AC and DC sub-networks. Under the phasor approximation, AC networks are represented by the well-known algebraic equations:

$$\underbrace{\begin{bmatrix} \boldsymbol{G} & -\boldsymbol{B} \\ \boldsymbol{B} & \boldsymbol{G} \end{bmatrix}}_{\boldsymbol{D}} \underbrace{\begin{bmatrix} \boldsymbol{v}_x \\ \boldsymbol{v}_y \end{bmatrix}}_{\boldsymbol{v}_{ac}} - \begin{bmatrix} \boldsymbol{i}_x \\ \boldsymbol{i}_y \end{bmatrix} = \boldsymbol{0} \tag{2.3}$$

where $\boldsymbol{G}$ (resp. $\boldsymbol{B}$) is the nodal conductance (resp. susceptance) matrix, $\boldsymbol{v}_x$ and $\boldsymbol{v}_y$ are vectors of real and imaginary components of the bus voltage, and $\boldsymbol{i}_x$ and $\boldsymbol{i}_y$ are the corresponding injected current components.

Similarly, by neglecting the series inductances of DC lines and cables, and lumping their shunt capacitances in the AC/DC converters [CB11] (see also sub-section 2.2.1), the DC grid becomes purely resistive; hence, the DC voltages and DC currents follow:

$$\boldsymbol{G}_{dc}\boldsymbol{v}_{dc} - \boldsymbol{i}_{dc} = \boldsymbol{0} \tag{2.4}$$

where $\boldsymbol{G}_{dc}$ the nodal conductance matrix, $\boldsymbol{v}_{dc}$ is the vector of DC bus voltages, and $\boldsymbol{i}_{dc}$ the vector of DC currents injected in the purely resistive part of the DC network.

This encompasses any AC-DC grid topology. If there are several disjoint AC sub-networks, the $\boldsymbol{G}$ and $\boldsymbol{B}$ matrices have a block-diagonal structure. The same holds true for $\boldsymbol{G}_{dc}$ in case of disjoint DC sub-networks.

2.1.2 Equipment connected to AC or DC grids

Modularity is also obtained by matching any equipment connected to the AC or DC grids with one of the following three generic components:

- an *injector* connected to a single AC bus
- an *AC two-port* connecting two AC buses
- an *AC/DC converter* connecting one AC and one DC bus.

Each component is modeled by a system of semi-implicit DAEs. Including algebraic equations and states offers remarkable modeling flexibility. In particular, each component model interfaces

with the network through the currents injected into it. Those currents (or current components) are involved in the DAEs as algebraic states. This allows processing the components separately during the simulation, and paves the way for parallel processing and acceleration of the dynamic simulations [APGV15].

Each of the above three generic components is considered hereafter in some more detail, with reference to Fig. 2.2.

2.1.3 Injector

Synchronous machines, synchronous condensers, static var compensators, motors, static loads, wind-turbine generators, etc. are well-known examples of injectors. The j-th injector attached to the k-th AC bus is modeled by:

$$\mathbf{\Gamma}_j \dot{\boldsymbol{x}}_j = \mathbf{\Phi}_j(\boldsymbol{x}_j, v_{xk}, v_{yk}) \tag{2.5}$$

where $\boldsymbol{x}_j$ is a state vector including both differential and algebraic variables, v_{xk} and v_{yk} are the bus voltage components. In this and subsequent models, $\mathbf{\Gamma}_j$ is a diagonal matrix with:

$$(\mathbf{\Gamma}_j)_{\ell\ell} = \begin{cases} 0 & \text{if the } \ell\text{-th equation is algebraic} \\ 1 & \text{if the } \ell\text{-th equation is differential.} \end{cases} \tag{2.6}$$

Note that $\boldsymbol{x}_j$ includes in particular the components of the current injected in the connection AC bus, i.e. $\boldsymbol{x}_j = [i_{xj}\ i_{yj}\ \ldots]^T$.

2.1.4 AC two-port

While an injector is attached to a single AC bus, an AC two-port is aimed at connecting two AC buses. Thus, the generic model of j-th AC two-port connected to the k-th and l-th AC buses is:

$$\mathbf{\Gamma}_j \dot{\boldsymbol{x}}_j = \mathbf{\Phi}_j(\boldsymbol{x}_j, v_{xk}, v_{yk}, v_{xl}, v_{yl}) \tag{2.7}$$

$\boldsymbol{x}_j$ includes (always with the other states of the AC two-port) the components of the currents injected in both AC buses, i.e. $\boldsymbol{x}_j = [i_{xoj}\ i_{yoj}\ i_{xej}\ i_{yej}\ \ldots]^T$ where subscript o denotes the origin and e the extremity.

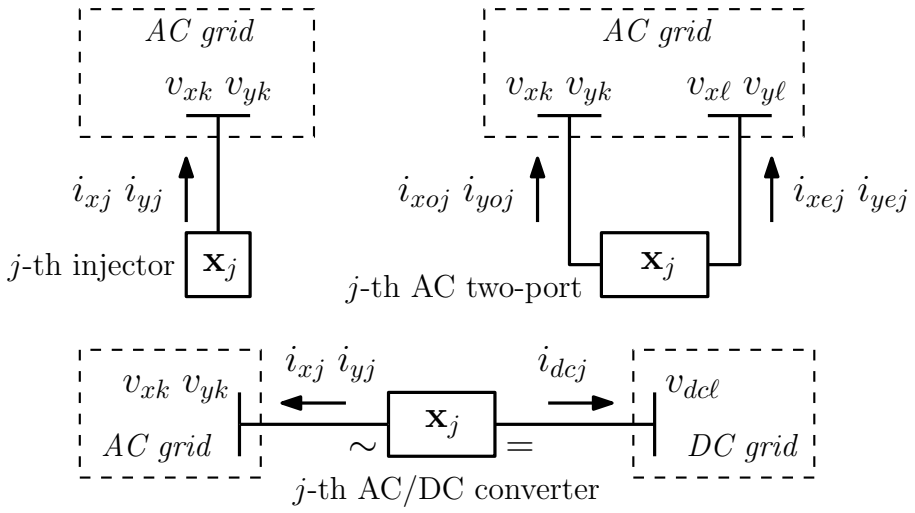

Figure 2.2: The three generic components and their associated variables

2.1.5 AC/DC converter

An AC/DC converter connects one AC with one DC bus. Thus, the j-th AC/DC converter connecting the k-th AC bus and the l-th DC bus is modeled by:

$$\mathbf{\Gamma}_j \dot{\boldsymbol{x}}_j = \mathbf{\Phi}_j(\boldsymbol{x}_j, v_{xk}, v_{yk}, v_{dcl}) \tag{2.8}$$

where v_{dcl} is the DC voltage of bus l. The state vector $\boldsymbol{x}_j$ includes (always with the other states of the AC/DC converter) the current components, i.e. $\boldsymbol{x}_j = [i_{xj}\ i_{yj}\ i_{dcj}\ \ldots]^T$.

Note that a point-to-point DC link can be modeled either as an AC two-port, or as the combination of two AC/DC converters and one DC line. In the latter case, a separate DC sub-network with two buses is created.

2.2 HVDC components modeling

2.2.1 DC line modeling

The branches of the HVDC grid model consist only of resistances. This simplification is justified by the fact that the DC network dynamics are much faster than the dynamics of concern in this work. Thus, the series inductances are neglected, while the shunt capacitances are accounted for in the terminal capacitors C_{term}, as shown in Fig. 2.3.

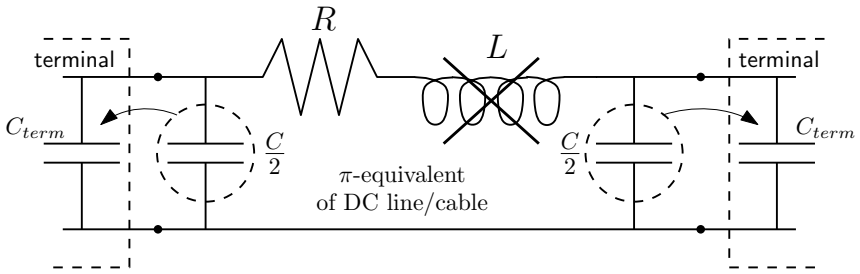

Figure 2.3: Model of HVDC line in phasor-mode simulation

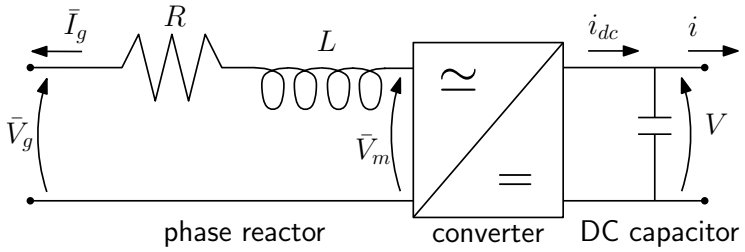

Figure 2.4: VSC representation

2.2.2 Two-level VSC

The generic model of the VSC used in this thesis, namely for the two-level VSC [1] is shown in Fig. 2.4. It consists of the AC phase reactor, the DC capacitor, and the controllers. The latter involve a PLL, current controllers, and outer controllers. On the AC side $\bar{V}_g$ and $\bar{V}_m$ denote the phasors of the AC grid voltage and the VSC modulated voltage, respectively, whereas $\bar{I}_g$ is the phasor of the AC current injected into the AC grid. On the DC side V is the DC voltage, i_{dc} the DC current leaving the converter, and i the current injected into the DC grid, all in per unit. The model is of the Type 6 in [CIG14, ACJ+14] and it has been inspired of various publications (in particular [CB11, RCGN12]). The model of the VSC and the DAE equations dictating its behavior are detailed hereafter.

The block diagram of the phase reactor is shown in Fig. 2.5. The dynamics of the xy components i_{gx}, i_{gy} of current $\bar{I}_g$ are described by the following equations:

$$\frac{di_{gx}}{dt} = \omega_N[-\frac{R}{L}i_{gx} + \frac{\omega_{ref}}{\omega_N}i_{gy} + \frac{1}{L}(v_{mx} - v_{gx})] \tag{2.9}$$

$$\frac{di_{gy}}{dt} = \omega_N[-\frac{R}{L}i_{gy} - \frac{\omega_{ref}}{\omega_N}i_{gx} + \frac{1}{L}(v_{my} - v_{gy})] \tag{2.10}$$

[1] the same model is applicable for a three-level VSC

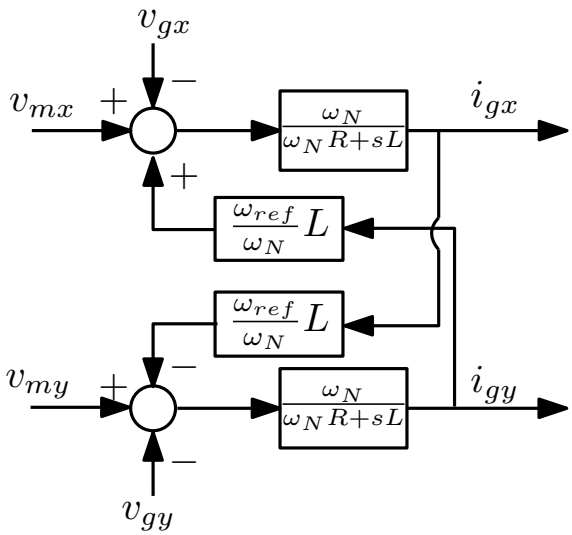

Figure 2.5: Phase reactor block diagram

where v_{gx}, v_{gy}, v_{mx} and v_{my} are the xy components of the grid voltage and modulated voltage phasors in per unit, ω_{ref} is the angular frequency of the xy reference frame in rad/s , and R, L are the parameters of the phase reactor, in per unit. Time t is in seconds, which explains the presence of the nominal frequency ω_N in the right-hand sides of (2.9) and (2.10).

On the DC side, the dynamics of the capacitor are expressed by (2.11):

$$\frac{dV}{dt} = \frac{i_{dc} - i}{2H_{dc}} \tag{2.11}$$

where H_{dc} the combined electrostatic constant of the VSC and the DC grid as discussed in Section 2.3. i_{dc}, i and H_{dc} are in per unit on the nominal power P_{nom} of the VSC in MW.

The connection between AC and DC side variables is given by the power balance equation, as follows:

$$i_{dc}\, V\, P_{nom} = -\left(i_{gx}\, v_{mx} + i_{gy}\, v_{my}\right) S_{nom} \tag{2.12}$$

where the losses in the VSC are neglected. S_{nom} is the nominal apparent power of the VSC in MVA.

The controls of the VSC are represented in the dq reference frame. The latter is provided by the Phase Lock Loop (PLL) that synchronizes the VSC to the grid. The PLL sets the reference frame of the VSC and provides an estimation θ of the grid voltage angle δ to be used by the controllers. It aims to align its d component with the grid voltage phasor $\bar{V}_g$ as shown in Fig. 2.6. The xy frame is rotating with speed ω_{ref}, whereas the dq frame of the PLL rotates with speed ω (in rad/s). In steady state, the grid voltage phasor $\bar{V}_g$ is aligned with the d axis, and, thus, the components v_{gd}

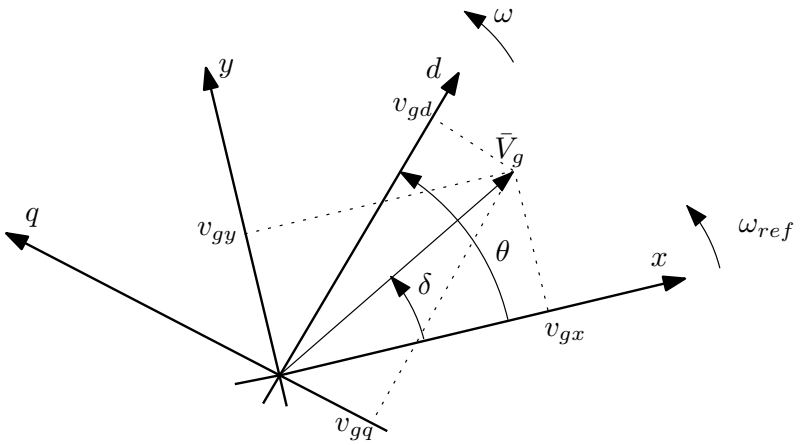

Figure 2.6: xy and dq reference frames

and v_{gq} of this voltage are equal to V_g and zero, respectively. In addition, the angle θ is equal to δ, the component i_{gd} of the current flowing through the phase reactor is the active current, and the component i_{gq} is the reactive current with opposite sign. Following a transient, the PLL adjusts the speed ω, until the d axis again coincides with the voltage phasor. A simple PLL model has been implemented in the VSC and it is shown in Fig. 2.7. Its equations are the following:

$$\frac{d\theta}{dt} = \omega - \omega_{ref} \tag{2.13}$$

$$\omega = K_{p\omega}\, v_{gq} + M_\omega \tag{2.14}$$

$$\frac{dM_\omega}{dt} = K_{i\omega}\, v_{gq}. \tag{2.15}$$

Equation (2.13) gives the predicted angle of the PLL. Equation (2.14) relates to the output of the PI controller, used to estimate the frequency of the system. Equation (2.15) describes the differential state of the integral part of the PI controller. The block $\boldsymbol{R}_{xy\to dq}$ in Fig. 2.7 denotes the change of reference frame from xy to dq. The transformation of voltage coordinates from the xy to the dq frame is given by the following equations (similar relations hold for the dq and xy current components):

$$v_{gd} = v_{gx}\, cos\theta + v_{gy}\, sin\theta \tag{2.16}$$

$$v_{gq} = -v_{gx}\, sin\theta + v_{gy}\, cos\theta. \tag{2.17}$$

Based on this transformation, Eqs. (2.9), (2.10) and (2.12) can be rewritten in dq terms as follows:

$$\frac{di_{gd}}{dt} = \omega_N[-\frac{R}{L}i_{gd} + \frac{\omega}{\omega_N}i_{gq} + \frac{1}{L}(v_{md} - v_{gd})] \tag{2.18}$$

$$\frac{di_{gq}}{dt} = \omega_N[-\frac{R}{L}i_{gq} - \frac{\omega}{\omega_N}i_{gd} + \frac{1}{L}(v_{mq} - v_{gq})] \tag{2.19}$$

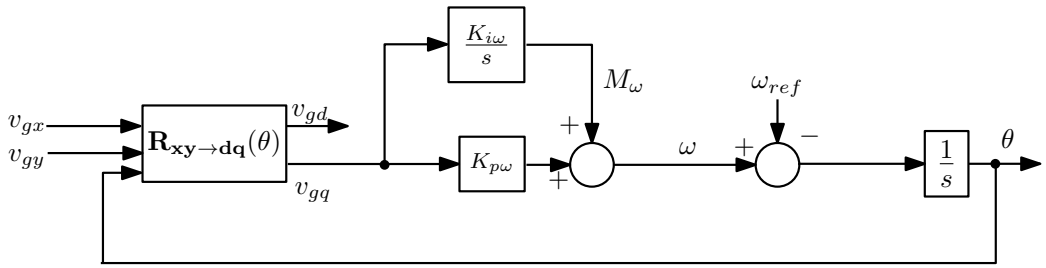

Figure 2.7: PLL block diagram

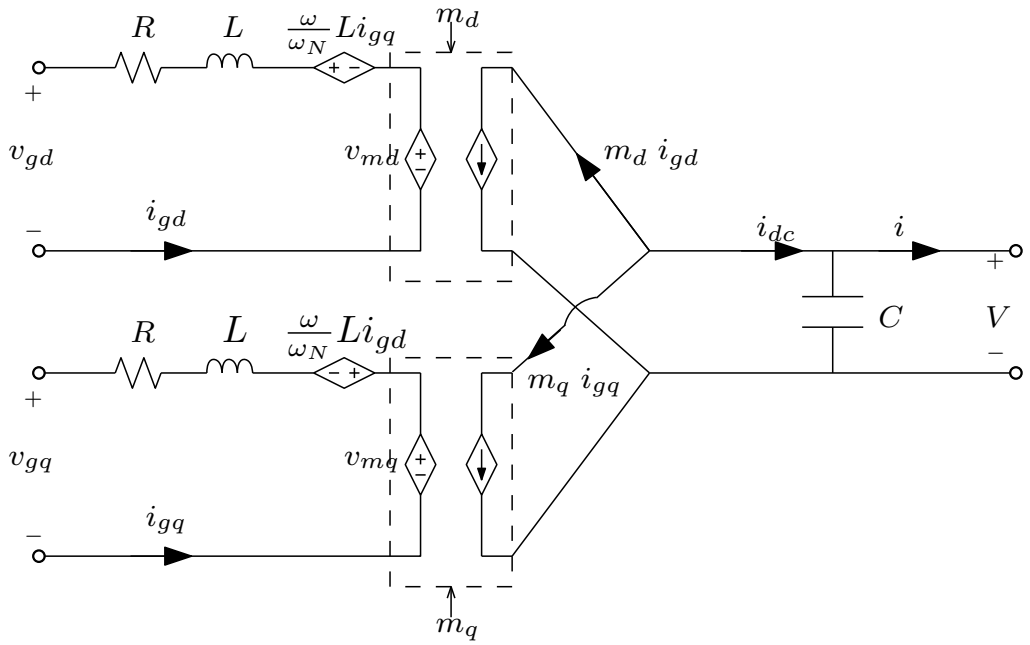

Figure 2.8: Circuit model of two-level VSC in dq-frame

$$i_{dc}\ V\ P_{nom} = -\left(i_{gd}\ v_{md} + i_{gq}\ v_{mq}\right) S_{nom} \tag{2.20}$$

From the above relations, a circuit model of the VSC can be derived in the dq frame [FPS+16], shown in Fig. 2.8, in which the modulation indices $m_d = \dfrac{v_{md}\ S_{nom}}{V\ P_{nom}}$ and $m_q = \dfrac{v_{mq}\ S_{nom}}{V\ P_{nom}}$ have been introduced.

The current controllers are used to control the VSC current components i_{gd}, i_{gq} to their references i_{gd}^{ref} and i_{gq}^{ref}, respectively. The structure described in [Rau14] is adopted here. The corresponding block diagram is given in Fig. 2.9. A PI controller is used for each component and decoupling terms are introduced to achieve independent control. In addition, the grid voltage components v_{gd}, v_{gq} are added to the output of the PI controllers for disturbance rejection purposes.

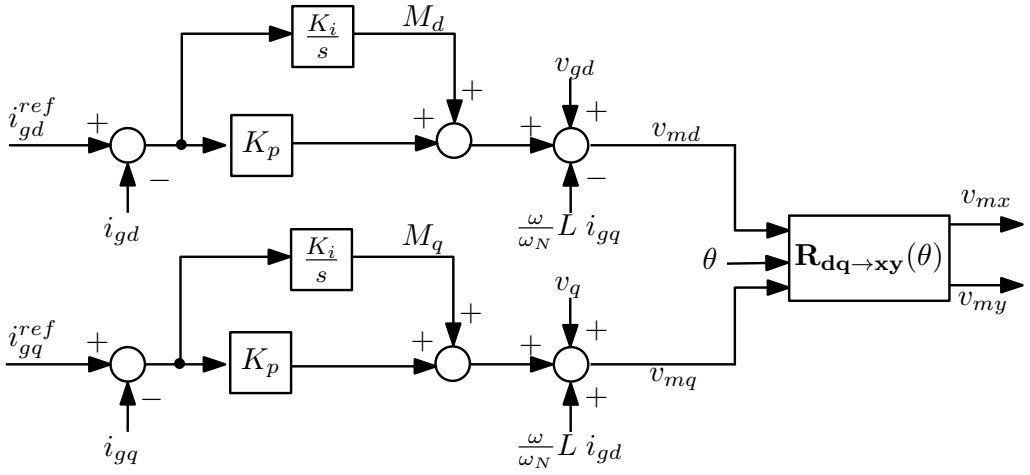

Figure 2.9: Current controller block diagram

The equations describing the current controllers are the following:

$$v_{md} = v_{gd} - \frac{\omega}{\omega_N} L i_{gq} + K_p(i_{gd}^{ref} - i_{gd}) + M_d \tag{2.21}$$

$$v_{mq} = v_{gq} + \frac{\omega}{\omega_N} L i_{gd} + K_p(i_{gq}^{ref} - i_{gq}) + M_q \tag{2.22}$$

$$\frac{dM_d}{dt} = K_i(i_{gd}^{ref} - i_{gd}) \tag{2.23}$$

$$\frac{dM_q}{dt} = K_i(i_{gq}^{ref} - i_{gq}) \tag{2.24}$$

where M_d, M_q are the states of the integral controllers and K_p, K_i the PI controller gains. $\boldsymbol{R}_{dq\to xy}$ is the operation of change from dq reference frame to xy (inverse of $\boldsymbol{R}_{xy\to dq}$).

The outer controllers provide the reference values i_{gd}^{ref} and i_{gq}^{ref}. Various strategies can be employed in order to control the power flow through the VSC, the AC/DC voltages, etc. Two generic controls are considered hereafter from which, by choosing appropriately the controller parameters, all strategies can be implemented.

The active current reference i_{gd}^{ref} is adjusted in order to satisfy the following equation:

$$\alpha_1 \left(P^{set} - P\right) + \beta_1 \left(V^{set} - V\right) = 0 \tag{2.25}$$

where P^{set} is the power setpoint of the VSC, and V^{set} its DC voltage setpoint. To bring the left-hand side of (2.25) to zero a PI controller is used as shown in Fig. 2.10.

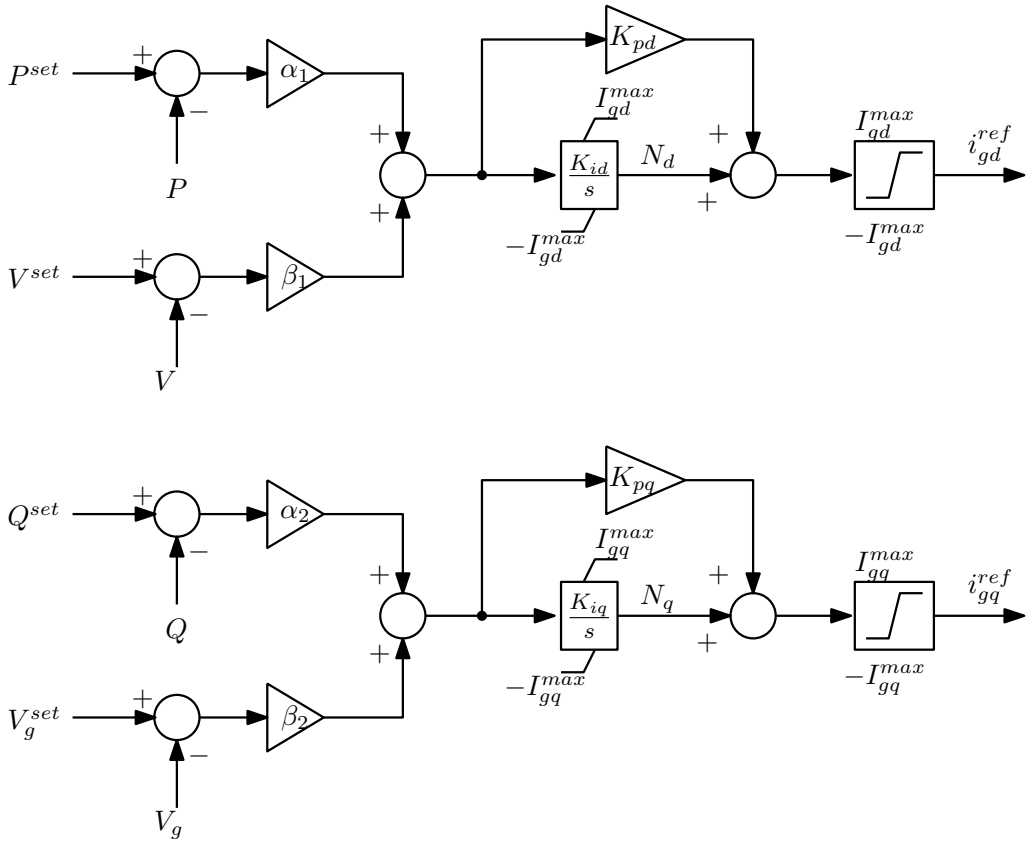

Figure 2.10: VSC outer controllers

Similarly the reactive current reference i_{gq}^{ref} is adjusted to satisfy

$$\alpha_2 \left(Q^{set} - Q\right) + \beta_2 \left(V_g^{set} - V_g\right) = 0 \tag{2.26}$$

where Q^{set} is the reactive power setpoint of the VSC, and V_g^{set} is its AC grid voltage magnitude setpoint. Another PI controller is used to this purpose, as shown in Fig. 2.10.

The following combinations α_1, α_2 and β_1, β_2 are of interest:

- $\alpha_1 = -1$, $\beta_1 = 0$: The VSC controls the power exchange with the AC grid to its reference P^{set}. Throughout this thesis, when reference is made to power P, it corresponds to the DC side power, counted positive when injected into the DC grid. The AC side active power could also be used with appropriate adjustment of the sign of α_1.
- $\alpha_1 = 0$, $\beta_1 = -1$: The VSC adjusts the power to control the DC voltage to its reference V^{set}.
- $\alpha_1 = -1$, $\beta_1 < 0$: The power of the VSC is adjusted in relation to the DC voltage following a linear $P - V$ characteristic.

- $\alpha_2 = -1$, $\beta_2 = 0$: The VSC controls the reactive power injected to the AC grid to its reference Q^{set}.
- $\alpha_2 = 0$, $\beta_2 = -1$: The VSC adjusts the reactive power to control the voltage V_g to its reference V_g^{set}.
- $\alpha_2 = -1$, $\beta_2 < 0$: The reactive power of the VSC follows a linear $Q - V_g$ characteristic.

The following equations are easily derived from Fig. 2.10:

$$i_{gd}^{ref} = K_{pd} \left(\alpha_1 \left(P^{set} - v_{gd}\, i_{gd} - v_{gq}\, i_{gq}\right) + \beta_1 \left(V^{set} - V\right)\right) + N_d \tag{2.27}$$

$$i_{gq}^{ref} = K_{pq} \left(\alpha_2 \left(Q^{set} + v_{gd}\, i_{gq} - v_{gq}\, i_{gd}\right) + \beta_2 \left(V_g^{set} - V_g\right)\right) + N_q \tag{2.28}$$

$$\frac{dN_d}{dt} = K_{id} \left(\alpha_1 \left(P^{set} - v_{gd}\, i_{gd} - v_{gq}\, i_{gq}\right) + \beta_1 \left(V^{set} - V\right)\right) \tag{2.29}$$

$$\frac{dN_q}{dt} = K_{iq} \left(\alpha_2 \left(Q^{set} + v_{gd}\, i_{gq} - v_{gq}\, i_{gd}\right) + \beta_2 \left(V_g^{set} - V_g\right)\right) \tag{2.30}$$

The tuning of the PI controller gains in Fig. 2.10 must take into account the values chosen for $\alpha_{1,2}$ and $\beta_{1,2}$. The work in [Rau14] has proposed ways to choose the PI gains depending on desired response times. In general, the inner controllers are tuned to achieve a response time in the order of 10 ms. In order to avoid interactions between the inner and the outer controllers, the latter are tuned to achieve a response time at least ten times slower, i.e. around 100 ms.

Both current references are limited to their maximum values I_{gd}^{max}, I_{gq}^{max}. Here priority has been given to the active current component in normal operation. Instead, the reactive component is limited by the room left by the active current. In this case, the per unit values of the limits in normal operation are given by:

$$I_{gd}^{max} = 1 \quad \text{and} \quad I_{gq}^{max} = \sqrt{1 - (i_{gd}^{ref})^2} \tag{2.31}$$

2.2.3 MMC model

This sub-section summarizes the comparison made in [FPS+16] of the model of a two-level VSC with that of an MMC.

The circuit model of an MMC derived in [FPS+16, SDM+14] is shown in Fig. 2.11, to be compared with Fig. 2.8.

It can be immediately identified that the AC side is identical in both the MMC and the two-level VSC. Therefore, the current and outer controllers described for the two-level VSC are also applicable to the MMC.

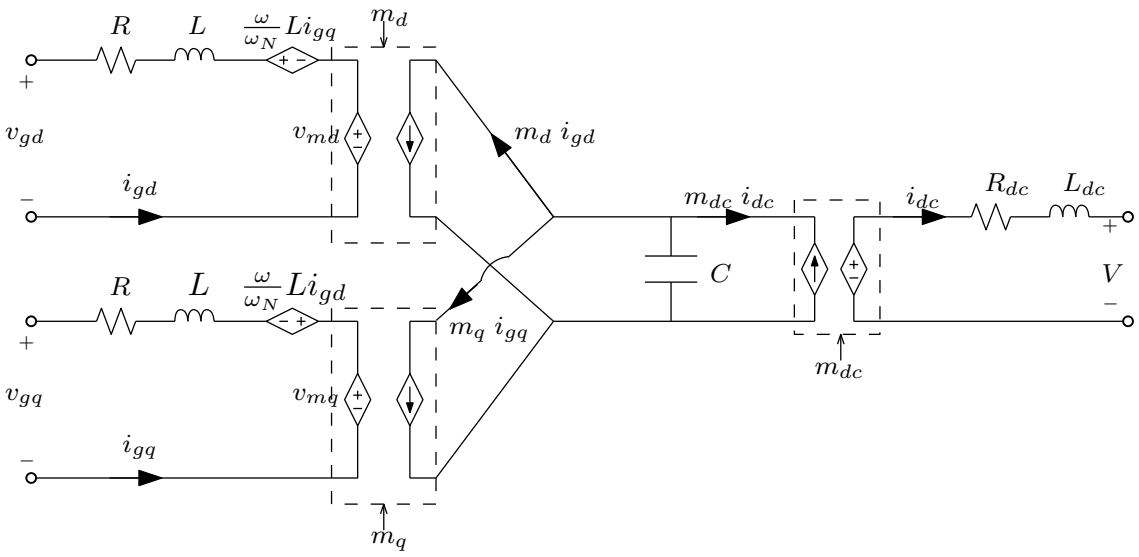

Figure 2.11: Circuit model of MMC in dq-frame

The difference between the two equivalent circuits is on the DC-sides of the two circuits. In particular, the equivalent capacitance of the MMC is not directly connected to the DC grid, i.e. it can be decoupled from it [SGM+15]. This in turn, can have significant impact on the DC voltage response since the total capacitance connected to an HVDC system may be greatly reduced [SGGD15].

Furthermore, the DC current of an MMC is an independent state variable and an additional PI controller (similar to the current controllers of the two-level VSC) is used to control this amount by providing the DC modulation index m_{dc}. In contrast, as observed in (2.12), the DC current i_{dc} of the two-level VSC is not an independent state variable, but is determined by the power balance between the AC and the DC sides.

The last main difference between the two models concerns the need for an internal energy control for the MMC. Indeed, the power balance between the AC and the DC side of an MMC is not automatically ensured (as for the two-level VSC model). Hence, an imbalance between the AC and DC powers would lead to charging or discharging the internal capacitor. An additional outer controller, the energy controller, ensures the power balance by keeping the energy stored internally in the MMC capacitors to its reference value. Several control schemes were proposed for this control [SGGD15], but this falls outside the scope of this thesis.

The above differences result in a model of the MMC slightly different than the one of a two-level VSC. Clearly, this can have important impact on its dynamic behavior. However, for the relatively slow phenomena considered in this work, these differences can be considered negligible, especially if an appropriate control structure is chosen for the MMC [FPS+16]. Therefore, while

this work is focused on the two-level VSC model, the controls developed and the conclusions reached are deemed to be valid also for the MMC topology with appropriate controls.

2.2.4 Offshore VSCs

The aforementioned control structure cannot be applied on AC networks without synchronous generators (i.e. with 100% power electronics-based generation) [DPD+18] since it requires a frequency for the VSC to synchronize to. Offshore wind farms belong to this category. In such a case, the VSC cannot follow a specific power setpoint, but should instead act as a "slack" bus, imposing the frequency and AC voltage on its AC side, and harvesting the power produced by the wind generators.

The detailed modeling and control of the offshore VSCs belongs to the category of grid-forming VSCs [DPD+18] and is out of the scope of this work. Therefore, a very simplified model is used for the AC side dynamics of an offshore VSC, similar to the one in [XYS07], neglecting all AC-side dynamics and controls, and simply setting the VSC modulated voltages (v_{md} and v_{mq}) to constant values. It is noted that the DC capacitor dynamics (2.11) and the power balance between AC and DC sides (2.12) are maintained.

2.3 DC voltage control

2.3.1 Need for voltage control

One of the most crucial aspects of the operation of an HVDC grid is the control of the DC voltage. This is achieved by controlling the power balance in the HVDC grid [Rau14]. To demonstrate this relation between power balance and DC voltage, let us consider an HVDC system of arbitrary topology, shown in Fig. 2.12.

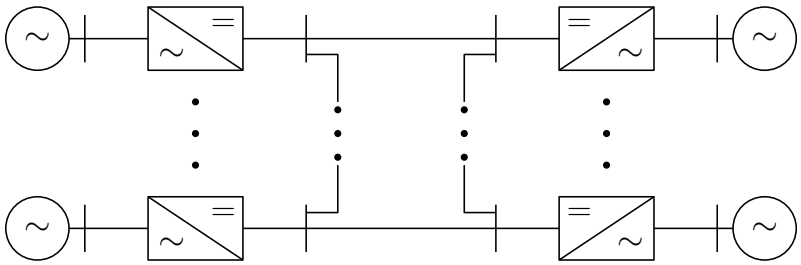

Figure 2.12: Example of HVDC system with arbitrary topology

Focusing on the DC side of the VSCs and replacing the VSCs and the cables with their equivalent models (shown in Fig. 2.4 and 2.3, respectively), the model of the MTDC grid shown in Fig. 2.13 is derived. It consists of the DC capacitors of the VSCs, the shunt DC capacitances of the branches, and the series resistances of the cables. The series inductances have been neglected, as discussed in Section 2.2.1.

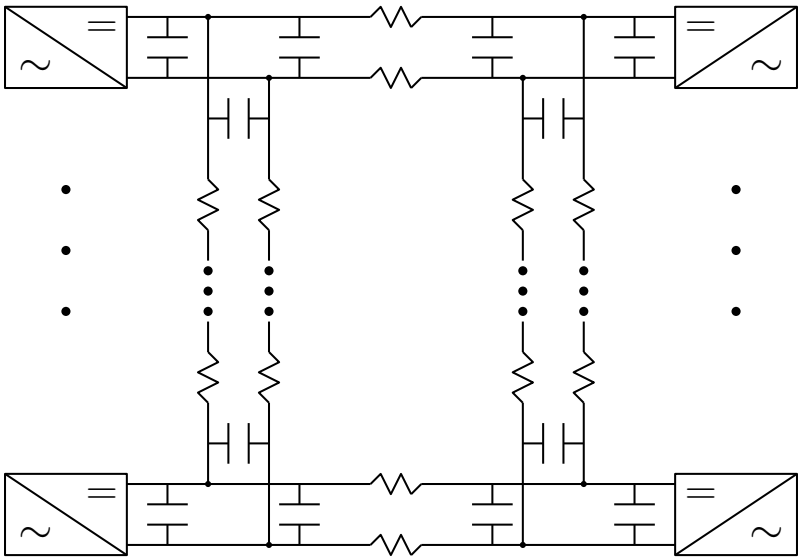

Figure 2.13: Model of MTDC grid (inductances neglected)

If the resistances are also neglected, then all the DC capacitances can be lumped into one equivalent capacitance C_{dc}^{tot}, leading to the simplified representation of the MTDC grid of Fig. 2.14, in which the DC grid is represented by a single DC bus. Therefore, in case of an imbalance between

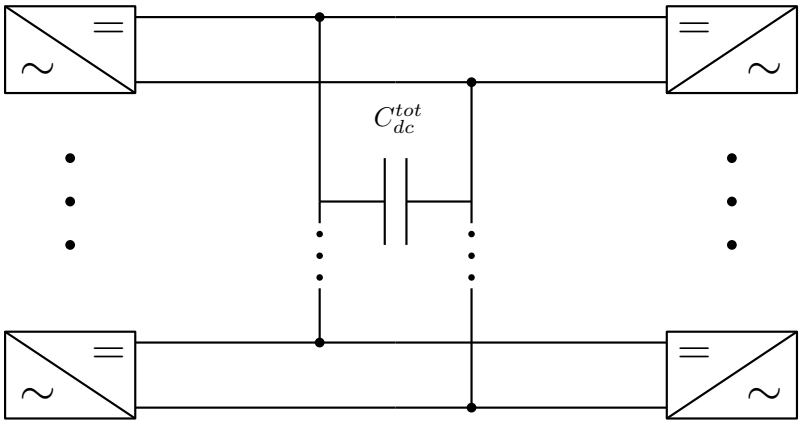

Figure 2.14: Simplified model of MTDC grid

the total power P_r injected into the grid by all rectifiers, and the total power P_i extracted from the

grid by all inverters, C_{dc}^{tot} will charge or discharge and, thus, the DC voltage will deviate from its desired value. Its rate of change is given as follows:

$$V\frac{dV}{dt} = \frac{P_r - P_i}{2H_{dc}^{tot}}. \tag{2.32}$$

H_{dc}^{tot} is the electrostatic constant of the DC grid in seconds, given by

$$H_{dc}^{tot} = \frac{1}{2}C_{dc}^{tot}\frac{V_b^2}{P_b} \tag{2.33}$$

where P_b is the base power of the DC grid and V_b the base DC voltage. These bases are used to convert V, P_r and P_i in per unit.

This expression is similar to the one for AC system frequency when there is an imbalance between the mechanical power P_m given by all turbines and the active power P_e produced by all generators. Similarly, the rate of change of angular frequency in response to a power imbalance is dictated by the total mechanical inertia H_{ac}^{tot} of the machines connected to the grid [KBL94] as follows:

$$\omega\frac{d\omega}{dt} = \frac{P_m - P_e}{2H_{ac}^{tot}}. \tag{2.34}$$

Large excursions of ω or V could lead to equipment tripping or damage. Hence the AC frequency and the DC voltage should be kept near their nominal values. However, while a typical value of the individual mechanical inertia constant of a conventional power plant is in the range of $2-5$ s, the electrostatic constant of an individual VSC is much smaller, namely in a range of $10-100$ ms (including the DC branch contribution). However, while there is usually a big number of conventional power plants in an AC interconnection, MTDC grids are expected to include a limited number of terminals. As a result, the total electrostatic inertia in the MTDC grid will be several orders of magnitude smaller than the mechanical inertia of AC systems. This necessitates having to control the power balance in an MTDC grid rapidly and tightly by adjusting the powers the VSCs inject and/or extract from the grid.

To this purpose, several control schemes have been proposed in which there is always at least one VSC adjusting its power to control the DC voltage. The strategies for a point-to-point link and for an MTDC grid are described hereafter.

2.3.2 Control of a point-to-point HVDC link

The most common control for a VSC point-to-point link is the Master-Slave scheme, which is also used in LCC connections. In this strategy one VSC is chosen to act as the Slave converter

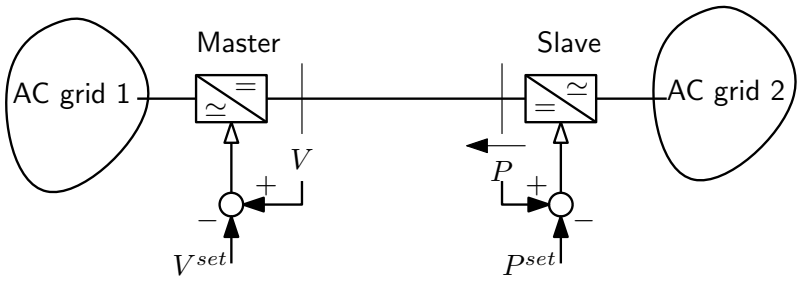

Figure 2.15: Master-Slave control of a point-to-point HVDC link

and the other as the Master. A simplified depiction of the Master-Slave scheme of a point-to-point HVDC link is given in Fig. 2.15. The Slave controls the power transfer in the link by controlling the power P to its setpoint P^{set} (i.e. by choosing $\alpha_1 = -1$ and $\beta_1 = 0$ in (2.25)). The Master adjusts its power to control the power balance in the DC grid by controlling the DC voltage V to its reference V^{set} (i.e. by setting $\alpha_1 = 0$ and $\beta_1 = -1$ in (2.25)).

As far as the reactive current control strategy is concerned, it can be selected independently in both ends, i.e. AC voltage control, reactive power control, etc. can be contemplated.

2.3.3 Control of an MTDC grid

The DC voltage control of an MTDC grid is not as straightforward as that of a point-to-point link, and several methods have been proposed in the literature. The most obvious option is to apply the same control as for a point-to-point link, i.e. the Master-Slave scheme. Assuming an MTDC grid consisting of N VSCs, one is selected as Master and the rest $N-1$ as Slaves. However, this configuration raises security concerns since a failure of the Master VSC would lead to the shut-down of the whole MTDC grid.

Alternatives to Master-Slave control have been proposed that provide redundancy in case of failure of the Master VSC. The voltage margin method [Hai12] uses a back-up Master VSC. The back-up VSC is normally operating as Slave, switching to Master only if the DC voltage exceeds a threshold. However, this method has poor dynamic performance and might require some communication in order to work properly. To solve this, the work in [TP14] proposes the use of multiple "master" converters, which control the voltages at different points in the grid.

The DC voltage droop method and its variants has received the most attention in the literature [DSR+12, Hai12, ACML+15, Rau14, BLM14, Vra13, EBVG15, BGG+14]. It is directly inspired by the AC frequency control practice and allows multiple converters to share any power imbalance in the HVDC grid. Namely, in a droop-controlled HVDC grid some of the VSCs are given a $P-V$

characteristic defined by a power setpoint (P^{set}), a voltage setpoint (V^{set}) and a droop gain (K_V). The power of the VSC then follows the relation:

$$P = P^{set} - K_V(V - V^{set}) \tag{2.35}$$

where positive value of P corresponds to rectifier operation[2]. This characteristic is shown in Fig. 2.16. Following a change in the power injected into the MTDC grid (e.g. change of WF power or tripping of a VSC), the DC capacitors will instantaneously cover this change. This leads to a change of the DC voltage and the adjustment of the VSC power following its characteristic (2.35). For instance, an increase of the DC voltage indicates a surplus of power, hence the VSC power decreases to restore the balance.

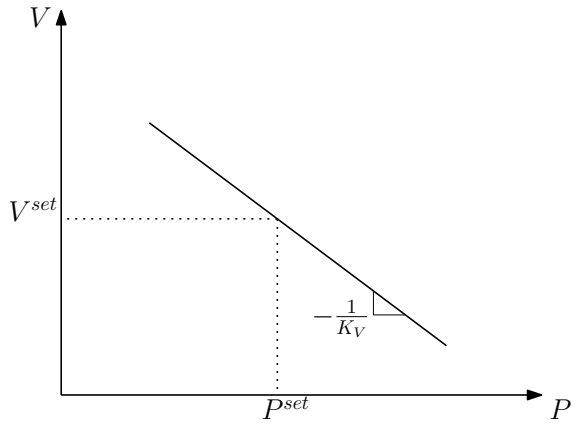

Figure 2.16: VSC droop characteristic

The magnitude of the DC voltage change is mainly determined by the droop gains of the VSCs [Hai12]. For example, let us assume an MTDC grid consisting of N VSCs (with same nominal power for simplicity), each VSC i with its own $P - V$ characteristic. If the losses are neglected then all VSCs have the same DC voltage V and the sum of their powers is equal to zero, i.e.:

$$\sum_{i=1}^{N} P_i = \sum_{i=1}^{N} \left(P_i^{set} - K_{Vi}(V - V_i^{set}) \right) = 0 \tag{2.36}$$

Assuming the outage of VSC j injecting power P_j before the disturbance, the remaining VSCs should adjust their power so that the power balance is again satisfied in the post-disturbance situation.

The total deviation of the post-disturbance powers P_i' from the initial powers will be equal to the

[2]This characteristic is achieved by setting $\alpha_1 = -1$ and $\beta_1 = -K_V$ in (2.25)

lost power P_j. i.e.:

$$\sum_{i=1,i\neq j}^{N} P_i' - \sum_{i=1,i\neq j}^{N} P_i = P_j \tag{2.37}$$

or by replacing P_i and P_i' with the equivalent expressions from (2.35):

$$\sum_{i=1,i\neq j}^{N} \left(P_i^{set} - K_{Vi}(V' - V_i^{set})\right) - \sum_{i=1,i\neq j}^{N} \left(P_i^{set} - K_{Vi}(V - V_i^{set})\right) = P_j \tag{2.38}$$

After performing some algebraic manipulations, (2.38) yields the following relation for the DC voltage deviation:

$$V' - V = \frac{-P_j}{\sum_{i=1,i\neq j}^{N} K_{Vi}} \tag{2.39}$$

The power deviation of a remaining VSC i is given by:

$$P_i' - P_i = \frac{K_{vi}}{\sum_{m=1,m\neq j}^{N} K_{Vm}} P_j \tag{2.40}$$

Equation (2.39) reveals that (in a lossless MTDC grid) the DC voltage deviation in steady-state depends on the magnitude of the power imbalance, and is inversely proportional to the sum of the droop gains K_{Vi}. Moreover, according to (2.40), the deviation of the power of VSC i depends on its relative contribution to DC voltage droop control. Obviously, if all VSCs had the same droop gain K_{Vi}, they would share equally the imbalance. In reality, the power sharing is also affected by the series resistances of the branches of the MTDC grid. In that case, a power-flow computation has to be used to find the post-disturbance operating point [Rau14].

The droop method is generally considered the most appropriate for multi-terminal HVDC operation due to its redundancy, good dynamic performance and its direct analogy with the AC frequency control practice. For the above reasons, it has also been adopted in this work.

2.4 Summary

This chapter has described the modeling and the basic control schemes of VSCs and HVDC networks. This work focuses on large scale studies and the interaction of the HVDC grids with the AC networks. The studies will rely on dynamic simulations under the phasor approximation. Following a brief description of the latter, the models of the various HVDC grid components have been described. Average-value generic models are used in this thesis, compliant with the phasor approximation, i.e. assuming balanced AC conditions and neglecting the fast switching dynamics.

A generic control structure of the VSC has been described whose parameters can be conveniently chosen to satisfy the desired objective, e.g. DC voltage or power control, etc.

The link between the DC voltage control and power balance in a DC network and its analogy with the AC frequency control have been presented. The Master-Slave approach, which is the most common strategy in point-to-point links has been described. The unsuitability of that approach for MTDC grids has been discussed, and alternatives schemes that share the effort between multiple VSCs have been considered, leading to adopt the DC voltage droop control.

Chapter 3

Examples of interactions between AC and HVDC systems

The aim of this chapter is to illustrate several cases of interactions between an HVDC grid and the adjacent AC systems, as well as the possibility to use the VSC control capabilities to improve the dynamics of the combined AC/DC system. In fact, ancillary services by MTDC grids are expected to play a significant role in the operation of future power systems [VR15], and they have already been included in the draft network code proposed by ENTSO-E [EE14a].

In this chapter, simulation results involving the models developed in Chapter 2 are presented, each addressing a different subject and pinpointing the necessity for the control schemes presented in the rest the thesis. Section 3.1 describes a long-term voltage instability case, corrected through post-disturbance redirection of the power through the MTDC grid. The possibility of frequency support among asynchronous AC areas through additional VSC control is demonstrated in Section 3.2. Section 3.3 illustrates the impact of an AC/DC converter outage on the MTDC grid and on the adjacent AC systems. Finally, Section 3.4 focuses on the response of a single VSC subject to a severe decrease of the short circuit capacity of the AC system to which it is connected. A summary of the chapter is made in Section 3.5.

All simulation results presented in this chapter and in the following ones were obtained with RAMSES, a power system dynamic simulation software developed at the university of Liège [AFV14], in which we have implemented the models detailed in Chapter 2, as well as the various controllers proposed in this thesis. RAMSES relies on the phasor approximation. The time step used is typically 5-20 ms.

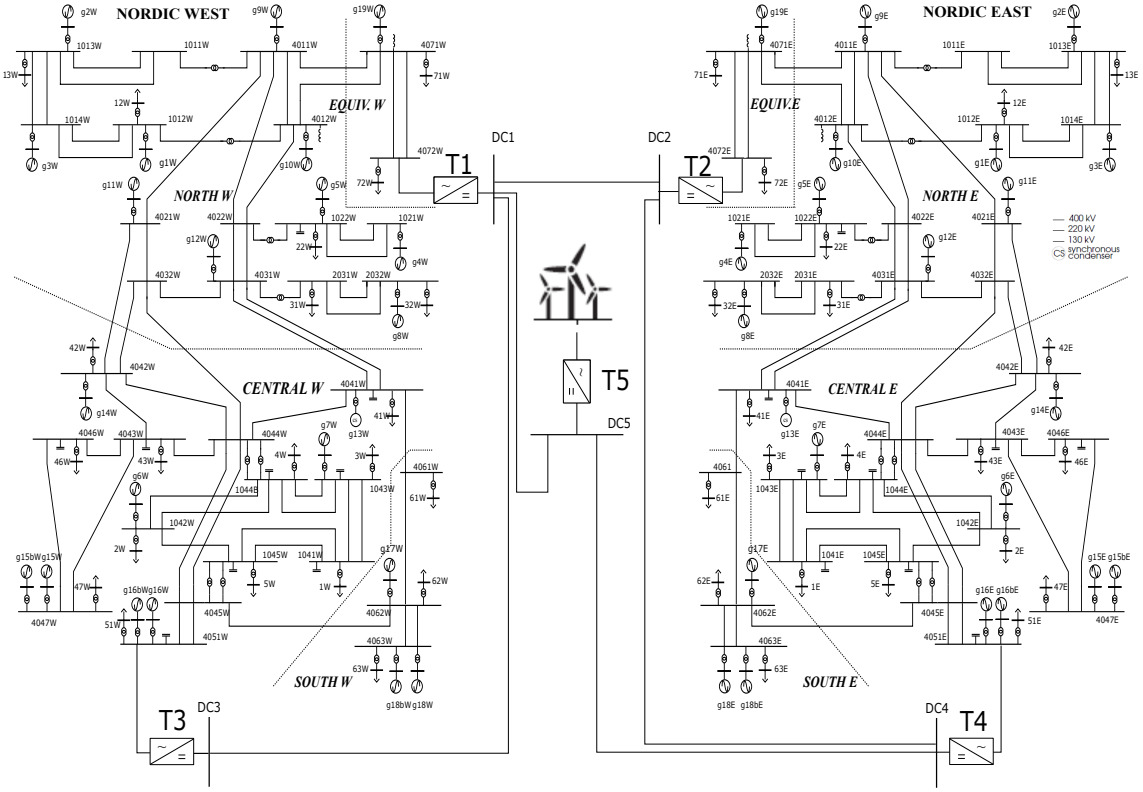

Figure 3.1: Double Nordic test system with MTDC grid

3.1 Case 1: Long-term voltage instability corrected by DC power redirection

3.1.1 Test system

The one-line diagram of the test system used in this example is shown in Fig. 3.1. It consists of two asynchronous AC areas (referred to as Nordic East and Nordic West), interconnected through a five-terminal HVDC grid, and an offshore wind farm.

Each AC area is based on the so-called Nordic test system, set up by the IEEE Task Force on "Test Systems for Voltage Stability Analysis and Security Assessment" and detailed in [IEE15]. Each Nordic system consists of four areas:

- "North" with hydro generation
- "Central" with much load and thermal power generation
- "Equiv" connected to the "North", it includes a very simple equivalent of an external system
- "South" with thermal generation, rather loosely connected to the rest of the system.

The nominal frequency of the system is 50 Hz. In the original configuration described in [IEE15], frequency is controlled through speed governors of generators in the North and Equiv. areas only. In addition, g20 is an equivalent generator with large inertia and participation in frequency control. The thermal units of the Central and South areas do not participate in primary frequency control.

Two operating points, labeled A and B, are described in [IEE15]. Operating point A is N-1 insecure. Its main characteristic is a heavy power transfer from North to Central through five long transmission lines, with several contingencies resulting in long-term voltage instability. These include the tripping of a line in the North-Central corridor or the loss of a generator in the Central area. Operating point B is a reinforced N-1 secure configuration of the system.

The Nordic East and West systems considered have undergone some adjustments compared to the original system shown in Fig. 3.2 [IEE15]. In particular, in both replicas, generator g20 has been removed and the nearby equivalent load has been accordingly adjusted. Also, the operating point of each system has been adjusted according to the case studied. In the long-term voltage instability scenario presented in this section, operating point B is chosen for Nordic West, and operating point A for the East. Each subsystem has two points of connection to the MTDC grid, as shown in Fig. 3.1.

All generators are represented with their automatic voltage regulators, excitation systems, Over-Excitation Limiters (OEL), speed governors and turbines as detailed in [IEE15]. The voltage-dependent loads are represented behind distribution transformers equipped with Load Tap Changers (LTC) reacting with various delays.

The HVDC components are modeled as detailed in Chapter 2. Among the five VSCs, all but T5 operate in DC voltage droop mode. The initial setpoints P^{set} and V^{set} for each VSC are set to the initial DC power and voltage, respectively. T5 harvests the power produced by the offshore wind farm, merely modeled as a power injection. The data of the VSCs and the HVDC lines are given in Appendix A.

3.1.2 Simulation results

The disturbance simulated is the tripping in the East system of line 4032E-4044E, one of the lines in the North-Central corridor of that system. As documented in [IEE15], this contingency leads to long-term voltage instability and final collapse of the system, unless remedial actions are taken.

The evolution of the 130-kV bus voltages in the Central area are shown in Fig. 3.3. Following the disturbance, the voltages are dropped due to the combined actions of LTCs and OELs, eventually collapsing at around 210 s. The instability mechanism has been described in detail in [IEE15] and associated references.

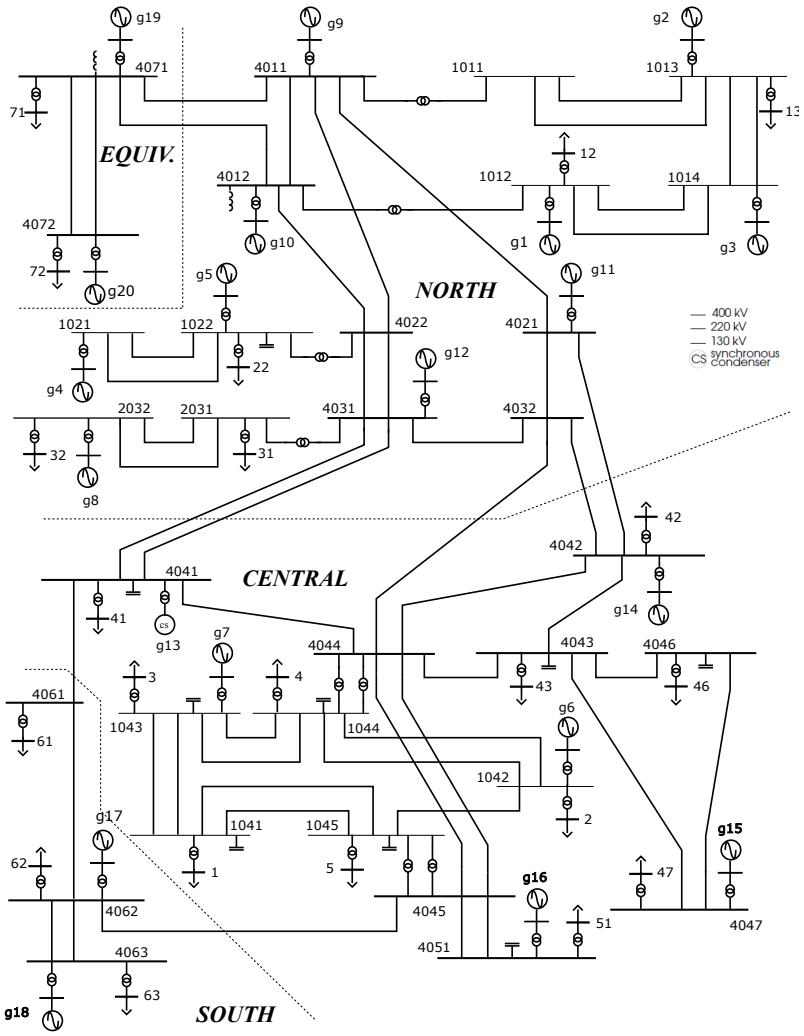

Figure 3.2: One-line diagram of Nordic test system in [IEE15]

System collapse can be avoided either by reducing the active power transferred through the remaining lines of the corridor or by injecting sufficient reactive power in the Central area, to prevent the OELs from taking over [PDPV15]. Traditional schemes to reduce the active power transfer require some kind of direct or indirect load reduction, either by under-voltage load shedding or by decreasing the LTC voltage setpoints. However, this can be also achieved by taking advantage of the MTDC grid, which allows to redirect the power through it.

This is illustrated in Figs. 3.4 and 3.5, which show the evolution of the 130 kV voltages in the Central area and the VSC DC powers, respectively. In this case, the power setpoints of T2 and T4 are adjusted at $t = 115$ s so that 320 MW are eventually rerouted through the MTDC grid, and injected directly by T4 into the Central area, hence bypassing the critical "North-Central" AC corridor. Figure 3.5 shows the DC side powers of the VSCs. The powers of T2 and T4 are adjusted

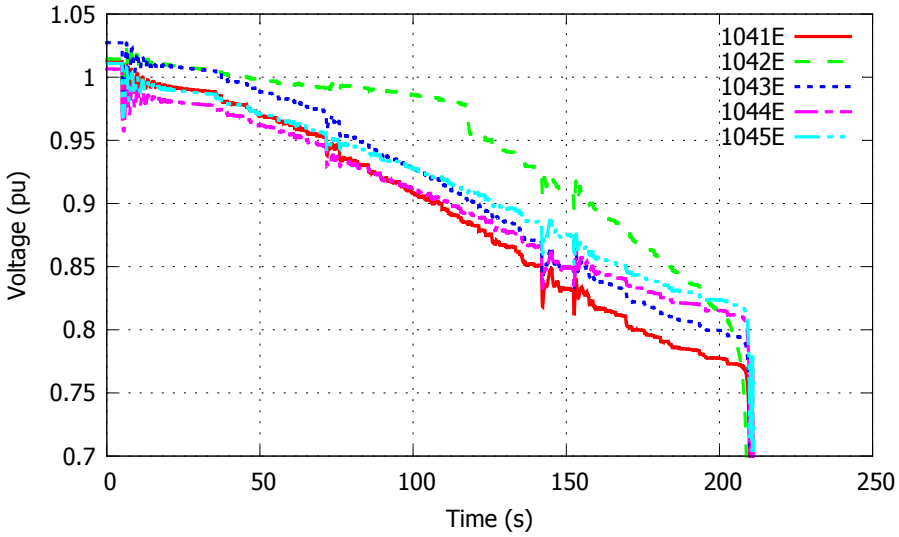

Figure 3.3: Case 1: 130-kV bus voltages in East Central area without intervention of the MTDC grid

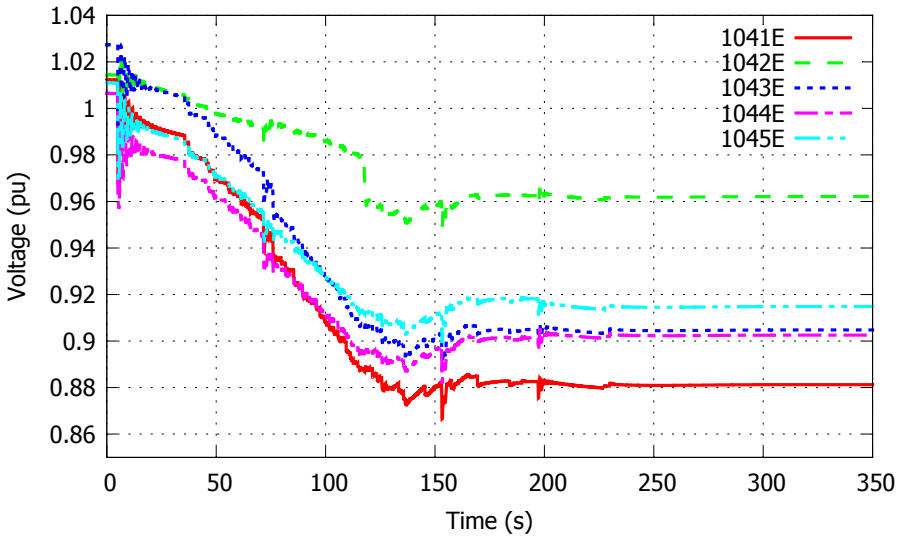

Figure 3.4: Case 1: 130-kV bus voltages in East Central area with sufficient MTDC grid corrective control

within 50 s, whereas the powers of T1, T3 and T5 remain almost completely unaffected. It is noted that the power is counted as positive when it injected into the MTDC system.

Figure 3.6, on the other hand, shows that rerouting only 100 MW is insufficient and does not prevent system collapse. Instead, injection of 320 MW is sufficient to arrest the voltage degradation as shown in Fig. 3.4. The voltages settle at low, but acceptable for a short period values.

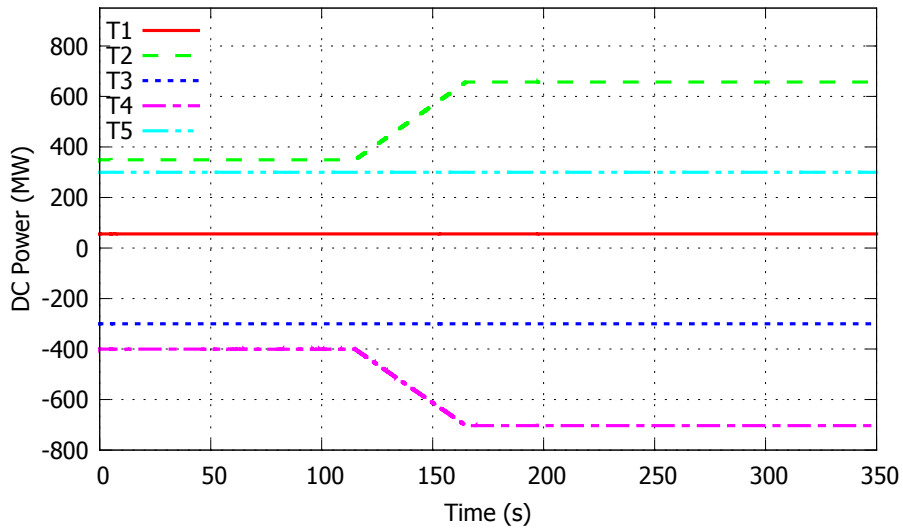

Figure 3.5: Case 1: VSC DC powers

3.1.3 Discussion

The type of scheme presented above falls in the category of post-disturbance corrective control. In order to calculate a sufficient amount of active power, it should be part of the security assessment of the East area that evaluates the response of the system to various contingencies or it should be implemented through a System Integrity Protection Scheme (SIPS) operating in closed loop.

In addition, the VSCs in this scenario are conveniently placed (T2 in the “Equiv” and T4 in the “Central” region). This allows considering the redirection of power from T2 to T4 as an effective countermeasure against voltage instability without affecting the West area. However, it becomes evident that, if both T2 and T4 were placed in the “Central” region, or if the redirection of power was not feasible (e.g. T2 was already injecting maximum power in the MTDC grid), the requested power injection to the “Central” would have to be taken by T1 or T3. In that case, the impact on the West area might not be negligible and precautions should be taken to prevent harming it.

Some aspects on whether an AC/DC system is correctively secure are discussed in more detail in Chapter 6.

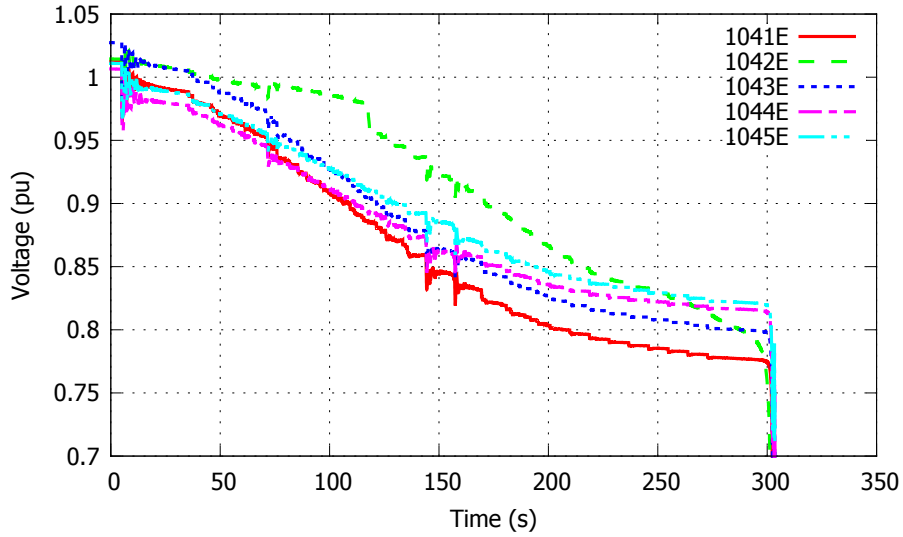

Figure 3.6: Case 1: 130-kV bus voltages in East Central area with insufficient corrective control

3.2 Case 2: Frequency support through MTDC grids

An example of frequency support between two asynchronous AC areas through an MTDC grid is provided in this section. In contrast to AC interconnections, most HVDC interconnected areas operate asynchronously, i.e. the various area frequencies are independent, and the speed governors of the machines in one do not respond to a frequency deviation in another.

3.2.1 Results without frequency support

The test system of Fig. 3.1 is used to demonstrate this. The reinforced operating point B is used for both West and East systems in order to focus on frequency dynamics unaffected by voltage behavior. In addition, the operating point of the East system has been slightly adjusted to free reserves on the thermal power plants and achieve a mixed system frequency behavior.

The disturbance considered is the loss of generator g1E in the East subsystem. This leads to the frequency evolutions shown in Fig. 3.7 for both AC areas. As expected the frequency of the East area is dropping rather sharply after the disturbance. Then the prime movers of the power plants in the East area take over and restore the power balance. Then the frequency recovers and settles at a value below the nominal. The correction of this steady-state error is the objective of the slower secondary frequency control [KBL94], which is not included here.

However, since the VSCs do not respond to the initial disturbance, the power balance in the West system is not affected and its frequency remains constant, equal to its nominal value.

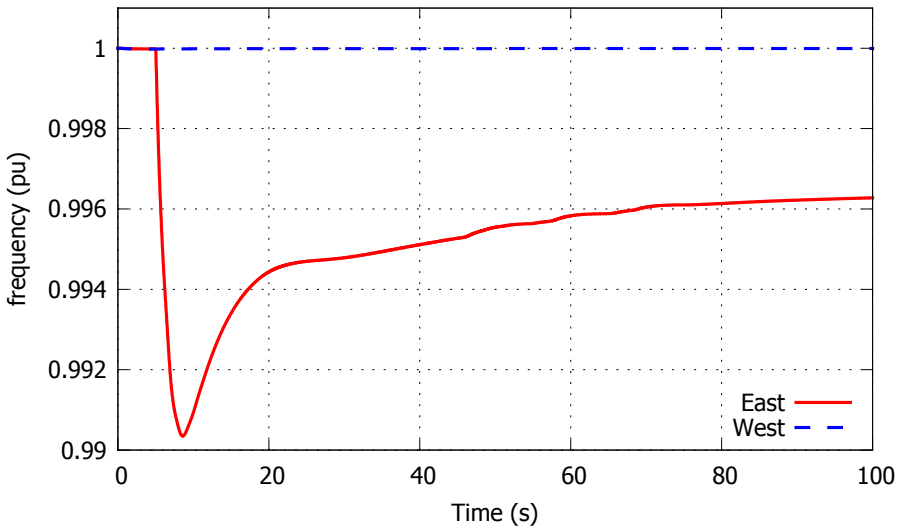

Figure 3.7: Case 2: AC frequency in Nordic East and West areas without support through MTDC

3.2.2 Results with frequency support

To enable frequency support among the two AC areas, the VSCs have to be provided with dedicated controllers responding to frequency deviations. This way, MTDC grids can act as "hubs" when one area is in emergency, adjusting the power transfer to that area, thus sharing the primary reserves of the various connected AC sub-systems [VR15].

One simple control scheme that has been proposed in the literature, e.g. in [HU10][1], is to add to the outer loops of the VSC (see Fig. 2.10) a factor proportional to the frequency deviation. Therefore, instead of Eq. (2.35) the DC power of a VSC in an MTDC grid satisfies (in steady-state) the following characteristic:

$$P = P^{set} - K_V(V - V^{set}) + K_f(f - f_N) \tag{3.1}$$

where K_f a pre-specified droop gain, f the locally measured frequency (which can be obtained from the PLL), and f_N the nominal frequency of the system (all variables in per unit). The block diagram of the power loop (see Fig. 2.10) is adjusted as shown in Fig. 3.8 to include the frequency droop term. The values of parameters α_1 and β_1 have been set to -1 and -K_V, respectively.

Figure 3.9 shows the evolution of the East and West frequencies when VSCs T1, T2, T3 and T4 are equipped with the aforementioned controller. This leads to a smaller frequency excursion in the East area, to the expense of an excursion in the West area, yet of lower amplitude.

[1] A more comprehensive overview of methods is provided in Chapter 5.

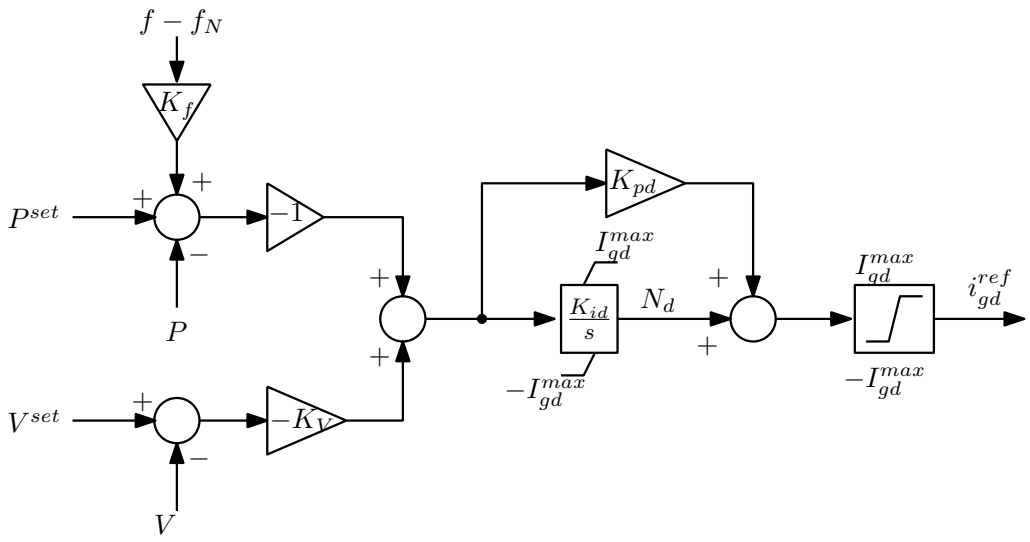

Figure 3.8: Power loop of VSC with frequency droop control

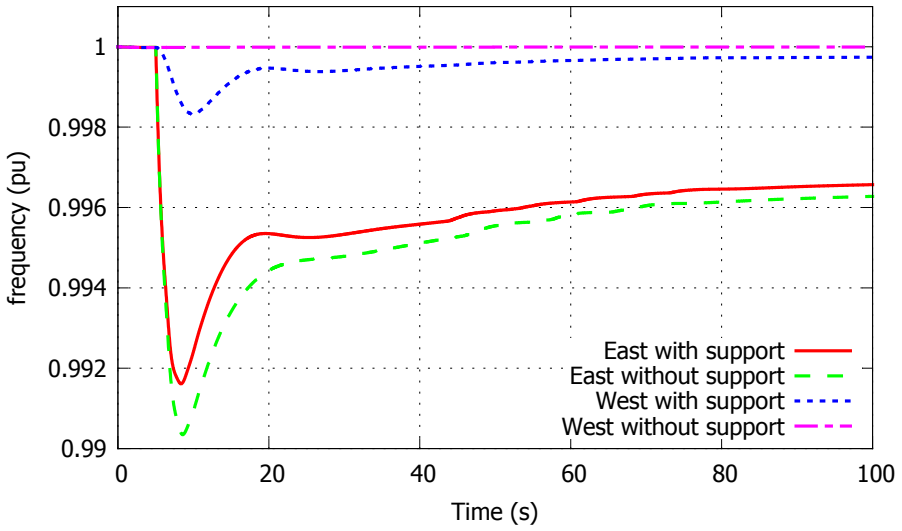

Figure 3.9: Case 2: AC frequency in Nordic East and West areas with support through MTDC

As shown in Fig. 3.10, T2 and T4 change the power they inject into the East area in response to the frequency deviation. T1 and T3 also change their power as dictated by the DC voltage droop control to reestablish the power balance in the MTDC grid, which results in the frequency deviation in the West area. The DC voltages also experience a deviation from their initial values, as shown in Fig. 3.11. Their values depend on the droop settings of the VSCs and the resistances of the HVDC branches.

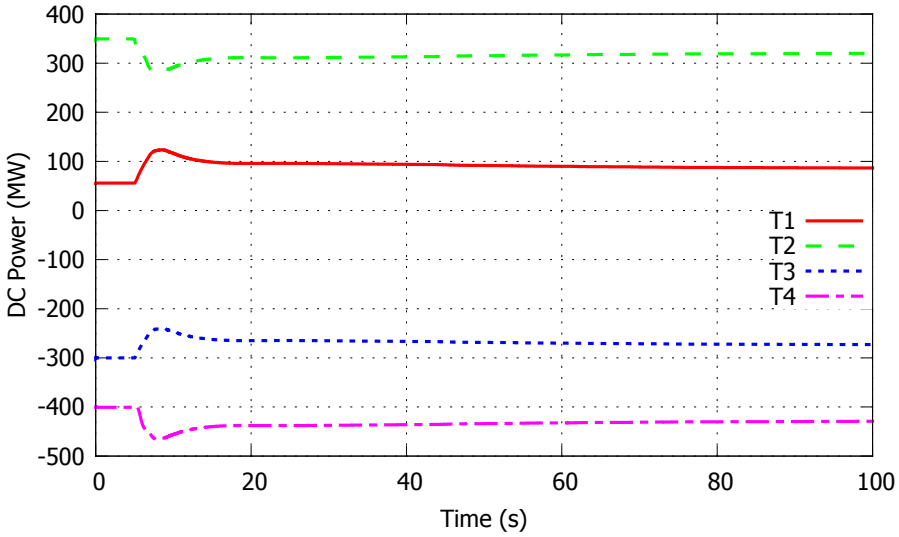

Figure 3.10: Case 2: VSC DC powers

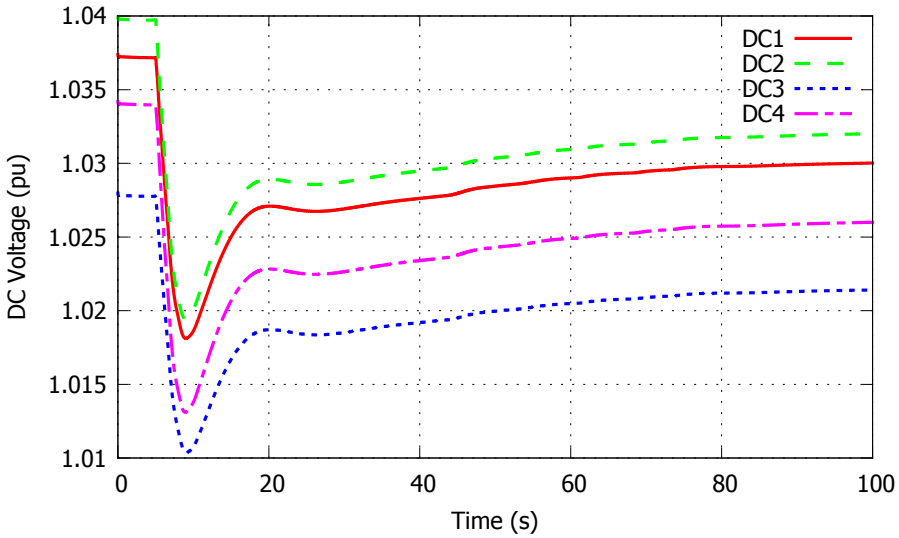

Figure 3.11: Case 2: MTDC grid DC voltages

3.2.3 Discussion

The above demonstrate that frequency support leads through an MTDC grid can improve the frequency response of an AC system. However, it leads to propagation of the disturbance to the DC grid and the other AC areas. Therefore, it might be necessary to limit the amount of support that can be provided so that the response of the MTDC grid variables (e.g. DC voltage limits), as well as of the other AC areas, remain acceptable.

In addition, adjusting continuously the power of a the VSCs according to (3.1) leads to a coupling between AC areas, originally designed to operate asynchronously. Adding a deadband around the nominal frequency would reduce this effect by preventing such continuous interactions between the primary controls of asynchronous areas.

Chapter 5 addresses in more detail the subject of frequency support between asynchronous AC areas.

3.3 Case 3: Tripping of a VSC in an MTDC grid

The aforementioned examples focused on disturbances occurring on the AC side of the AC/DC system. However, the introduction of MTDC grids will necessitate the consideration of DC-side contingencies. This section describes the impact of a sudden loss of a VSC on the MTDC grid and the AC systems. In fact, since MTDC grids are expected to transfer large amounts of power over long distances, the loss of a VSC may significantly impact the security of the adjacent AC systems.

3.3.1 Simulation results

The test system of Section 3.1 is again considered. The disturbance studied is the loss of VSC T4. T4 is operating as inverter before the disturbance, thus its outage creates a power surplus in the MTDC grid. As shown in Fig. 3.12, the remaining VSCs (except T5) react to this by rapidly adjusting their powers and restoring the power balance in the MTDC grid, according to their voltage droop gains K_V. In this example, the same values of K_V have been chosen for T1, T2, T3. Therefore, they share almost equally the power of T4 (small differences are observed due to the resistive losses in the MTDC grid). As a result, approximately 66.7% of the power of T4 is covered by T1 and T3 combined, and the rest 33.3% by T2.

This surplus of power also causes the DC voltages to rise, as shown in Fig. 3.13. They settle at a higher value as dictated by the voltage droop parameters of the VSCs.

The impact of the disturbance on the AC areas should not be neglected. First, as shown in Fig. 3.14, the tripping of T4 followed by the rapid adjustment of power through the DC voltage droop control causes an over-frequency in the West area and an under-frequency in the East area. These frequency excursions are corrected by the primary controls of both areas. However, while the frequency in the West system reaches a steady-state, the one of the East experiences some large transients and indicates system collapse at around 160 s.

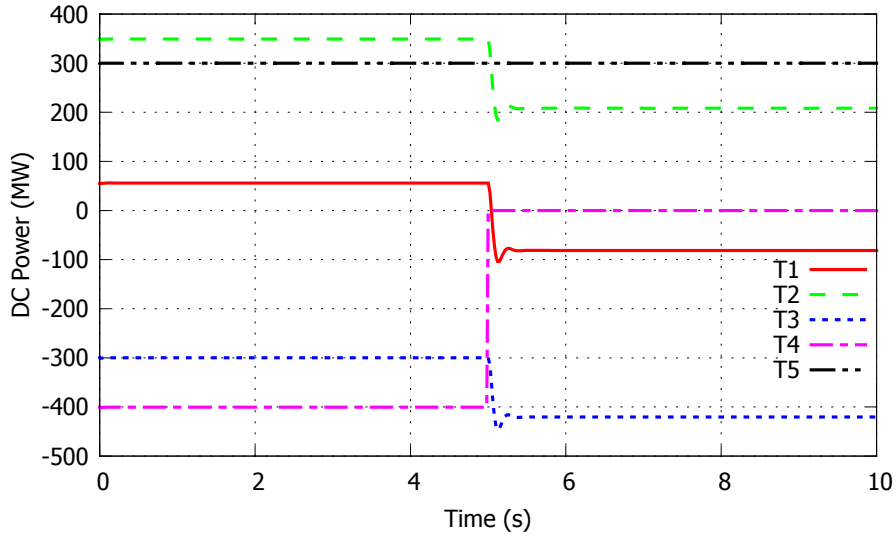

Figure 3.12: Case 3: VSC DC powers

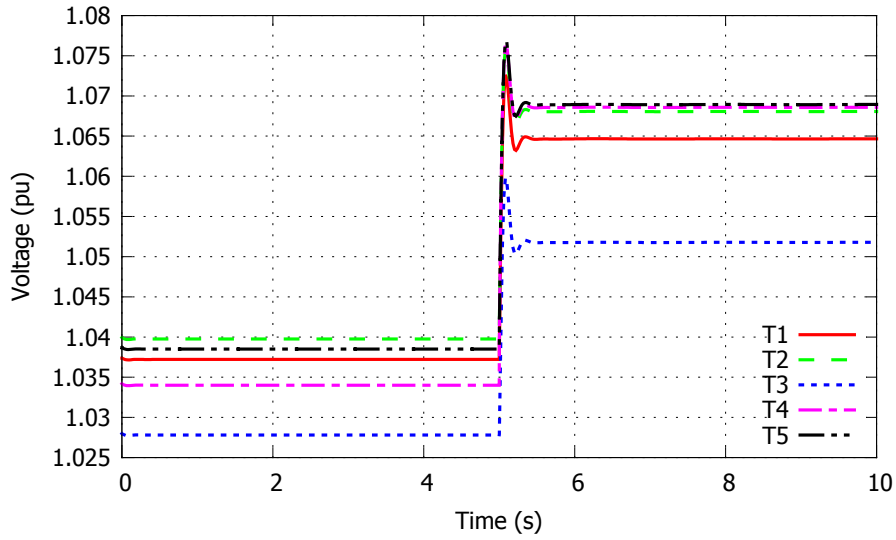

Figure 3.13: Case 3: MTDC grid DC voltages

In fact, the East system collapses due to long-term voltage instability as shown in Fig. 3.15. The mechanism is similar to the long-term voltage instability case discussed in Section 3.1. Indeed, part of the power of T4 is covered by T1 and the rest by the hydro plants in the North area. This power is forced to pass through the heavily loaded "North-Central" corridor of the East system. The latter is thus not secure with respect to the outage of T4.

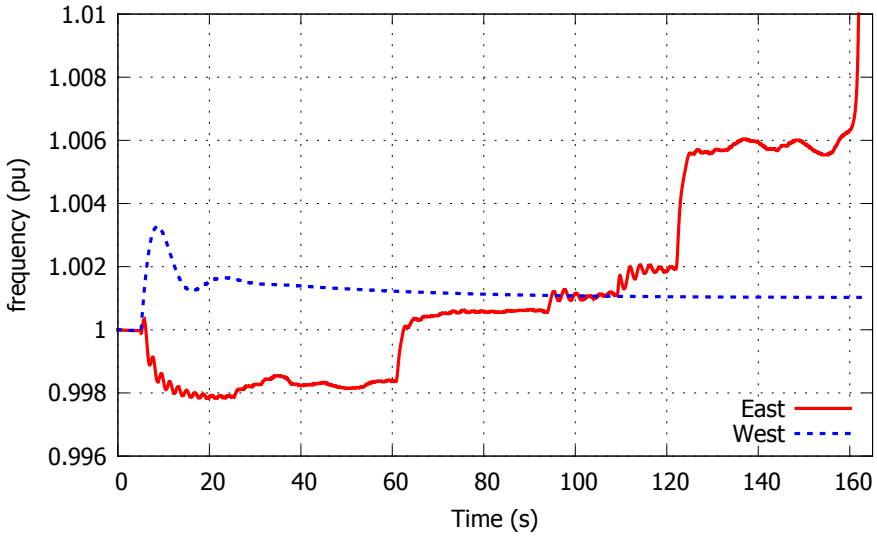

Figure 3.14: Case 3: Nordic East and West frequencies

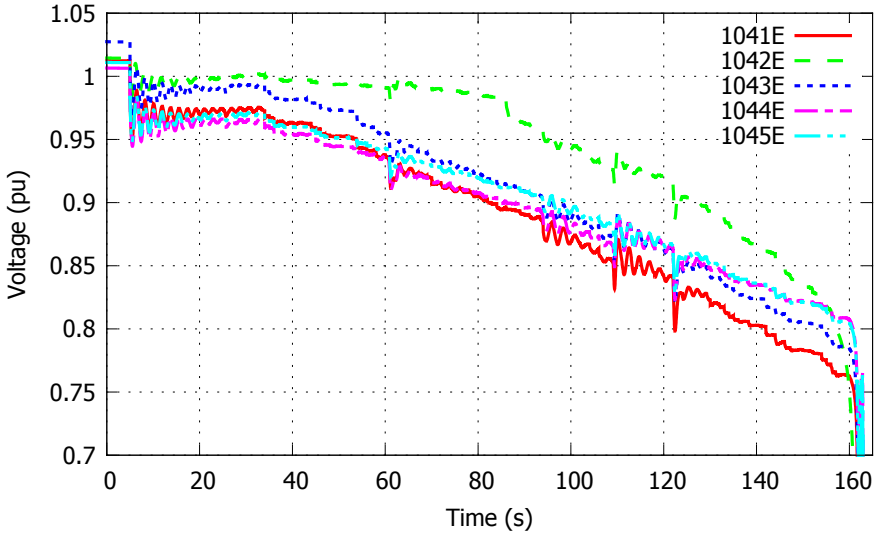

Figure 3.15: Case 3: 130-kV bus voltages in East Central area

3.3.2 Discussion

Using a local control scheme allows to quickly restore the power imbalance in the MTDC grid, but it has its limitations. First, since it simply uses a proportional control, a steady-state error remains, proportional to the size of the disturbance. This steady-state error should be corrected to ensure correct operation of the MTDC grid. In addition, some objectives, e.g. desired MTDC grid power flow, and constraints, e.g. DC branch overloads, cannot be satisfied without a full view of the HVDC system and some coordination between the VSCs.

Last but not least, the security aspect for DC side contingencies should be taken into account. Both the MTDC grid and the AC systems, should be able to withstand the loss of single components including DC grid contingencies.

The above aspects are discussed in Chapters 4 and 6.

3.4 Case 4: Stability of a VSC connected to weak AC grid

3.4.1 Context of study

The last illustrative example does not directly deal with an MTDC grid, but focuses on the behavior of a VSC subject to a sudden decrease of the Short Circuit Capacity (SCC) of the AC system it is connected to. The case study presented here has been discussed in more detail in [PDP+18b].

The system that is investigated is shown in Fig. 3.16. It consists of a point-to-point HVDC link and a simplified representation of the 50-Hz AC system by a Thévenin equivalent involving an ideal voltage source (with magnitude E) and a small reactance X_s, in parallel with a larger reactance X_w. The fast dynamics of the network are neglected, a simplification typical of phasor simulation. Therefore the xy components of the voltage $\bar{V}_g$ are given as follows:

$$v_{gx} = E - X_{eq} i_{gy} \tag{3.2}$$

$$v_{gy} = X_{eq} i_{gx} \tag{3.3}$$

where i_{gx} and i_{gy} are the xy components of the current $\bar{I}_g$ injected into the AC network by the VSC (see also Fig. 2.4). The reference axes xy rotate at nominal angular frequency, and the phase angle of the voltage source is taken equal to zero.

The Slave VSC is connected to the AC system through its phase reactor. The VSC controls the current $\bar{I}_g$ flowing through the phase reactor by adjusting the voltage $\bar{V}_m$. In turn, the current is adjusted so that the VSC controls its active power P, as well as the AC voltage magnitude V_g at the connection point of the HVDC link. The Master VSC is controlling the DC voltage at its DC bus by adjusting its power, thereby ensuring the power balance of the HVDC link.

The static limit of the active power that can be absorbed by the AC system, is given by the well-known formula (e.g. [Ber09]):

$$P_{max}^{st} = \frac{V_g \, E}{X_{eq}} \tag{3.4}$$

corresponding to a 90° phase angle difference and an equivalent reactance X_{eq} between the voltage-controlled nodes. Let us assume for simplicity that E is equal to 1 pu and the VSC

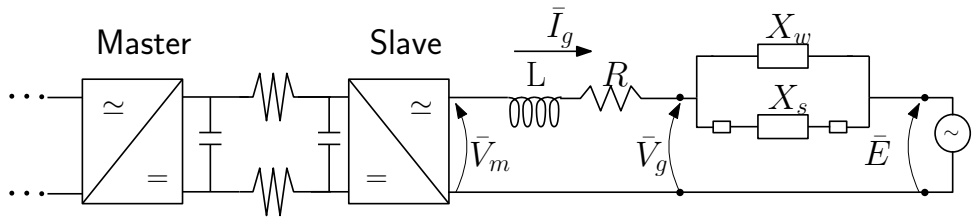

Figure 3.16: Test system of case study

controls its terminal voltage V_g to 1 pu. The expression of P^{st}_{max} becomes merely:

$$P^{st}_{max} = \frac{1}{X_{eq}} = \text{SCC} \tag{3.5}$$

Clearly, if some lines are tripped in the AC system, the equivalent impedance X_{eq} seen by the VSC increases and the maximum power is reduced. If the active power P that the VSC seeks to inject is larger than the new reduced limit P^{st}_{max}, operation is impossible and instability will necessarily result.

Before the disturbance (i.e. with the short reactance X_s in operation), the AC system is adequately strong to absorb the full power of the VSC. Therefore, the power transferred through the VSC before the disturbance can be larger than the SCC of the post-disturbance weak grid.

However, we show in the remaining of this section this example demonstrates that stability is not guaranteed even for lower powers, but depends on the disturbance conditions. A complementary investigation of the impact of the various control loops (outer loops, PLL) using small-signal analysis is detailed in Appendix C.

The system is subject to a large disturbance requiring to consider its non-linear behavior. Therefore, upper and lower limits on i^{ref}_{gd}, i^{ref}_{gq}, v_{md}, v_{mq} and ω (see Figs. 2.10, 2.9 and 2.7) have to be considered. Furthermore, the analysis should also consider changes of control logic. Namely, since the tripping of a line is usually preceded by a fault, it is important to include the low voltage behavior of the VSC.

3.4.2 Low voltage behavior of VSC

In order to avoid sudden disconnection of multiple converters, many grid codes require Fault-Ride-Through (FRT) capability by the VSCs [EE14b, Wei15]. In addition, for the duration of the fault, the VSC is required to boost its reactive current injection in order to support the voltage, while limiting the active current is needed to avoid exceeding the nominal current. Then, after fault clearing, the VSC should ramp up its active power back to its pre-disturbance value. For

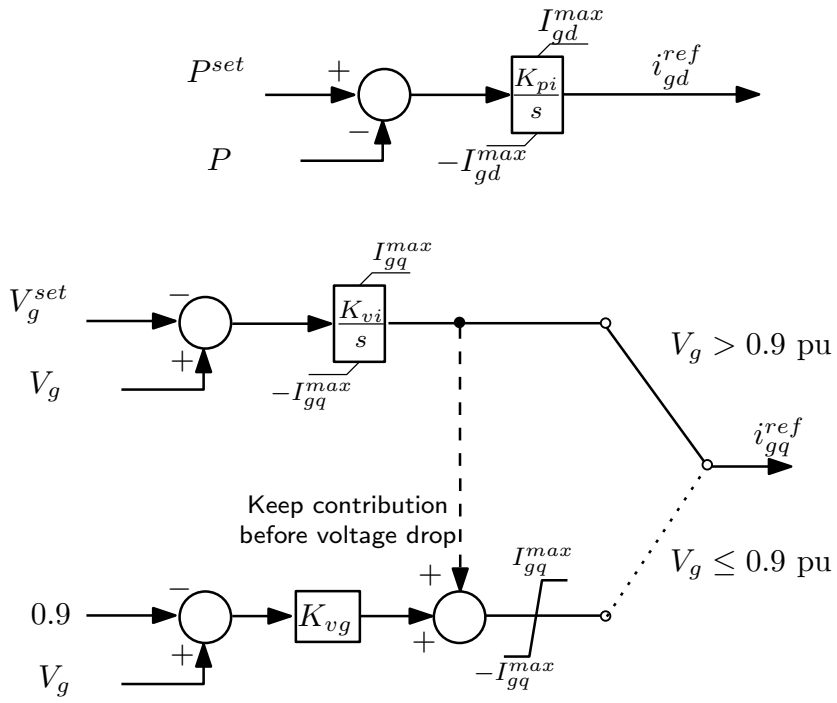

Figure 3.17: Outer loops of VSC including low-voltage support

example, the German grid code specifies that the active power should be restored with a gradient of at least 20% of its nominal value per second [VDN07]. Other grid codes, e.g. in UK [Nat13], are even more constraining by demanding faster active power recovery.

This behavior is modeled as shown in Fig. 3.17 relative to the outer loops of the VSC.

In normal operation an integral control is used for both active power[2] and voltage control. Priority is given to the active current, which can increase up to the maximum VSC active current αI^{max}, α being the fraction of the maximum current I^{max} allocated to active current ($0 < \alpha \leq 1$). Namely, the upper limits shown in Fig. 3.17 are given by:

$$I_{gd}^{max} = \alpha I^{max} \text{ and } I_{gq}^{max} = \sqrt{(I^{max})^2 - \left(i_{gd}^{ref}\right)^2}. \tag{3.6}$$

In case the voltage drops below 0.9 pu the priority switches to reactive current, i.e.

$$I_{gd}^{max} = \alpha\sqrt{(I^{max})^2 - \left(i_{gq}^{ref}\right)^2} \text{ and } I_{gq}^{max} = I^{max} \tag{3.7}$$

and the voltage control loop is replaced by a proportional controller with gain K_{vg} driven by the voltage difference $V_g - 0.9$. It is noted that the i_{gq} contribution of the voltage control before the

[2]This case study focuses on the AC side of the VSC, so P and P^{set} refer to the AC power (in contrast to Fig. 2.10).

fault is kept and added as a constant term to the contribution of that proportional controller. In addition, the voltage control integrator is frozen to prevent windup during the fault.

After fault clearing and the subsequent recovery of the voltage above 0.9 pu, the integral voltage control is restored in operation and priority is once again given, albeit gradually, to the active current. This is achieved by ramping up the active current limit I_{gd}^{max}.

3.4.3 Case 4.1 - Tripping of short reactance with fault

The disturbance considered is a solid three-phase fault in the middle of the short reactance ($X_s = 0.1$ pu), cleared after five cycles (0.1 s) by disconnecting the reactance X_s. X_w is set to 2 pu, thus leading to $P_{max}^{st} = 0.5$ pu after fault clearing. K_{vg} (see Fig. 3.17) is set equal to 2.5 pu and the active power recovery rate is 20 $\%/s$. The response times of the inner loops, the PLL and the outer loops are 10, 50 and 100 ms, respectively. I^{max} has been set equal to 1 pu and $\alpha = 1$. The nominal active power of the VSC has been selected as the base power. The values of the reactances in pu refer to this base.

Figures 3.18, 3.19 and 3.20 show the evolution of respectively the VSC terminal bus voltage V_g, the active power P and the reactive power Q. Three initial operating points are considered: (i) $P^{set} = 0.44$ pu, $P^{set} = 0.45$ pu, and $P^{set} = 0.8$ pu. The selection of the initial operating points has been made according to the results of the small-signal analysis of Appendix C. $P^{set} = 0.44$ pu corresponds to a marginally stable point, $P^{set} = 0.45$ pu to a marginally unstable point and $P^{set} = 0.8$ pu to an absence of equilibrium after the tripping of the line.

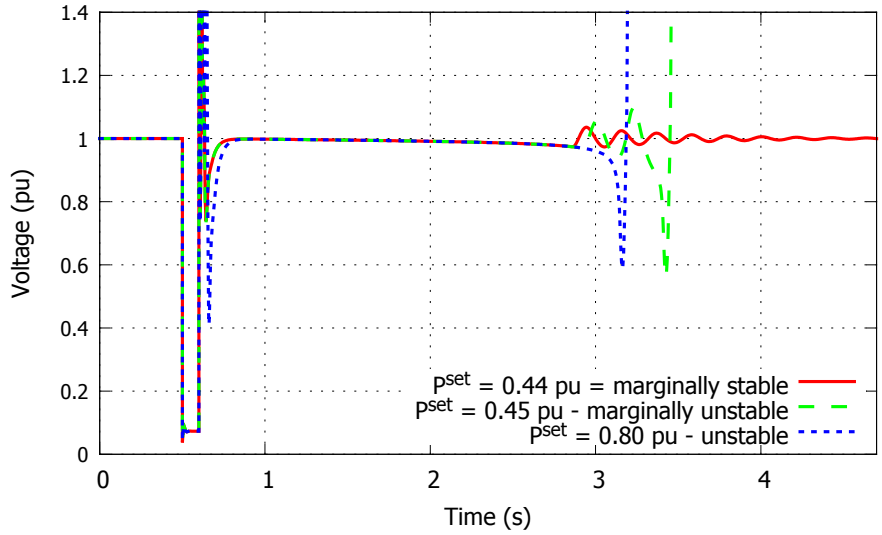

Figure 3.18: Case 4.1 - Voltage at VSC terminal

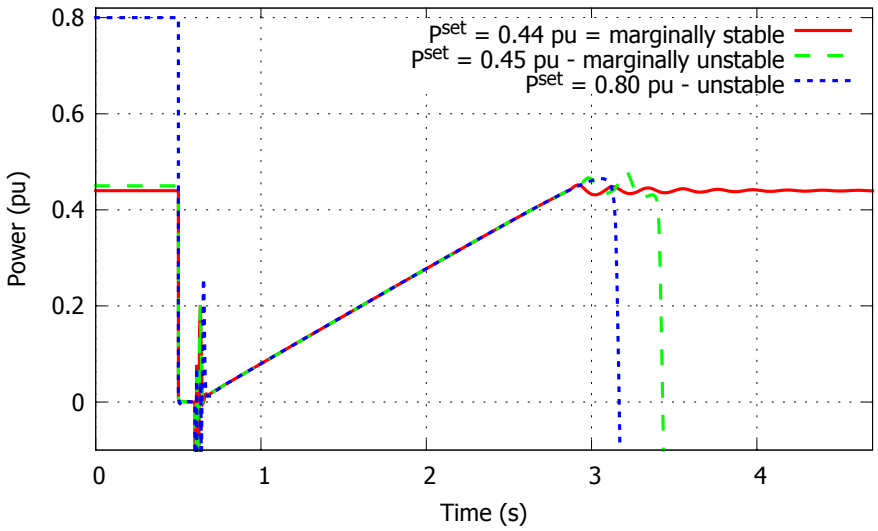

Figure 3.19: Case 4.1 - VSC active power

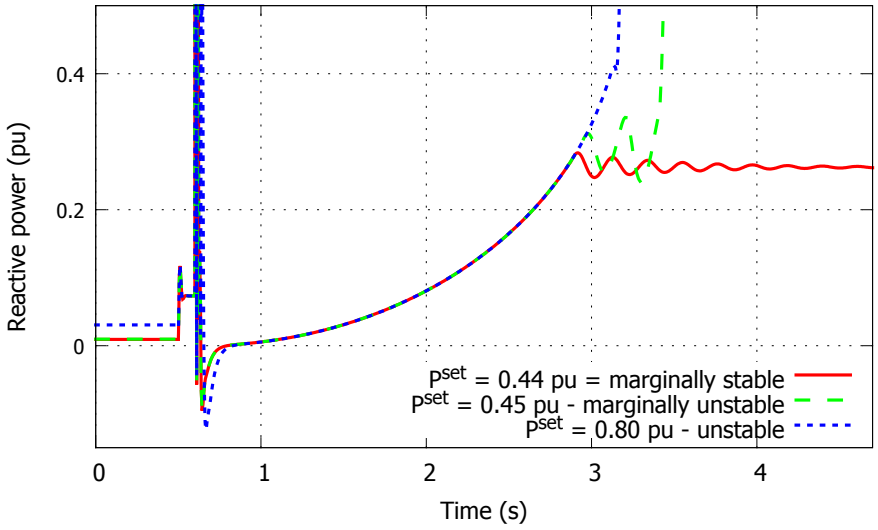

Figure 3.20: Case 4.1 - VSC reactive power

Following the fault, the VSC voltage drops below the threshold of 0.9 pu, as shown in Fig. 3.18, and the VSC enters the reactive support mode by giving priority to the reactive current. Since, the full capability of the VSC is devoted to reactive power, the active power drops to 0 pu during the fault (see Fig. 3.19).

After the clearing of the fault and the tripping of the reactance X_s, there is a large fast transient caused by the voltage and phase angle variations. An overvoltage spike is observed immediately after fault clearing. This is corrected by VSC controls, which swiftly restore the voltage near its

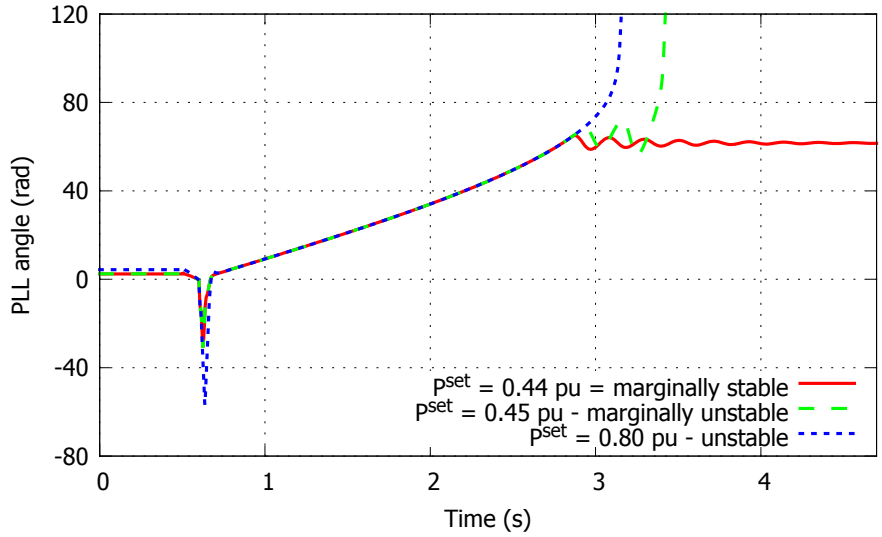

Figure 3.21: Case 4.1 - PLL angle

nominal value. The spike is due to the reactive current, which reached a high value during the fault and takes a short time to decrease, combined with the large Thévenin reactance (see Fig. 3.20). One cannot preclude that an overvoltage protection trips the VSC. If not, the VSC enters the active power restoration mode and ramps up its active power as shown in Fig. 3.19.. As expected, in the unstable case ($P^{set} = 0.8$ pu), the reference power is infeasible and the attempt to recover it leads to collapse. As far as the $P^{set} = 0.45$ case is concerned, the system becomes oscillatory unstable. For $P^{set} = 0.44$ pu, the power experiences some oscillations, but eventually reaches a stable steady state.

The angle θ of the PLL, defined in the block diagram of Fig. 2.7, is shown in Fig. 3.21, for all cases. For the stable case, the angle increases almost linearly, as the power is ramped up and settles at 61°. On the contrary, it raises monotonically in the two unstable cases indicating that the VSC cannot be resynchronized with the AC grid.

3.4.4 Case 4.2 - Tripping of short reactance without fault

Whether the fault-ride-through behavior of the VSC is activated depends on the type of the disturbance, the system under concern, etc., and is not a priori known.

We consider next a case where the SCC is decreased without a fault. Thus, the short reactance X_s is removed at $t = 0.6$ s, leaving the Thèvenin reactance equal to X_w. The evolutions of the VSC voltage and active power are shown in Figs. 3.22 and 3.23, respectively, for various initial operating points.

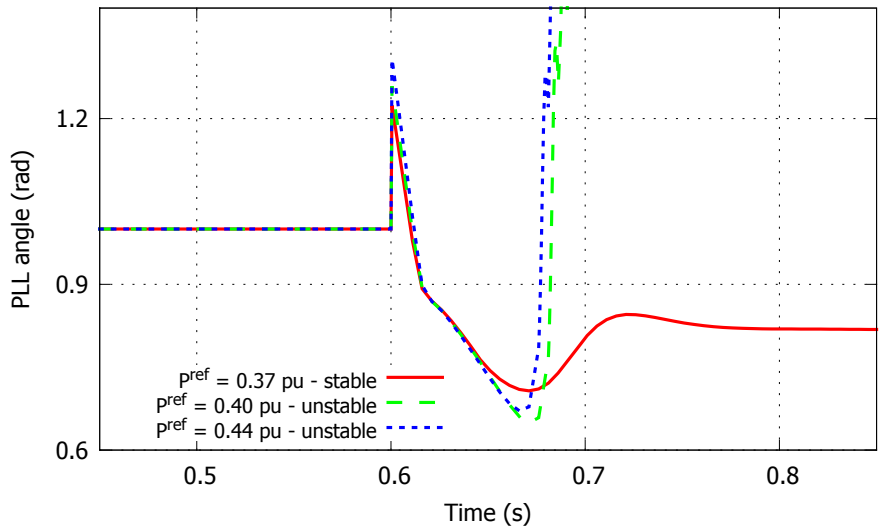

Figure 3.22: Case 4.2 - Voltage at VSC terminal

Figure 3.23 reveals that the case of $P^{set} = 0.44$ pu, identified as stable in Case 4.1, is no longer stable. In contrast, almost immediate collapse is observed after the disturbance. This paradoxical at first glance result is explained as follows. After an initial increase caused by the sudden angle change and the time it takes for the VSC to track the new angle, the voltage drops below 0.9 pu, but not much. Thus, the magnitude of the reactive current i_{gq} injected is smaller than in case 4.1 and leaves room for the whole active current i_{gd}. The latter is not reduced and the VSC attempts to force the pre-disturbance active power immediately.

In order to identify a secure operating point, the pre-disturbance power P^{set} has been decreased in steps of 0.01 pu. The first stable operating point is found for $P^{set} = 0.37$ pu. However, as seen in Fig. 3.22, the voltage has dropped significantly and settled below the threshold of 0.9 pu, indicating that the VSC has been locked in the reactive support mode. Nevertheless, since the active power is successfully restored, the operating point is considered stable.

3.4.5 Discussion

In view of the large transients, the adequacy of the generic model used should be further investigated, as well as the appropriateness of the phasor approximation in the AC system. Methods to detect the imminent instability, as well as countermeasures, such as fast power reduction or simply tripping of the HVDC link should be contemplated. Due to the speed with which the phenomena evolve, relying on a communication signal might not be desirable. This constitutes a challenge since the emergency control should depend entirely on local signals readily available to the VSC.

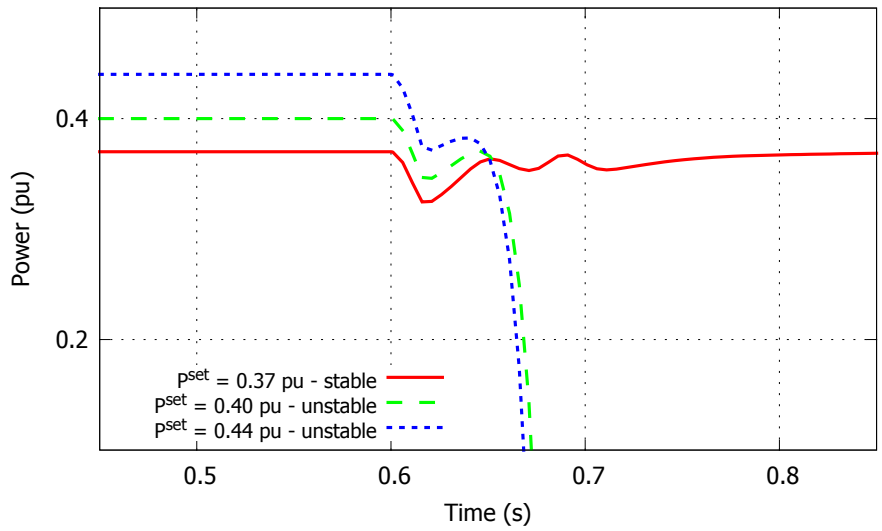

Figure 3.23: Case 4.2 - VSC active power

Alternatives to the generic control scheme of Chapter 2 have been proposed in the literature to increase the stability limit of VSCs connected to weak grids, e.g. the adaptive control of [EFHG15] and the power synchronization method of [ZHN10]. However, these methods focused in small-signal analysis and their response to severe events, such as the one considered in this section, should be further investigated.

In the rest of the thesis the AC grids are assumed strong enough to accommodate the power produced by the VSCs, leaving the aforementioned problems as subjects of future research.

3.5 Summary

This chapter has presented a set of examples illustrating the behavior of combined AC/DC grids. These examples have demonstrated that the MTDC grid can be effectively used to support the AC systems in post-disturbance situations, a service that might prove very valuable in future power systems. This service can be with negligible impact on the other AC systems connected to the MTDC grid, as in the long-term voltage instability case in Section 3.1, or by propagating a fraction of the disturbance, as in the frequency support case in Section 3.2.

On the other hand, the integration of MTDC grids may also introduce new disturbances and security issues, as described in Section 3.3. The necessity to assess the impact of a disturbance in the DC grid on the AC systems, as well as the DC grid itself has been highlighted. In addition, schemes that can restore the systems to a secure operating point following such a disturbance have

to be investigated.

In contrast, the last example described a case study where a severe disturbance in the AC grid can have a strong impact on a DC connection.

Chapter 4

Hierarchical control of MTDC grids

This chapter describes the proposed hierarchical control structure for an MTDC grid. It consists of three levels, a primary, a secondary and a tertiary one. This structure is, up to some point, inspired of the existing and well-proven framework for AC frequency control.

The chapter is organized as follows. Section 4.1 presents the motivation for this work, discusses existing works on the subject, and gives an overview of the proposed control structure. Sections 4.2 focuses on the proposed secondary control. Simulation results from its application on a five-terminal MTDC grid are presented in Section 4.3. The tertiary level is detailed in Section 4.4. Results of the tertiary level and its coordination with the secondary control are provided in Section 4.5. A summary of the chapter is offered in Section 4.6.

4.1 Introduction

4.1.1 Motivation and literature review

As explained in Section 2.3, the secure and robust operation of an MTDC grid relies on tightly controlling its power balance despite the relatively small energy storage capacity. Various methods have been proposed to tackle this issue. Most of them resort to the DC voltage droop technique (see Section 2.3) to quickly correct a power imbalance at MTDC grid level and, hence, stabilize DC voltages [DSR+12].

However, as demonstrated in Section 3.3, these local controls alone cannot steer the MTDC grid towards a desired operating point or remove system-wide violations, such as DC branch overloads. For this reason, other works have been devoted to updating the power and/or DC voltage setpoints

transmitted to the VSCs. To this purpose, the authors of [AEAG14] and [GCL+15] propose an Optimal Power Flow (OPF) to determine and send setpoints to the VSCs at regular time intervals, with the objective of minimizing losses. The work in [NTP16] computes the power and voltage setpoints by solving a multi-objective optimization. The coordinated control detailed in [Rau14] uses repeated DC power flow computations to update the voltage and power setpoints at regular time intervals. Similarly, a method is proposed in [Hai12, HEU15] to estimate the setpoint corrections to be sent to the VSCs so that the power flows through selected AC/DC terminals are restored. A comparison of various re-dispatch schemes is offered in [BV15] with the same objective of correcting the voltage offset left by voltage droop control after a disturbance. The ability of the various schemes to track the desired power setpoints is also evaluated.

Reference [EBVG15] proposes a three-level control structure inspired of AC frequency control practice. Primary control consists of a simple current-based droop scheme. The secondary level involves a slow Proportional-Integral (PI) control to reset the VSC powers to their reference values, and a redispatch scheme updating the power references at regular time intervals. Reference is made to OPF for tertiary control.

Coming back to DC voltage control, several alternatives have been also proposed. The work in [TP14] relies on multiple "master" converters whose voltage setpoints are determined by (centrally) solving a security-constrained OPF. The latter minimizes MTDC grid losses while keeping DC voltages within limits after the outage of a VSC. Reference [BLM14] introduces the pilot voltage droop concept, in which a common DC voltage is communicated to all converters for them to share the powers more efficiently. In addition, two methods are used for power setpoint tracking, namely a simple PI controller and a setpoint redispatching by a central entity. A different approach is followed in [ZBAR15], where fast communication is used to match at each time step the sum of DC currents injected by wind farms with the sum of DC currents of the grid-side converters.

As already mentioned, the optimal operation and the minimization of losses in an MTDC grid have already been addressed in the literature [TP14, GL15, NTP16, AEAG14]. However, this optimization should be compliant with the traditional N-1 security criterion, i.e. the MTDC grid should be able to continue operating following the outage of any single component, without experiencing equipment damage or cascading outages. The work in [TP14] considered N-1 constraints, but not explicitly in its OPF formulation. Instead, it relied on an iterative procedure and used a genetic algorithm to reach a solution.

4.1.2 Overall structure of proposed scheme

The proposed MTDC grid hierarchical control consists of a primary, a secondary and a tertiary level. This structure is inspired by the hierarchical control structure for AC frequency, a simplified diagram of which is shown in Fig. 4.1a [EE12]. The primary frequency control is responsible for restoring the power balance and stabilizing the frequency in the first seconds following a disturbance. Local measurements are used during this stage to ensure a reliable and fast response, while distributing the effort over several specified generation units. Then, secondary frequency control takes over with the objective to restore the primary reserves, cancel the frequency offset of the droop control and restore the power transfer through the interconnections. This process requires coordination of several plants, hence it is slower and lasts for some minutes. The tertiary control has the task of freeing the frequency reserves in order to prepare the system for the next contingency; a process that involves redispatching of the power plants, or starting new units. It can last from several minutes to hours.

The same philosophy is adopted here for the DC voltage control, whose proposed overall structure is shown in Fig. 4.1b. The primary control is responsible for stabilizing the DC voltages, and should achieve this in a time-frame of some milliseconds. During the next seconds (up to a few minutes) the secondary control should correct the DC voltage deviations and adjust the power transfer in the AC/DC converters. At last, the tertiary control should ensure that the MTDC grid satisfies some security criteria, a procedure that takes some minutes, depending on the system complexity.

The primary level has been already discussed in Chapter 2. It consists of several VSCs operating in DC voltage droop mode and adjusting their power according to the DC voltage droop characteristic given by (2.35).

The secondary level is coordinated, i.e. it receives measurements from the MTDC system and sends back setpoints to the AC/DC converters. Its purpose is twofold: (i) to smoothly drive the MTDC system from one operating point to another, and (ii) correct DC node voltage and branch current violations.

The objective of the tertiary level is to calculate and provide appropriate references to the secondary level, in order to optimize its operation. In addition, it incorporates a notion of N-1 security, in order to guarantee that the system can continue operating in case of component failures.

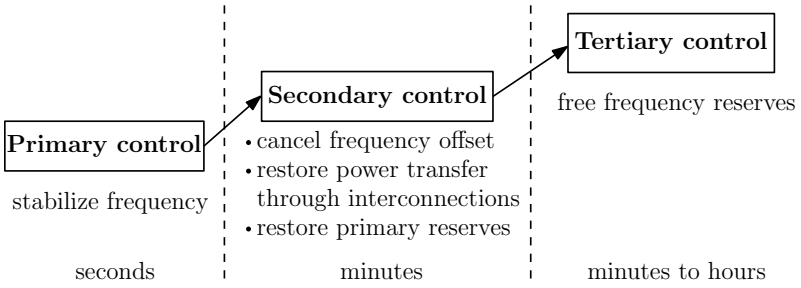

(a) Hierarchical control of AC frequency

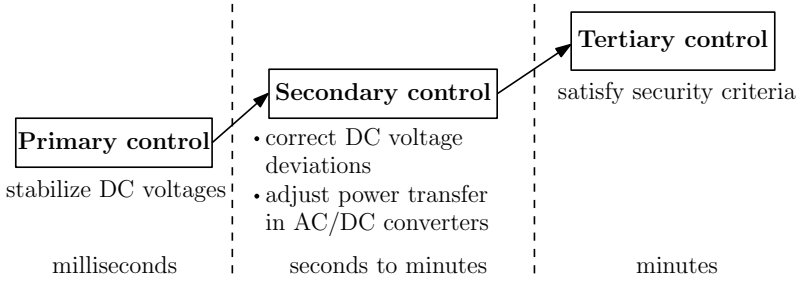

(b) Proposed hierarchical control of DC voltage

Figure 4.1: Analogy between AC frequency and DC voltage control

4.2 Secondary control[1]

4.2.1 Overview

The secondary control should satisfy the following requirements:

1. accommodate the varying power injections by renewable sources;
2. prevent or correct DC voltage and current violations;
3. smoothly drive the system from the current to a desired operating point;
4. avoid excessive impact on the adjacent AC systems and provide additional services (such as frequency support).
5. be robust with respect to model inaccuracies as well as disturbances, such as outages of AC/DC converters or DC cables/lines, and avoid extensive communication between controllers.

Optimization-based approaches are the most appealing owing to their ability to handle constraints. However, most optimization methods proposed in the literature have been devised to operate in open loop. Hence, they cannot account for model inaccuracies, component failures, etc. This was

[1]The material of this section is largely based on [PDPV17b].

our main motivation for resorting to Model Predictive Control (MPC) [2] [Mac02, QB03].

Following a similar categorization to the one in [NTP16], the MTDC grid is assumed to be connected through dispatchable and non-dispatchable VSCs, respectively[3]. Dispatchable VSCs are assigned a $P - V$ droop characteristic according to Eq. (2.35). They either participate in DC voltage control or keep their power to a constant value (i.e. $K_V = 0$) as specified, for instance, by market agreements. They are generally connected to strong AC areas. The non-dispatchable VSCs, on the other hand, have their power varied by external factors. For instance, a VSC connecting an offshore Wind Farm (WF) to the MTDC grid is considered non-dispatchable, since it transfers the power collected by the WF, usually operating in Maximum Power Point Tracking (MPPT) mode. Hence, they do not participate in DC voltage control (i.e. $K_V = 0$).

Supervisory control should act primarily on dispatchable terminals. Adjustments of non-dispatchable terminals (e.g. to decrease the infeed of a WF [FE07, SMS+12]) should be reserved for cases where a limit violation cannot by removed by acting on dispatchable terminals only.

The overall control structure is shown in Fig. 4.2. The lower layer includes a total of N terminals, out of which N_D (resp. $N - N_D$) are dispatchable (resp. non-dispatchable). The upper layer consists of a Power Rescheduler and the MPC-based controller, both acting at the same discrete times. Their respective functions are explained in the next sub-sections.

4.2.2 MPC description

MPC is a mature control technique that has been used for years in the process industry [GHRVC11, QB03]. In the recent years, it has received attention in the area of power system control. For example, it has been proposed for control of distribution networks [VV13, BV18], automatic generation control [VHRW08a], control of microgrids [PWK+17], and damping of wide-area electromechanical oscillations [WGW11].As far as HVDC systems are concerned, several applications have been proposed. At the level of an individual power converter, MPC has been used in [KCV+09] to control the switches of a VSC and in [MFM14] for fast power tracking.

As indicated by its name, the difference with other more conventional control schemes lies on the use of a model of the controlled process. This model is used to predict (i.e. estimate) the behavior of the system in the future. MPC relies on solving on-line an optimization problem to calculate the optimal control actions satisfying a pre-specified objective. For instance, it could be formulated as an optimal control problem or as a minimization of the difference between the predicted system outputs and the desired outputs [Sol17].

[2] also called Receding Horizon Control

[3] In this chapter, the terms “VSC” and “AC/DC terminal” are used interchangeably.

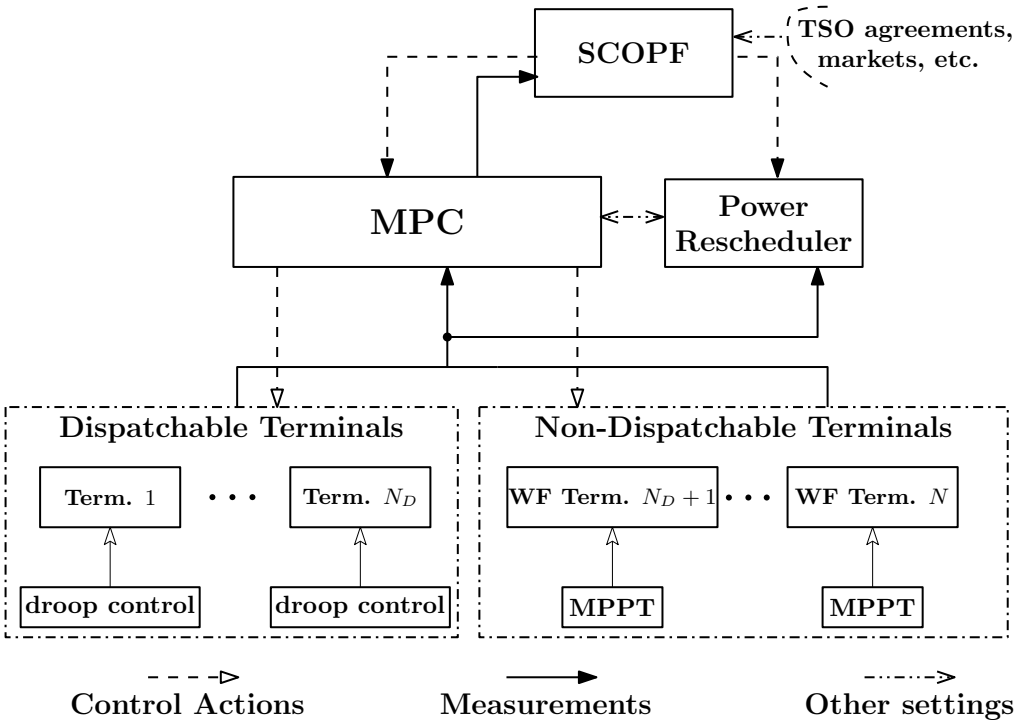

Figure 4.2: Overall control structure

In many applications, a simplified linear model of the system is used. This allows to formulate the optimization problem as a convex linear or quadratic programming problem, for which efficient solution algorithms exist [Bem18]. More complex formulations leading to non-linear MPC have also been proposed [QB00]. However, due to various obstacles (e.g. computing times, although computational power and optimization algorithms have improved during the recent years), the majority of practical MPC applications rely on linear or quadratic programming.

Simply stated, MPC consists of computing a sequence of control changes which minimizes a multi-time-step objective and satisfies constraints in the future [Mac02]. At a given discrete time k, using the latest available measurements, the controller computes a sequence of optimal control actions to be applied from k to $k + N_c - 1$, so that the system meets a desired target at $k + N_p$. N_c and N_p are referred to as control and prediction horizons, respectively. Out of this sequence, only the first component is applied. Then, after a sampling period T, i.e. at time instant $k + 1$, the procedure is repeated for the updated control and prediction horizons, using the newly received measurements, which reflect the system response to the applied control actions at and before time k. This yields a closed-loop behavior, that can account for unexpected behavior and approximation of the system model.

The control and prediction horizons are illustrated in Fig 4.3. In general, the prediction horizon

is chosen greater than the control horizon, i.e. $N_p \geq N_c$, so that the controller takes into account the anticipated effect of the control actions on the system. If the controller does not have to consider changes beyond the control horizon, which is the case in this work, the horizons can be set equal, i.e. $N_c = N_p$, to decrease the computational burden (i.e. decrease the number of decision variables).

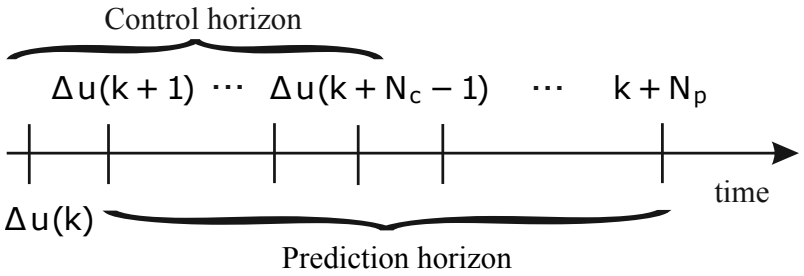

Figure 4.3: Prediction and control horizons

A hypothetical example of MPC operation is presented in Fig. 4.4 for a single-input single-output system, with $N_c = N_p = 3$ steps. In this case, the optimal control actions are calculated so that the y-axis variable is close to its target value (inside a tolerance δ). At the discrete time k a new target is received by the MPC and a control sequence $\Delta\mathbf{u}(k)$, $\Delta\mathbf{u}(k+1)$ and $\Delta\mathbf{u}(k+2)$ is calculated to bring the variable under concern inside the tolerance. Only the first action $\Delta\mathbf{u}(k)$ is applied. New measurements are received at time $k+1$. Based on them, the MPC calculates a new sequence of control actions at $k+1$ in order to reach the target at the end of the (receding) prediction horizon.

Due to model inaccuracies, measurement noise and other uncertainties, the system response to the action $\Delta\mathbf{u}(k)$ is not exactly the one predicted by the model. These inaccuracies are corrected by the closed-loop behavior of MPC, which eventually brings (after several steps) the system output into the desired interval, as depicted by the magenta circles in Fig. 4.4. In fact, an open-loop approach would consist of applying the control actions calculated at time k, i.e. $\Delta\mathbf{u}(k)$, $\Delta\mathbf{u}(k+1)$ and $\Delta\mathbf{u}(k+2)$. In this case, the new measurements at $k+1$ would not be exploited, and the resulting response could be quite different from what was predicted. This is depicted by the black squares in Fig. 4.4, which also show that the objective is eventually not satisfied.

The above receding horizon principle can be simply formulated as follows [Sol17].

Typically it relies on an optimization problem, aiming at minimizing or maximizing a function (e.g. minimizing a cost) under various constraints. Assuming $\boldsymbol{x}(k+1), \ldots, \boldsymbol{x}(k+N_p)$ are state variables, grouped into the vector $\boldsymbol{X}(k)$, and $\boldsymbol{u}(k), \ldots, \boldsymbol{u}(k+N_c-1)$ into $\boldsymbol{U}(k)$, the optimization problem can be written as:

$$\min_{\boldsymbol{X},\boldsymbol{U}} \quad J(\boldsymbol{X}(k), \boldsymbol{U}(k)) \tag{4.1}$$

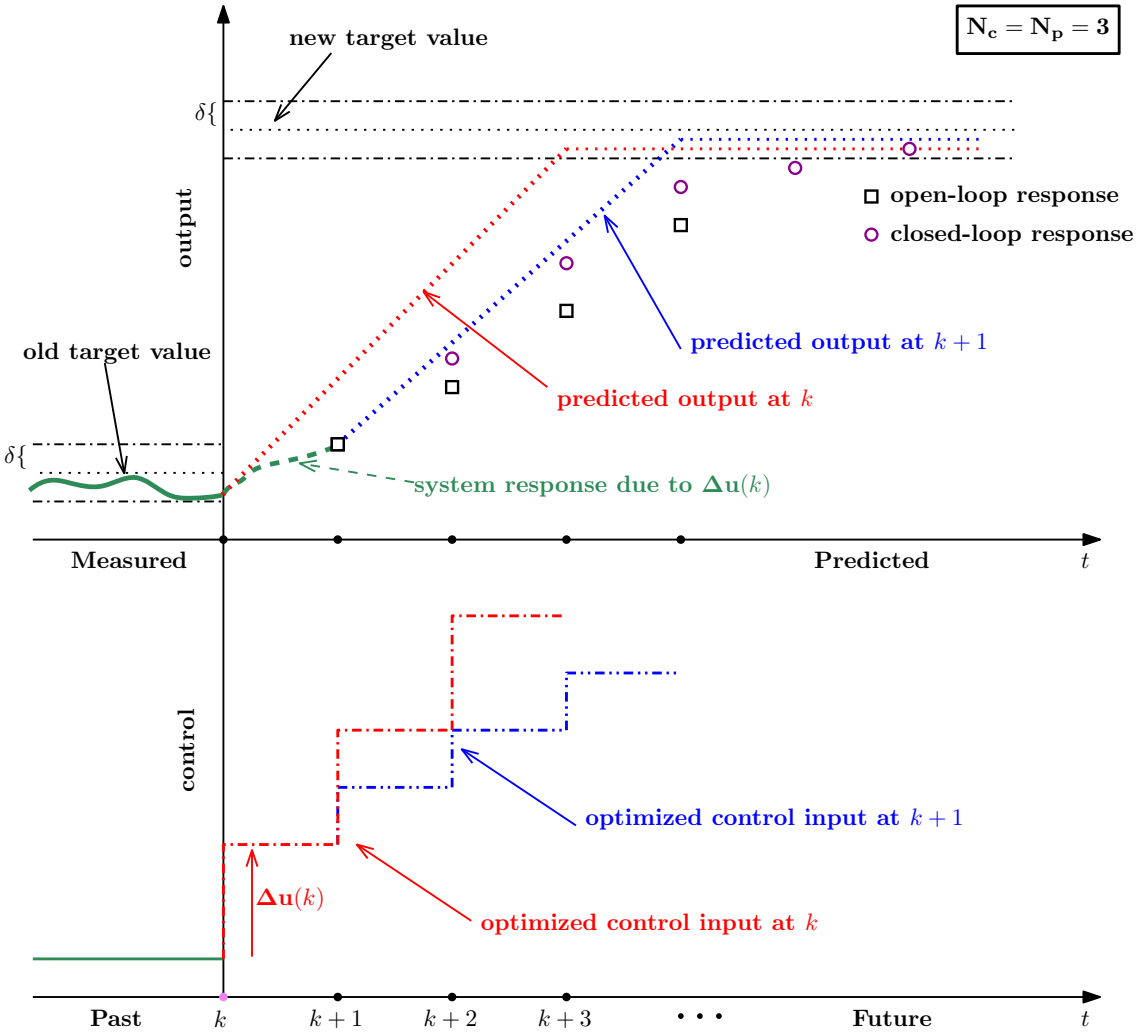

Figure 4.4: Example of basic principle of MPC

subject to the system evolution equality constraint, expressed symbolically through the function $\boldsymbol{f}$:

$$\boldsymbol{X}(k+1) \;=\; \boldsymbol{f}(\boldsymbol{X}(k), \boldsymbol{U}(k)) \tag{4.2}$$

and the state-output relation:

$$\boldsymbol{Y}(k) \;=\; \boldsymbol{g}(\boldsymbol{X}(k)) \tag{4.3}$$

where $\boldsymbol{Y}(k)$ is a vector grouping the outputs $\boldsymbol{y}(k+1), \ldots, \boldsymbol{y}(k+N_p)$ which have to be controlled, and are obtained from the state variables through the function $\boldsymbol{g}$. For simplicity of presentation, the output variables are assumed to be all directly measured.

In addition, constraints are imposed on outputs and controls according to:

$$\boldsymbol{y}(k+N_p \mid k) \in \boldsymbol{\mathcal{Y}} \tag{4.4}$$

$$\boldsymbol{u}(k+i) \in \boldsymbol{\mathcal{U}} \qquad i=0,\ldots,N_c-1 \tag{4.5}$$

where $\boldsymbol{y}(k+N_p \mid k)$ denotes the predicted output at the end of prediction horizon, given the current output $\boldsymbol{y}(k)$. The control $\boldsymbol{U}(k)$ is such that $\boldsymbol{y}(k+N_p \mid k)$ falls in the acceptable set $\boldsymbol{\mathcal{Y}}$, which defines the desirable output. The latter can be either a particular set-point or a targeted range of values. This is also known as terminal constraint, and is likely to guarantee the stability of the control scheme, if properly chosen [Mac02]. Alternatively, and depending on the application, variable constraints may be imposed at all steps of the prediction horizon (i.e. $\boldsymbol{y}(k+i+1 \mid k) \in \boldsymbol{\mathcal{Y}},\ i=0,\ldots,N_p-1$). Similarly, the constraints (4.5) require that $\boldsymbol{u}$ stays within the acceptable set $\boldsymbol{\mathcal{U}}$ over the control horizon. These limits must be satisfied, insofar as they reflect hard constraints on available control means.

Given the above-mentioned principle illustrated in Figs. 4.3 and 4.4, the procedure at time step k is the following:

1. Obtain measurements $\boldsymbol{y}(k)$.
2. Compute the optimal control sequence $\boldsymbol{u}(k+i),\ i=0,\ldots,N_c-1$.
3. Apply $\boldsymbol{u}(k)$ to the system.

Most of the systems behave in a non-linear manner that can be described by (ordinary) differential equations. Unfortunately, in most cases, solving non-linear differential equations is complicated. Therefore, functions $\boldsymbol{f}$ and $\boldsymbol{g}$ are obtained after time discretization and algebraization of the differential equations. Then, it is left to the closed-loop nature of MPC to compensate for the errors.

It should be noted that in most MPC applications (e.g. Chemical Engineering, food processing, automotive, aerospace applications, etc.), the dynamics of the system are such that, after a single control change $\Delta\boldsymbol{u}(k)$, the state variables reach steady values after a time larger than the sampling period T of the MPC controller. In such a case, the dynamics of the system have to be taken into account in the system evolution function $\boldsymbol{f}$.

An MTDC grid is characterized by very fast dynamics (in the order of milliseconds) and, thus, with the proper choice of the sampling period T (e.g. in the order of 5 seconds), the state variables have reached steady values before the next control change is applied. This justifies the use of a sensitivity-type model, as detailed in the sequel.

4.2.3 Applications of MPC on power systems and HVDC grids

Following the recent advances, power systems are requested to operate under more and more constraints (environmental, economical and security). This has led to increasing interest for MPC-based schemes and several publications in the literature. Indicatively, MPC has been proposed for (among others):

- control of distribution networks [BV18, VV13];
- alleviation of thermal overloads in the transmission network [OMGV07];
- voltage stability enhancement [HG06, GHRVC11];
- automatic generation control [VHRW08b].

Other works propose MPC in order to provide ancillary services to the grid. The works in [FIDM14, AIT13] aim at improving the stability of power systems by enabling the converters to contribute to oscillation damping. The coordination of several VSCs and AC systems for improved secondary frequency control was the subject of other works [MND+16, MM18].

Closer to the work of this thesis, MPC has been proposed for MTDC grid control in [JC15]. However, that work is more economy oriented with a time horizon in the order of hours, and does not address system control in the presence of limit violation or after an unforeseen outage. The transition between operating points is not considered either. Instead, the MPC-based scheme proposed in this work is aimed at steering the VSCs with a response time ranging from seconds up to a couple of minutes.

4.2.4 Power Rescheduler: updating the VSC reference powers

The Power Rescheduler block in Fig. 4.2 calculates the power references $\boldsymbol{P}^{ref}$, which are the desired VSC power flows. For all dispatchable VSCs, it receives a power schedule $\boldsymbol{P}^{sch}$, provided by the tertiary level (see Section 4.4). This schedule is assumed to be updated only infrequently. In the meantime, to cope with the variability of the non-dispatchable VSC powers, it is necessary to adjust the power references of the dispatchable VSCs. This can be achieved through a variety of procedures. One simple option, considered in this work, is to use VSC participation factors ρ_i, as explained hereafter.

First, for non-dispatchable VSCs, the reference power is taken equal to the last available measurement, i.e.

$$P_i^{ref} = P_i^m \qquad i = N_D + 1, \ldots, N \tag{4.6}$$

which amounts to considering that the non-dispatchable VSC powers are not going to change. A forecasted value (of the WF powers) could be used instead but, in view of the short horizon covered by the controller, this may not be very relevant.

Next, the power references of the dispatchable VSCs are adjusted according to ($i = 1, \ldots, N_D$):

$$P_i^{ref} = P_i^{sch} - \rho_i \left(\sum_{l=1}^{N_D} P_l^{sch} + \sum_{l=N_D+1}^{N} P_l^{ref} + P_{losses} \right) \tag{4.7}$$

where P_{losses} is an estimate of the losses in the MTDC grid and $\rho_i \geq 0$. The sum of the participation factors should be always equal to one, i.e.:

$$\sum_{i=1}^{N_D} \rho_i = 1. \tag{4.8}$$

If the MTDC grid losses were constant, the non-dispatchable powers invariable, and the power measurements P_i^m infinitely accurate, the parenthesis in (4.7) would be zero. In a real situation, it will differ from zero due to change of the grid losses, measurement noise and variations of the non-dispatchable powers. While the latter are reflected through (4.6), change of the losses and measurement noise are not considered in (4.7). Nevertheless, using MPC easily accommodates the above simplifications.

The illustrative example of a hypothetical system is given in Fig. 4.5. Grid losses are neglected for simplicity. Figure 4.5.(a) shows the initial schedule provided to the Power Rescheduler, corresponding to a WF power of 100 MW. It states that 50 MW are injected in area A, 10 MW in area B and the rest in area C. The participation factors are such that the injection in area A does not deviate from 50 MW, while 60% of the WF power change is covered by area B and the rest by area C. Figure 4.5.(b) shows the power references given by (4.7) after an increase of the WF power by 50 MW.

4.2.5 MPC: constrained optimization problem

The objective of the MPC block in Fig. 4.2 is to smoothly steer the VSCs to the reference powers given by the Power Rescheduler, while obeying the following constraints:

- lower and upper limits on DC node voltages;
- lower and upper limits on the power of each VSC;
- limit on the rate of change of each VSC power;
- upper limit on each DC branch current, etc.

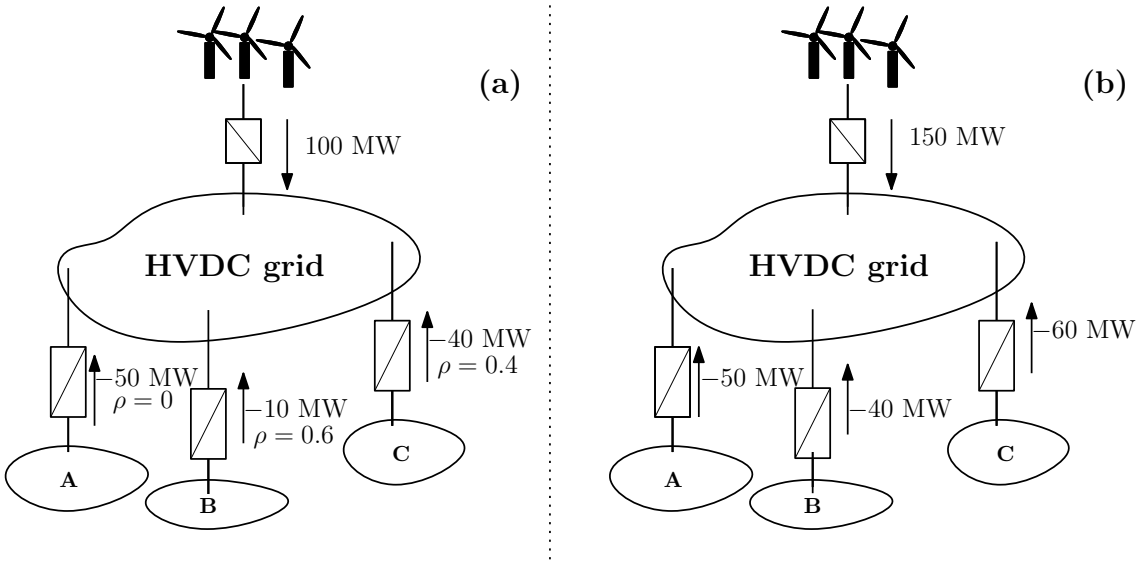

Figure 4.5: VSC power references: (a) in base case; (b) after a 50 MW increase of WF power

To this end, the controller receives measurements at regular time intervals. At time k the following measurements are used:

- $\boldsymbol{P}^m(k)$ the vector of VSC powers;
- $\boldsymbol{V}^m(k)$ the vector of DC node voltages;
- $\boldsymbol{I}^m(k)$ the vector of DC branch currents.

Based on these measurements, a reference trajectory [QB03] is defined with the objective of steering the VSC powers to the reference values $\boldsymbol{P}^{ref}$ in N_c control steps. That trajectory is linear and defined as follows ($j = 1, \ldots, N_c$):

$$\boldsymbol{P}^{ref}(k+j) = \boldsymbol{P}^m(k) + \frac{j}{N_c}(\boldsymbol{P}^{ref} - \boldsymbol{P}^m(k)). \tag{4.9}$$

The MPC objective consists of minimizing the deviations with respect to that reference trajectory:

$$\min_{\boldsymbol{V},\boldsymbol{I},\boldsymbol{P},\boldsymbol{\epsilon},\boldsymbol{\zeta},\Delta\boldsymbol{P}^{set},V_{avg}} \sum_{j=1}^{N_c} \left|\left|\boldsymbol{P}^{ref}(k+j) - \boldsymbol{P}(k+j)\right|\right|^2_{\boldsymbol{W}} + v\sum_{j=1}^{N_c} ||\boldsymbol{\epsilon}(k+j)||^2 + q\sum_{j=1}^{N_c} ||\boldsymbol{\zeta}(k+j)||^2 \tag{4.10}$$

where $\mathbf{W}$ is a diagonal weighting matrix assigned to the deviations of VSC powers $\boldsymbol{P}$ from their references $\boldsymbol{P}^{ref}$. Non-dispatchable terminals are assigned a weight w_{ND} higher than the weight w_D of dispatchable VSCs in order to resort to them when actions on dispatchable VSCs only are not sufficient. $\boldsymbol{\epsilon}$ and $\boldsymbol{\zeta}$ are vectors of slack variables used to relax constraints in case of infeasibility, with the respective weighting factors v and q.

The minimization is subject to the following constraints:
for $j = 1, \ldots, N_c$:

$$\boldsymbol{V}^{low}(k+j) - \boldsymbol{\epsilon}(k+j) \leq \boldsymbol{V}(k+j) \leq \boldsymbol{V}^{up}(k+j) + \boldsymbol{\epsilon}(k+j) \tag{4.11}$$

$$\boldsymbol{P}^{min} \leq \boldsymbol{P}(k+j) \leq \boldsymbol{P}^{max} \tag{4.12}$$

$$\Delta\boldsymbol{P}^{min} - \boldsymbol{\zeta}(k+j) \leq \boldsymbol{P}(k+j) - \boldsymbol{P}(k+j-1) \leq \Delta\boldsymbol{P}^{max} + \boldsymbol{\zeta}(k+j) \tag{4.13}$$

$$\boldsymbol{I}^{low}(k+j) \leq \boldsymbol{I}(k+j) \leq \boldsymbol{I}^{up}(k+j) \tag{4.14}$$

$$\boldsymbol{\epsilon}(k+j) \geq \mathbf{0}, \quad \boldsymbol{\zeta}(k+j) \geq \mathbf{0} \tag{4.15}$$

$$\Delta\boldsymbol{P}^{set}(k+j-1) = \boldsymbol{S}_P \left[\boldsymbol{V}(k+j) - \boldsymbol{V}(k+j-1)\right] \tag{4.16}$$

$$\boldsymbol{P}(k+j) = \boldsymbol{P}(k+j-1) + \Delta\boldsymbol{P}^{set}(k+j-1) - \boldsymbol{K}_V \left[\boldsymbol{V}(k+j) - \boldsymbol{V}(k+j-1)\right] \tag{4.17}$$

$$\boldsymbol{I}(k+j) = \boldsymbol{I}(k+j-1) + \boldsymbol{S}_I \, \Delta\boldsymbol{P}^{set}(k+j-1) \tag{4.18}$$

$$V_{avg}(k+j) = V_{avg}(k) + \frac{j}{N_c}\left(V_{avg}^{ref} - V_{avg}(k)\right). \tag{4.19}$$

Constraint (4.11) sets the range of admissible DC voltages at the VSC buses. Any violation of these limits ($\epsilon \neq 0$) is heavily penalized in the objective function by setting the weighting factor v to a large value. Note that $\boldsymbol{V}^{low}$ and $\boldsymbol{V}^{up}$ evolve with time, in order to bring the voltages progressively inside the desired range. Similarly, constraint (4.14) keeps the branch currents $\boldsymbol{I}$ between limits, which vary with time for the same purpose. This variation is further detailed in Section 4.2.8.

Constraint (4.12) relates to the minimum and maximum power of each VSC.

Constraint (4.13) stems from the AC networks. Too fast changes in the power injections into or from the AC areas could cause problems, such as unacceptable frequency or voltage deviations. Therefore, this constraint limits to $\Delta\boldsymbol{P}^{min}$ and $\Delta\boldsymbol{P}^{max}$ the power change of each VSC between two discrete time steps. The slack variables $\boldsymbol{\zeta}$ are also heavily penalized in the objective function by choosing a large value for the weighting factor q.

Equations (4.16), (4.17) and (4.18) are used to predict future values of voltages, powers and currents in response to the control changes $\Delta\boldsymbol{P}^{set}$, which are defined by:

$$\boldsymbol{P}^{set}(k+j) = \boldsymbol{P}^{set}(k+j-1) + \Delta\boldsymbol{P}^{set}(k+j-1). \tag{4.20}$$

For uniformity the notation ΔP^{set} is also used for actions on the non-dispatchable terminals, although they are not assigned a setpoint P^{set}. Since the non-dispatchable terminals do not participate in DC voltage control, ΔP^{set} is actually the desired change in power ΔP.

The prediction horizon is equal to the control horizon N_c. The transition model relies on the sensitivity matrices $\boldsymbol{S}_P$ and $\boldsymbol{S}_I$, which, as already mentioned, is justified by the fast response of the power electronics based VSCs compared to the MPC sampling time, in the order of a few seconds. The derivation of those matrices is detailed Appendix B.

The above linear model is initialized at the last received measurements:

$$\boldsymbol{V}(k) = \boldsymbol{V}^m(k) \quad \boldsymbol{P}(k) = \boldsymbol{P}^m(k) \quad \boldsymbol{I}(k) = \boldsymbol{I}^m(k). \tag{4.21}$$

The last constraint (4.19) is aimed at restoring the average DC voltage:

$$V_{avg}(k+j) = \frac{1}{N}\sum_{i=1}^{N} V_i(k+j) \qquad j = 0, \ldots, N_c \tag{4.22}$$

to a given reference V_{avg}^{ref}. The main motivation is that, in an MTDC system, no bus has its voltage tightly controlled; instead, DC voltages evolve according to the droop characteristic of Eq. (2.35) (where an infinite K_V would be required to have constant voltage). Equation (4.19) prevents the voltage profile from somewhat "floating". Without this constraint, if the term P_{losses} in (4.7) is underestimated by the Power Rescheduler when setting $\boldsymbol{P}^{ref}$, the MPC controller would progressively increase the DC voltages (until one of them hits its limit) in order to decrease the losses and, hence, the deviations from the reference powers. Conversely, if the MTDC grid losses are overestimated, the MTDC voltages would be pushed to their lower limits. V_{avg}^{ref} can be simply set to the nominal DC voltage (i.e. to 1 pu) or it can be chosen to minimize the grid losses for a desired power flow.

By keeping the DC voltages around the reference, Eq. (4.19) contributes to keeping voltages within their limits. However, controlling the average does not ensure that all voltages settle in the desired range. This is why the constraints (4.11) are also included in the formulation.

Each control output ΔP_i^{set} is communicated to the corresponding VSC i. The cumulative setpoint change is applied through the outer loops of Fig. 2.10 as shown in Fig. 4.6.

4.2.6 Sensitivity and parameter update after topological changes

Following a significant event, the behavior of the MTDC grid may change significantly, and the sensitivities and/or reference powers may become outdated. Two cases have to be considered, as detailed next.

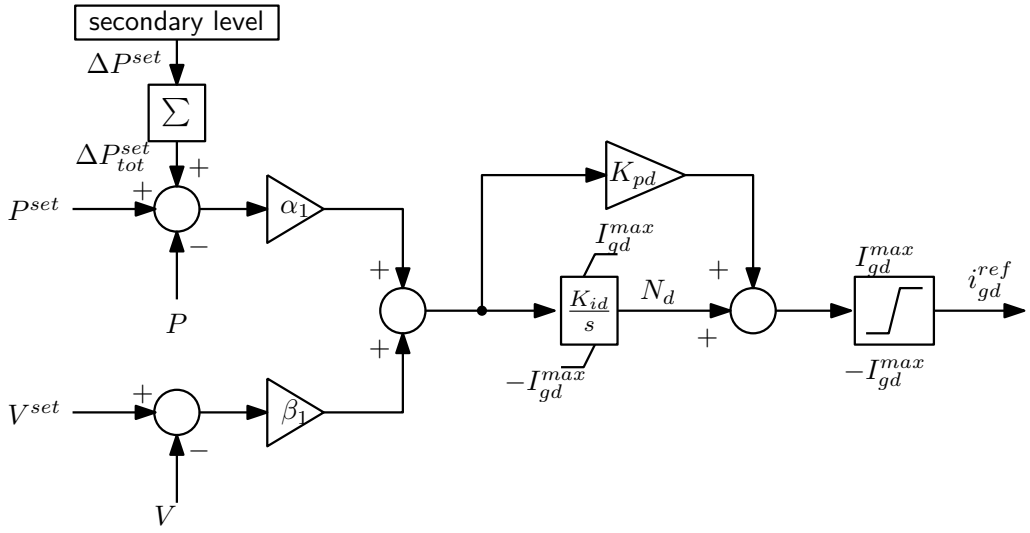

Figure 4.6: Connection of secondary level actions to VSC outer controllers. The $\sum$ block denotes a discrete integrator, i.e. its output ΔP^{set}_{tot} is calculated as $\Delta P^{set}_{tot}(k) = \Delta P^{set}_{tot}(k-1) + \Delta P^{set}(k)$

Tripping of a dispatchable VSC

If the i-th VSC has been taken out of service, the droop gain $K_{v,i}$ is set to zero, and matrices $\boldsymbol{S}_P$ and $\boldsymbol{S}_I$ are recalculated. $\mathbf{S_P}$ is updated by simply subtracting $K_{v,i}$ from the i-th diagonal entry.

As far as the Power Rescheduler is concerned, the scheduled power P^{sch}_i and the participation factor ρ_i must be set to zero for the tripped VSC. The participation factors and/or the schedule values of the remaining VSCs are adjusted accordingly. The participation factors should be adjusted so that (4.8) holds true, whereas the update of the $\boldsymbol{P}^{sch}$ values should follow pre-defined rules, e.g. to redirect the power of the tripped VSC to a specific area.

This can be illustrated on the simple example of Fig. 4.5. Consider the outage of the VSC connected to Area B. Assuming that the zero participation of Area A is unchanged, the participation factor of Area C becomes $\rho = 1$ to satisfy (4.8). Then, from (4.7), the new power references are: -50 MW for Area A, 0 MW for Area B and -50 MW for Area C.

Tripping of a DC branch

Matrices $\boldsymbol{S}_P$ and $\boldsymbol{S}_I$ are recalculated by removing the contribution of the tripped branch, and the corresponding constraints (4.14) are removed. The Power Rescheduler does not need to be updated (unless the HVDC grid splits).

4.2.7 Actions on WF terminals

Some works [EBVG15, AS13, MS15] investigated the possibility of implementing primary DC voltage support by WF converters. Specifically, by adjusting the blade pitch angle, the wind farms can reduce their active power output in order to keep some primary reserves or provide support in case of DC overvoltage. Therefore, they could also be equipped with a droop characteristic. However, this would require dedicated market rules establishing economic incentives to compensate for the long-term sub-optimal operation of the WF. This option is not considered in this work; instead it is assumed that the WFs are normally operating in MPPT mode. In emergency conditions, however, the controller can send corrective actions to WFs in order to reduce their output temporarily. These actions are to be considered in case of an emergency. Hence, the deviation of WF terminals from their reference value is assigned a higher cost w_{ND} in the objective function (4.10).

Specifically for WF terminals, after the emergency cause has been dealt with, they should return to MPPT operation. To do so, the controller has a "reset mechanism", inspired by the method proposed in [SBGV16]. Namely, (4.6) is modified as follows for WF terminal i ($j = 1, \dots, N_c$):

$$P_i^{ref}(k+j) = P_i^m(k) - \frac{j}{N_c}\Delta P_i^{cor}(k) \tag{4.23}$$

where $\Delta P_i^{cor}(k)$ is the cumulated correction that has been sent to terminal i up to time k, i.e.:

$$\Delta P_i^{cor}(k) = \sum_{j=-\infty}^{k-1} \Delta P_i^{set}(j) \tag{4.24}$$

Clearly, $\Delta P_i^{cor}(k)$ cannot be positive, i.e. the MPC cannot force the WF to produce more than the maximum power received from wind. If it is equal to zero, then (4.23) is the same as (4.6). Otherwise, (4.23) gives an estimate of the MPPT WF power, if no correction had been sent. The proposed controller will aim to restore the WF to its maximum available power once the constraint necessitating WF curtailment is no longer active.

4.2.8 Progressive bound tightening

In normal operation, the DC voltages must remain between the specified minimum $\boldsymbol{V}^{min}$ and maximum $\boldsymbol{V}^{max}$ values, and the branch currents are below their limits $\boldsymbol{I}^{max}$. In this case, the bounds in constraints (4.11) and (4.14) are ($j = 1, \dots, N_c$):

$$\boldsymbol{V}^{low}(k+j) = \boldsymbol{V}^{min} \qquad \boldsymbol{V}^{up}(k+j) = \boldsymbol{V}^{max} \tag{4.25}$$

$$\boldsymbol{I}^{low}(k+j) = -\boldsymbol{I}^{max} \qquad \boldsymbol{I}^{up}(k+j) = \boldsymbol{I}^{max}. \tag{4.26}$$

If, after a disturbance, a terminal DC voltage or a branch current exceeds its limit, the controller should alleviate this violation before it leads to equipment tripping or damage. On the other hand, abrupt corrections should be avoided. Therefore, after a violation is identified, the bounds in (4.11) and (4.14) are progressively tightened. More precisely, if the DC voltage V_i^m measured at terminal i violates its lower limit V_i^{min}, the latter is progressively enforced by specifying ($j = 1, \ldots, N_c$):

$$V_i^{low}(k+j) = V_i^m(k) + \frac{j}{N_c}\left(V_i^{min} - V_i^m(k)\right) \tag{4.27}$$

This is shown in Fig. 4.7. The leftmost dash-dotted line is the linearly evolving V_i^{low}, considered at time k, reaching V_i^{min} at the end of the control horizon, at time $k + N_c$. After a new measurement is collected, at time $k + 1$, the bound is updated according to the rightmost dash-dotted line.

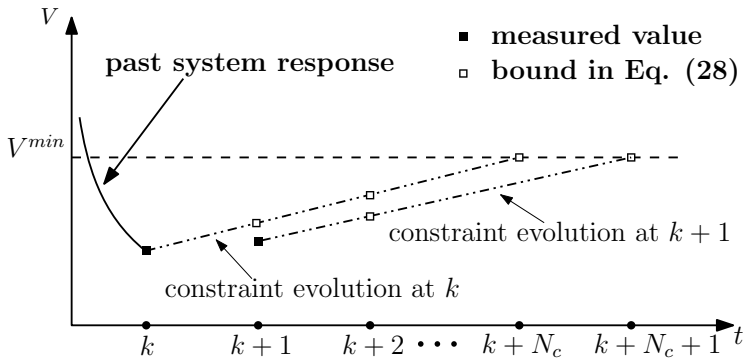

Figure 4.7: DC Voltage progressive constraint tightening based on (4.27)

Of course similar expressions hold for the upper voltage limit and for the current limits as well.

In this thesis, a linear function has been chosen for the progressive constraint tightening. Other functions, e.g. exponential, could be also used, if faster correction is required.

This way of alleviating the violations assumes that thermal limits can be exceeded for some time. In HVDC systems, however, some violations may not be tolerated at all. For example, the DC voltage limits have to be chosen with a security margin from the real technical limits because a DC voltage outside limits may cause immediate tripping of the converter. In fact, the soonest the controller can alleviate a violation is after a delay of one time step. For faster reaction, other methods (relying only on local information, or event-based schemes) should be considered.

4.2.9 Selection of control horizon

The control horizon can be chosen to obtain a desired 5% settling time. The latter can be easily calculated by neglecting the losses of the MTDC grid and assuming no voltage or current limit is reached. From (4.9) the VSC powers after one control step of the MPC will be:

$$\boldsymbol{P}(k+1) = \boldsymbol{P}(k) + \frac{\boldsymbol{P}^{ref} - \boldsymbol{P}(k)}{N_c} \tag{4.28}$$

Therefore, the error $\delta\boldsymbol{P}$ after one step will be:

$$\delta\boldsymbol{P}(k+1) = \boldsymbol{P}^{ref} - \boldsymbol{P}(k+1) = \frac{N_c - 1}{N_c}\left(\boldsymbol{P}^{ref} - \boldsymbol{P}(k)\right) \tag{4.29}$$

Following the same logic for the next steps, the error at the n-th step will be:

$$\delta\boldsymbol{P}(k+n) = \left(\frac{N_c - 1}{N_c}\right)^n \left(\boldsymbol{P}^{ref} - \boldsymbol{P}(k)\right) \tag{4.30}$$

Numerical example: Assuming that a settling time of 40 s is chosen, this translates to a total of 8 steps for a sampling time of 5 s. Therefore, by substituting $n = 8$ in (4.30) the maximum control horizon N_c is found as follows:

$$\delta P(k+8) \leq 0.05\left(P^{ref} - P(k)\right) \Rightarrow \left(\frac{N_c - 1}{N_c}\right)^8 \leq 0.05 \;\; \Rightarrow \;\; N_c^{max} = 3 \text{ steps.} \tag{4.31}$$

4.3 Simulation results with secondary control

4.3.1 Test system

The proposed secondary control has been tested on the system of Fig. 3.1, consisting of two asynchronous AC areas and one offshore wind farm, connected through a five-terminal HVDC grid. The focus is on the MTDC grid response, thus, the N-1 secure configuration for both AC areas has been selected.

Among the five VSCs, all but T5 operate in DC voltage droop mode with $K_v = 5$ pu (on the VSC nominal power base). The initial setpoints P^{set} and V^{set} for each VSC are set equal to its initial DC power and voltage. The initial power flow in the MTDC grid is shown in Fig. 4.8.

The effectiveness of the secondary level is first presented through various test cases, also documented in [PDPV17b].

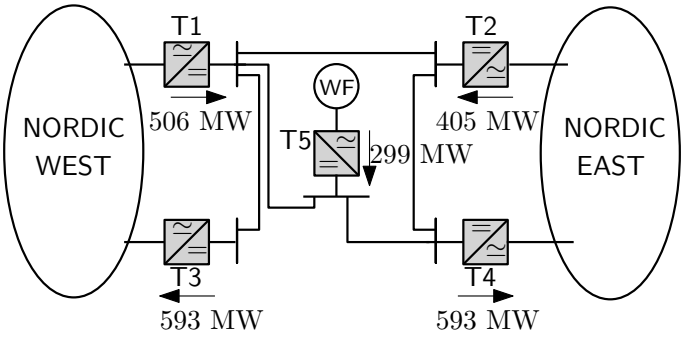

Figure 4.8: Test system topology and initial power flow

4.3.2 MPC Parameters

A control horizon of $N_c = 3$ steps has been considered for the MPC with a sampling time $T = 5$ s. The control actions are applied 1 s after receiving the measurements, to account for the time needed to process them, solve the optimization problem and communicate corrections to the VSCs. The weighting factors w_D, w_{ND}, q and v in the objective function (4.10) are taken equal to 1, 10^2, 10^3 and 10^6, respectively. These values have been chosen based on the importance of each variable, and no further fine-tuning has been contemplated. The same participation factor $\rho = 0.25$ has been assumed for all four dispatchable VSCs. Since steady state is assumed at the beginning of the simulation, V_{avg}^{ref} is taken equal to the average of the initial DC voltages (1 pu).

For all VSCs, the active power limits have been set to $P^{min} = -10$ and $P^{max} = +10$ pu (on a 100 MW base), the DC voltage limits to $V^{min} = 0.96$ and $V^{max} = 1.04$ pu. For simplicity, the rate of change limits have been set to large values ($\Delta P^{min} = -10$ pu and $\Delta P^{max} = +10$ pu), and were not considered in the simulations. The DC branch current limits have been set to $I^{max} = 10$ pu, except for both branches connected to T5, which have a lower capacity with $I^{max} = 3.5$ pu. The term P_{losses} is neglected when calculating the references of the dispatchable VSCs in Eq. 4.7.

4.3.3 Scenario 1: WF power decrease and change in schedule

This first scenario includes the following events:

- from $t = 11$ to $t = 31$ s: gradual (although accelerated) decrease of the WF power from 299 to 100 MW;
- at $t = 51$ s: update of the scheduled powers P_i^{sch} of all dispatchable VSCs. The new schedule, corresponding to the new WF production, is as follows: 500 MW in T1, 600 MW in T2, -800 MW in T3, and -400 MW in T4.

Figure 4.9 shows the DC powers of the converters. As expected, following the WF power decrease, all converters inject more power in the MTDC grid. The corrections calculated and sent by the MPC controller are shown in Fig. 4.10. They start at $t = 15$ s. Since all dispatchable terminals have the same participation factor ρ_i, the system is steered to an operating point where all VSCs are asked to cover the same fraction of the lost WF power.

Following the schedule change at $t = 51$ s, the VSC powers are smoothly adjusted to follow their new references obtained from (4.7). Since the latter neglects MTDC grid losses, the VSC powers do not reach their reference values exactly. The final discrepancies $P - P^{ref}$ are: 6.4 MW for T1, 6.1 MW for T2, 6.7 MW for T3, and 6.3 MW for T4. Their sum (25.5 MW) is the total DC power lost. They are (almost) equally distributed over the four VSCs because the latter were given the same weight w_D in the objective function (4.10).

The DC voltages and their average V_{avg} are shown in Fig. 4.11. The decrease of the WF power causes a temporary power deficit in the MTDC grid, which is temporarily covered by the discharging of the DC capacitors, leading to the drop of the DC voltages. The magnitude of the DC voltage drop is determined by the droop gains of the VSCs. However, the centralized controller smoothly restores the average voltage to its reference value (1 pu), and all voltages eventually settle near this value.

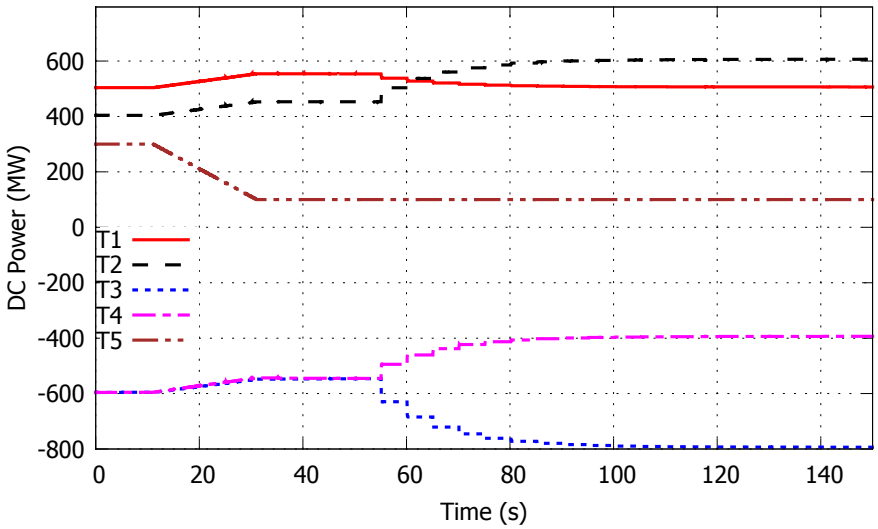

Figure 4.9: Scenario 1: DC powers of VSCs

The values of P^{sch} of the VSCs at various time instants and the values P^{ref} as calculated by (4.6) and (4.7) are shown in Table 4.1 (rounded to the nearest integer). It is noted that the initial P^{sch} values are taken equal to the initial DC powers of the VSCs.

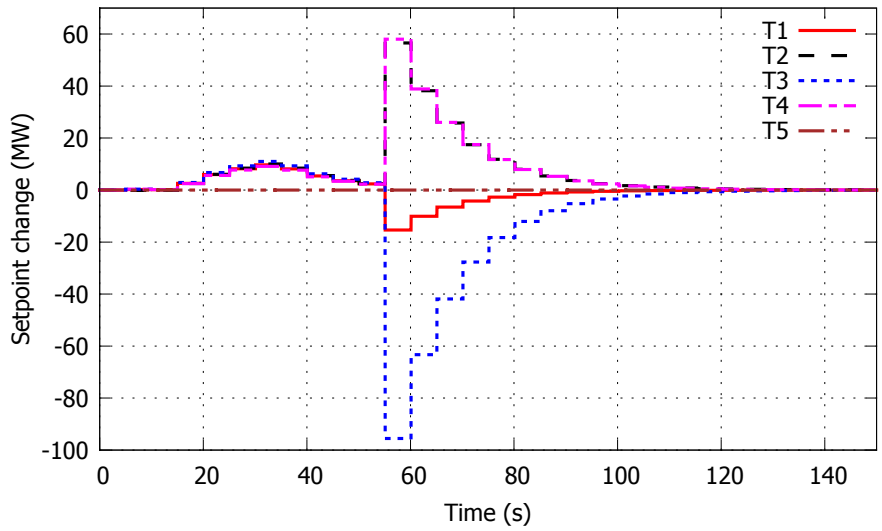

Figure 4.10: Scenario 1: setpoint changes $\Delta \boldsymbol{P}^{set}$

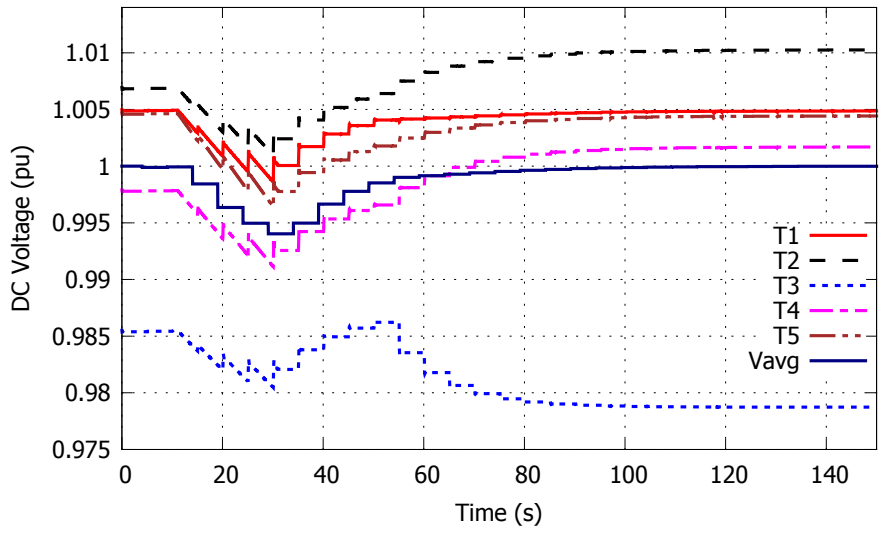

Figure 4.11: Scenario 1: MTDC grid voltages

4.3.4 Scenario 2: outage of an AC/DC terminal

This scenario involves the inadvertent tripping of Terminal T3 at $t = 5$ s.

Following this outage, the power references $\boldsymbol{P}^{ref}$ are updated by the Power Rescheduler. As explained in Section 4.2.6, the scheduled power of T3 and its participation factor are set to zero, while the participation factors of the remaining dispatchable VSCs are adjusted. Several options can be thought of for this adjustment. As in [EBVG15], it was assumed that, after the tripping

Table 4.1: P^{sch} and P^{ref} values at various time instants (MW)

Time		T1	T2	T3	T4	T5
$t = 4$ s	P^{sch}	506	405	-593	-593	-
	P^{ref}	500	400	-600	-600	299
$t = 19$ s	P^{sch}	506	405	-593	-593	-
	P^{ref}	520	419	-580	-580	220
$t = 34$ s	P^{sch}	506	405	-593	-593	-
	P^{ref}	550	449	-549	-549	100
$t = 54$ s	P^{sch}	500	600	-800	-400	-
	P^{ref}	500	600	-800	-400	100

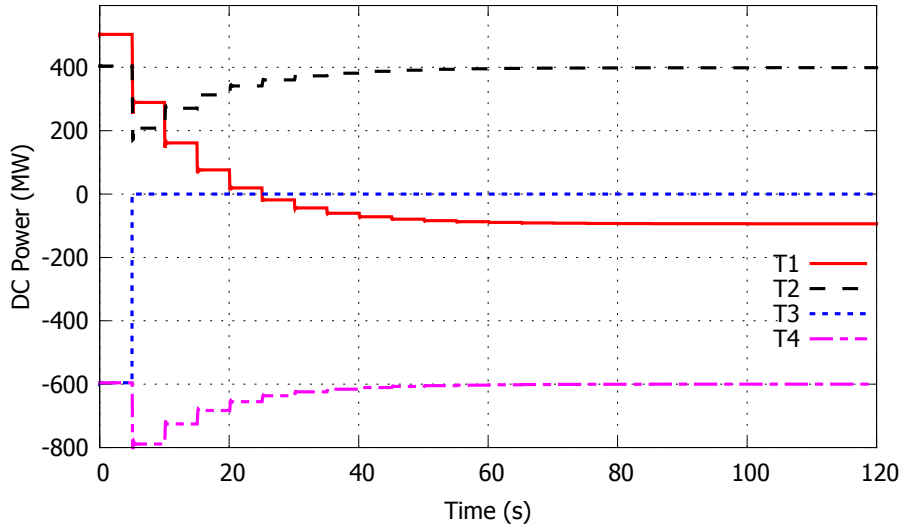

Figure 4.12: Scenario 2: DC powers of VSCs

of a VSC connected to an AC area, the power transfer to that area is taken over by the remaining VSCs connected to it. This leads to setting, once the loss of T3 is known, $\rho_1 = 1$ for T1, and $\rho_2 = \rho_4 = 0$ for T2 and T4. The same can be achieved by setting $\rho_1 = \rho_2 = \rho_4 = 1/3$ (i.e. the remaining VSCs keep sharing any change of the WF power), and $P_1^{sch} = P_1^{sch,pre} + P_3^{sch,pre}$, where $P^{sch,pre}$ denotes the pre-disturbance scheduled power. The second option is adopted here.

The VSC powers are shown in Fig. 4.12. Immediately after the outage of T3, thanks to voltage droop control, T1, T2 and T4 adjust rapidly their power to restore the power balance of the MTDC grid. As can be seen in Fig. 4.13, the controller starts acting at $t = 10$ s. It redirects the lost power to T1, with the result that the powers of T2 and T4 progressively return to their pre-disturbance values (see Fig. 4.12).

The corresponding DC voltage evolutions are shown in Fig. 4.14. Since T3 was operating as inver-

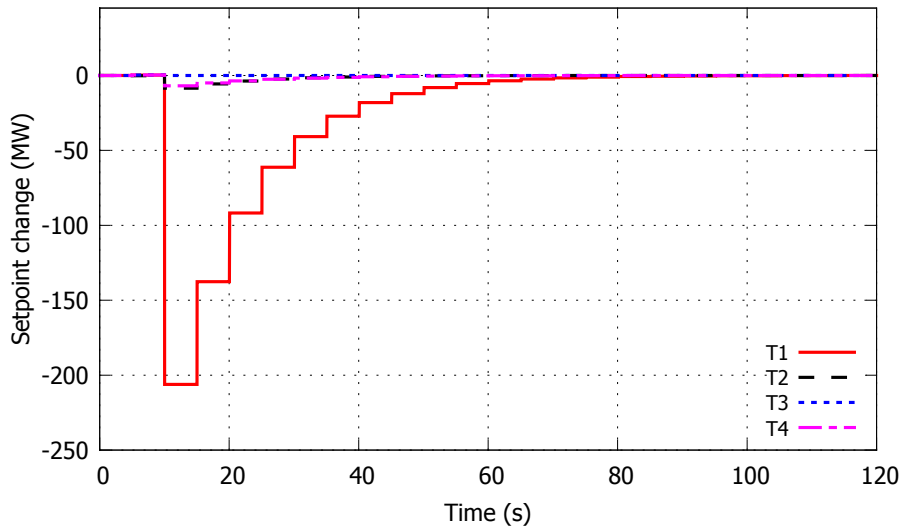

Figure 4.13: Scenario 2: setpoint changes $\Delta \boldsymbol{P}^{set}$

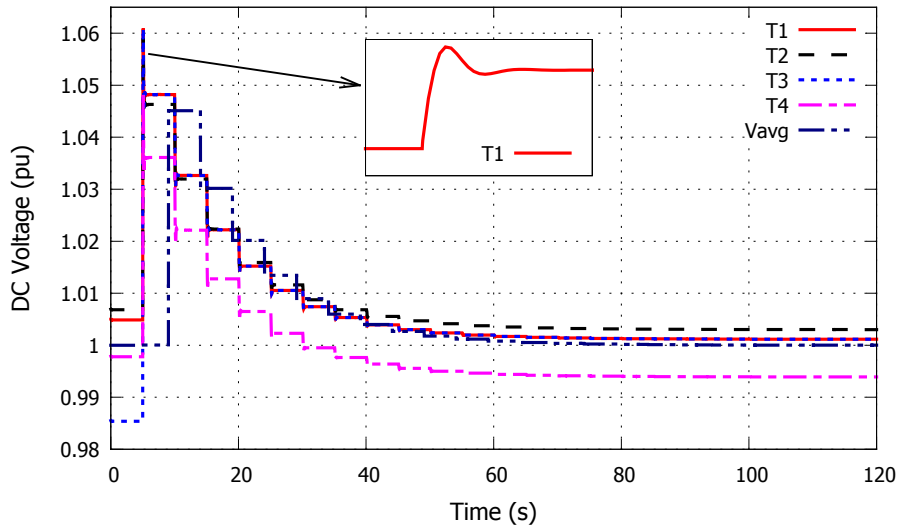

Figure 4.14: Scenario 2: MTDC grid voltages

ter before the disturbance, the DC voltages rise rapidly after its tripping. As revealed by zooming on the first milliseconds after the disturbance (shown only for T1), the DC voltages exhibit an overshoot and are stabilized at a higher value by the DC voltage droop control. However, this alone is not satisfactory, since the DC voltages exceed the allowed upper limit of 1.04 pu, and the average DC voltage has drifted from its reference value. Both issues are corrected by the controller smoothly bringing the DC voltages in the specified range and the average voltage to its reference.[4]

[4]In this figure (and similar ones), the actual DC voltage evolutions are shown, while the average voltage is the one computed by the controller from the received measurements. This explains the (four second) lag that affects the curve

Without the centralized control, the DC voltages would remain at the values immediately after the disturbance and the violations observed at some buses would not be corrected.

While the powers are satisfactorily rerouted in the minute that follows this severe disturbance, the resulting operating point may not be acceptable (e.g. insecure) over a longer period of time. It is the tertiary level role to subsequently modify the power schedule (see Section 4.4).

To illustrate the robustness of the MPC scheme, simulation results in the presence of modeling errors are provided in Table 4.2.

Table 4.2: Scenario 2 - Final operating points with various methods

Method	VSC Power (MW) T1	T2	T4	V_{avg} (pu)
MPC & accurate model	-110	407	-592	1.00
MPC & inaccurate model	-110	407	-592	1.00
Open-loop & accurate model	-110	-406	-590	1.00
Open-loop & inaccurate model	-192	-343	-447	0.97

The first two lines of the table show the final operating points reached when using MPC, respectively without and with model inaccuracy. The latter consist of assuming erroneous entries in the $\boldsymbol{K}_V$ matrix used by the controller. Namely, $K_v = 10$ pu has been assumed for T1 and T2, instead of the actual $K_v = 5$ pu value used in the VSC model. Comparing the first two rows of the table shows that the MPC-based controller brought the system to the same final operating point, thus compensating for the unknown error. It is noted that due to the change of the MTDC grid losses, the steady-state power of T1 will not correspond exactly to the sum of the pre-disturbance powers of T1 and T3.

The last two rows of the table relate to an optimization-based correction method acting in open loop. The latter simply consists of a single-step ($N_c = 1$) minimization of the objective (4.10) under the constraints (4.11)-(4.19).[5] The so-obtained corrections are applied only once, i.e. without exploiting successively updated measurements as MPC does. With an accurate model, this open-loop correction yields almost the same operating point, showing negligible differences compared to the MPC solution (first two rows). However, if the $\boldsymbol{K}_V$ matrix is affected by the aforementioned errors, the resulting operating point is significantly impacted, as shown by the last row of the table. More precisely, T1 does not compensate for the loss of T3 as expected, and the effective average voltage deviates from its setpoint.

of the average voltage.

[5] Except constraint (4.13), which has been removed as it is specific to multi-step control

4.3.5 Scenario 3 - Branch overload alleviation

The last scenario demonstrates the efficiency of the proposed control in correcting branch current violations. As the controller acts on the non-dispatchable terminal T5, it also illustrates the reset mechanism described in Section 4.2.7.

The following events are involved:

- from $t = 11$ to $t = 31$ s: large, gradual (although much accelerated) increase of the WF power by 550 MW;
- at $t = 80$ s: the average voltage reference V_{avg}^{ref} is increased from 1 to 1.03 pu. This change could emanate from the tertiary level of control.

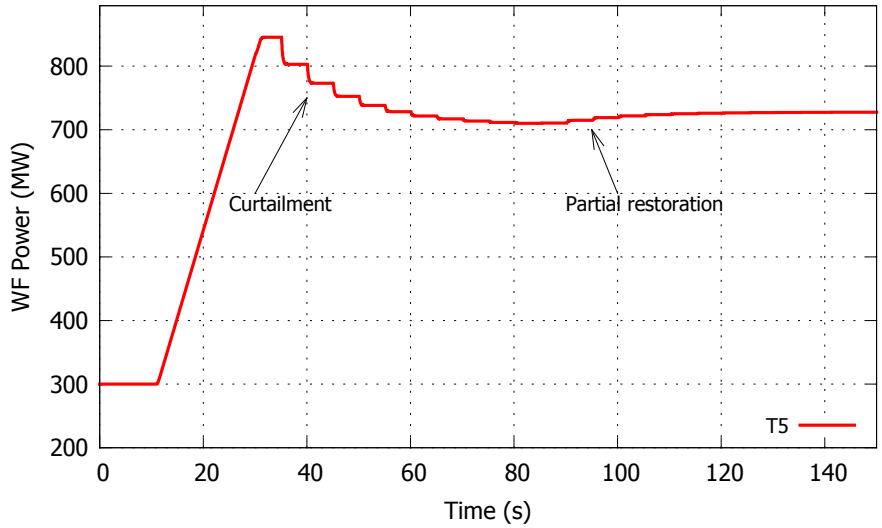

Figure 4.15: Scenario 3: DC power of VSC T5

Figure 4.15 shows the power injected in the DC grid by T5. It can be seen that at $t = 35$ s, a fraction of this power is curtailed by the controller. This curtailment is dictated by the overload of the two branches connected to T5, as can be seen in Fig. 4.16. The limit of branch T5-T4 (of 3.5 pu) is the first to be exceeded, and the controller redirects the power injected by T5 through branch T5-T1, which avoids curtailing the WF power. However, after $t = 30$ s both branches have their limits exceeded and the controller starts decreasing the WF power. Eventually, some 140 MW are curtailed and the branch currents are brought back below their limits at $t = 80$ s. In the same time interval, the DC voltages are adjusted so that their average is brought to 1 pu, as can be seen from Fig. 4.17.

Following the change of the V_{avg}^{ref} reference at $t = 80$ s, the controller increases all the DC

voltages. As a result, the DC currents decrease slightly and temporarily, and their respective constraints are no longer active. Thus, the MPC scheme identifies that some more WF power can be accommodated, and it increases the power of T5. This restores a small part of the WF power previously curtailed, until the DC branch current constraints become active again.

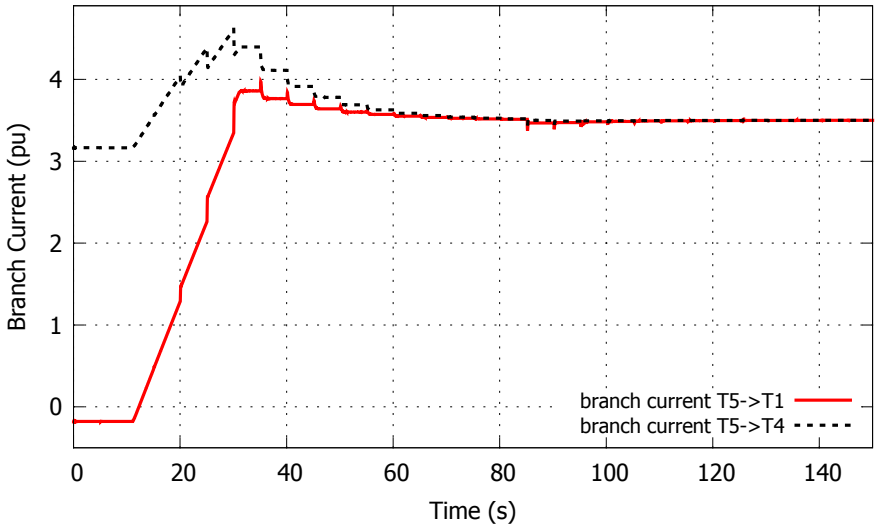

Figure 4.16: Scenario 3: Branch currents

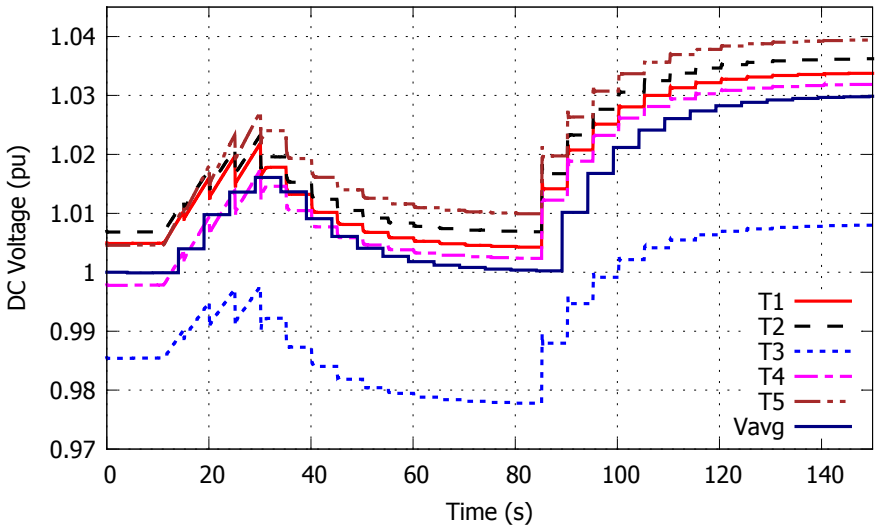

Figure 4.17: Scenario 3: MTDC grid voltages

4.4 Tertiary control

4.4.1 Objectives

The objectives of the tertiary control are the following:

- minimize the power losses in the MTDC grid;
- gather as much as possible energy produced by the wind power plants connected to the grid;
- satisfy a desired power in specific VSCs (e.g. to have a desired power exchange between two AC areas);
- ensure the system has margin to operate within limits following the outage of any single MTDC grid component ("N-1" situation).

The above are addressed by formulating and solving a Secure-Constrained Optimal Power Flow Problem (SCOPF) for the MTDC grid. In most works in the literature [Wig15, CDW16, MZL+17, IWCA15], an SCOPF is formulated taking into account the entire AC/DC interconnection, thus extending the conventional SCOPF for AC grids [CMP+11].

The SCOPF proposed here focuses on the MTDC grid. Thus, it is much simpler due to the reduced size of the problem and the absence of reactive power transfer. The security of the entire AC/DC interconnection will instead be addressed in Chapter 6.

Note that the SCOPF considers the security of the MTDC grid after a contingency, but before the secondary MPC-based controller has acted, since the latter will further improve the operating point of the MTDC grid.

The outputs of the SCOPF are the vector of scheduled power values $\boldsymbol{P}^{sch}$ and the average DC voltage reference V_{avg}^{ref}. In general, an increase of V_{avg}^{ref} would lead to lower losses and better utilization of the MTDC grid. However, increasing it too much could lead to violating the upper DC voltage limits after a disturbance, e.g. the tripping of a VSC in inverter mode.

V_{avg}^{ref} is used in (4.19), i.e. in the MPC controller, whereas $\boldsymbol{P}^{sch}$ is required by the Power Rescheduler to calculate the power references from (4.7). The tertiary level requires as an input a vector $\boldsymbol{P}^{des}$, which includes the desired power transfers through specific VSCs. These VSCs include:

- non-dispatchable VSCs: the desired power is the present or a forecasted value;
- dispatchable VSCs: the desired power is the power requested to be transferred through a subset of the dispatchable VSCs. This could result from inter-TSO or market agreements, etc.

4.4.2 SCOPF formulation

Based on the above, the SCOPF consists of solving a multi-objective optimization problem. The objective function consists of minimizing a weighted average of the MTDC grid losses and the deviations of the VSC powers from their desired values. The former is the sum of all the VSC powers (neglecting the losses in the VSCs) [GL15], which results in the following:

$$\min_{\boldsymbol{P}_0,\boldsymbol{V}_0,\boldsymbol{I}_0,\boldsymbol{P}_j,\boldsymbol{V}_j,\boldsymbol{I}_j,\boldsymbol{\alpha},\boldsymbol{\beta}} \sum_{i=1}^{N} P_{0,i} + \sum_{i=1}^{N} w_i (P_{0,i} - P_i^{des})^2 \tag{4.32}$$

where $P_{0,i}$ is the DC power of the i-th VSC in the base case ("N-0" situation), and w_i a weighting factor.

The minimization is subject to the following constraints:

- for the "N-0" situation:

$$\boldsymbol{P}_0 = \text{diag}(\boldsymbol{V}_0)\, \boldsymbol{G}\, \boldsymbol{V}_0 \tag{4.33}$$

$$\boldsymbol{I}_0 = \boldsymbol{A}\, \boldsymbol{V}_0 \tag{4.34}$$

$$\{\boldsymbol{I}^{min}, -\boldsymbol{P}^{max}, \boldsymbol{V}^{min}\} \leq \{\boldsymbol{I}_0, \boldsymbol{P}_0, \boldsymbol{V}_0\} \leq \{\boldsymbol{I}^{max}, \boldsymbol{P}^{max}, \boldsymbol{V}^{max}\} \tag{4.35}$$

  where $\boldsymbol{P}_0$, $\boldsymbol{V}_0$, $\boldsymbol{I}_0$ are the vectors of DC powers, voltages and branch currents, respectively, in the "N-0" situation. $\boldsymbol{G}$ is the indefinite conductance matrix of the MTDC grid, and $\boldsymbol{A}$ relates the DC voltages to DC branch currents (see also Appendix B).
- for the "N-1" situation (tripping of j-th component):

$$\boldsymbol{P}_j = \text{diag}(\boldsymbol{V}_j)\, \boldsymbol{G}_j\, \boldsymbol{V}_j \tag{4.36}$$

$$\boldsymbol{I}_j = \boldsymbol{A}_j\, \boldsymbol{V}_j \tag{4.37}$$

$$\{\boldsymbol{I}_j^{min}, \boldsymbol{V}_j^{min}\} \leq \{\boldsymbol{I}_j, \boldsymbol{V}_j\} \leq \{\boldsymbol{I}_j^{max}, \boldsymbol{V}_j^{max}\} \tag{4.38}$$

  for each VSC $i = 1, \ldots N$:

$$0 \leq (P_{j,i} + P_i^{max}) \perp \alpha_{j,i} \geq 0 \tag{4.39}$$

$$0 \leq (P_i^{max} - P_{j,i}) \perp \beta_{j,i} \geq 0 \tag{4.40}$$

$$P_{j,i} - d_{j,i}\,(P_{0,i} - K_{V,i}\,(V_{j,i} - V_{0,i}) - \alpha_{j,i} + \beta_{j,i}) = 0 \tag{4.41}$$

  where $\boldsymbol{P}_j$, $\boldsymbol{V}_j$ and $\boldsymbol{I}_j$ are the vectors of VSC powers, DC voltages and branch currents, respectively, after the outage of component j (either a VSC or a DC branch). α and β are

auxiliary variables used to include the VSC power ratings in the optimization. $d_{j,i}$ is equal to one, unless the disturbance j is the tripping of the i-th VSC, in which case it is equal to zero. $\boldsymbol{G}_j$ and $\boldsymbol{A}_j$ are equal to $\boldsymbol{G}$ and $\boldsymbol{A}$, respectively, unless the tripped j-th component is a DC branch. In that case the contribution of the tripped branch is removed from the two matrices.

Priority can be given in (4.32) to specific VSCs by choosing appropriate values for the weighting factors w_i. For example, for VSCs connecting wind farms to the MTDC grid, a large weighting factor is used to gather as much power as possible from them. It is set to 0 for VSCs whose power is not required to be close to a desired value, but instead depends on the rest.

Constraint (4.33) expresses that $\boldsymbol{P}_0$ and $\boldsymbol{V}_0$ should satisfy the power flow equations of the MTDC grid. Equality constraint (4.34) yields the DC branch currents. Constraints (4.35) relate to the maximum (i.e. $\boldsymbol{I}^{max}$, $\boldsymbol{P}^{max}$ and $\boldsymbol{V}^{max}$) and minimum (i.e. $\boldsymbol{I}^{min}$, $-\boldsymbol{P}^{max}$ and $\boldsymbol{V}^{min}$) values of the DC branch currents, VSC powers and DC voltages, respectively.

As far as the "N-1" case is concerned, constraint (4.36) denotes the power flow equations after the tripping of the j-th component. Similarly, equality constraints (4.37) give the DC branch currents after the outage and constraints (4.38) specify that the currents and DC voltages must remain between limits after the outage. Note that the current and voltage limits, in the N-1 situation, denoted as $I_j^{min,max}$ and $V_j^{min,max}$, respectively, can be different from the limits for normal operation.

It is noted that if a VSC is connected radially to the rest of the MTDC grid, the outage of its DC branch is not included in the SCOPF. Instead, only the outage of the VSC is considered. The impact on the remaining MTDC system is the same in steady-state in both cases (the VSC is tripped and no current is flowing through the radial branch).

Constraints (4.39)-(4.41) relate to the power of each VSC in the post-disturbance case, and ensure that it is between the maximum and minimum limits P^{max} and $-P^{max}$, respectively. The auxiliary vectors $\boldsymbol{\alpha}$ and $\boldsymbol{\beta}$ are introduced to appropriately model the behavior of a VSC in droop mode when it reaches one of its power limits. A VSC cannot be overloaded; when it reaches its maximum (resp. minimum) power P^{max}, its power stops increasing (resp. decreasing), hence, this is equivalent to a change of its behavior. Thus, each VSC in droop mode follows the piece-wise

characteristic shown in Fig. 4.18, described by the following equations[6]:

$$\begin{cases} P = -P^{max} & \text{and} \quad V \geq \frac{P^{max}+P_0}{K_V} + V_0 \\ P = P_0 - K_V(V - V_0) & \text{and} \quad \frac{-P^{max}+P_0}{K_V} + V_0 \leq V \leq \frac{P^{max}+P_0}{K_V} + V_0 \\ P = P^{max} & \text{and} \quad V \leq \frac{-P^{max}+P_0}{K_V} + V_0 \end{cases} \tag{4.42}$$

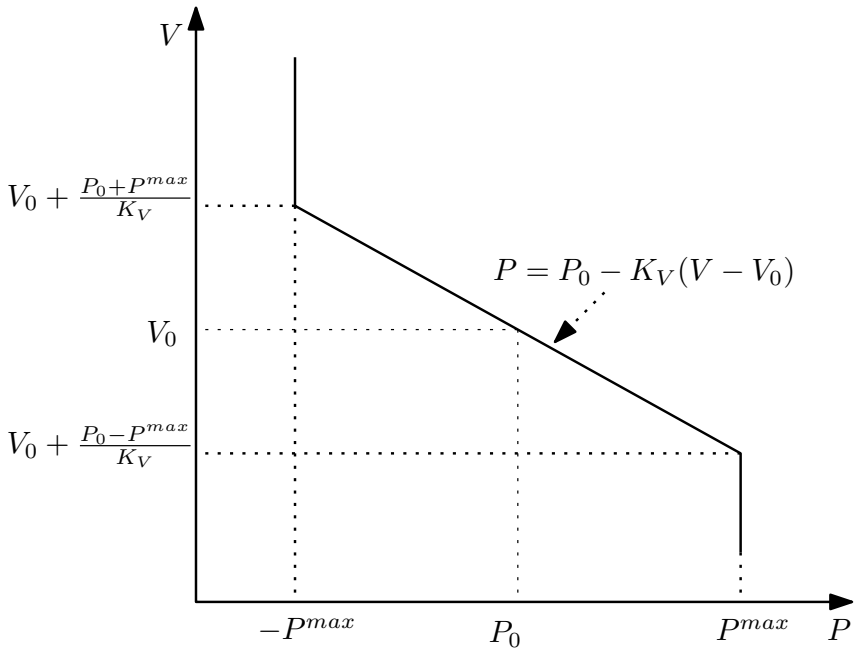

Figure 4.18: Piece-wise droop characteristic of VSC

Equation (4.42) indicates that when the VSC reaches one of its power limits, it switches to constant power control (i.e. $K_v = 0$). In order to include this change of behavior in the SCOPF formulation without resorting to integer variables, complementarity constraints [RRS05] (denoted with the $\perp$ symbol) are used. Specifically, constraints (4.39) and (4.40) can be re-written as follows:

$$(P_{j,i} + P_i^{max})\ \alpha_{j,i} = 0 \tag{4.43}$$

$$P_{j,i} + P_i^{max} \geq 0 \ \text{ and } \ \alpha_{j,i} \geq 0 \tag{4.44}$$

$$(P_i^{max} - P_{j,i})\ \beta_{j,i} = 0 \tag{4.45}$$

$$P_i^{max} - P_{j,i} \geq 0 \ \text{ and } \ \beta_{j,i} \geq 0 \tag{4.46}$$

[6]Parameters (P^{set}, V^{set}) have been replaced by (P_0, V_0) in (4.32)-(4.42), implicitly taking $P_0 = P^{set}$ and $V_0 = V^{set}$. In fact, an infinite number of pairs (P^{set}, V^{set}) can yield the same power flow (P_0, V_0). Here, $P_0 = P^{set}$ and $V^0 = V^{set}$ has been taken to simplify the presentation.

It can be verified by enumerating the various cases that constraints (4.39)-(4.41) represent correctly the piece-wise characteristic (4.42). For instance, when the i-th VSC is upper limited following the j-th disturbance:

1. from (4.43): $\alpha_{j,i} = 0$;
2. from (4.45): $\beta_{j,i} \geq 0$;
3. (4.41) with $d_{j,i} = 1$ yields: $P_i^{max} - P_{0,i} + K_{V,i}\,(V_{j,i} - V_{0,i}) + \beta_{j,i} = 0$;
4. since $\beta_{j,i} \geq 0$: $P_i^{max} - P_{0,i} + K_{V,i}\,(V_{j,i} - V_{0,i}) \leq 0$;
5. therefore the following relation holds for the DC voltage: $V_{j,i} \leq V_{0,i} + \frac{P_{0,i} - P_{j,i}}{K_{V,i}}$

This shows that the VSC operates on the rightmost vertical piece of the characteristic in Fig. 4.18.

More information on complementarity constraints, as well as methods to achieve better convergence to the solution, were presented in [RRS05] and its references.

The resulting formulation is a nonlinear quadratic problem for which several solvers can be found. Here, the optimization is solved in Matlab with the use of the *fmincon* function relying on the interior-point algorithm. In the cases considered in the simulation results of Section 4.5, the required time for the algorithm to converge to the solution was approximately 20-35 s.

4.4.3 Outputs given to secondary level

The output of the optimization is a set of powers P_0 and DC voltages V_0. From the former, the new scheduled powers of the dispatchable VSCs are given to the Power Rescheduler as follows:

$$P_i^{sch} = P_{0,i} \quad \text{for} \quad i = 1, \ldots, N_D \tag{4.47}$$

The term P_{losses} in (4.7) is taken equal to the losses in the base case, i.e.:

$$P_{losses} = \sum_{i=1}^{N} P_{0,i} \tag{4.48}$$

If it is found from the SCOPF that the power of e.g. a wind farm has to be reduced to ensure the security of the MTDC grid, it is necessary to force the secondary MPC to curtail some of its power. This is done by setting to $P_{0,i}$ the maximum power (P_i^{max} in (4.12)) of the corresponding non-dispatchable i-th VSC.

Finally, the average DC voltage reference V_{avg}^{ref} is taken equal to the average value of the voltages

V_0, i.e.:

$$V_{avg}^{ref} = \frac{1}{N}\sum_{i=1}^{N} V_{0,i} \tag{4.49}$$

4.4.4 Discussion

The above SCOPF formulation has been kept as simple as possible. Other constraints could be incorporated, such as a desired power transfer between AC areas or a maximum change of power injection to an AC area after a contingency (e.g. to prevent unacceptable frequency deviations).

In addition, transient dynamics have not been taken into account. The SCOPF ensures that steady-state limits of DC voltages and currents will be respected. Thus, it is implicitly assumed that a transient violation of these limits after the disturbance can be tolerated and rapidly corrected by the VSC controls. The analysis could be coupled with EMT simulations involving detailed modeling of the VSCs and the lines/cables to appropriately tune the VSC controls and check in detail that the security limits are satisfied. This analysis, however, was not further considered here.

Furthermore, different values of I^{max}, V^{max} and V^{min} have been assumed between normal and post-contingency situation. The limits for the N-0 case should be at least as constraining as the ones used in the secondary level controller, otherwise the MPC would not satisfy the operating point calculated by the SCOPF. On the other hand, a wider range can be selected for the N-1 cases in the SCOPF constraints.. Although it is highly unlikely that the DC voltage limits can be significantly relaxed, small branch overloads might be tolerated for a short period of time, i.e. the time required by the MPC controller to remove the current violation. Assuming that the MPC-based secondary control will succeed alleviating the overload, I_j^{max} in (4.38) can be set to higher value than I^{max} in (4.35). However, the tertiary level has to ensure that following a disturbance, there remains sufficient margin for the secondary level to act. Namely, the voltages and currents after the disturbance should not lead to further equipment tripping before the secondary control has time to correct the violations.

Finally, the formulation of a multi-objective optimization problem requires attention when tuning the weighting factors. Here, more weight is given first to harvesting the WF power, then to satisfying the desired powers of the dispatchable VSCs, and lastly to losses minimization. Situations might occur where the optimization, pursuing the maximum WF power harvest, increases the losses in the MTDC grid, thus pushing the DC voltages to their lower limit.

4.5 Simulation results with tertiary control

Results of the application of the tertiary level are presented on the five-terminal DC grid previously considered in this chapter (see Fig. 4.8). The SCOPF formulation is solved for two cases including all N-1 contingencies[7]:

- Case 1: the desired powers P^{des} of T3, T4 and T5 are set equal to -3, -4 and 2 pu, respectively;
- Case 2: the desired powers P^{des} of T3, T4 and T5 are set equal to -9, -9 and 9 pu, respectively;

The following limits are used in the optimization:

- for the pre-contingency situation: same limits as for the secondary level, i.e. $V^{min} = 0.96$ pu, $V^{max} = 1.04$ pu, $P^{max} = 10$ pu, $I^{max} = 10$ pu for all HVDC branches except the ones connected to the WF that have a limit $I^{max} = 3.5$ pu;
- for the (immediate) post-contingency situation: larger voltage and maximum current deviations are allowed, i.e. $V^{min} = 0.90$ pu, $V^{max} = 1.10$ pu and $I_j^{max} = 110\%\ I^{max}$ pu.

The weighting factors of T1 and T2 are set to zero, for T3 and T4 they are set to $w_3 = w_4 = 10$ and for T5 a value $w_5 = 10^3$ is chosen.

The results of the SCOPF are shown in Tables 4.3 and 4.4. For comparison purposes the results of a simple "N-0" OPF considering (4.32)-(4.35) only are also included.

Table 4.3: OPF and SCOPF results for Case 1

	SCOPF		**OPF**	
VSC	$\boldsymbol{P}_0$ (pu)	$\boldsymbol{V}_0$ (pu)	$\boldsymbol{P}_0$ (pu)	$\boldsymbol{V}_0$ (pu)
T1	3.35	1.04	3.34	1.04
T2	1.70	1.04	1.70	1.04
T3	-3	1.0306	-3	1.0306
T4	-4	1.0347	-4	1.0347
T5	2	1.0395	2	1.0395
Losses (pu)	0.05		0.04	

[7] except of the tripping of the branch connecting T5 to the rest of the MTDC grid

Table 4.4: OPF and SCOPF results for Case 2

	SCOPF		OPF	
VSC	P_0 (pu)	V_0 (pu)	P_0 (pu)	V_0 (pu)
T1	3.95	1.0376	2.01	1.0344
T2	3.20	1.04	6.07	1.04
T3	-6.86	1.0159	-9	1.0055
T4	-4.15	1.0348	-6.02	1.0325
T5	4.03	1.04	7.28	1.04
Losses (pu)	0.17		0.34	

The SCOPF and the OPF reach an almost identical operating point in the first case, as shown in Table 4.3. The small differences can be attributed to rounding off and solver accuracy. In fact, there is no constraining contingency for the first case since the power flows in the MTDC grid are small. Therefore, the solution satisfies the desired powers of T3, T4 and T5, and it is steered towards the maximum DC voltage limit in order to reduce the losses.

The second case, detailed in Table 4.4, shows that a quite different operating point is reached when an N-1 security constraint becomes active. In both cases, the capability of the branches connecting the WF to the MTDC grid is smaller than the produced power. Therefore, it is required to reduce the WF power. However, the optimal WF power resulting from the SCOPF is almost half of the one from the OPF, since the system would not be secure in case of the outage of one of the two branches.

It is interesting to note that the losses are higher with the OPF. This is because of the higher WF power injected into the network.

4.5.1 Coordination with secondary level

The coordination between the secondary and the tertiary level, as well the ability of the former to track the operating point given by the latter is demonstrated here. In addition, the dynamic simulations reported here served as a validation of the results of the SCOPF. The system of Fig. 3.1 is again simulated, starting from the operating point shown in Fig. 4.8, and considering the following events:

- at $t = 11$ s: the tertiary level provides a new secure operating point for the current production of the WF; the desired powers of T3 and T4 are set to -6 pu;
- at $t = 81$ s: tripping of branch connecting the VSCs T2 and T4. This constraining contingency leads to a violation of the long-term current limit of the branch between T4 and

Table 4.5: SCOPF results with short-term relaxation of I^{max}

VSC	T1	T2	T3	T4	T5
$\boldsymbol{P}_0$ (pu)	1.40	6.06	-6	-4.29	2.99
$\boldsymbol{V}_0$ (pu)	1.0344	1.04	1.0154	1.0324	1.0362
Losses (pu)			0.17		
V_{avg}^{ref} (pu)			1.0317		

T5.

Figures 4.19 and 4.20 show the powers and the DC voltages of the VSCs.

At $t = 11$ s, the new values of $\boldsymbol{P}^{sch}$ and V_{avg}^{ref} shown in Table 4.5 are sent to the Power Rescheduler. It is noted that due to N-1 security constraints the desired power of T4 (-6 pu) is not satisfied, but is instead increased to -4.29 pu (see Table 4.5). The secondary level successfully steers the MTDC grid to the received operating point. However, following the tripping of the branch T2-T4, the MPC controller reduces (resp. increases) the power of T1 (resp. of T3 and T4). As revealed in Fig. 4.21, this was necessary to restore the DC current of branch between T4 and T5 below its maximum limit I^{max}, as well as the DC voltage at bus T2.

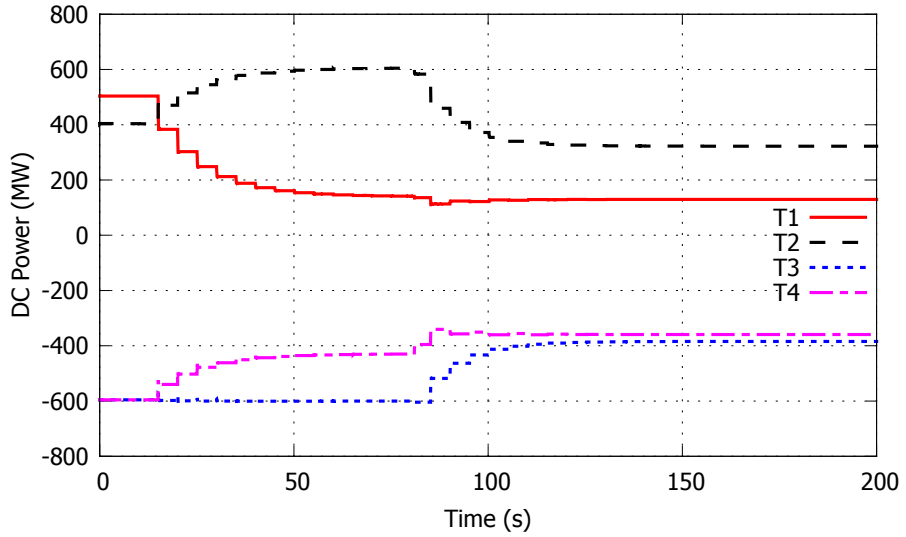

Figure 4.19: VSC powers

It is highlighted that the DC current in branch T4-T5 right after the disturbance has been allowed to reach a value of 110% of the I^{max} value (namely 3.85 pu instead of 3.5 pu). This constraint relaxation allowed the tertiary level to further optimize the operation of the MTDC grid, knowing in advance that the secondary level would correct such short-term violations, in case the contingency occurs.

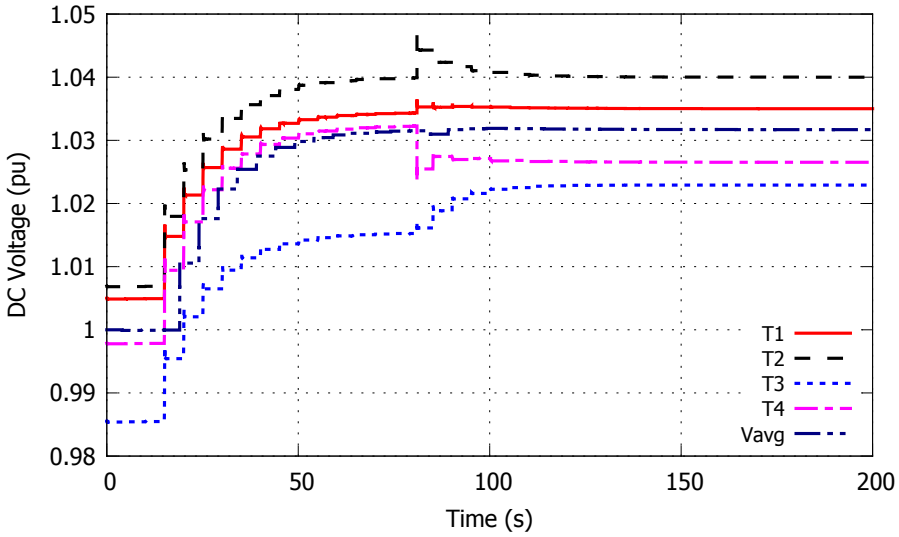

Figure 4.20: MTDC grid voltages

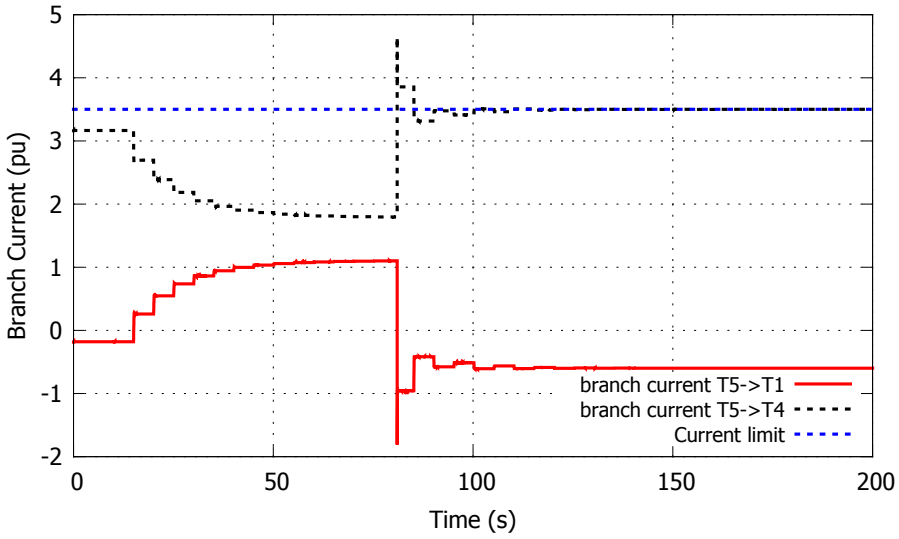

Figure 4.21: Branch currents

If the relaxation of the branch current was not considered, the SCOPF would result in the operating point given by Table 4.6. To satisfy the more constraining limit, the N-0 case power of T4 would need to be further increased from -4.29 pu (see Table 4.5) to -3.89 pu.

To validate the result of the SCOPF, the same dynamic simulation as in Figs. 4.19-4.21 has been performed with the lower limit. Figure 4.22 shows the DC currents flowing through branches T1-T5 and T4-T5. It can be seen that the DC current in branch T4-T5 rises to its maximum and settles at this value after a short transient. A short adjustment period is also observed after the

Table 4.6: SCOPF results without short-term relaxation of I^{max}

VSC	T1	T2	T3	T4	T5
$\boldsymbol{P}_0$ (pu)	1.87	5.18	-6	-3.89	2.99
$\boldsymbol{V}_0$ (pu)	1.0353	1.04	1.0162	1.0334	1.0371
Losses (pu)			0.15		
V_{avg}^{ref} (pu)			1.0324		

disturbance. This is due to the secondary level adjusting the setpoints of the VSCs to alleviate DC voltage violations and restore the average DC voltage to its reference value. Apart from this adjustment, the current settles at its limit as expected.

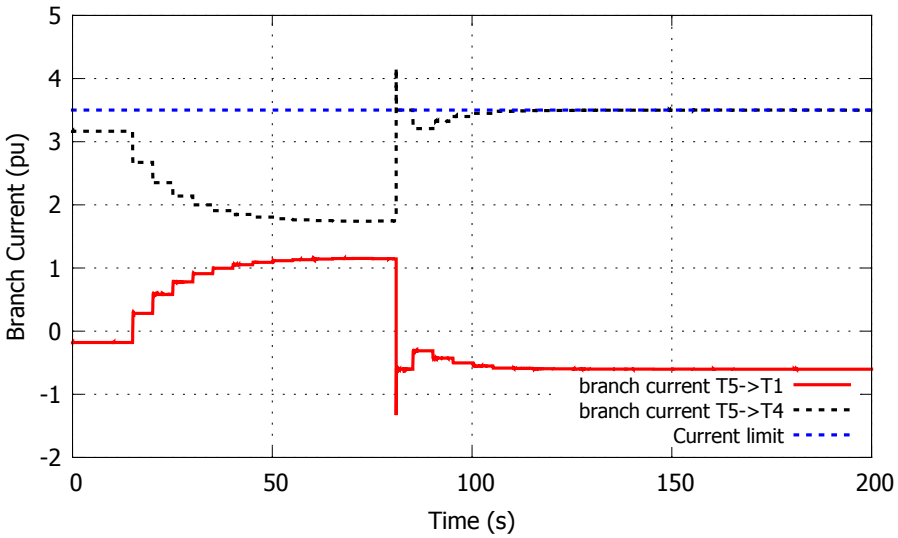

Figure 4.22: Branch currents without short-term relaxation of I^{max}

4.6 Summary

A three-level hierarchical control structure for MTDC grids has been proposed in this chapter. The structure is based on the DC voltage droop control as a primary level, an MPC-based secondary level, and an SCOPF as a tertiary level.

The primary level ensures the stability of the MTDC grid by enabling multiple VSCs to adjust their power and correct power imbalances. The secondary level monitors the whole MTDC grid and coordinates the VSCs to steer the MTDC grid towards a desired operating point, while respecting constraints. The tertiary level aims at optimizing the operation of the MTDC grid taking into account security constraints. The security constraints specify that the MTDC grid can reach an

acceptable operating point following the loss of a single HVDC component, taking into account that the secondary level can contribute in alleviating short-term violations.

Chapter 5

Frequency support among asynchronous AC areas through MTDC grids

The subject of this chapter is the description of two methods for frequency support among asynchronous AC areas through MTDC grids. The basic mechanism has been already illustrated using the example of Section 3.2. The support in the example relied on a simple frequency droop control that is considered the state-of-the-art in the literature. Both alternatives described in this chapter are inspired of MPC. However, they approach the subject from a different perspective aiming to satisfy different objectives.

The chapter is organized as follows. Section 5.1 reviews the methods that have been proposed in the literature. Section 5.2 details the first scheme [PDPV17a, PDPV17c], while Section 5.3 provides simulation results illustrating its performance. The second scheme [PDP+18a] is described in Section 5.4. The corresponding simulation results are provided in Section 5.5. Finally, Section 5.6 summarizes the main results of the chapter.

5.1 Introduction

Frequency support to an AC area by VSCs and MTDC grids has been the subject of quite a number of publications. In the majority of them, a supplementary proportional (droop) control is added to the control structure of the VSC, enabling it to react to frequency deviations [HU10, WAA+15, SPG13]. A variant of the droop scheme was proposed in [Vra13], where different values of droop

are used depending on the severity of the disturbance. A different approach was described in [ZBA+13], but it can be used for inertia emulation only and not for sharing primary reserves between asynchronous AC areas.

A number of publications are devoted to control strategies enabling both primary frequency control and inertia emulation response by offshore wind farms connected to the main onshore network through an MTDC grid [Phu12, PCG12, SMS+12]. In this application, the main idea is to enable the offshore converters to change the frequency (or the voltage magnitude) they impose on the AC offshore grid [FE07]. This in turn triggers the controllers of the offshore wind turbines, which modify their active power production to provide inertial or primary frequency support. An alternative method based on directly communicating the onshore frequency deviation to the offshore wind farm was proposed in [MS15].

A drawback of the simple frequency droop control is the strong interaction with its DC voltage droop counterpart. This has been shown to reduce the efficiency of both control schemes, and adjustment of the frequency droop gain is required to achieve the desired participation to frequency support [ADPG15]. However, even this adjustment is valid only for a given configuration of the system. Namely, if one VSC is not participating to DC voltage droop control as expected, the support provided to the AC area undergoing the frequency deviation will be significantly reduced. An alternative was proposed in [PGV15], using integral control of the power setpoint to deal with this issue.

In addition, with the exception of [MS15], the study of frequency support to AC areas by MTDC grids has focused on AC-side disturbances. Cases like the outage of a VSC, which could lead to significant frequency deviations, as well as troublesome DC voltage problems have not been investigated. In this case, a "compromise" should be sought between frequency support and maintaining an acceptable DC voltage profile of the system. Conventional control structures would require a rather complex set of rules and correct limits to deal with the above cases, the design of which is not obvious.

In general, there are two options to consider for frequency support through HVDC grids: (i) a continuously active regulation, and (ii) an activation only after large disturbances. In the first scheme, each VSC adjusts its power exchange with the AC grid in response to the frequency deviation resulting in a partial coupling between the balancing controls of the various AC systems, originally decoupled. In contrast, the second scheme considers frequency support by the VSCs as an emergency control scheme, inactive for small deviations around its nominal value [BCH14]. Frequency support is then activated when unusually large frequency deviations or Rates Of Change Of Frequency (ROCOF) are detected.

Some works have investigated the possibility to use the MTDC grid in order to "reach a frequency

consensus" between the interconnected asynchronous AC areas [JPSE11, AWD+15], i.e. eventually bring all frequencies to the same value. This is not the track followed in this work, whose aim is to consider frequency support as an "emergency" control scheme, as also suggested in [BCH14]. Therefore, for small frequency deviations the frequency support scheme remains inactive. This also serves the purpose of preventing continuous interactions between the frequency controls of AC systems which were otherwise planned to operate asynchronously. On the other hand, in response to a large enough frequency deviation in one AC area, the VSCs connected to the latter sense the frequency deviation and correspondingly adjust the power transfer through the MTDC grid, thus taking advantage of the primary reserves of other AC areas.

5.2 Scheme 1 - Predefined participation

In the first scheme, the participating VSC is controlled to provide in steady state a pre-defined fraction of the total power injection needed to support the frequency in the AC area of concern, as for a power plant under speed governor control. This can be achieved by changing the power setpoint P^{set} of the P-V characteristic (2.35) until the above objective is satisfied. As pointed out in [PGV15], in order a VSC in frequency droop mode to achieve the desired power participation, some kind of integral action is required so that the total change of its power setpoint counteracts the impact of the resulting DC voltage deviation on its power flow (according to (2.35)).

Clearly, the added control should not jeopardize the operation of the MTDC grid as well the other AC areas. This imposes to obey constraints on the DC voltage, on the rate of change of powers, etc. Furthermore, a concern which, to the authors' knowledge, has not received proper attention is the controller behavior when the other AC areas do not "cooperate" as expected, e.g. when the VSCs of one area do not participate as expected in DC voltage control and, hence, do not provide the power requested by the frequency controlling VSCs.

Finally, it is highly desirable for each VSC to rely only on local measurements readily available. By so doing, fast and reliable performance can be achieved without resorting to communication between converters, which can be subject to delays and failures.

5.2.1 Controller objective

The proposed controller bears the spirit of an "emergency" scheme, thus being inactive in normal operation. Its activation is triggered by frequency deviation with some hysteresis. As shown in Fig. 5.1, as long as frequency stays inside a pre-specified range $[f^{on}_{min}, f^{on}_{max}]$, the controller remains idle (OFF state), while it is activated as soon as frequency leaves the deadband (ON state). Once

the controller has been activated, it remains active until the frequency is restored inside a narrower range $\left[f_{min}^{off}, f_{max}^{off}\right]$ by the secondary frequency controller of the AC system.

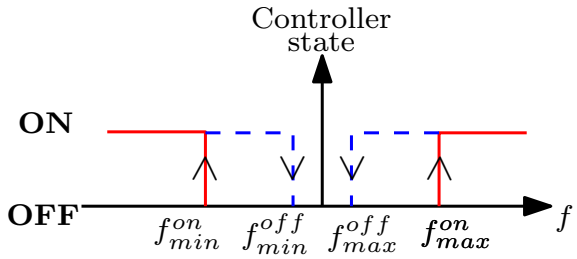

Figure 5.1: Controller activation logic

Let $t^\star$ be the time when the control is activated, and $P(t^\star)$ the power injected by the VSC into the MTDC grid at that time.

The main objective of frequency control is to adjust P so that the steady-state participation of the VSC is proportional to the frequency deviation from its nominal value f_N, i.e.

$$\lim_{t\to\infty} \left[P(t) - P(t^\star) - K_f \left(f(t) - f_N \right) \right] = 0. \tag{5.1}$$

The measurements used at time k are:

$P^m(k)$: the power flowing through the converter
$V^m(k)$: the voltage at its DC bus
$f^m(k)$: the frequency at its AC bus
$r_f^m(k)$: the rate of change of frequency at its AC bus.

These measurements are readily available in the converter sub-station. Specifically, AC frequency can be measured through the PLL. Note that multiple VSCs supporting the same AC area will not measure exactly the same frequency, since the local measurements may be impacted by the initial disturbance and by the resulting electromechanical oscillations.

The first scheme for frequency support is actually inspired by the formulation of the secondary MPC-based controller of Chapter 4, the difference being that the frequency support scheme concerns a single VSC. Similar to the secondary level, a reference evolution (or "trajectory" [QB03]) is defined with the objective of bringing the VSC power from its currently measured value to a value satisfying (5.1) in a finite number N_c of control steps: for $j = 1, \ldots, N_c$:

$$P^{ref}(k+j) = P^m(k) + \frac{j}{N_c} \left[P(t^\star) + K_f (f(k+N_c) - f_N) - P^m(k) \right]. \tag{5.2}$$

It is easily checked, that the reference power at the end of the control horizon satisfies the participation defined by (5.1), if the frequency was already at its final value. This point is further discussed later in this chapter.

In the MPC spirit, a constrained-optimization problem is set up. This requires a simplified model for the DC voltage and power as well as for the AC frequency response, as described next.

5.2.2 DC Voltage and power model

As detailed in Chapter 3, the DC voltage droop control is used to maintain the balance of the MTDC grid. By assuming that the MTDC grid dynamics are almost instantaneous, a steady-state model can be used to predict the DC voltage (V) and power (P) changes in response to the calculated control actions (ΔP^{set}): for $j = 1, \ldots, N_c$:

$$P(k+j) = P(k+j-1) + \Delta P^{set}(k+j-1) - K_v(V(k+j) - V(k+j-1)) \tag{5.3}$$

$$V(k+j) = V(k+j-1) + s_v \Delta P^{set}(k+j-1) \tag{5.4}$$

The setpoint variation $\Delta P^{set}(k+j-1)$ is defined as the change of setpoint P^{set} between two subsequent discrete times, i.e.:

$$\Delta P^{set}(k+j-1) = P^{set}(k+j) - P^{set}(k+j-1).$$

The sensitivity s_v in (5.4) takes into account the DC voltage droop gains of all VSCs and the topology of the MTDC grid. Its derivation is detailed in Section 5.2.5.

At each sampling time, the above model is initialized to the latest received measurements $P^m(k)$ and $V^m(k)$, i.e.

$$P(k) = P^m(k) \text{ and } V(k) = V^m(k).$$

The model used for the DC grid is static, which is justified by the speed of power electronics, DC voltage and VSC controls, compared to the sampling period of the discrete controller, in the order of some hundrends milliseconds.

The prediction model can also be used in point-to-point HVDC links where the Master-Slave control logic is used instead of the droop control [Rau14]. However, the proposed control can only be applied on the Slave VSC since the Master converter adjusts its power to control its DC voltage. In this case, the droop gain K_v in (5.3) is equal to zero, and the value of s_v accounts only for the expected DC voltage change due to change of losses.

5.2.3 AC frequency model

A model of the AC system frequency is used to predict the future evolution. A simplified model is considered in this work with a minimal requirement of parameters from the Transmission System Operator (TSO) of the AC system.

Figure 5.2 depicts a simplified frequency response model [KBL94] serving as the basis to derive the model used in the MPC. The following variables are involved:

- P_m: the total mechanical power produced by the conventional power plants,
- P_e: the total electrical power consumed in the AC system, produced by the generators,
- P: the DC power (counted positive for rectifier operation) drawn from the AC system (assuming only one VSC),
- r_f: the ROCOF,
- Δf: the frequency deviation from its nominal value,
- H: the total inertia constant of the (synchronous machines) rotating masses in the AC system.

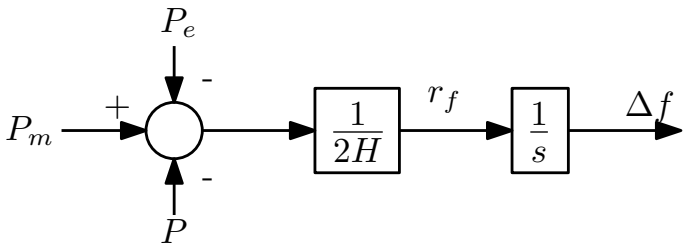

Figure 5.2: Simplified frequency response model

Figure 5.2 shows that, at every time instant:

$$r_f = \frac{P_m - P_e}{2H} - \frac{P}{2H}. \tag{5.5}$$

In order to derive a simplified model for inclusion in the MPC formulation the following assumptions are made:

1. P_m and P_e remain constant throughout the whole prediction horizon of the MPC, and equal to their values from the latest time of measurement i.e. $P_m(k)$ and $P_e(k)$. This assumption neglects the contribution of the prime movers of the power plants and the load self-regulation effect. However, by keeping the prediction horizon short enough, this approximation is easily compensated by the MPC closed-loop nature.

2. The VSC power P, which is adjusted by the MPC at each sampling time, has an instantaneous response and is also constant between two consecutive time instants. This is justified by the very fast response of power electronics and VSC controls, compared to the AC frequency dynamics.

Based on the aforementioned assumptions and (5.5), r_f can be considered constant between two consecutive actions of the MPC. Subsequently, the frequency change between time instants $k+j$ and $k+j-1$ is given by: for $j = 1, \ldots, N_c$:

$$f(k+j) - f(k+j-1) = \frac{P_m(k) - P_e(k) - P(k+j)}{2H} T_s \tag{5.6}$$

where T_s is the sampling time. This equation can be decomposed as follows:

$$f(k+j) - f(k+j-1) = \frac{P_m(k) - P_e(k) - P(k)}{2H} T_s + \frac{P(k) - P(k+j)}{2H} T_s \tag{5.7}$$

It is not realistic to assume precise knowledge of the total mechanical and electrical powers in the AC system, at the rate of the controller. However, the fraction in the first term in the right hand side of (5.7) is equal to the ROCOF at time k, i.e. $r_f(k)$, which can be measured directly by the VSC through its PLL. Consequently, $P_m(k)$ and $P_e(k)$ can be eliminated from (5.7) resulting in the following frequency prediction: for $j = 1, \ldots, N_c$:

$$f(k+j) - f(k+j-1) = r_f(k) T_s + \frac{P(k) - P(k+j)}{2H} T_s \tag{5.8}$$

In (5.8) the total inertia constant H is used to calculate the effect of the DC power change on the AC frequency. However, the exact value of this parameter is also unknown. In addition, (5.8) assumes that only one VSC is changing its DC power to support the AC frequency, which might not be the case since an AC area can be connected to an MTDC grid with more than one VSCs. For these reasons a sensitivity s_f is introduced. The value of s_f requires an approximation of H and should consider the fact that more than one VSCs may be participating in frequency support. All things considered, the AC frequency prediction model is the following:

$$f(k+j) = f(k+j-1) + r_f(k) T_s + \left(P(k) - P(k+j)\right) s_f T_s \tag{5.9}$$

The AC frequency model is initialized to the latest frequency and ROCOF measurements, namely:

$$f(k) = f^m(k) \quad \text{and} \quad r_f(k) = r_f^m(k).$$

5.2.4 Constrained optimization problem

The constrained optimization at the heart of the proposed control consists in minimizing the deviations with respect to the aforementioned reference values:

$$\min_{V,P,f,\epsilon,\Delta P^{set}} \sum_{j=1}^{N_c}[P^{ref}(k+j) - P(k+j)]^2 + v\sum_{j=1}^{N_c}[\epsilon(k+j)]^2 \tag{5.10}$$

subject to the following constraints: for $j = 1, \ldots, N_c$:

$$V^{low}(k+j) - \epsilon(k+j) \leq V(k+j) \leq V^{up}(k+j) + \epsilon(k+j) \tag{5.11}$$

$$\epsilon(k+j) \geq 0 \tag{5.12}$$

$$P^{min} \leq P(k+j) \leq P^{max} \tag{5.13}$$

$$V(k+j) = V(k+j-1) + s_v\,\Delta P^{set}(k+j-1) \tag{5.14}$$

$$P(k+j) = P(k+j-1) + \Delta P^{set}(k+j-1) - K_v\,(V(k+j) - V(k+j-1)) \tag{5.15}$$

$$f(k+j) = f(k+j-1) + [r_f(k) - s_f\,(P(k+j) - P(k))]\,T_s \tag{5.16}$$

where ϵ is a slack variable, and v a weight penalizing voltage violations.

Inequality (5.11) specifies that the DC voltage should not exceed the secure limits V^{low} and V^{up}. In case the optimization problem becomes infeasible, these constraints are relaxed, with the ϵ variable taking a nonzero value. The constraint violation is, however, kept as small as possible by setting the weight v to a high value. Note that V^{low} and V^{up} evolve with time $k+j$ in order to bring the voltage progressively inside the desired range defined by V^{min} and V^{max}. This is achieved with the same method described in Section 4.2.8.

Constraint (5.13) imposes the VSC power to stay within limits.

Equations (5.14), (5.15) and (5.16) make up the DC voltage, power and AC frequency prediction model, respectively. The predicted variables do not vary after the last action has been applied. Hence, there is no need to take the prediction horizon larger than the control horizon N_c. s_v is the sensitivity of the DC voltage of a given VSC to the setpoint change ΔP^{set} of the same VSC. Its derivation is explained in the next section.

The formulation can accommodate other constraints, such as maximum rate of change of power and/or DC voltage, maximum steady-state participation to frequency control, etc.

As demonstrated in [PDPV17a], it is not mandatory to include a model of frequency dynamics in the formulation. Instead, the future frequency values could be set to the latest measurement

$f^m(k)$, updated at each time step k. This is equivalent to assuming $s_f = 0$ and $r_f = 0$ in (5.16), removing the need for a ROCOF measurement. Extensive tests in [PDPV17a] have shown that this approximation is still properly compensated by the closed-loop MPC scheme. Nevertheless, the simple prediction model (5.16) improves the frequency support, especially during the first moments after the activation of the controller.

The output ΔP^{set} is applied to the VSC through the outer loops as shown in Fig. 5.3, similar to Fig. 4.6.

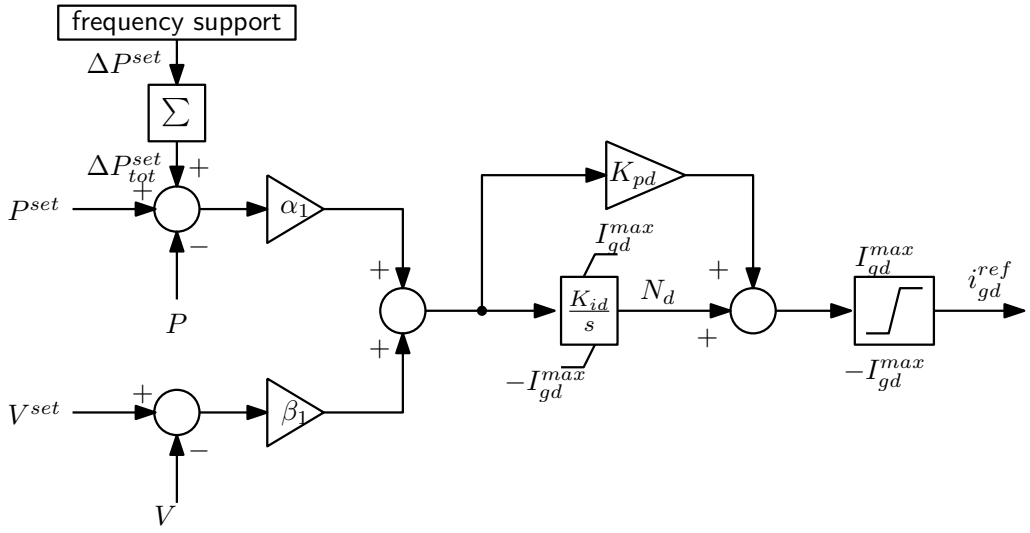

Figure 5.3: Connection of frequency support actions to VSC outer controllers. The $\sum$ block denotes a discrete integrator, i.e. its output ΔP^{set}_{tot} is calculated as $\Delta P^{set}_{tot}(k) = \Delta P^{set}_{tot}(k-1) + \Delta P^{set}(k)$

5.2.5 Determination of the sensitivity s_v

The starting point to determining the sensitivity s_v is the sensitivity matrix $\boldsymbol{S}_P$ used in the secondary level of Chapter 4 and giving the relation between the DC voltage changes and the VSC power setpoint changes. Its derivation has been detailed in Appendix B as follows:.

$$\Delta \boldsymbol{P}^{set} = \boldsymbol{S}_p \, \Delta \boldsymbol{V} \quad \text{or} \quad \Delta \boldsymbol{V} = \boldsymbol{S}_v \, \Delta \boldsymbol{P}^{set} \tag{5.17}$$

$$\text{where:} \quad \boldsymbol{S}_p = \boldsymbol{S}_v^{-1} = \boldsymbol{J}_{dc} + \mathbf{diag}(K_{v1} \dots K_{vc}). \tag{5.18}$$

If an AC area is connected to the MTDC grid through more than one VSCs, it is possible that a frequency excursion in that area activates frequency control in more than one terminals. Considering the c-th terminal, its DC voltage varies under the combined effect of several power changes

as follows:

$$\Delta V_c = \sum_{i \in \mathcal{A}} [\boldsymbol{S}_v]_{ci} \, \Delta P_i^{set} \tag{5.19}$$

where $\mathcal{A}$ denotes the set of activated terminals. In order to control each of them independently of the others, an approximate sensitivity factor s_v is sought. It can be obtained under the following reasonable approximations:

1. The controllers of all terminals connected to the same area have the same parameters (in particular the same sampling period T_s);
2. the control action calculated by each controller at each time step is proportional to the corresponding frequency droops K_f (see Eq. (5.2)), i.e.

$$\forall i, c \in \mathcal{A} : \quad \frac{\Delta P_i^{set}}{K_{f,i}} \approx \frac{\Delta P_c^{set}}{K_{f,c}}. \tag{5.20}$$

From (5.20), the various power changes can be expressed in terms of the c-th one:

$$\Delta P_i^{set} = \frac{K_{f,i}}{K_{f,c}} \Delta P_c^{set} \tag{5.21}$$

Substituting this result in (5.19) yields:

$$\Delta V_c = \sum_{i \in \mathcal{A}} [\boldsymbol{S}_v]_{ci} \, \frac{K_{f,i}}{K_{f,c}} \Delta P_c^{set} \tag{5.22}$$

from which the sensitivity is obtained as:

$$s_v = \sum_{i \in \mathcal{A}} [\boldsymbol{S}_v]_{ci} \, \frac{K_{f,i}}{K_{f,c}}. \tag{5.23}$$

This sensitivity accounts for the effect on DC voltages of all the VSCs supporting the frequency of an area. Note that no information is exchanged between terminals in the course of controlling frequency. In addition, the sensitivities (5.23) need not be updated often, but only after a topological change in the MTDC grid. Once again, the approximations embedded in (5.23) are corrected by the closed-loop MPC scheme.

5.2.6 Discussion

One could argue [VC18] that the desired participation to frequency support could be achieved using a simple frequency droop (see Section 3.2). Indeed, as shown in [ADPG15], an appropriate

adjustment of the frequency droop gain could lead to the correct participation without communication. However, the following conditions have to be satisfied:

- the losses of the MTDC grid do not change;
- no VSC reaches its rated power;
- frequency support is only activated in one area.

If at least one of the above conditions is not satisfied, then the pre-defined droop gain will not lead to the correct participation. That was the main motivation to resort to some kind of integral action, choosing MPC for its ability to provide adaptive response and respect constraints.

Another suggestion, in [VC18], was to remove the DC voltage droop and keep only the frequency droop control when frequency support is activated. However, it was noted in the same reference that the frequency deviations of the other areas are not negligible. Therefore, if frequency support was to be activated at all terminals, the DC voltages would not be controlled. With the proposed method, the voltage droop is kept active at all times, while the DC voltage constraints ensure that frequency support is frozen as soon as a voltage limit is reached.

Obviously, if communication between the VSCs was assumed (even a limited one), the proposed control could be adjusted to take into account the received information, and its response could be further improved.

5.3 Simulation results for Scheme 1

5.3.1 Test system and modeling

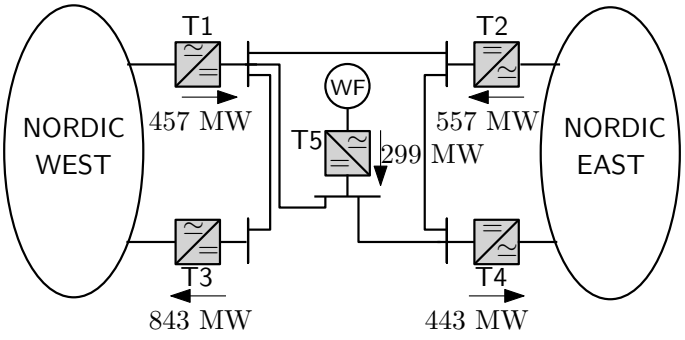

Figure 5.4: MTDC grid initial power flow

The proposed control scheme has been tested on the system of Fig. 3.1. The power flow in the MTDC grid has been slightly adjusted, as shown in Fig. 5.4. The adjustment mainly concerns the power of T3 which has been increased in order to simulate a significant VSC outage.

Among the five VSCs, all but T5 operate in DC voltage droop mode with $K_v = 5$ pu (on the VSC nominal power base), and are equipped with the proposed frequency control with a gain $K_f = 20$ pu. A deadband of ± 200 mHz is used for the activation of the controller and of ± 10 mHz for its deactivation (see Fig. 5.1).

All discrete controllers have a sampling time $T = 0.5$ s, which is long compared to the time constants of power electronics but short with respect to frequency dynamics. In order to synchronize the VSCs acting on the same AC area, the controls ΔP^{set} are applied at discrete times kT $(k = 1, 2, \ldots)$, assuming that each controller is relying on a GPS-synchronized clock. Each VSC collects the measurements $P^m(k), V^m(k)$ and $f^m(k)$ at times $kT - 0.1\,s$ $(k = 1, 2, \ldots)$ to account for the time needed to solve the optimization problem.

The control and prediction horizons have been set both to $N_c = 3$ to obtain a fast response time. The weighting factor v (see (5.10)) has been chosen to 10^4.

The active power limits of each VSC have been set equal to the VSC nominal active power of 1000 MW, i.e. $P^{min} = -10$ and $P^{max} = +10$ pu on a 100 MW base . The voltage limits at the DC buses of T1 - T4 have been chosen equal to $V^{min} = V^o - 0.05$ and $V^{max} = V^o + 0.05$ pu, where V^o is the initial DC voltage. The nominal DC voltage of all VSCs is ± 320 kV. For simplicity, the simulation results do not consider the frequency response model (5.16), as in [PDPV17a]. Results with a frequency response model have been reported in [PDPV17c].

A total of five scenarios are demonstrated. The first two concern an AC-side disturbance, for which a comparison between the proposed controller and the conventional frequency droop scheme is performed. The last three scenarios show the performance of the proposed scheme in a more intricate case, initiated by a DC-side disturbance. The hierarchical control structure for the MTDC grid described in Chapter 4 is not considered here.

The proposed scheme has also been validated experimentally. The control was implemented on a small-scale DC grid, in collaboration with Ecole Centrale de Lille [AAB+18]. The mock-up DC grid involves DC cables and VSCs, on which the ideas presented in the previous sections were tested. More details on the implementation steps, as well as a sample of the experimental results, are reported in Appendix D.

5.3.2 Disturbance in the AC system

The first two scenarios correspond to the tripping of generator g8E in the East subsystem (see Fig. 3.1), which activates frequency control by T2 and T4.

A comparison is conducted with the conventional frequency droop control using the same droop K_f. To facilitate the comparison, the droop control is also implemented as a discrete-time controller with the same sampling time as the RHC-based control ($T = 0.5$ s). The droop control is activated when frequency exits the same deadband (± 200 mHz) as in the proposed MPC-based control.

Scenario 1

Figure 5.5 shows the frequencies in both AC areas, with and without frequency support by T2 and T4. As expected, the activation of frequency support by T2 and T4 leads to a less pronounced frequency dip, and a higher final value, to the expense of a frequency deviation in the West subsystem, although milder. However, the proposed control leads to a higher power infeed than the conventional droop. The reason is the enforcement of the desired steady-state participation according to (5.1), in contrast to the conventional frequency droop control.

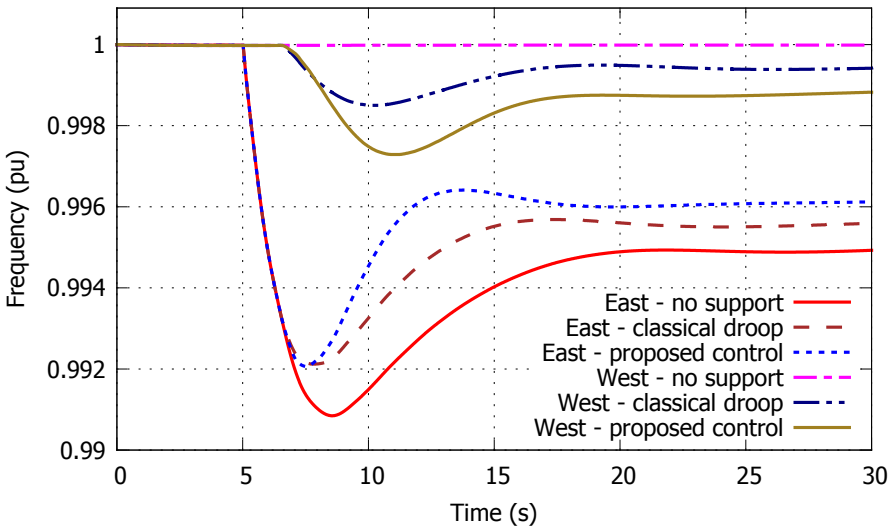

Figure 5.5: Scenario 1: AC system frequencies

This is further illustrated in Fig. 5.6, which shows the DC power of T4 for both schemes. It is noted that frequency control is activated at $t = 6$ s and, hence, the first control action is applied at $t = 6.5$ s in both cases. The MPC-based scheme provides the correct participation in steady

state (approx. 80 MW) compared to the conventional droop scheme whose effect is partially counteracted by the DC voltage droop control (yielding a participation of approx. 40 MW). T2 exhibits a similar response.

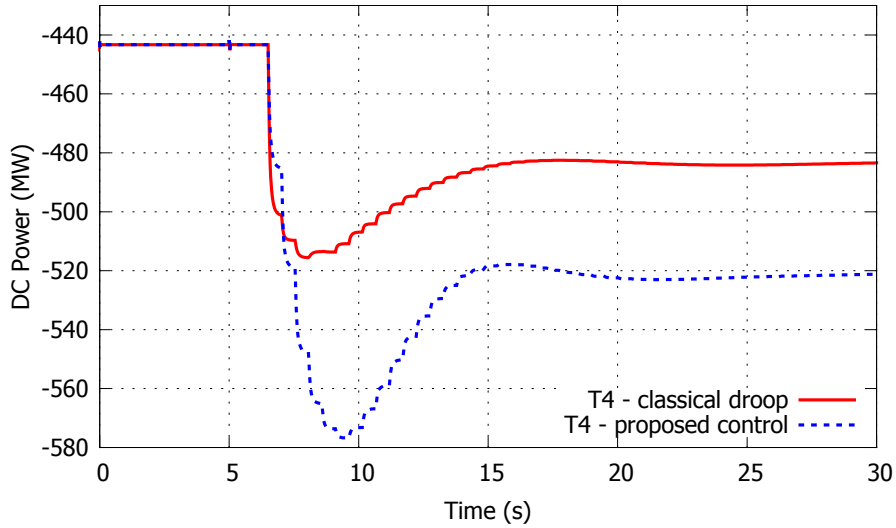

Figure 5.6: Scenario 1: DC power of T4

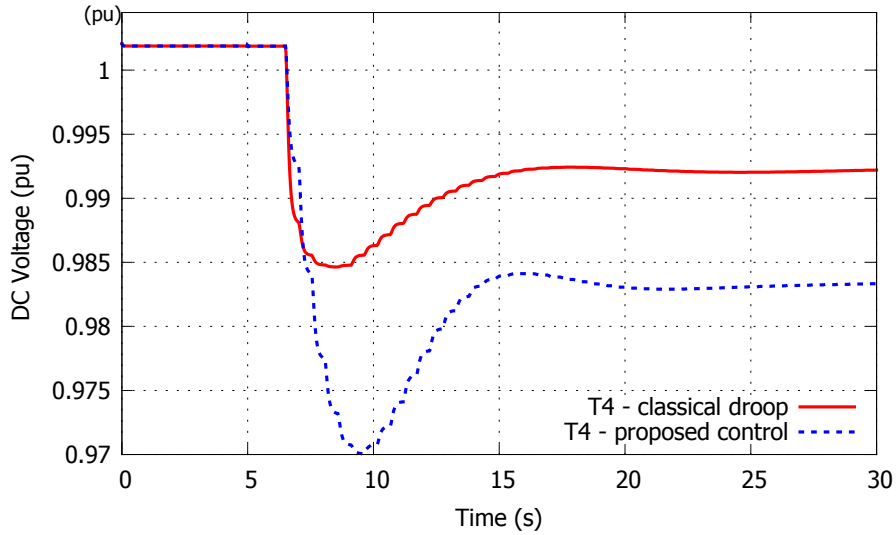

Figure 5.7: Scenario 1: DC voltage at bus DC4

The DC voltage at bus DC4 is shown in Fig. 5.7. The other DC voltages experience similar variations. Clearly, by enforcing the required participation through MPC, the DC voltages of the grid experience larger deviations. However, this is acceptable since these deviations are kept between the specified operating limits.

The control steps (ΔP^{set}) of the proposed controller are shown in Fig. 5.8 for both T2 and T4. The largest corrections are observed immediately after the activation of frequency support. In steady-state, the desired participation has been satisfied, hence the actions calculated by the MPC (i.e. the inputs to the discrete integrator in Fig. 5.3) are equal to zero.

It must be highlighted that the time response of the proposed frequency control is comparable to that of a conventional power plant. This is important in order to limit the impact of the initial disturbance on the West system. Indeed, if faster response was provided (as made possible by power electronics), the West system might experience a larger frequency drop.

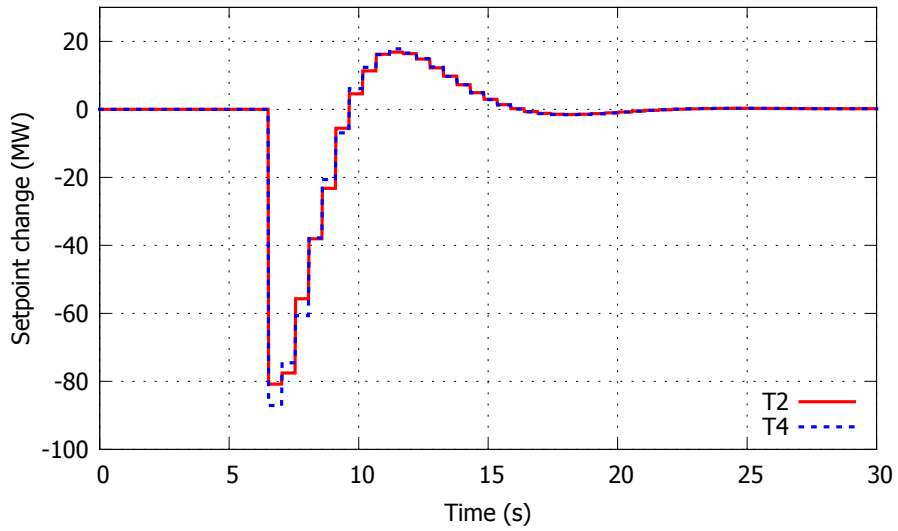

Figure 5.8: Scenario 1: Control steps ΔP^{set} in T2 and T4

Finally, Fig. 5.9 shows, for T4, a plot of the power deviation $P(t) - P(t^\star)$ as function of the frequency change $f - f_N$, superimposed to the dotted line which corresponds to the desired steady-state participation $K_f\,(f - f_N)$. Before frequency control activation, the T4 power does not deviate significantly from its initial value (see horizontal upper part of the trajectory), whereas after its activation, it eventually converges to point A on the frequency droop line, confirming that (5.1) is satisfied. Point B corresponds to the steady state reached with the conventional droop scheme.

Scenario 2

The purpose of this scenario is to demonstrate the safe behavior of the MPC scheme in case of unexpected non-cooperation between the two areas.

It involves the same initial generator outage, but now T3 does not participate in DC voltage control

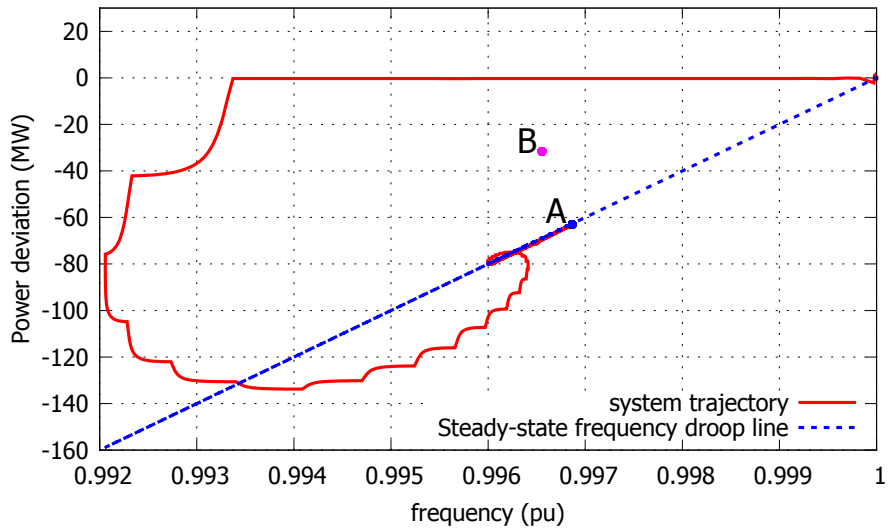

Figure 5.9: Scenario 1: Power deviation vs frequency for T4

as expected. Specifically, it is assumed that T3 is operating in constant power mode ($K_v = 0$). This could be the result of a non-reported action by the transmission system operator of the West system, due to stressed conditions in that system. It must be emphasized that the sensitivity s_v has not been updated to account for this "hidden failure".

After the tripping of g8E, frequency support is activated in T2 and T4 as in the previous scenario. However, the whole power requested by T2 and T4 is now provided by T1 alone. Indicatively, the DC power of T2 is shown in Fig. 5.10, while the same power in Scenario 1 is repeated for comparison. It can be seen that with the conventional control, T2 provides even less support than in Scenario!1. The reason is the larger DC voltage deviation, due to the non-participation of T3, which further reduces the frequency support by T2 and T4. On the contrary, the proposed controller, eventually provides the same power as in Scenario 1, in spited of the failure of T3. The DC voltage at bus DC2 is shown in Fig. 5.11. It can be seen that the proposed MPC-based control leads to a larger DC voltage deviation since it requires a larger change of the power setpoint of T2 in order to satisfy the desired participation. However, when the lower limit is approached, the controller automatically adapts its behavior to avoid further DC voltage degradation. Following the recovery of the East system frequency, the controller removes some of the power it had to inject in the AC system. Hence, the DC voltage recovers and settles inside the allowed operating zone.

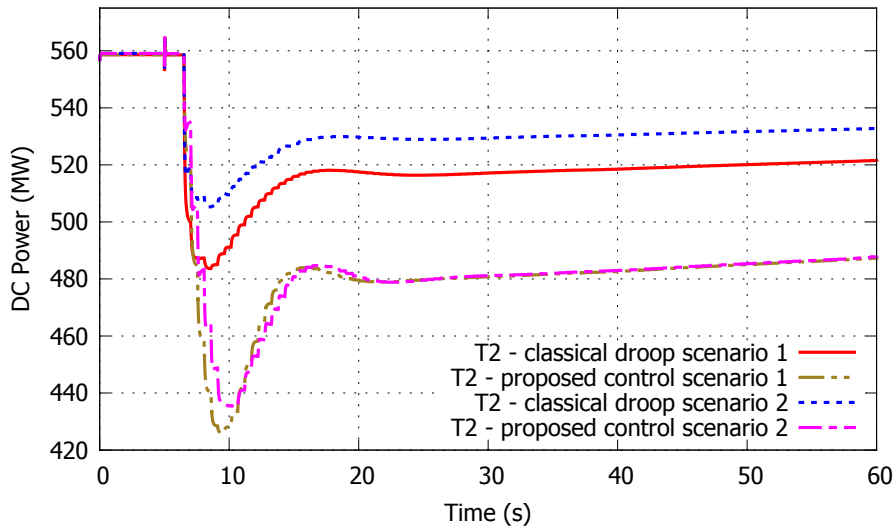

Figure 5.10: Scenario 2: DC power of T2

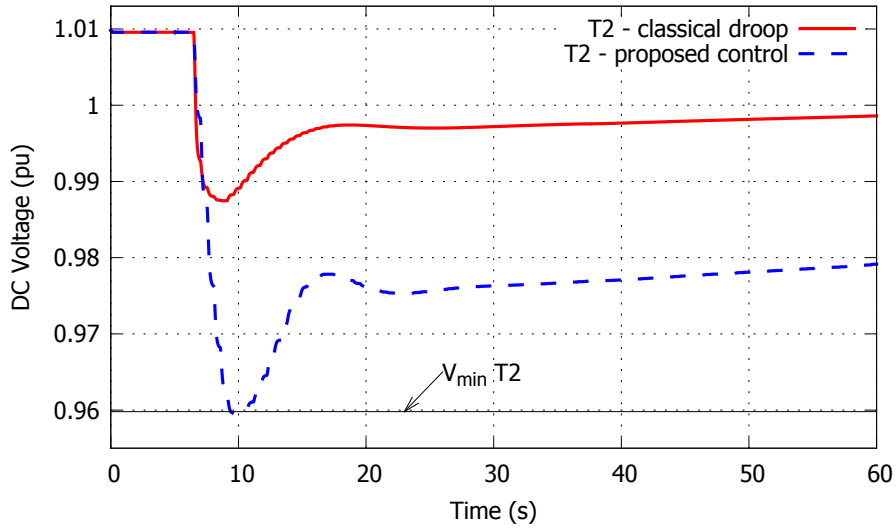

Figure 5.11: Scenario 2: DC voltage at bus DC2

5.3.3 Disturbance in the MTDC system

The following scenarios deal with a disturbance in the MTDC system, i.e. the tripping of terminal T3 at $t = 3$ s. In all cases, this event is followed by a very fast power adjustment of T1, T2 and T4, under the effect of DC voltage droop control. The outage is expected to cause a significant frequency deviation in both AC systems, but in opposite directions. Indeed, since the West system is missing the 843 MW injected by T3, it will experience under-frequency. The East system, on the other hand, will experience over-frequency. Each of the following scenarios relates to a different

outcome:

1. Scenario 3: only T1 is equipped with the proposed MPC control.
2. Scenario 4: only T2 and T4 are equipped with that control.
3. Scenario 5: all remaining terminals (T1, T2 and T4) are equipped with that control.

Scenario 3

When frequency support is activated in T1 only, the system evolves as shown in Figs. 5.12 to 5.14.

Figure 5.12 shows the frequencies of both systems with and without the support by T1. It can be seen that the frequency support activation slightly improves the response in both AC areas.

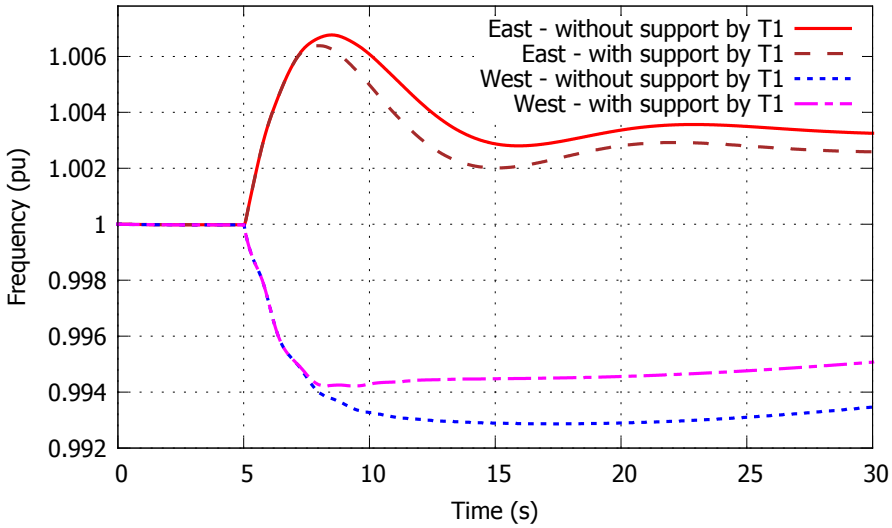

Figure 5.12: Scenario 3: AC system frequencies

The DC powers of the VSCs are shown in Fig. 5.13. Due to DC voltage droop control, the powers of T1, T2 and T4 change rapidly to restore the power balance of the MTDC grid. Then, at $t = 6.5$ s, frequency support is activated in T1. At this point, the choice of the correct reference value $P(t^\star)$ has to be stressed. This value should be recorded after the VSC power has settled under the effect of the DC voltage droop control. Otherwise, the VSC will not provide the desired participation that corresponds to the new configuration of the system. Given that the DC voltage response is much faster than the AC frequency response, it can be assumed that the MTDC grid will have reached steady voltages before the frequency of the AC network leaves the specified deadband. For this reason, it has been chosen to set $P(t^\star)$ to the last power measurement taken before the controller activation.

Finally, the DC voltages at buses DC1, DC2 and DC4 are shown in Fig. 5.14. Following the tripping of T3 they all rise very fast but are promptly stabilized by the DC voltage droop control. However, the DC voltage of T1 settles outside its limit. Therefore, following the activation of frequency support, the controller not only pursues to change the power of T1 in order to satisfy the desired participation, but also to bring the DC voltage below the maximum limit. As expected, the voltage at bus DC1 eventually settles on its upper limit.

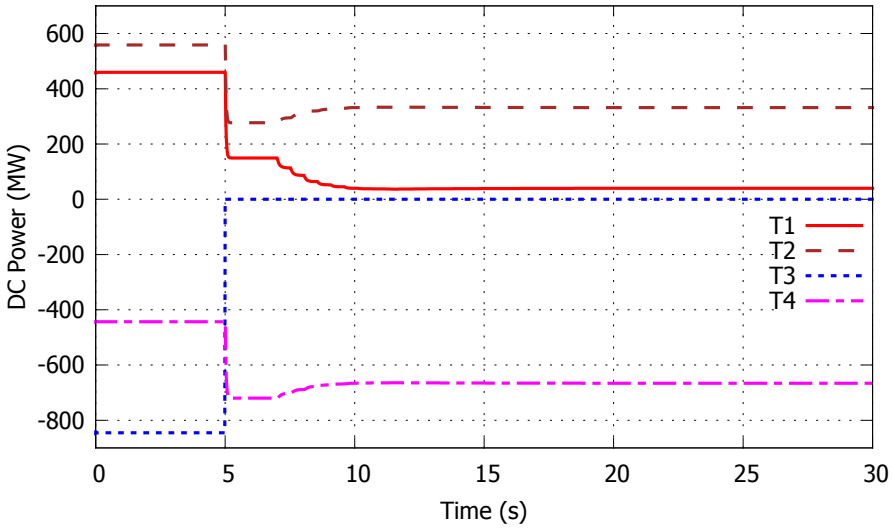

Figure 5.13: Scenario 3: DC power of VSCs

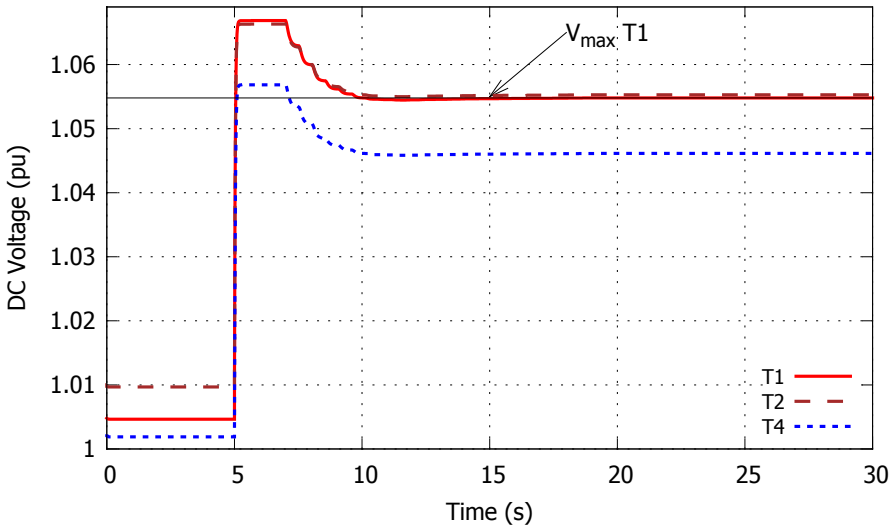

Figure 5.14: Scenario 3: MTDC grid voltages

It fact, in this case the proposed controller automatically provides more power than the amount

specified by the desired droop gain. The reason is that the change of the T1 power setpoint required in order to bring the DC voltage to its limit is greater than the one required to satisfy the desired participation to frequency support. This behavior is beneficial, since providing more power to the West system favors the response of the combined AC/DC system, i.e. it improves the frequency response of both East and West subsystems and the DC voltages in the DC grid. It should be also noted that if the opposite was true, i.e. the change of power setpoint required to satisfy the desired frequency participation was greater than the one needed to bring the DC voltage to its limit, the controller would eventually provide the desired participation and the DC voltage would settle inside its desired operating range. Therefore, it can be concluded that in this case the proposed scheme will provide at least the desired participation.

Scenario 4

Figures 5.15 to 5.17 show the evolution of the system when T2 and T4 are equipped with the proposed controller instead of T1. As in scenario 3, following the tripping of T3, DC voltages are promptly stabilized by the DC voltage droop control, as shown in Fig. 5.15.

However, following the activation of frequency support by T2 and T4 at $t = 6.5$ s, the controllers do not try to support the frequency of East system by increasing their injection in the DC system, because this would aggravate the DC voltage violation. Instead, as shown in Fig. 5.16, they act towards the opposite direction to bring their DC voltages (shown in Fig. 5.15) below their limits.

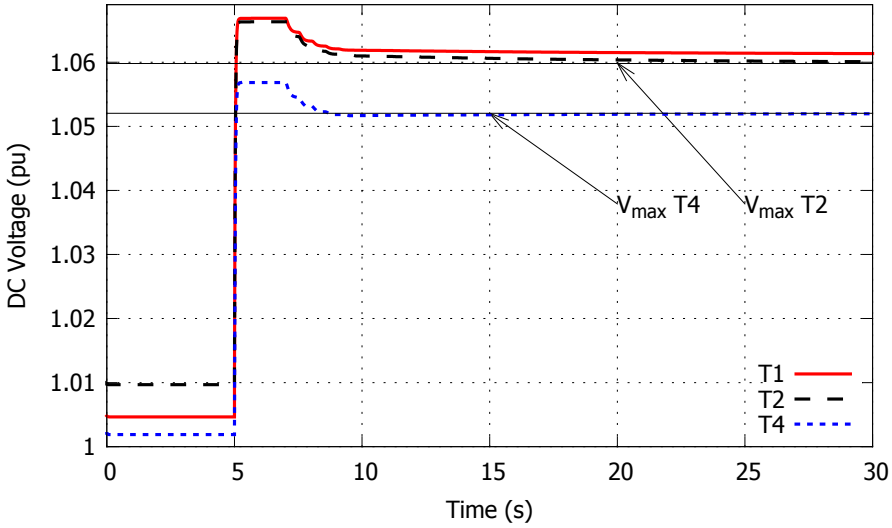

Figure 5.15: Scenario 4: MTDC grid voltages

Figure 5.17 reveals a slow shift of power from T2 to T4. This is because the DC voltage of T4

is restored a little below its limit before the DC voltage of T2 is also corrected. Therefore, since no communication between the VSCs has been assumed, the controller of T4 senses that it could inject some more power in the DC grid. On the other hand, since T2 keeps its DC voltage at the requested limit, it modifies its power setpoint to cover for the power change of T4. Eventually, this power shift stops when both DC voltages are at their limits.

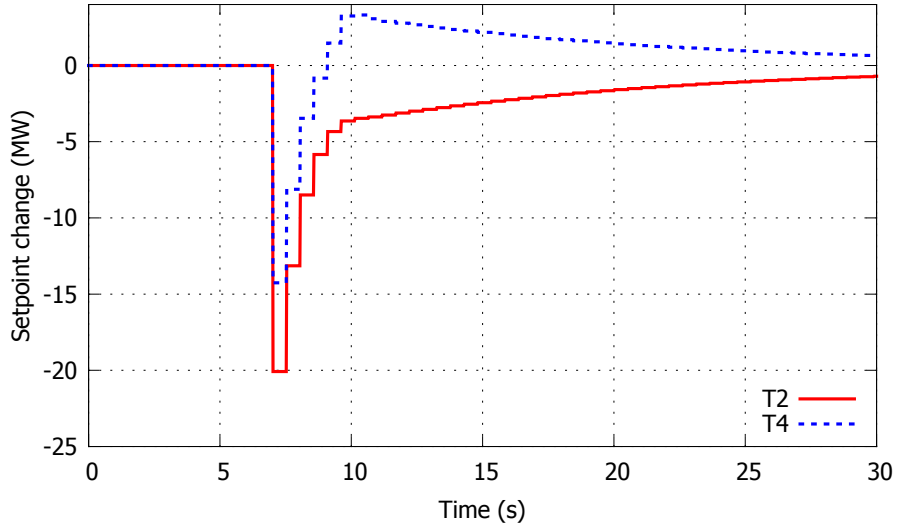

Figure 5.16: Scenario 4: Control steps ΔP^{set} in T2 and T4

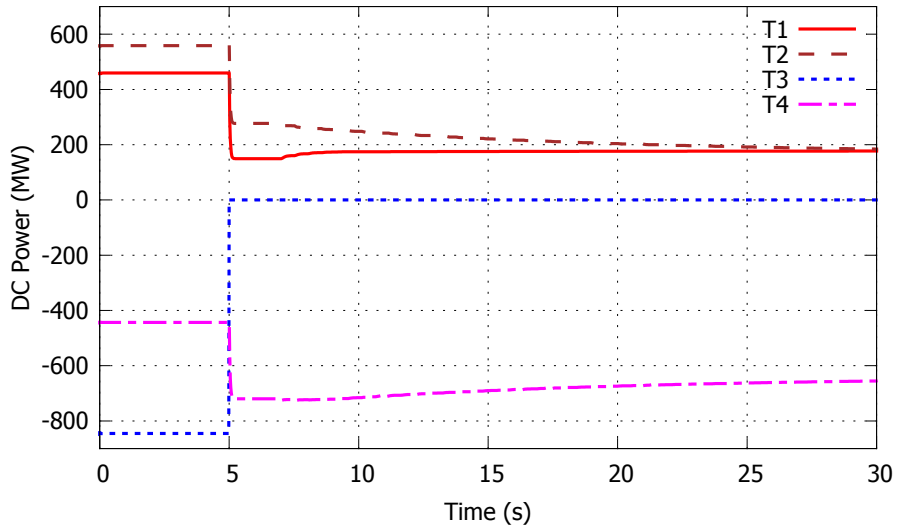

Figure 5.17: Scenario 4: DC power of VSCs

It should be highlighted that if the initial disturbance was not severe enough to cause the DC voltage violation, the frequency controllers would behave as expected, i.e. they would draw power

from the East subsystem to mitigate the frequency increase.

Scenario 5

In this last scenario, T1, T2 and T4 are all provided with the proposed frequency control scheme. Thus, at $t = 6.5$ s, the three VSCs start adjusting their power setpoints, first to restore the DC voltages below their limits, as in scenarios 3 and 4, then to satisfy their desired participatios to frequency support. Thus, initially, all VSCs decrease their injection in the DC grid to correct the DC voltages. This is achieved at approximately $t = 12.5$ s, as shown in Fig. 5.18. Since all DC voltages are restored below their limits, the actions of all controllers are towards satisfying the desired participation to frequency support.

As previously, T1 decreases its power injection into the DC grid, as shown in Fig. 5.19. Furthermore, since the East system experiences over-frequency, T2 and T4 also attempt to increase their power injections into the DC grid. This leads to again increasing the DC voltages of the system, as shown in Fig. 5.18, with the outcome that the maximum DC voltage constraint of T1 becomes active. At the same time, since the DC voltages of T2 and T4 have not reached their limits yet, they keep changing their power output in order to satisfy their own participation to frequency control of the East system, as shown in Fig. 5.19.

Eventually, the system reaches a steady state when the desired participation of T2 and T4 has been satisfied, whereas T1 is operating at its maximum DC voltage limit. It is also noted that eventually T1 provides more power to the West subsystem than specified by its droop gain. As in Scenario 3, this is beneficial since a larger part of the pre-disturbance power exchange between the two areas is restored.

This severe scenario was aimed at demonstrating the ability to preserve DC grid operation even when all VSCs switch to frequency support control mode. Clearly, this situation arises since no communication is utilized and all VSCs aim at supporting frequency. However, the system could be reset (e.g. by the slow, centralized controller of 4) in order to restore the DC voltage near its nominal value, resume normal operation and restore the whole power transfer between the two areas.

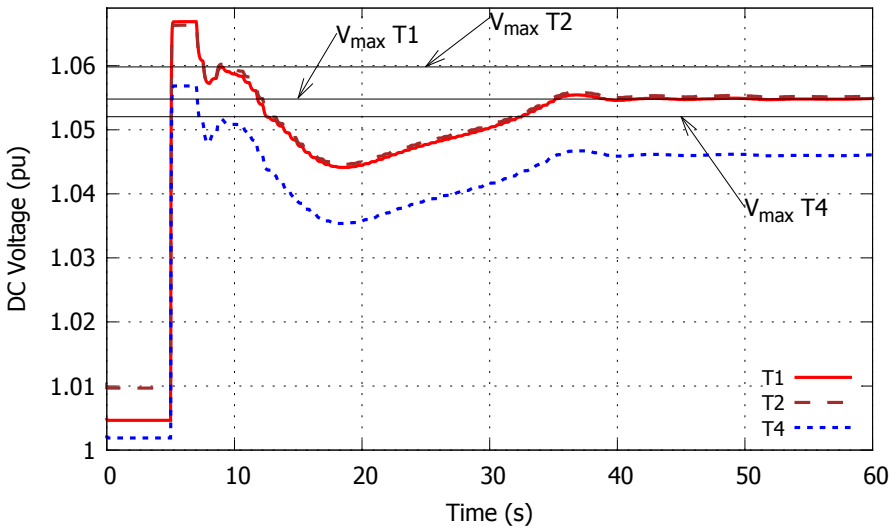

Figure 5.18: Scenario 5: MTDC grid voltages

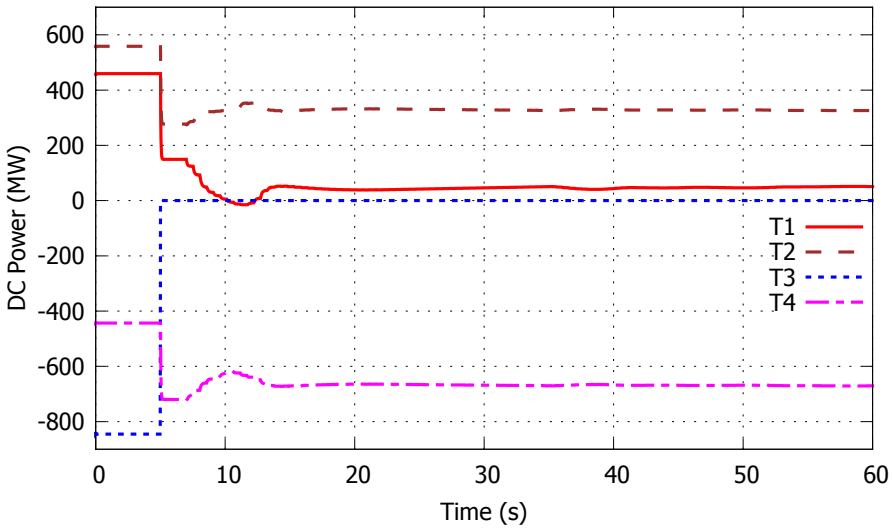

Figure 5.19: Scenario 5: DC power of VSCs

5.4 Scheme 2 - Frequency containment

5.4.1 Overall controller description

The second option for frequency support approaches the problem from a different perspective. Despite the various implementation differences of the methods for primary frequency support in the literature, the main idea remains the same: a frequency droop gain is selected relating

the power of the VSC with the AC frequency deviation, sometimes complemented by an inertia emulation gain to provide some derivative response [FPB17]. This is inherited from AC systems and power plants, where the droop method has been the norm for several decades. However, although the droop control has proven indispensable for continuous regulation of frequency by conventional units (if the small frequency deadband present in many speed governors is ignored), the same does not necessarily hold true for the VSCs. In fact, simply specifying a frequency droop gain prevents from utilizing the VSC maximum capacity in emergency cases, e.g. when an Under-Frequency Load Shedding (UFLS) threshold is approached. Instead, we can think of a more adaptive control scheme that will provide as much support as possible in stressed situations, especially when operating the future AC systems with a lower number of synchronous machines.

A novel possibility for provision of frequency support by VSCs is proposed in this section, refraining from the requirement to select a frequency droop gain, and exploiting the almost instantaneous response of VSCs. The main idea is to provide as much power as required (or as possible) to prevent the triggering of UFLS relays or at least reduce the amount of load shedding. Typically, these relays have multiple shedding steps with various frequency thresholds. For example, in [EE14b] UFLS schemes with a maximum of ten shedding steps between 49 and 48 Hz are described. Avoiding or reducing UFLS can be translated into keeping frequency above the first frequency threshold of the relays. To achieve this, an MPC-based scheme is proposed that changes the VSC power setpoint P^{set} of its P-V characteristic (2.35), as soon as such a violation is predicted.

Clearly, the added control should not jeopardize the operation of the MTDC grid as well the other AC areas. This imposes to obey constraints on the DC voltages, on the rate of change of powers, etc. As for Scheme 1, only local measurements readily available to each VSC are used.

5.4.2 Constrained optimization problem

Instead of a reference trajectory, the objective here is to minimize the total control effort, while satisfying DC voltage, power and frequency constraints. The complete quadratic programing problem at the heart of the proposed controller is described by Eqs. (5.24)-(5.31) hereafter:

$$\min_{\Delta P^{set},\epsilon,\zeta,V,P,f} \sum_{j=0}^{N_c-1} [\Delta P^{set}(k+j)]^2 + w_1 \sum_{j=1}^{N_c} \epsilon^2(k+j) + w_2 \sum_{j=1}^{N_c} \zeta^2(k+j) \tag{5.24}$$

subject to the following linear constraints, for $j = 1, \ldots, N_c$:

$$V^{low}(k+j) - \epsilon(k+j) \leq V(k+j) \leq V^{up}(k+j) + \epsilon(k+j) \tag{5.25}$$

$$P^{min} \leq P(k+j) \leq P^{max} \tag{5.26}$$

$$f^{min} - \zeta(k+j) \leq f(k+j) \leq f^{max} + \zeta(k+j) \tag{5.27}$$

$$\epsilon(k+j), \zeta(k+j) \geq 0 \tag{5.28}$$

$$P(k+j) = P(k+j-1) + \Delta P^{set}(k+j-1) - K_v(V(k+j) - V(k+j-1)) \tag{5.29}$$

$$V(k+j) = V(k+j-1) + s_v \Delta P^{set}(k+j-1) \tag{5.30}$$

$$f(k+j) = f(k+j-1) + r_f(k)T_s + [P(k) - P(k+j)]\, s_f T_s \tag{5.31}$$

The first term in the objective function (5.24) aims to minimize the total control effort. By minimizing the $\mathcal{L}_2$ norm, the overall control effort is distributed throughout the whole control horizon N_c and a smooth response is achieved. Again, the prediction horizon has been taken equal to the control horizon.

Constraint (5.25) specifies that the DC voltage should remain between some security limits V^{low} and V^{up}. These limits evolve with time $k+j$ to bring the voltage progressively inside the desired range defined by V^{min} and V^{max}, as for the first scheme (see also (5.11)). Constraint (5.26) specifies that the VSC power must remain between the values P^{min}, P^{max} corresponding to the capability of the VSC. Constraint (5.27) keeps the AC frequency inside the limits f^{min} and f^{max}. Both constraints (5.25) and (5.27) can be relaxed by making variables ϵ and ζ larger than zero in case of infeasibility. Progressive constraint tightening could be also applied to constraint (5.27), but is not considered here. However, both ϵ and ζ are kept to small values by selecting large weighting factors w_1 and w_2 in the objective function (5.24). Since the DC voltage constraint is critical to avoid VSC tripping or damage, the weighting factors are chosen such that $w_1 \gg w_2 \gg 1$.

Equations (5.29)-(5.31) make up the prediction model. The same model as for the first option is considered here.

The controller operation for $N_c = 3$ steps is illustrated in Fig. 5.20. As long as the MPC does not predict any frequency violation, the first term in the objective function (5.24) ensures that no action is taken. Suppose now that, at time k, the controller receives measurements and identifies that the minimum frequency limit is going to be violated, unless corrective actions are taken. The solution of the quadratic programming problem (5.24)-(5.31) is a sequence of control actions $\Delta P^{set}(k)$, $\Delta P^{set}(k+1), \ldots, \Delta P^{set}(k+N_c-1)$ required to keep the frequency above its minimum value, if possible. The controller then applies the first action $\Delta P^{set}(k)$ and discards the rest of the sequence. At time $k+1$, new measurements are received and the whole procedure is repeated for the updated control horizon. As shown in Fig. 5.20, the updated frequency measurement at $k+1$ differs from the one predicted at time k due to model simplifications, uncertainties, etc. However, the closed-loop nature of the MPC can compensate for such modeling errors.

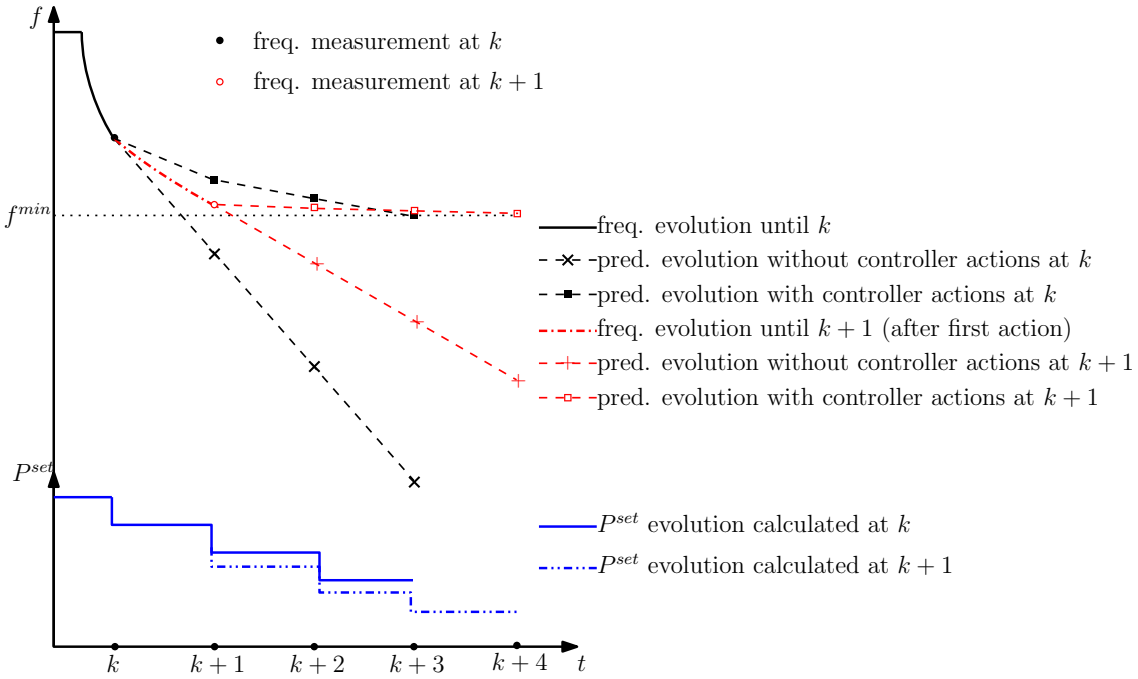

Figure 5.20: Illustrative example of proposed controller operation

It has to be emphasized that the success of the VSC in keeping frequency above this limit cannot be ensured. Instead, the various constraints, in particular (5.25) and (5.26) may prevent this. Nevertheless, the proposed scheme is expected to provide the maximum possible support to the system.

It is also noted that other constraints could be also accommodated by the formulation, such as maximum power available for frequency support, maximum rate of change of frequency, maximum power requested from the other AC area, etc. For simplicity, the formulation has been kept to the minimal set given by (5.24)-(5.31).

5.4.3 Discussion

The first scheme for frequency support required a deadband (see Fig. 5.1) to prevent continuous interactions between the AC areas, and avoid activation of frequency support on all VSCs. The size of the deadband should be sufficiently large to satisfy the above requirements. However, too large a deadband would decrease the effectiveness of the controller, since it would be activated with a larger delay. Thus, a compromise has to be found regarding the size of the deadband.

The formulation of the second scheme removes the need for a deadband. The first term in the objective function (5.24) ensures that no action is taken, unless a violation of a frequency threshold

is predicted (or a DC voltage violation has already been observed). The frequency threshold depends on the UFLS settings, and no particular tuning is required; here it has been simply set above the UFLS threshold with a sufficient margin.

It is expected that the activation of the proposed controller will be somewhat delayed since it has first to wait for the frequency to drop significantly. However, as demonstrated by simulation results, the controller counteracts this delay with a very fast response.

As a final remark, due to the wide range $[f^{min}, f^{max}]$ of this scheme, it is considered extremely improbable that frequency support is activated on more than one VSC simultaneously. This assumption cannot be made for other methods, which use a small frequency deadband, e.g. Scheme 1 presented in Section 5.2 of this thesis or the schemes in [SMS+12, ADPG15]). This characteristic has to be considered by a TSO when performing security assessment of its AC area, and will be further elaborated in Chapter 6.

5.5 Simulation results for Scheme 2

5.5.1 Test system

This second control scheme has been also tested on the system shown in Fig. 5.4.

All distribution buses are assumed to be equipped with UFLS relays. Each relay uses the local frequency calculated from the bus voltage phasor measurements. If the frequency drops below a threshold for more than 100 ms, a fraction of the load connected to the bus is shed. The frequency thresholds and the curtailed blocks for each relay are shown in Table 5.1. The settings were tuned to match this particular version of the Nordic East system, and avoid an overshoot of its frequency following triggering of the relays.

Table 5.1: UFLS relay settings

Level	Threshold (Hz)	Threshold (pu)	% of load shed
1	49	0.98	2.5
2	48.9	0.978	2
3	48.8	0.976	1
4	48.7	0.974	1
5	48.5	0.97	5

The disturbance considered is the tripping of generators g1E and g3E in the Nordic East area. The system response is shown for the following cases:

- Case 1: the VSCs do not respond to frequency deviations, i.e. there is no support from the West area.
- Case 2: all VSCs are equipped with a traditional frequency droop control.
- Case 3: all VSCs are equipped with the proposed MPC-based control (Scheme 2).
- Case 4: same as Case 3, but with adjusted DC voltage limits to investigate the system behavior when a DC voltage constraint becomes active.

5.5.2 Case 1: System response without frequency support

The system is simulated without any support from the MTDC grid. The frequency evolution is shown in Fig. 5.21. Following the disturbance, the system frequency drops rapidly below the threshold of 0.98 pu. Consequently, the first level of all UFLS relays is triggered between 2.8 and 4.3 seconds after the disturbance. Since the first load curtailment was not enough to arrest the frequency decline, the second level of all relays was also triggered. The total load shed is 435.9 MW, i.e. 4.5% of the load of the whole East system.

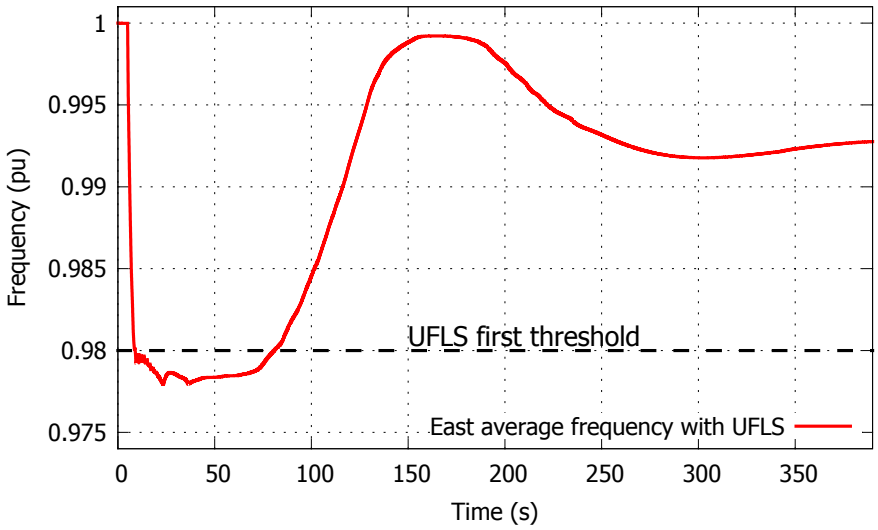

Figure 5.21: Average frequency of East area - Case 1

Following the second load shedding, the frequency of the East area recovers and eventually settles at around 0.993 pu (49.65 Hz). The rather slow response of frequency in Fig. 5.21 is due to the bulk of the imbalance covered by the hydro governors in the North and of the actions of the LTCs. The latter have an indirect impact on frequency response by restoring the voltages (and, thus, the active powers) of the voltage-dependent loads.

5.5.3 Case 2: System response with frequency droop control

The inadequacy of the simple droop control to exploit the available VSC capacity to prevent UFLS is illustrated in this case. To this purpose, a frequency droop control is added to the control structure of all VSCs (except T5). In the following simulation results, a typical value of 20 pu has been selected for K_f.

Figure 5.22 shows the frequency of the East subsystem when VSCs T2 and T4 are equipped with the conventional droop control. The case without load shedding is also shown (red solid line) for comparison purposes. As in case 1, the frequency drops quickly below the UFLS threshold and load shedding takes the necessary countermeasures. In total, 140.6 MW of load are shed, at 14 buses. Following the load curtailment, the East frequency recovers above 0.99 pu.

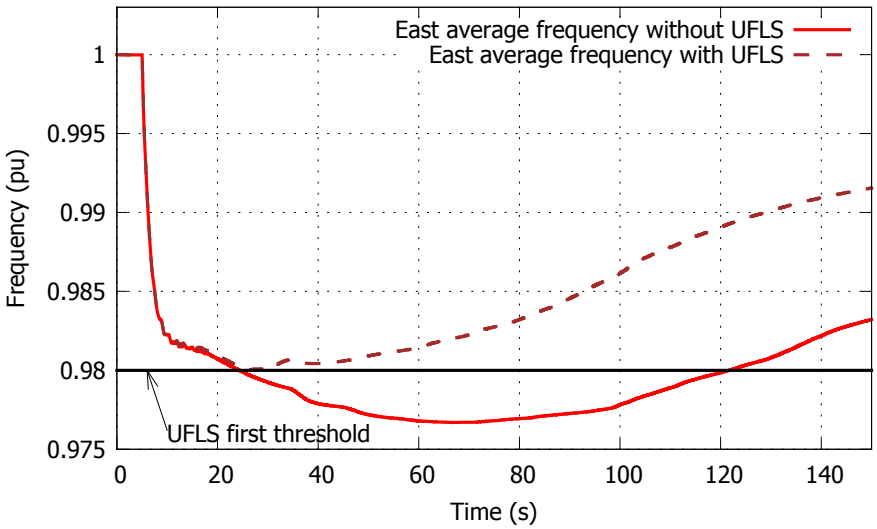

Figure 5.22: Frequency of East area - Case 2

The DC powers of VSCs T1-T4 are shown in Fig. 5.23. As expected, the powers of T2 and T4 decrease following the disturbance (i.e. more power is injected into the East subsystem). The powers of T1 and T3 increase due to DC voltage droop control to restore the power balance in the MTDC grid and stabilize the DC voltages. Following the load shedding after $t = 20$ s and the subsequent restoration of the East frequency, all VSC powers partially return to their initial values.

The DC voltages are shown in Fig. 5.24. The demand of power from the East system leads to a drop of the whole DC voltage profile. The voltages follow the evolution of the East frequency and recover following the UFLS.

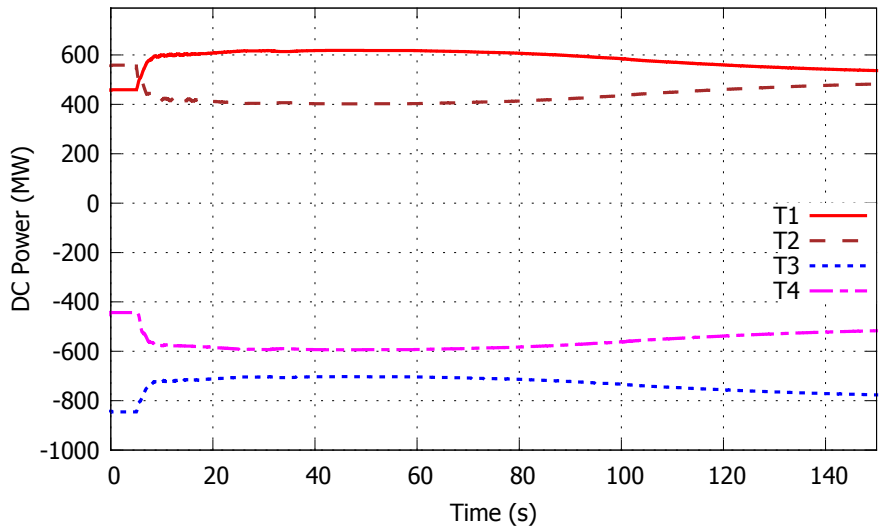

Figure 5.23: VSC DC powers - Case 2

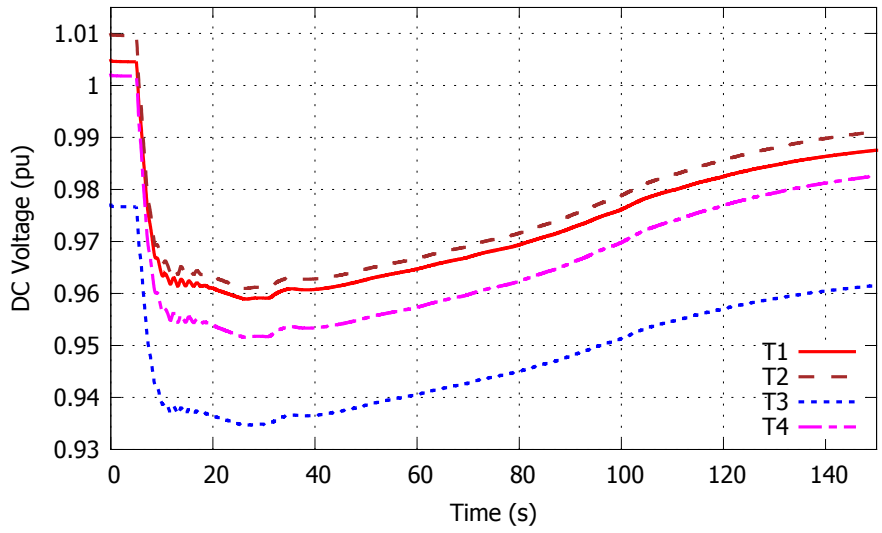

Figure 5.24: MTDC grid DC voltages - Case 2

5.5.4 Case 3: System response with MPC-based control

In this case, all VSCs (except T5) are equipped with the proposed Scheme 2 for frequency support.

The DC voltage limits have been chosen equal to $V^{min} = 0.90$ and $V^{max} = 1.10$. The active power limits of each VSC have been set equal to the VSC nominal active power i.e. $P^{min} = -10$ and $P^{max} = +10$ pu on a 100 MW base. The weighting factors w_1 and w_2 have been selected equal to 10^3 and 10^6, respectively.

The frequency limits in (5.27) are set to $f^{min} = 0.985$ pu and $f^{max} = 1.015$ pu, respectively. In fact, following large disturbances, the local frequency signals include the effect of electromechanical oscillations, which could trigger UFLS in some locations. Therefore, the lower frequency limit f^{min} has been selected slightly higher than the UFLS relays threshold to prevent inadvertent load shedding.

All discrete controllers have a control horizon of $N_c = 4$ steps and a sampling time $T_s = 0.25$ s, which is long enough compared to the time constants of power electronics but short with respect to frequency dynamics. In order to synchronize the VSCs acting on the same AC area, the controls ΔP^{set} are applied at discrete times kT_s ($k = 1, 2, \dots$), assuming that each controller is relying on a GPS-synchronized clock. Each VSC collects the measurements $P^m(k)$, $V^m(k)$, $f^m(k)$ and $r_f^m(k)$ at times $kT_s - 0.05$ s ($k = 1, 2, \dots$) to account for the time needed to solve the optimization problem. The value of the sensitivity s_f for T2 and T4, used in the frequency prediction model (5.31), is calculated using the pre-disturbance inertia of the Nordic East system and is not updated during the simulation.

The system response is shown in Figs. 5.25 to 5.27. To begin with, Fig. 5.25 shows that the proposed controller successfully manages to keep the East frequency above the f^{min} threshold, with just a very small violation, which can be attributed to the approximations embedded in the formulation. Nevertheless, load shedding has been successfully prevented by the fast support from the MTDC grid. Obviously, this increased support is reflected on the West system frequency which experiences a larger drop than with the conventional frequency droop control. However, this drop is acceptable and does not cause any problem in the West area. In this rather extreme case, the total support provided is approximately 620 MW for an initial disturbance of 1300 MW. Furthermore, the proposed scheme is selective since the MPC controllers of T1 and T3 did not react to the frequency drop in the West system.

Figure 5.26 displays the DC powers of VSCs T1-T4. Following the disturbance, the powers of T2 and T4 quickly decrease to support the AC system. As soon as the frequency starts recovering, the controllers identify that enough power has been injected in the AC grid and they stop adjusting the power setpoints of the VSCs. It is interesting to note that T2 provides slightly more power than T4. This is due to electromechanical oscillations affecting the local measurement of the ROCOF, especially the one sensed by T2, which is closer to the disturbance. This difference could be reduced by filtering those measurements.

The DC voltages are shown in Fig. 5.27. They decrease under the effect of the controllers, eventually settling at a value above the lower limit V^{min} involved in the MPC formulation.

It is important to note that, in contrast to Case 2, there is no restoration of the VSC power following the AC frequency restoration. The reason is that the frequency is inside the MPC allowed range

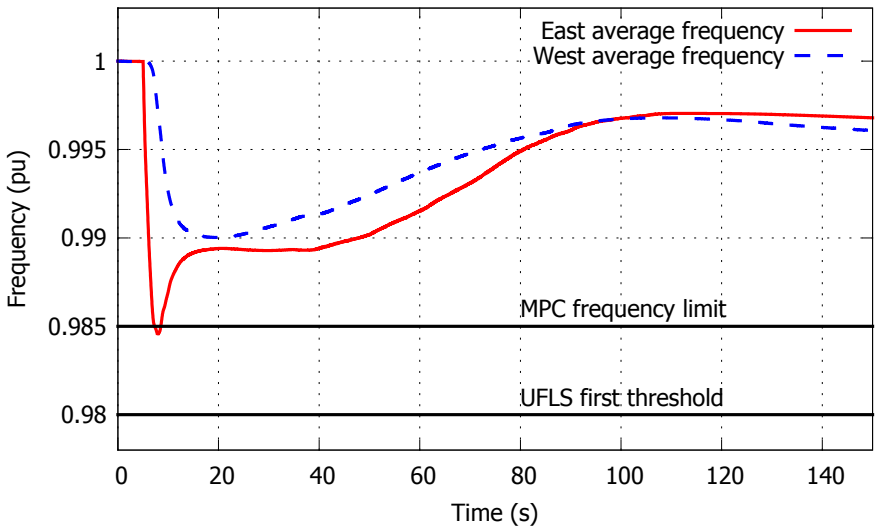

Figure 5.25: Frequency of East area - Case 3

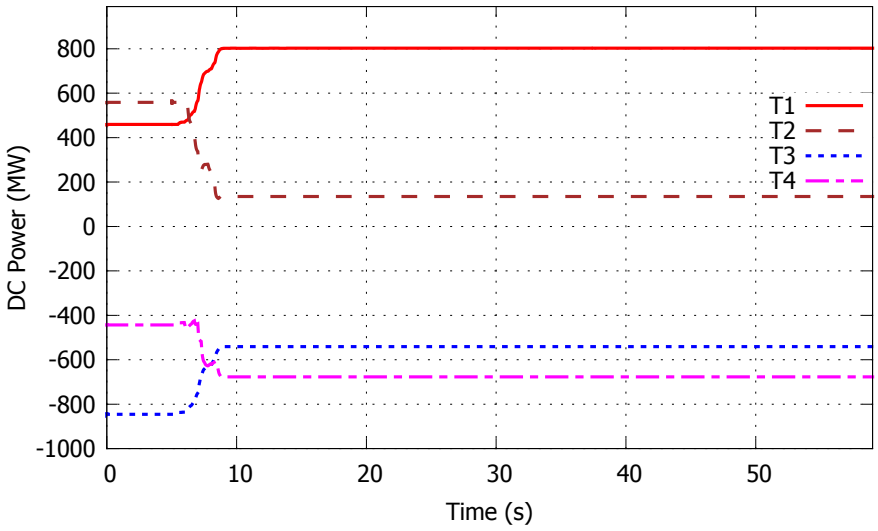

Figure 5.26: VSC DC powers - Case 3

and the controller does not take actions anymore, as can be seen in Fig. 5.26. In addition, due to the absence of any restoration of VSC power, the steady-state frequency of the East area (where the initial generator outage occurred) is higher than the steady-state frequency of the West area. These “drawbacks” of the proposed control method can be easily resolved at a slower time frame by a centralized control of the MTDC grid, as the one proposed in Chapter 4.

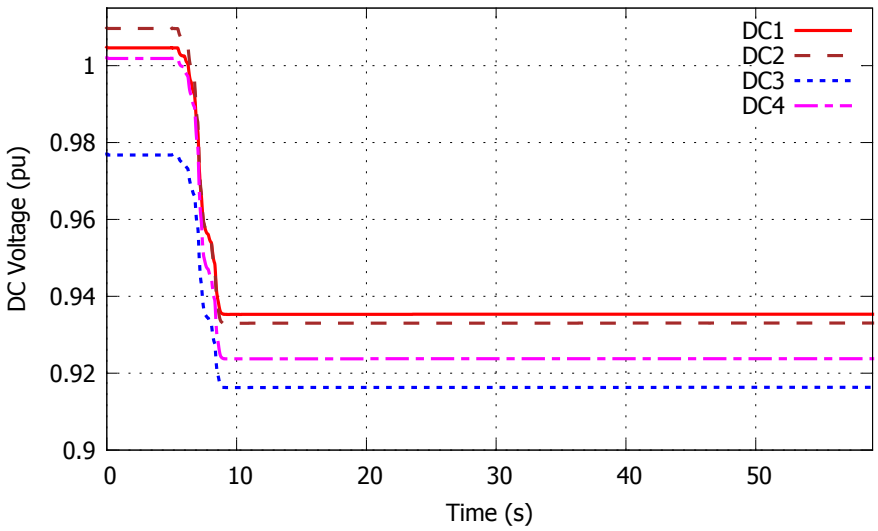

Figure 5.27: MTDC grid DC voltages - Case 3

5.5.5 Case 4: Effect of DC voltage constraints

This last case demonstrates the effect of activating a DC voltage constraint while in progress of supporting frequency.

If the DC voltage of the controller violates its limit, the term corresponding to ϵ in the objective function (4.10) becomes dominant due to the large value selected for the weighting factor w_1. Consequently, the MPC redirects its efforts to keeping the DC voltage above its limit, which is equivalent to switching the VSC to DC voltage control. Obviously, frequency support becomes less effective as long as the DC voltage of the VSC is at (or below) its limit. Furthermore, the DC voltages are not identical throughout the MTDC grid, but depend on the grid topology and the power flows, in contrast to frequency in AC systems. Therefore, assuming that more than one VSCs have been equipped with the proposed controller with the same limits V^{min}, V^{max}, it is reasonable to assume that this constraint will become active in one VSC (not known beforehand) before the others.

Coming back to the test system of Fig. 5.4, two cases are envisaged: (i) one of T1 or T3 reaches first its V^{min} limit while providing the power requested by T2 and T4, and (ii) one of T2 or T4 reaches first its V^{min} limit. Case (i) would only affect the share between T1 and T3 of the total power requested by T2 and T4. Therefore, the effect on the frequency support to the East subsystem would be negligible, and this case is not further detailed. On the other hand, case (ii) could have a significant impact on the overall frequency support. To demonstrate this, the voltage limits of VSCs T2 and T4 only have been set to the more constraining values of $V^{min} = 0.95$ and

$V^{max} = 1.05$ pu.

The frequency in the East system is shown in Fig. 5.28. Initially, the frequency behavior is similar to the one of Fig. 5.25 with only a small violation of the threshold of 0.985 pu. However, the frequency starts declining again and drops below this threshold until approximately 60 s where it slowly recovers above this threshold. The cause for this second frequency decline can be found in Figs. 5.29 and 5.30, showing the VSC DC powers and voltages, respectively. Following the activation of frequency support on T2 and T4, their DC voltages are quickly depressed with T4 dropping below its limit. Therefore, T4 starts drawing a little power to smoothly restore the DC voltage at its limit, leading to the second frequency decline.

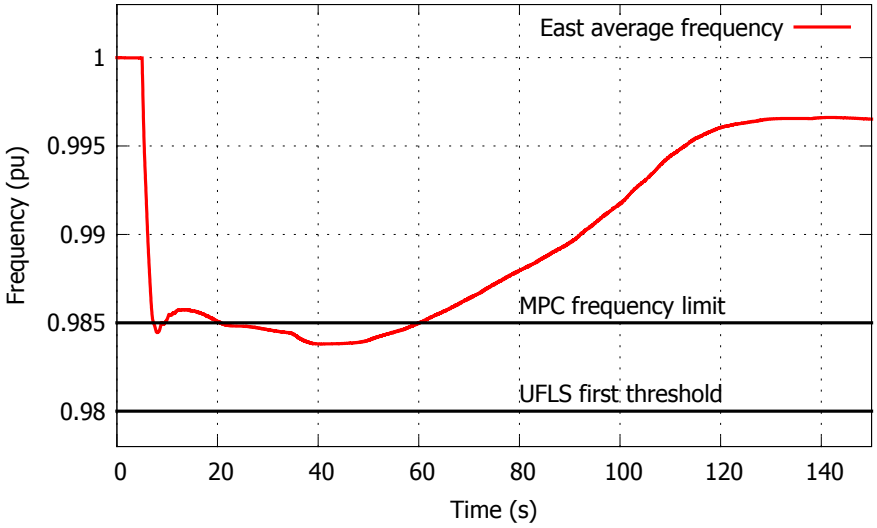

Figure 5.28: Frequency of East area - Case 4

Meanwhile, the DC voltage of T2 is still above its limit; hence, when the frequency drops again below the threshold, T2 starts injecting more power in the AC grid. However, this power is provided mainly by T4, whose behavior has become similar to that of a master VSC, leading to a slow shift of power from T4 to T2. This power shift stops when the voltage of T2 also reaches its minimum value. Clearly, this situation arises since no communication is utilized to inform VSCs that the behavior of the MTDC grid voltages has significantly been altered. However, as mentioned in scenario 5 of the first scheme (where a similar shift of power was observed) the slower centralized controller could restore the DC voltage near its nominal value, thus “unblocking” the VSC whose voltage constraint is active. This in turn would enable to resume the frequency support. Finally, it should be noted that even in this case, UFLS has been successfully prevented.

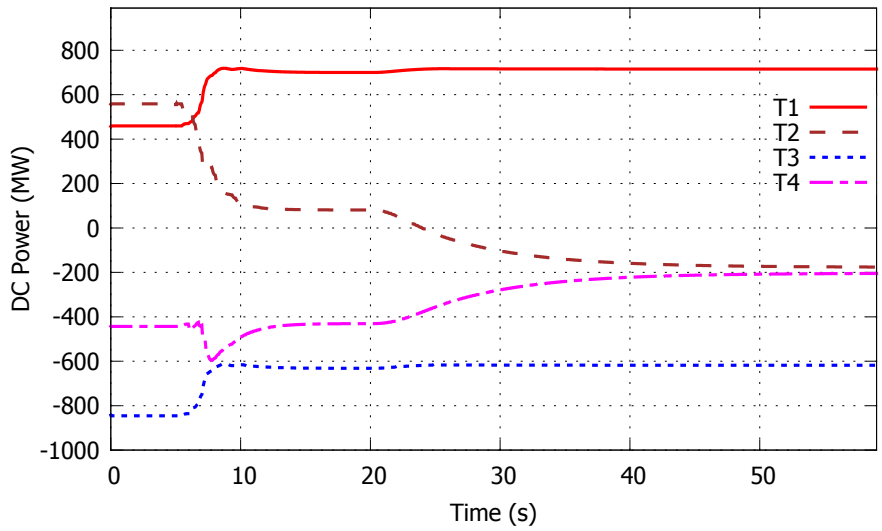

Figure 5.29: VSC DC powers - Case 4

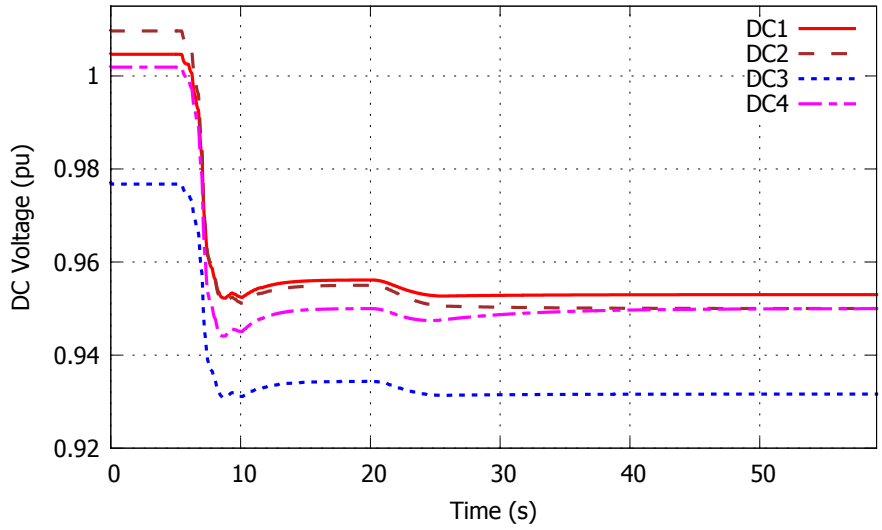

Figure 5.30: MTDC grid DC voltages - Case 4

5.6 Summary

This chapter has discussed two schemes for provision of frequency support among asynchronous areas interconnected through an MTDC grid. Both methods are inspired of MPC in order to explicitly account for constraints, but target different objectives. Relying only on local measurements, each method solves a constrained optimization problem and adjusts the power setpoint of the VSC to satisfy its objective. The latter can be either to provide a desired participation to frequency

support (as defined by a droop gain) or to provide as much power as required (if this power is attainable) to keep the frequency inside limits and prevent UFLS.

Simulation results have shown the effectiveness of the methods in achieving their objectives, while respecting DC grid constraints. The results focused on a test system consisting of two asynchronous AC areas. Nevertheless, the expansion to MTDC grids connected to more areas is quite straightforward.

Chapter 6

Security assessment and control in mixed AC/DC systems

Security assessment is among the main functions of a TSO. This chapter discusses some challenges that security assessment will face due to the integration of MTDC grids and the resulting interconnection of multiple asynchronous AC areas. A conceptual framework is proposed to address these challenges and ensure the security of the combined AC/DC system. The need for cooperation between the various TSOs, and the exchange of relevant information between them is highlighted in order to take advantage of the control flexibility that MTDC grids can provide.

6.1 Introduction

System operation is classified into several states depending on the operating conditions, as shown in Fig. 6.1, inspired of the original reference [DL74] [1].

In "normal" operation, the system is operating with all variables within normal range and without equipment overloading. In this state, the system can be either in the "secure" or in the "alert" state. If it is secure, it is able to withstand predefined "credible" contingencies without violating any of the constraints. The classical "N-1" security rule considers the outage of any single transmission or generation component as a credible contingency. By extension the current operating point is referred to as "N-0". The "alert" state typically arises following a disturbance or a change in the operating condition, e.g. a load increase. In this state the system is still operating with all variables

[1] A similar classification is made in [ENT12, FC78]. In these references, the "normal" state denotes exclusively a secure operating point and not a point without violations of operational constraints in N-0 situations as in Fig. 6.1.

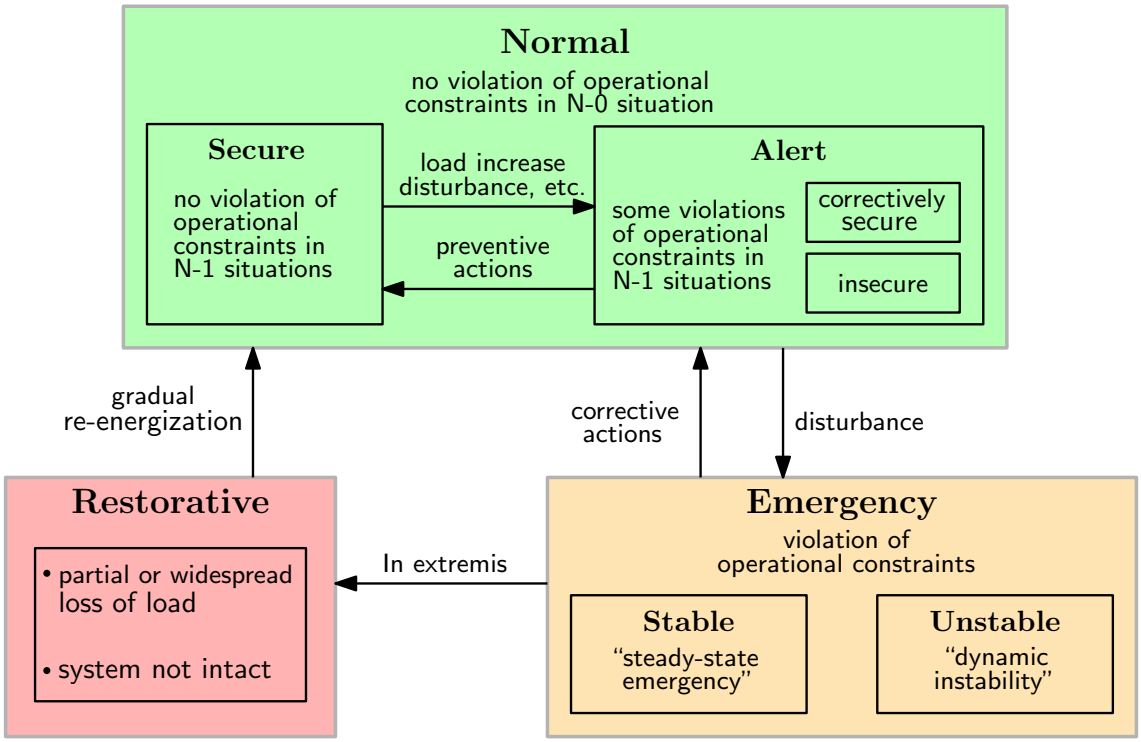

Figure 6.1: Classification of system states [DL74]

within limits, but, it is unable to withstand some contingencies out of a predefined list. It is usually considered that the TSO should take preventive actions (e.g. start new units) in order to bring the system back to the "secure" state, i.e. to comply with the N-1 rule. Alternatively, the TSO could assess whether the system is "correctively secure", i.e. whether there are corrective actions that would bring the system back to the "normal" state, if applied after a contingency occurs. Of course, those actions should be implemented in a time interval compatible with the allowed duration of the limit violation.

Unforeseen contingencies (or foreseen contingencies while the system is in the "alert" state) and extreme events could drive the system to the "emergency" state. In this state the system may experience violation of operational limits and other adverse phenomena, such as interruption of power supply in some zones. As indicated in Fig. 6.1, a system in the "emergency" state could still be stable. In this case, referred to as "steady-state emergency" [DL74], some operational constraints are not satisfied, e.g. some voltages are outside limits or some equipment is overloaded, but they may be tolerated for some time until corrective actions are taken to bring the system back to the "normal", and preferably "secure", state. However, the system could also become unstable and reach the "dynamic instability" condition. Dynamic instability usually takes place in a very short period and remedial actions to restore secure operation have to be taken immediately. If not, the system runs the risk of collapse, resulting in uncontrolled loss of supply in a widespread area

(blackout).

If a blackout has occurred, the system is in the "restoration" state. In this state, the system is no longer intact, but has gone through a partial loss of load and generation. To restore normal operation, the system should be gradually re-energized, with the reconnection of the lost generating units and loads.

One of the main objectives of a TSO is to ensure that the system is secure, i.e. it is not brought to the emergency state in response to credible contingencies. This function is referred to as security assessment. As discussed in [CIG07], it can be classified into Static Security Assessment (SSA) and Dynamic Security Assessment (DSA). The former aims at verifying that the post-contingency operating state of the system (bus voltages, line limits) is inside limits. It assumes that the system transition between the pre- and post-contingency states takes place without any loss of stability. On the other hand, DSA considers also the transition to the post-contingency state, and evaluates whether this transition takes place without losing stability or experiencing unacceptable transients with high impact on the quality of service.

Security assessment can be performed either off-line or on-line. Off-line security assessment has been historically conducted to determine stability limits for forecasted scenarios. Since this requires significant computational effort, the assessment is made well in advance. However, due to the fast changing nature of modern power systems and the improvement of computational tools, many TSOs turned to on-line DSA [CIG07]. To this purpose, several methodologies have been proposed and implemented world-wide. In general, the components of most on-line DSA systems can be divided into the components shown in Fig. 6.2 [CIG07].

Each component serves a different function. The necessary information from the network is collected by the "Measurement" block. This information is used in the "Modeling" and "Computation" components. The former sets up the model of the system for use in the security assessment, including models of the external systems, etc. The latter uses the system model and the information brought by the measurements to compute the system response to contingencies and possibly determine remedial actions. The task "Reporting and Visualization" is to display the results of the security assessment in a simple and meaningful manner, so that the human operators can extract useful information and take appropriate decisions. The "Control" component is in charge of the implementation of the control actions either automatically specified by the "Computation" part or invoked by the operator. Finally, the "Other functions" block concerns other important requirements, such as archiving the whole information for future reference.

Most works have addressed the secure operation of mixed AC/DC grids through optimal power flow calculations. For example, in [WAA+15] the classical Secure-Constrained Optimal Power Flow (SCOPF) formulation performed by the TSO of an AC grid, is extended to combined AC/DC

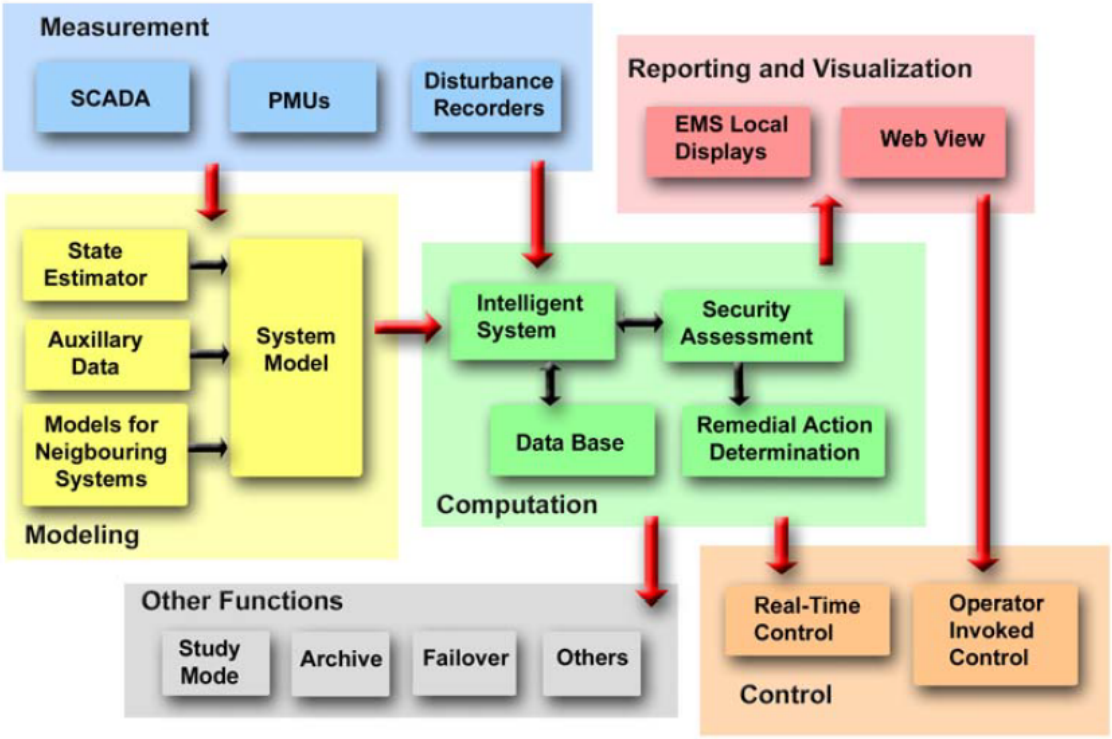

Figure 6.2: The components of an on-line DSA system [CIG07]

grids including DC component outages and control variables. The same spirit is followed in [CDW16] and [TAGS16] where a SCOPF formulation for mixed AC/DC grids including preventive and corrective controls is proposed. The work in [MZL+17] proposed a hierarchical SCOPF using Benders Decomposition for mixed AC/DC grids. A centralized approach for AC/DC OPF is also described in [SKS17] including a model of losses for the VSCs.

In the above cases, SCOPF is intended to be performed in a centralized manner assuming that a single entity is responsible for ensuring the security of the whole system. This is the best option insofar as the MTDC grid is embedded in one AC system operated by one TSO. However, future MTDC grids are expected to interconnect multiple synchronous and asynchronous areas. Solving the combined SCOPF will probably not be feasible, owing to the computational complexity. Therefore, alternatives should be investigated so that the computational burden is not increased prohibitively, the information exchange is minimal and the autonomy of the TSOs is preserved.

In fact, several works proposing distributed or collaborative methodologies for security assessment (or OPF) have been published in the literature, e.g. [WGE07], [HNA+07]. In these works each TSO operates its own system assuming simplified equivalent representations of the external systems and iterating with the other TSOs in order to reach a consensus. This is necessary in

synchronously connected systems since a disturbance in one area can have a significant impact on the rest, possibly raising security concerns if overlooked.

Instead, a distributed OPF involving an MTDC grid was proposed in [IWCA15] with the objective of maximizing social welfare. Three alternatives concerning the operation of the system were discussed. The first consists of a centralized approach, with a single entity having complete knowledge and control of the system. The second assumes the creation of an MTDC grid operator. The third option involves the extension of the area of responsibility of each TSO to include the MTDC grid components directly connected to it. This results in a distributed scheme requiring information exchange between the various TSOs, as well as iterations in order to reach a common solution.

The concept of an independent DC grid operator is also proposed in [GL15]. There, it is defined as "a private or public entity, which coordinates, controls and monitors the operation of the DC transmission system involving one or several power park modules and one or several TSOs". The task of the DC grid operator is to solve an OPF for the DC grid, taking into account voltage and current limits in the pre-contingency operation. In case a contingency has taken place, the OPF is solved again to identify a new operating point without violations.

As already illustrated, MTDC grids can contribute to the security of power systems through corrective control. This thesis has provided examples specifically for frequency support (see Chapter 5) and for long-term voltage stability (see Section 3.1). Since MTDC grids will require significant investment by all TSOs connected to it, all TSOs would expect to benefit from it in terms of security. Thus, the MTDC grid can be considered as a "common asset", i.e. an infrastructure to which all adjacent TSOs have access to request support, if relevant. Furthermore, the fast response of VSCs make them very good candidates for effective post-contingency corrective control. However, conflicts are expected to arise when multiple TSOs want to act at the same time on the MTDC grid, or when the action of one TSO comes to the expense of insecure operation of another AC grid.

To the author's knowledge, apart from [IWCA15] (which did not consider any security criteria), no work in the literature has addressed the problem of identifying corrective actions involving the MTDC grid, when there are conflicts between the various TSOs.

This chapter outlines a general framework to integrate MTDC grids into the existing tools for security assessment of the TSOs. Emphasis is put on the determination of the remedial MTDC grid actions and on resolving possible conflicts between the various TSOs. The focus is on MTDC grids interconnecting asynchronous AC systems, each operated by a single TSO. In reality, multiple TSOs can operate various parts of an AC system. Frameworks for security assessment among synchronous AC areas have already been proposed in the literature (e.g. [WGE07]), and an initial

investigation for synchronous HVDC links has been made in [DV13], where the coordination of multiple HVDC links between synchronous areas during "alert" and "emergency" conditions is discussed. In addition, although there is already significant experience on security assessment of synchronous AC areas (e.g. from the operation of the European interconnection), there is comparatively less material in the literature when asynchronous areas are concerned.

The above are investigated in the rest of the chapter, which is organized as follows: Section 6.2 describes the method for security assessment in all-AC grid. Section 6.3 discusses the challenges brought to security assessment with the integration of MTDC grids. The framework for security assessment of combined AC/DC grids is outlined in Section 6.4 and illustrative examples are offered in Section 6.5. Section 6.6 summarizes the ideas presented in the chapter.

6.2 Security assessment in all-AC grids

Before the introduction of the MTDC grid, each TSO would have the task to assess the security of its own area, i.e. simulate the response of its AC system following each contingency out of a list of credible contingencies. If the post-contingency state is not acceptable, remedial actions have to be contemplated that would mitigate the effects of the disturbance and alleviate any possible violations. Such remedial actions could involve generation rescheduling, compensation switching, startup of fast units, change of topology, transformer tapping and, in the very last resort, load shedding. The remedial actions can be preventive (i.e. pre-contingency) or corrective (i.e. post-contingency, if the contingency occurs). Preventive actions inflict a direct increase in operating costs since they cause deviation of the operating point of the system from its previous (presumably "optimal") state. An SCOPF can be used in order to identify them. In contrast, corrective actions do not increase operating costs, unless the contingency actually occurs. Under the pressure of the electricity market, there is a trend for the TSOs to "amend" the original strict definition of a secure system by operating it at a "correctively-secure" point [CMP+11].

One further option for the TSO would be to identify the cheapest post-contingency remedial actions. However, this is not so obvious since it requires having prices at an unknown operating point in the future; indeed, it is not known when and if the contingency will actually occur. In fact, when facing an emergency situation, the cost of corrective actions plays relatively little role, the highest priority being to stop system degradation. Therefore, the focus of this work is on simply identifying whether there is at least one acceptable post-contingency corrective control. More precisely, any post-contingency corrective action will be considered acceptable provided it does not entail shedding load.

This can be described in more formal, mathematical terms as follows. Let k be the number of a

harmful contingency causing the system to be insecure. Whether the system is correctively secure can be found by searching for a solution to the optimization problem:

$$\min_{\Delta \boldsymbol{u}_k} ||\Delta \boldsymbol{u}_k||^2_{\boldsymbol{W}} + ||\Delta \boldsymbol{u}_k^{ls}||^2_{\boldsymbol{W}_{ls}} \tag{6.1}$$

subject to the following system and control constraints

$$\boldsymbol{g}_k(\boldsymbol{x}_k, \Delta \boldsymbol{u}_k, \Delta \boldsymbol{u}_k^{ls}) = \boldsymbol{0} \tag{6.2}$$

$$\boldsymbol{h}_k(\boldsymbol{x}_k, \Delta \boldsymbol{u}_k, \Delta \boldsymbol{u}_k^{ls}) \leq \boldsymbol{L}_k \tag{6.3}$$

$$\left|\Delta \boldsymbol{u}_k^{ls}\right| \leq \overline{\Delta \boldsymbol{u}_k^{ls}} \tag{6.4}$$

$$|\Delta \boldsymbol{u}_k| \leq \overline{\Delta \boldsymbol{u}_k} \tag{6.5}$$

where $\boldsymbol{x}_k$ is the post-contingency state of the system and $\Delta \boldsymbol{u}_k$ the post-disturbance corrective control actions. $\boldsymbol{W}$ is a diagonal positive-definite matrix that assigns a weighting factor to each control action. The term $\Delta \boldsymbol{u}_k^{ls}$ corresponds to load shedding actions, which are heavily penalized through matrix $\boldsymbol{W}_{ls}$.

The objective (6.1) is the minimization of the total control effort. No specific weight tuning is assumed since the objective is not to find the cheapest solution but to identify if there is at least one acceptable solution. Therefore, all corrective actions except load shedding could have the same weight.

Constraints (6.2) and (6.3) enforce the feasibility of the post-contingency post-control state. A static formulation has been considered here, but integration of dynamic aspects should be envisaged. The equality constraint (6.2) represents the AC power flow equations in the post-contingency operation. The inequality constraint (6.3) includes the physical limits of the various components, in particular operational bounds on branch currents and voltage magnitudes. These limits are gathered in vector $\boldsymbol{L}_k$. Constraints (6.4) and (6.5) avoid unrealistic control adjustments, by specifying the upper bounds $\overline{\Delta u_k^{ls}}$ and $\overline{\Delta u_k}$. They may account for the time taken to implement the corrective actions.

If, for the contingency of concern, the total load shedding is below a threshold, then the system is flagged as correctively secure for that contingency.

Note that several solutions of the above optimization problem, each for a different selection of matrix $\boldsymbol{W}$, may be acceptable. Nevertheless, we assume that it is enough to find one of them to assess the system as correctively secure for the contingency of concern.

6.3 Challenges of security assessment with an MTDC grid

Let us consider the generic system of Fig. 6.3 consisting of M asynchronous AC areas connected to the same MTDC grid including N VSCs ($N \geq M$). Each area can be connected to the MTDC grid through one or more VSCs.

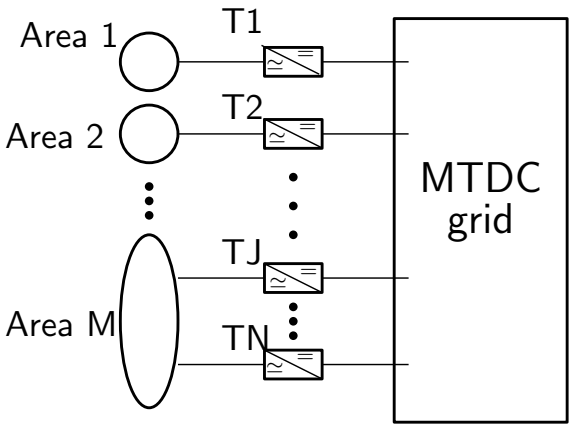

Figure 6.3: Generic system of M areas and N terminals

In order to encompass the MTDC grid in the security assessment, some modifications of the previous framework have to be made. The most significant ones concern the system model, the candidate remedial actions and the update of the list of plausible contingencies, as discussed next.

6.3.1 Modeling requirements for security assessment

The definition of an appropriate system boundary plays a significant role when performing security assessment. The main idea when identifying a boundary is to keep enough detail so that the response of the system model is not significantly modified when replacing what is beyond the boundary by a much simpler model. The part of the model encircled by the boundary that belongs to the external system is referred to as a buffer zone. Specifying a very small buffer zone could lead to loss of important information, whereas a widespread zone would increase prohibitively the computational cost. For example, in [WFGV17] the boundary is extended to include a buffer zone around the studied area. This allows retaining its impact on the voltages of the system under concern, hence providing more accurate results.

As mentioned at a few places in this thesis, a unique feature of HVDC connections between asynchronous AC areas is that they act as "firewalls" preventing the propagation of the effects from one side to the other, unless a control action changes the power flow in the HVDC grid. The boundary used in the AC system has to be adjusted accordingly.

Let us come back to the system of Fig. 6.3. Each AC TSO has to select the part of the system that will be modeled in detail, in addition to its own area. For a given TSO - say the one of Area 1 - three options can be envisaged, shown in Fig. 6.4:

1. Option A: the model includes only Area 1 and the part of the HVDC grid directly connected to that area.
2. Option B: the model includes Area 1 and the complete HVDC grid.
3. Option C: the whole AC/DC system is modeled in detail.

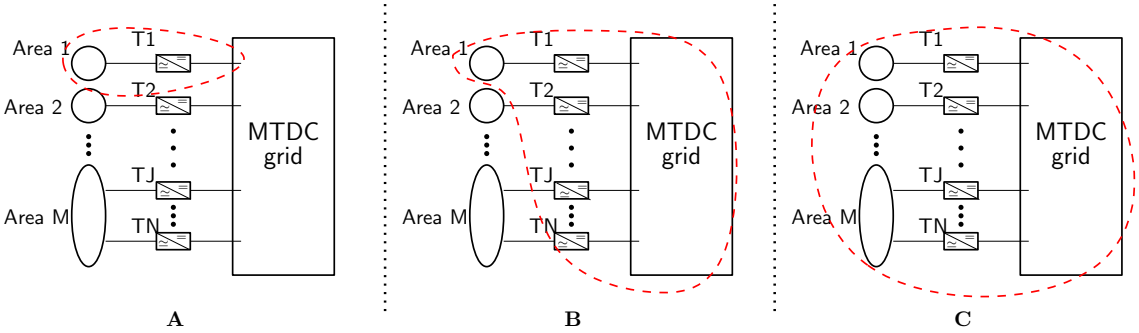

Figure 6.4: Possible boundaries for security assessment

Obviously, Option C provides the best possible accuracy. However, the computational complexity of security assessment is dramatically increased due to (i) the larger size of the system model and (ii) the number of possible contingencies/scenarios that have to be assessed.

Therefore, a choice has to be made between options A and B. The size of the future MTDC grids in terms of number of buses is not expected to be large. Thus, the difference in complexity between both options can be considered negligible. Keeping the whole MTDC grid (Option B) in the model facilitates the simulation of HVDC grid control schemes, while choosing boundary A requires to identify appropriate models for the DC grid response and control schemes, with insignificant gain in computation speed.

For the above reasons, it seems appropriate for a TSO to follow Option B and represent the entire MTDC grid together with its own AC system in its security assessment.

6.3.2 Representation of external AC systems

The representation of the external systems, i.e. the systems outside the selected boundary, is important for two main reasons: (i) to take into account their impact on the response of the system under concern, and (ii) to ensure that the negative effects of a disturbance do not propagate to the external systems.

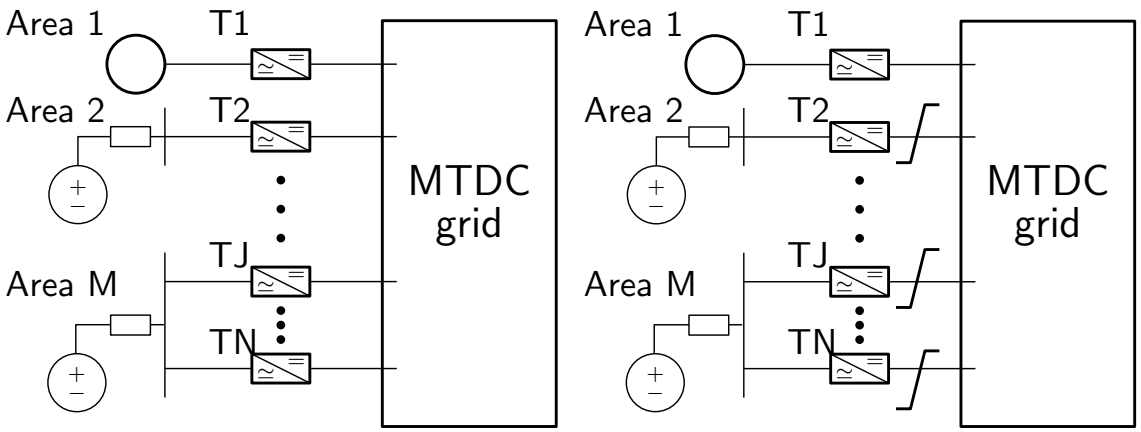

(a) Thévenin equivalents

(b) Thévenin equivalents with VSC limits

Figure 6.5: Representation of external AC systems

Several methodologies have been proposed in the abundant literature for identifying external equivalents in AC interconnected systems (e.g. [FLB07, WV17, FGWV09] and their references). However, due to the firewall property of HVDC connections, the responses of two asynchronous AC systems are coupled only through the MTDC grid controls that can alter the power transfer between both areas. For example, such controls are the frequency support of Chapter 5, and the emergency control scheme against long-term voltage instability illustrated in Section 3.1.

A first step would be to completely neglect the dynamics of the external systems by replacing each one by a Thévenin equivalent, as sketched in Fig. 6.5a. This representation could be sufficient for moderate changes in the power transfer through the MTDC grid, i.e. when the change has a little impact on the power balance and/or the power flows in the external AC system.

However, the dynamic response of the external AC system can have an impact on the response of the MTDC grid. An example has been demonstrated in Section 5.2, where it was shown that if frequency support is activated in both asynchronous AC systems, the participation of the MTDC grid to frequency support differs from the expected one. Not taking into account such dependencies could lead to an optimistic assessment of the scenario.

One option would be to replace the external AC systems by dynamic equivalents that approximate their behavior. However, such models should be properly updated to provide a reasonable fitting to the original system. The representation proposed here consists of a simple Thévenin equivalent complemented with upper and lower limits on the deviation of a VSC power from its operating point, as sketched in Fig. 6.5b. Violation of a VSC limit would result in unacceptable behavior of the AC area to which it is connected. Each TSO should receive the limits on all VSCs, and determine the corrective actions so that these limits are satisfied. The calculation of such limits is rather straightforward when an AC area is connected to the MTDC grid through a single VSC.

However, when two or more VSCs are involved (e.g. Area M in Fig. 6.5b), this calculation is not obvious.

The development of a grid code could be considered, which would oblige a TSO to provide and update in regular intervals the values of the above limits. ENTSO-e has already provided a list of requirements that a DC network would be committed to provide (e.g. fault ride-through, frequency support, etc.) [EE14a]. This could be complemented by requirements from the AC TSOs towards the MTDC grid. For example, the grid code could include a pre-specified short-circuit capacity at the point of connection of the VSCs, or that the AC system should tolerate a fast change of power of the VSC for support to the other AC areas.

The selection of the appropriate representation depends on various criteria, one of which is the controls chosen for the MDTC grid. For example, if a simple frequency support scheme based on $P-f$ droop is used, an equivalent dynamic model of frequency dynamics would be a good option. Instead, if the frequency support scheme of Section 5.4 is considered, a simplified representation with limits on the VSC power deviation would suffice.

6.3.3 Contingency list

MTDC grids are expected to carry large amounts of power over long distances. Therefore, a disturbance in an MTDC grid can have a significant impact on the surrounding AC systems and should be contemplated in the security assessment. MTDC grid disturbances mainly include:

- tripping of a converter station (or one pole of a bipolar configuration).
- Tripping of a DC branch (line or cable). This could result, for example, from selective isolation after a DC fault [HL17].
- Loss of a part (or even the whole) MTDC grid for a short period of time. As discussed in [HL17], outage of a part of the HVDC grid could result from non-selective or partially selective DC fault clearing. If a non-selective fault clearing strategy is adopted, the whole MTDC grid is shut down temporarily. Then, the faulted component is isolated and the whole system is restarted. Instead, the partially selective strategy preserves a healthy part of the MTDC grid, whereas the rest is shut down temporarily until the faulted component is identified and isolated.

The DC disturbances considered here are outages of either a converter station or an individual DC branch assuming selective fault clearing, without simulation of the DC fault.

This list of DC contingencies is added to the list of AC contingencies that have to be considered in the security assessment.

6.3.4 Remedial actions

As shown in Fig. 6.2, the "Computation" component of the DSA involves the determination of remedial actions, after the security assessment has identified some contingencies as harmful.

The possibility of using the MTDC grid in the remedial actions must definitely be taken into consideration. Indeed, VSC-based MTDC grids offer the possibility of fast control and can be used effectively in post-contingency situations. The cost of these actions will depend on various factors. For instance, redirection of power between two VSCs could come at little cost, if they are connected to the same area, or could be expensive if the power exchange with the neighboring areas is affected.

All three levels of the hierarchical control structure detailed in Chapter 4 could be used for the actuation of corrective controls. The fast automatic schemes should be local with no or limited communication in order to provide fast response (e.g. frequency support). When this is not possible because wide-area information is required (e.g. long-term voltage instability) the control action could be applied through the secondary or tertiary level. Since in emergency conditions the objective is to stabilize the AC system, the N-1 MTDC grid criterion can be temporarily relaxed by bypassing the tertiary level and activating the control action directly through the secondary control. The security of the MTDC grid can be reinstated after the emergency has been dealt with. Note that the response time of the MTDC grid controls should be also taken into consideration. Having a full view of the MTDC grid and its controls would enable each TSO to also take these dynamic aspects into account.

A clear distinction can be made between remedial actions for AC and DC contingencies. It is reasonable to assume that following an AC contingency, only one TSO requests corrective actions from the MTDC grid, since the probability of two independent AC contingencies occurring at the same time in different AC areas can be considered negligible. However, a DC contingency may lead to a situation where more than one TSO requests support from the MTDC grid. These actions will probably be conflicting. Therefore, a way to solve (or avoid) these conflicts should be contemplated. An example of such conflict has been already presented in Section 5.3.3, where following the tripping of a VSC, frequency support was requested by both Nordic East and Nordic West areas.

6.4 Security assessment of AC/DC systems

6.4.1 General framework

The framework outlined hereafter assumes that all TSOs are willing to cooperate, exchange information, and do their best efforts to ensure the security of the combined AC/DC system. As shown in Fig. 6.6, it relies on the existence of a coordinating entity, referred to as "DC TSO". The DC TSO exchanges information with all connected AC TSOs in order to coordinate them and resolve conflicts[2].

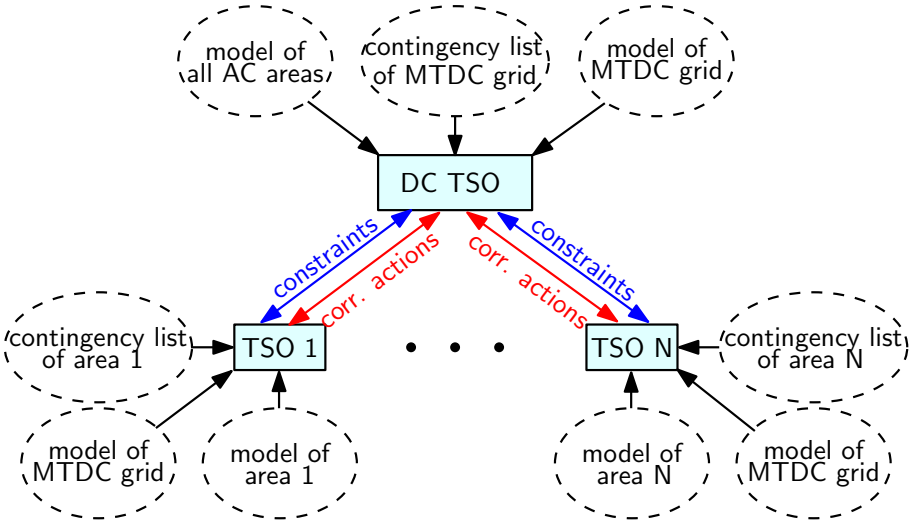

Figure 6.6: Framework for security assessment of AC/DC system

The AC TSOs have a model of their own AC system and the MTDC grid, and perform security assessment taking into account constraints they receive from the DC TSO about the other AC areas. Instead, the DC TSO has a model of the whole AC/DC system, and it performs security assessment of the complete system, but for the MTDC grid contingencies only. Although the model used for the security assessment by the DC TSO would be significantly larger (i.e. inside boundary C in Fig. 6.4), the number of DC contingencies to be investigated would be small. This allows to perform security assessment with a full view of the system without prohibitive increase in computational complexity.

The different cases for AC and DC contingencies are further discussed in the following.

[2]Its role bears similarity with that of a regional security coordinator, such as CORESO [ENT]

6.4.2 AC contingencies

First, the case of an AC contingency is considered. As mentioned before, propagating the effects of a disturbance from one area to the others has to be avoided.

For the i-th TSO, an optimization problem similar to the one described by Eqs.(6.1)-(6.5) can be considered, with the addition of DC grid controls (the subscript k relative to contingency k is dropped to simplify the notation):

$$\min_{\Delta \boldsymbol{u}_i, \Delta \boldsymbol{v}_i, \Delta \boldsymbol{u}_i^{ls}} ||\Delta \boldsymbol{u}_i||^2_{\boldsymbol{W}_u} + ||\Delta \boldsymbol{v}_i||^2_{\boldsymbol{W}_v} + ||\Delta \boldsymbol{u}_i^{ls}||^2_{\boldsymbol{W}_{ls}} \tag{6.6}$$

subject to:

$$\boldsymbol{g}_i(\boldsymbol{x}_i, \Delta \boldsymbol{u}_i, \Delta \boldsymbol{v}_i, \Delta \boldsymbol{u}_i^{ls}) = \boldsymbol{0} \tag{6.7}$$

$$\boldsymbol{h}_i(\boldsymbol{x}_i, \Delta \boldsymbol{u}_i, \Delta \boldsymbol{v}_i, \Delta \boldsymbol{u}_i^{ls}) \leq \boldsymbol{L}_i \tag{6.8}$$

$$\left|\Delta \boldsymbol{u}_i^{ls}\right| \leq \overline{\Delta \boldsymbol{u}_i^{ls}} \tag{6.9}$$

$$|\Delta \boldsymbol{v}_i| \leq \overline{\Delta \boldsymbol{v}_i} \tag{6.10}$$

$$|\Delta \boldsymbol{u}_i| \leq \overline{\Delta \boldsymbol{u}_i} \tag{6.11}$$

where $\Delta \boldsymbol{v}_i$ denotes a control action on a converter and functions g_i and h_i now also involve those controls. The subscript i denotes a control action calculated by TSO i. The diagonal entries of $\boldsymbol{W}_u$ and $\boldsymbol{W}_v$ are the weighting factors for AC and DC control actions, respectively. The updated vector $\boldsymbol{L}_i$ includes also the physical and operational bounds of the DC equipment.

Since the MTDC grid is also included in the model of TSO i, the vector $\Delta \boldsymbol{v}_i$ leads to modifying the DC grid power flows. If the external systems are simply replaced by Thévenin equivalents (as in Fig. 6.5a), then the resulting DC grid power flows are only limited by the MTDC grid constraints and the VSC ratings. However, the MTDC grid actions have to be approved by the other TSOs. In accordance with the framework shown in Fig. 6.6, TSO i has to inform the DC TSO of its corrective MTDC actions. Based on this information, the DC TSO evaluates whether those actions cause a problem in the other AC areas. If not, the corrective actions are accepted and the i-th AC area is correctively secure with respect to the contingency of concern. Otherwise, the DC TSO computes and sends back to the i-th TSO constraints on the available MTDC grid actions, to be added to its security assessment model, formally:

$$\boldsymbol{h}_i^{th}(\Delta \boldsymbol{v}_i) \leq \boldsymbol{L}_i^v \tag{6.12}$$

where (6.12) includes the VSC limits L_i^v set by all external AC areas on the MTDC grid actions available to TSO i, as discussed in Section 6.3.2.

To avoid performing twice the security assessment for the contingencies requiring actions from the MTDC grid, the DC TSO could update and post the constraints in real time. Therefore each AC TSO could incorporate them directly in its security assessment.

6.4.3 DC contingencies

The assessment of MTDC grid contingencies is performed by the DC TSO. Since it has a full view of the system this analysis is rather straightforward and the corrective actions can be identified by solving the following optimization problem, which minimizes the total control effort over all AC areas:

$$\min_{\Delta \boldsymbol{u}, \Delta \boldsymbol{v}, \Delta \boldsymbol{u}^{ls}} ||\Delta \boldsymbol{u}||^2_{\boldsymbol{W}_u} + ||\Delta \boldsymbol{v}||^2_{\boldsymbol{W}_v} + ||\Delta \boldsymbol{u}^{ls}||^2_{\boldsymbol{W}_{ls}} \tag{6.13}$$

where $\Delta \boldsymbol{u} = [\Delta \boldsymbol{u}_1 \ \dots \ \Delta \boldsymbol{u}_N]$ and $\Delta \boldsymbol{u}^{ls} = \left[\Delta \boldsymbol{u}_1^{ls} \ \dots \ \Delta \boldsymbol{u}_N^{ls}\right]$.

The minimization is subject to the following constraints: for $i = 1, \dots, N$:

$$\boldsymbol{g}_i(\boldsymbol{x}_i, \Delta \boldsymbol{u}_i, \Delta \boldsymbol{v}, \Delta \boldsymbol{u}_i^{ls}) = \boldsymbol{0} \tag{6.14}$$

$$\boldsymbol{h}_i(\boldsymbol{x}_i, \Delta \boldsymbol{u}_i, \Delta \boldsymbol{v}, \Delta \boldsymbol{u}_i^{ls}) \leq \boldsymbol{L}_i \tag{6.15}$$

$$\left|\Delta \boldsymbol{u}_i^{ls}\right| \leq \overline{\Delta \boldsymbol{u}_i^{ls}} \tag{6.16}$$

$$|\Delta \boldsymbol{u}_i| \leq \overline{\Delta \boldsymbol{u}_i} \tag{6.17}$$

and the following constraint for the DC grid control actions:

$$|\Delta \boldsymbol{v}| \leq \overline{\Delta \boldsymbol{v}} \tag{6.18}$$

The above procedure results in a single set of MTDC actions $\Delta \boldsymbol{v}$ as well as suggested AC actions $\Delta \boldsymbol{u}_i$ for each AC area $i = 1, \dots, N$. The latter are suggested to the AC TSOs, and will not necessarily be applied. For instance, an AC TSO could opt for other corrective actions taking into account the MTDC grid actions calculated by the DC TSO.

Although it has been assumed that all TSOs are willing to coordinate and respect the recommendations of the DC TSO, it is still possible that a disagreement arises between the DC and AC TSOs regarding the DC control actions calculated by the former. In such a case, it should be the responsibility of the AC TSO to provide appropriate constraints to the DC TSO. Then, the latter should perform a new security assessment taking into account the updated constraints.

6.4.4 AC-DC contingencies

A clear distinction between AC and DC contingencies was assumed in the previous analysis. However, this distinction might not always be obvious, especially when combined events are considered. An example of such event has been illustrated in Section 3.4 where an AC contingency (loss of line and dramatic decrease of SCC) led to instability. Such an event would most probably result in tripping of the VSC or in fast decrease of its power. The latter could emanate from offline analysis and setting up of defense plans. Consequently, such an event would impact the other AC areas since the lost power would be compensated by the remaining VSCs.

This type of event could be treated as an AC contingency. Therefore, the TSO of the AC area in which the initial contingency occurs should ensure that the impact on the other AC areas is between limits. Namely, the change of the powers of the remaining VSCs should be between the limits specified by (6.12). In the example of Section 3.4, and assuming that the VSC is connected to an MTDC grid instead of a point-to-point link, the change in the MTDC grid power flows is not due to a corrective action of the TSO, but is rather the natural response of the system. The fast evolution of such events does not leave adequate time for corrective actions; therefore, the TSO should resort to preventive actions by either enhancing its AC grid or by adjusting the power transfer in the VSC.

6.4.5 Discussion

The proposed framework has been described in an abstract and conceptual form to ease presentation and maintain generality. In reality, it may be required to also investigate dynamic aspects. If dynamic simulations have to be performed, the complexity of identifying “optimal” actions increases significantly. Nevertheless, exchanging constraints between the DC and AC TSOs enables taking advantage of the control capabilities of the MDTC grid, without violating its “firewall” property.

Preventive controls have not been considered in the above analysis. In fact, they are similar to the ones following a DC contingency, in the sense that multiple TSOs may request them simultaneously. Therefore, in principle the same methodology can be applied, i.e. rely on the DC TSO with a full view of the system to calculate them. To keep the computational burden tractable, the number of contingencies assessed by the DC TSO should be kept as low as possible. Several methods can be contemplated. For example, a filter could be applied so that only the contingencies already assessed as insecure are further considered by the DC TSO.

6.5 Illustrative examples

The following simulation results illustrate a few aspects that were discussed in the above framework. Two scenarios, involving respectively an AC and a DC contingency, are presented. The initial operating point of the MTDC grid for both scenarios is shown in Fig. 6.7.

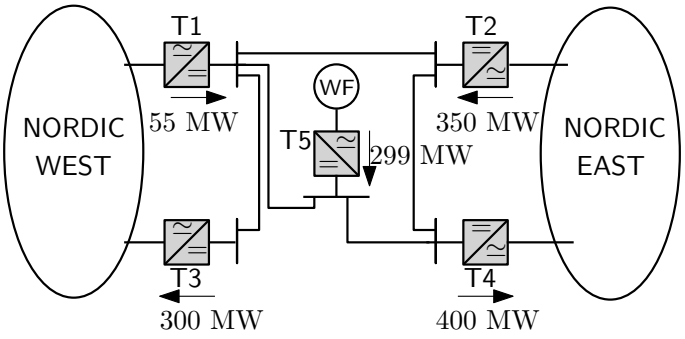

Figure 6.7: Operating point of MTDC grid

6.5.1 AC contingency

The first case concerns the long-term voltage instability scenario presented in Section 3.1. Nordic East is operating at point A (N-1 insecure), and Nordic West at point B (N-1 secure) [IEE15]. As already described, the outage of line 4032E-4044E (see Fig. 3.1) causes the degradation of the Nordic East system operation due to the combined actions of LTCs and OELs, resulting in the collapse of the East system. Section 3.1 demonstrated that a corrective action consisting of rerouting 320 MW through the MTDC grid can stop the degradation.

This corrective action should be performed through the secondary level of the MTDC grid controller described in Chapter 4 (instead of ramping up directly the setpoints of T2 and T4 as in Section 3.1). The same parameters as in Chapter 4 are used for the coordinated MPC. Therefore, at $t = 115$ s, the scheduled powers P_{sch} of T2 and T4 are adjusted by -320 MW and 320 MW, respectively. As shown in Fig. 6.8, this corrective control is sufficient to stabilize the East system, and restore the voltages in its Central zone to acceptable values.

The evolution of the VSC powers following this corrective control are shown in Fig. 6.9. In contrast to the results of Fig. 3.5, the power change of T4 is not covered exclusively by T2, but it is shared between T2 and T3. This share was automatically made by the MPC-based secondary controller. As unveiled by Fig. 6.10, this is due to the DC voltage of T2 hitting its upper limit. In

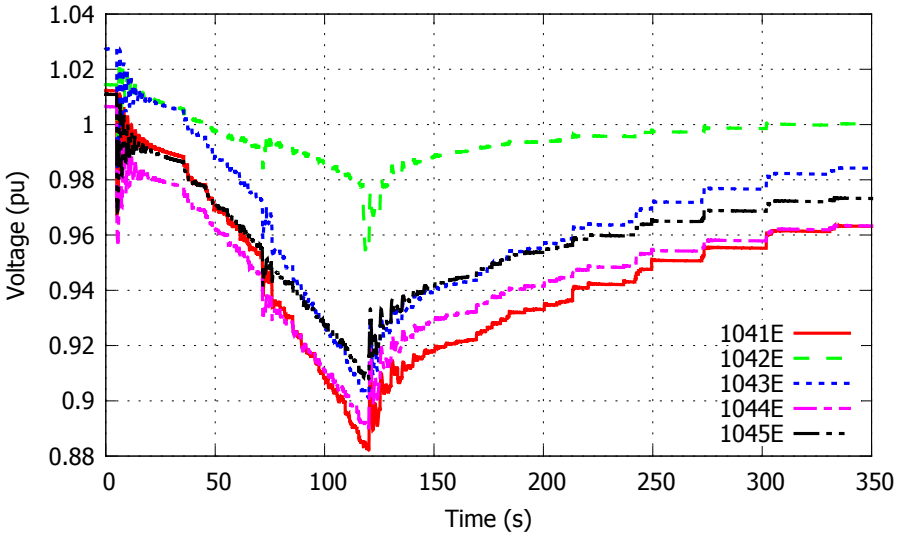

Figure 6.8: AC contingency: 130-kV bus voltages in Central area of East system

fact, covering the full change of the power of T4 would require increasing the DC voltage of T2 above this limit. Instead the MPC-based coordinated controller compensated by acting on T3.

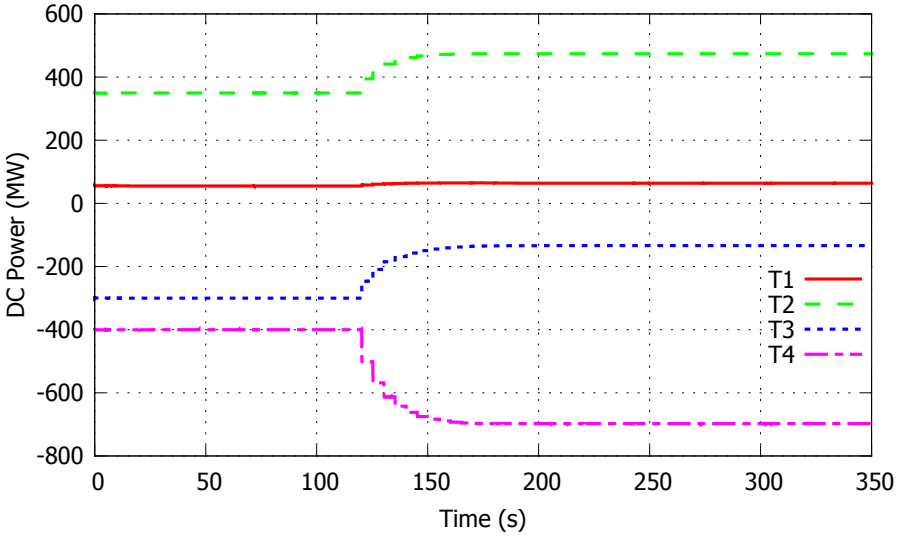

Figure 6.9: AC contingency: VSC DC powers

Including the MTDC grid in the security assessment of an AC TSO allows to take into account the response of the MTDC grid controllers and identify whether a given support request is feasible. In this specific example, the TSO of the East system would be able to identify that the power redirection through the MTDC grid would result in support from the other system due to MTDC grid constraints.

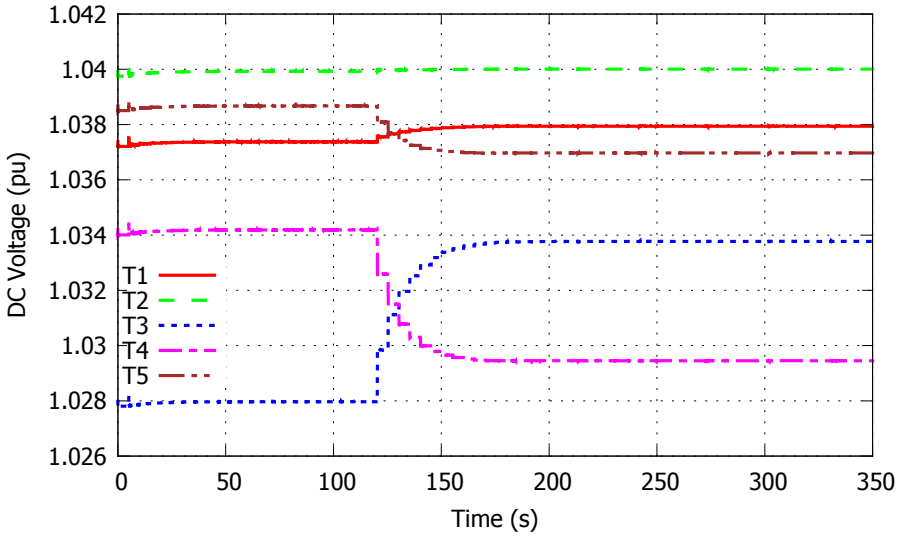

Figure 6.10: AC contingency: MTDC grid voltages

In addition, the speed of action of the MTDC grid controls can be taken into account. This is illustrated in Fig. 6.11 which shows the voltage at bus 1041E in the Nordic East area for the same corrective action (i.e. redirection of 320 MW) but different tunings of the MPC. In particular, the response time of the secondary controller is increased by varying the number of control steps N_c (see also Section 4.2.9). As expected, the effectiveness of the corrective action decreases for slower responses of the control. For N_c = 6, the coordinated MPC is slower and leads to lower steady-state voltages. If the control horizon is further increased to $N_c = 12$, the emergency action is not sufficient to restore viable operation, and the system settles at a pseudo-stable but unacceptable operating point due to some LTCs hitting their tap ratio limits [VCV07].

As a proof of concept, Fig. 6.12 shows the response of the voltage at bus 1041E after replacing the Nordic West system with a Thévenin equivalent (as sketched in Fig. 6.5). No difference is observed compared to the case with detailed representation of the Nordic West area.

Finally, let us assume that the TSO of the Nordic West system has specified that the power of T3 should not go above the value of -200 MW. This could be the result of stressed conditions in that system due to e.g. increased loading in its Central zone. Now, the corrective actions calculated by the TSO of the Nordic East system should also obey this constraint. Figures 6.13 and 6.14 show the voltages in the Central area of the East system and the VSC DC powers when that additional constraint on the power of T3 is also taken into account. The corrective action here consists of changing the scheduled powers of T1, T2 and T4 by 200, 120 and -320 MW, respectively. This action is applied at 115 s resulting in the stabilization of the Nordic East system.

It is noted that the DC voltage of T2 hits again its upper limit as shown in Fig. 6.15. As a result,

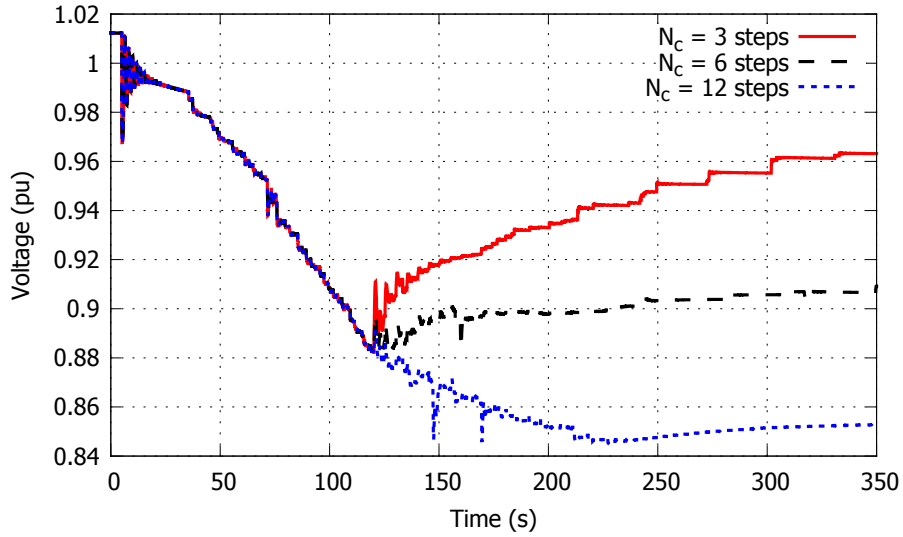

Figure 6.11: AC contingency: Voltage at bus 1041E for various tunings of the second-level MTDC grid controller

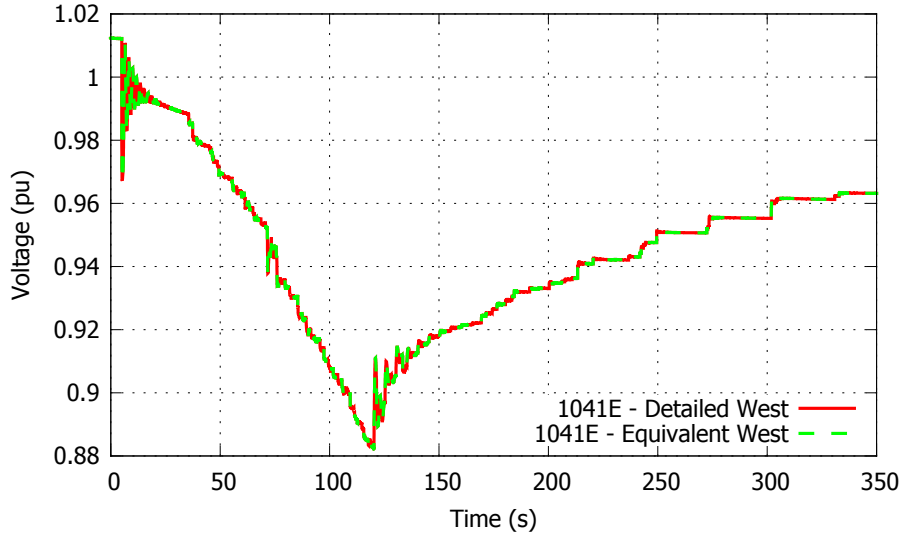

Figure 6.12: AC contingency: Voltage at bus 1041E - Representation of Nordic West as a Thévenin equivalent

the desired operating point cannot be satisfied and the VSC powers in steady state deviate from their scheduled values. Therefore, some power is drawn by T3, but the constraint of -200 MW is respected.

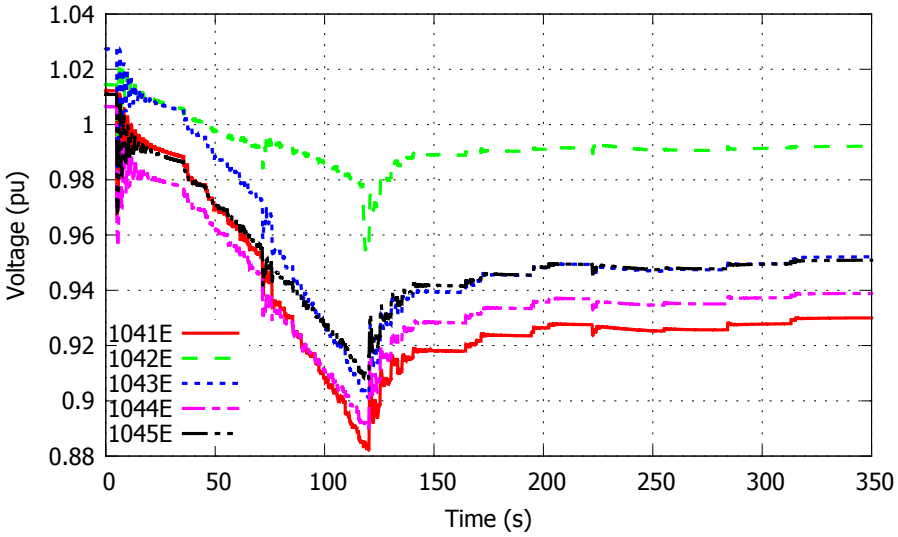

Figure 6.13: AC contingency: 130-kV bus voltages in Central area of East system with constraint on power change of T3

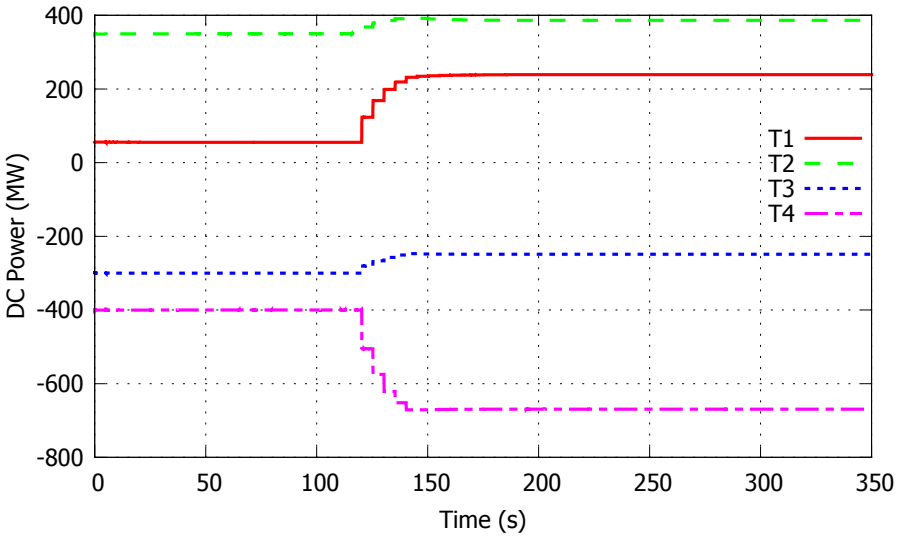

Figure 6.14: AC contingency: VSC DC powers with constraint on power change of T3

6.5.2 DC contingency

The second case involves the tripping of VSC T2. For this scenario, both Nordic East and Nordic West systems operate at point A detailed in [IEE15], which is N-1 insecure. As shown in Fig. 6.7, T2 initially injects 350 MW into the MTDC grid. Hence, following its outage, the remaining VSCs increase their injections to immediately restore the balance, as shown in Fig. 6.16. Next, the secondary control of the MTDC grid takes actions in order to restore the power exchange between

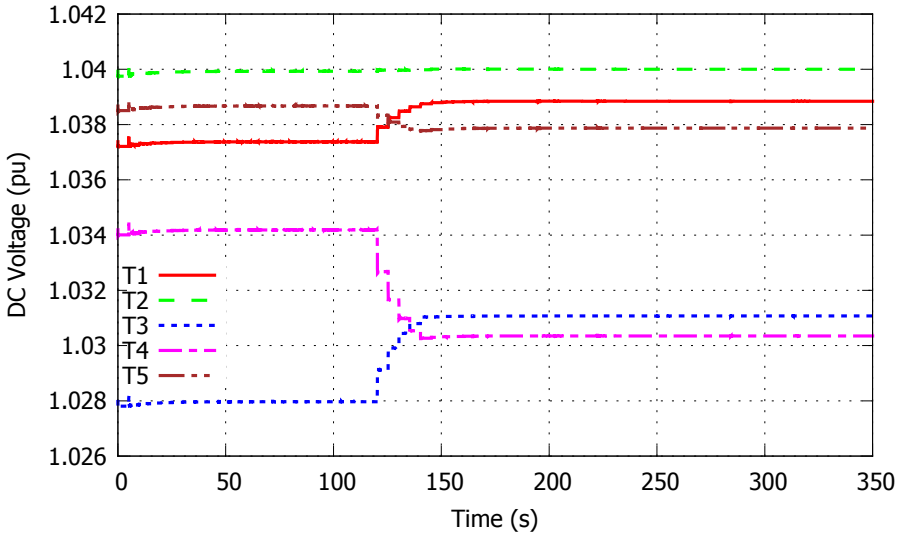

Figure 6.15: AC contingency: MTDC grid voltages

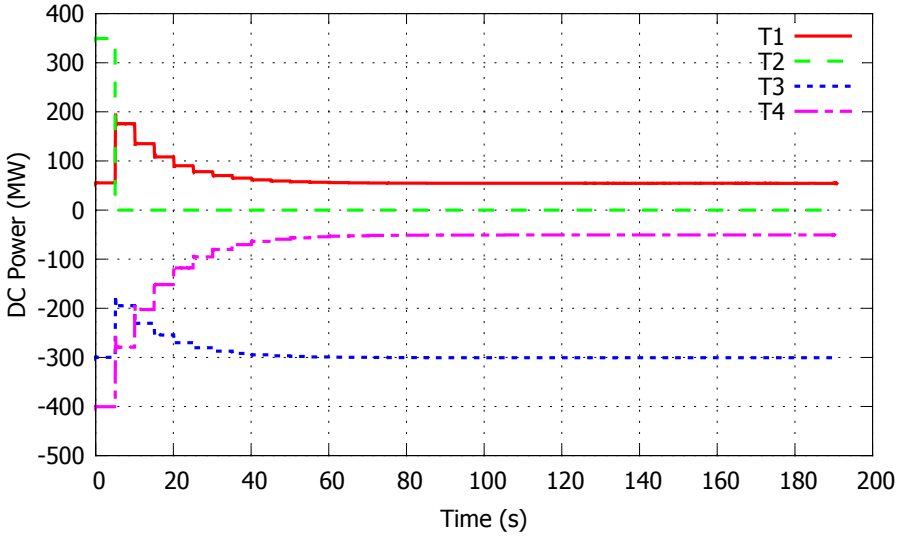

Figure 6.16: DC contingency: VSC DC powers

the two AC areas by redirecting the lost power of T2 through T4.

As a result, more power is drawn from T4, which has to flow through the North-Central corridor of the Nordic East system. This leads to long-term voltage instability and final collapse of the East system at 190 s. Instead, the West system returns to its original operating point, as shown by the dashed curve in Fig. 6.17, relative to the voltages at buses 1041E and 1041W in the East and West system, respectively.

Since T2 is out of operation, it is evident that this instability can be avoided (assuming only MTDC

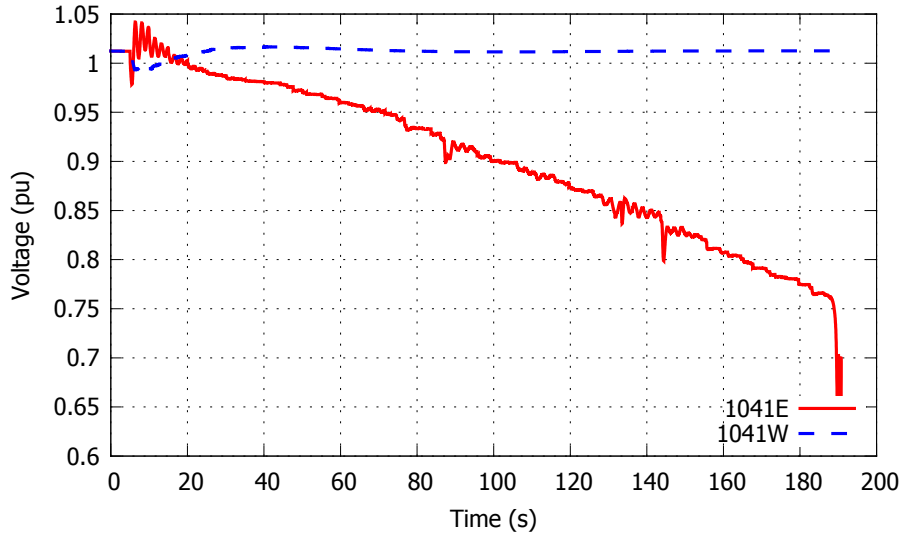

Figure 6.17: DC contingency: Voltages at buses 1041E and 1041W without corrective control

corrective actions) by preventing the restoration of power exchange by the MTDC grid secondary controller and, thus, by soliciting power from the West area.

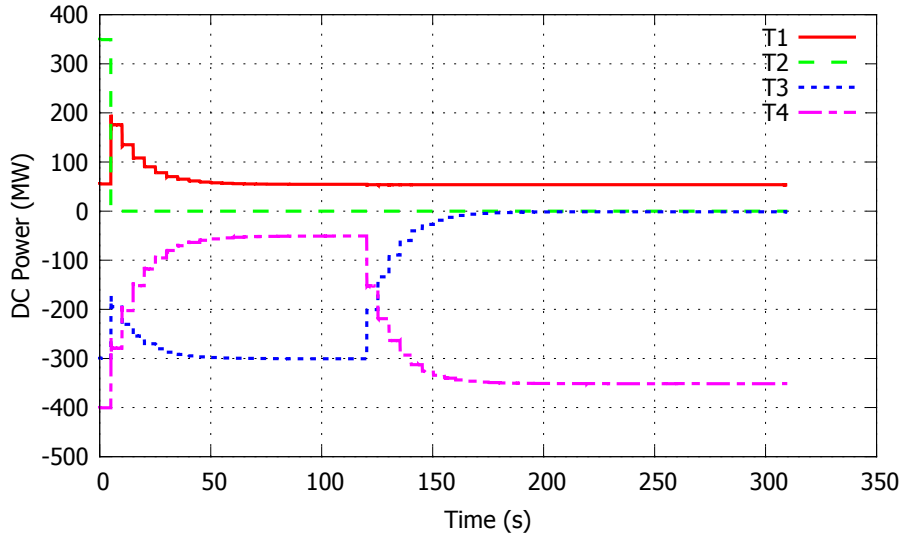

Figure 6.18: DC contingency: VSC DC powers

One option is to adjust the P^{sch} values of T3 and T4 by 300 MW and -300 MW, respectively, as shown in Fig. 6.18. This adjustment successfully prevents long-term voltage instability in the East system, as shown by the solid curve in Fig. 6.19. However, the increased request of power from T3 now results in instability of the West system and its subsequent collapse as revealed by the evolution of the voltage at bus 1041W in Fig. 6.19.

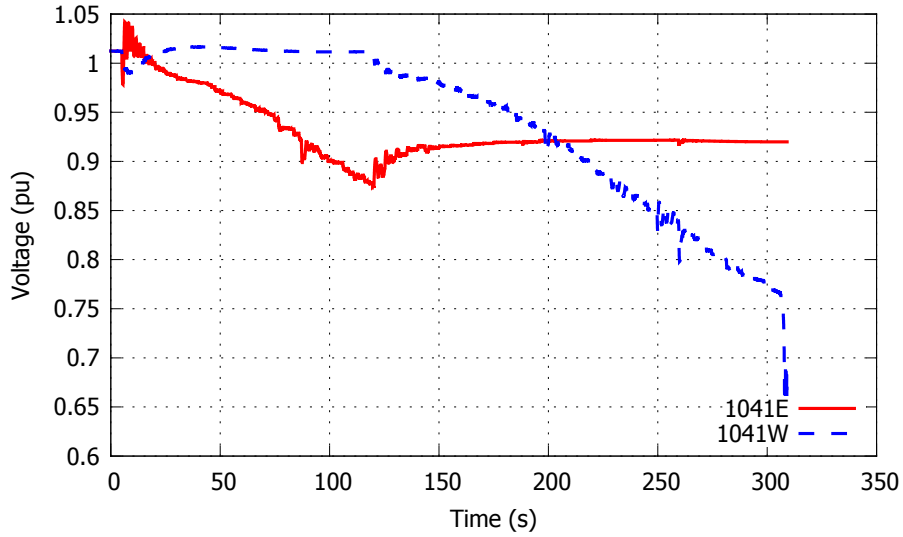

Figure 6.19: DC contingency: Voltages at buses 1041E and 1041W with corrective control destabilizing Nordic West

The second option is to adjust the power of T1 by 300 MW, instead of T3, as shown in Fig. 6.20. Therefore, following the outage of T2 and the initial adjustment of the VSC powers by the secondary controller, the P^{sch} values of T1 and T4 are adjusted at $t = 115$ s. Figure 6.21 shows that this corrective control successfully prevents instability in East system, without jeopardizing the operation of Nordic West.

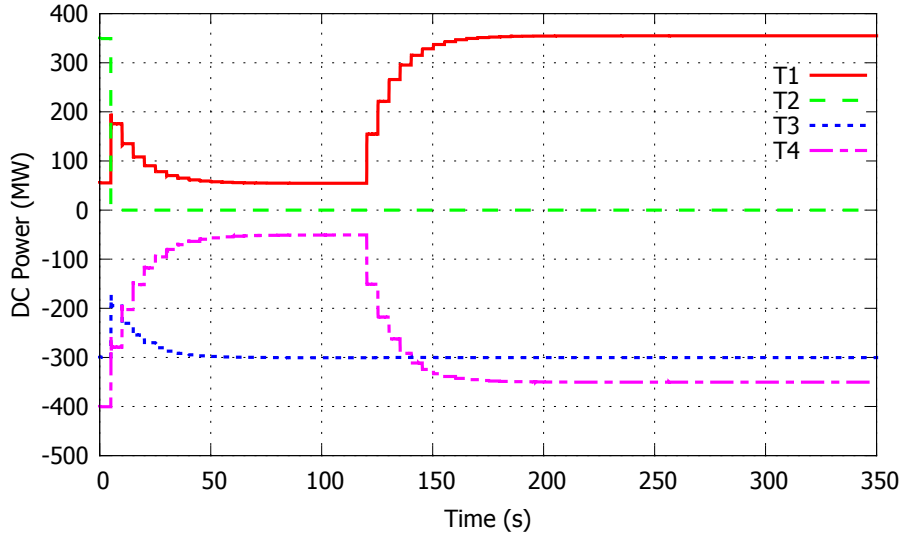

Figure 6.20: DC contingency: VSC DC powers

The DC TSO should arbitrate between the above possible alternatives and choose the most appro-

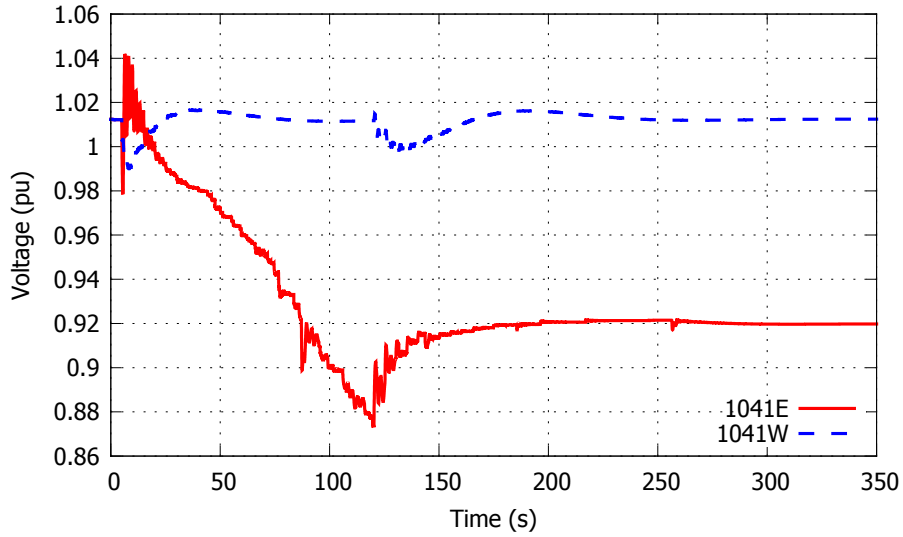

Figure 6.21: DC contingency: Voltages at buses 1041E and 1041W with effective corrective control

priate one. This scenario involves only two asynchronous AC areas and some iterations between the two TSOs would also resolve the conflict without the intervention of the DC TSO. However, the complexity is expected to increase significantly when more TSOs are connected to the MTDC grid.

6.6 Summary

This chapter has proposed a conceptual framework for security assessment of a mixed AC/DC grid involving multiple asynchronous AC areas connected through an MTDC grid. Taking advantage of the control flexibility brought by MTDC grids, especially in post-disturbance corrective control, poses several challenges to the security assessment. To address these challenges, the proposed framework assumes the establishment of a coordinating entity (referred to as DC TSO) that has full view of the system and exchanges information with the AC TSOs. A distinction is made between AC contingencies originating in the jurisdiction of an AC TSO, and DC contingencies inside the MTDC grid. The former are assessed by the TSO of the system they occurred in, considering MTDC grid actions subject to constraints gathered by the DC TSO. Instead, DC contingencies are assessed by the DC TSO to avoid conflicting actions between the AC TSOs.

Chapter 7

General conclusion

7.1 Summary of work and main contributions

Undoubtedly, the importance of HVDC connections for the future power systems will go increasing. This thesis has focused on MTDC grids, in particular on developing methods and schemes to take the most of the benefits they can bring to the power system. Centralized and decentralized schemes have been proposed in order to control the MDTC grid, provide auxiliary services to the AC areas connected to it, and ensure secure operation of the combined AC/DC system.

The proposed control of MTDC grids has been somewhat inspired of the current practice for AC frequency control. A hierarchical structure is described consisting of primary, secondary and tertiary control. The primary level is based on the DC voltage droop control to ensure the power balance in the MTDC grid and stabilize the DC voltages. Several VSCs follow a $P - V$ characteristic and adjust their powers in response to DC voltage deviations. This configuration provides redundancy against the failure of a VSC.

The secondary level monitors the MTDC grid and coordinates the VSCs in order to steer the system towards a desired operating point, alleviating system-wide violations (e.g. DC branch overloads) in the process. This control is inspired of MPC, a closed-loop optimization-based scheme, acting at discrete times. MPC can accommodate a simplified sensitivity-based model of the MTDC grid to predict its future response. Based on this model, it calculates a set of control actions (namely VSC power setpoint changes) that smoothly drive the system towards the desired operating point. The formulation of the MPC encompasses DC voltage and branch current constraints to ensure that the system remains or returns between limits. In case a violation is observed, the MPC takes actions to smoothly restore an acceptable operating point. A distinction is made between dispatchable and non-dispatchable VSCs. The latter refer to VSCs whose power cannot be specified,

but depend on external factors (e.g. wind farm terminals). The secondary level acts primarily on dispatchable VSCs. Actions on the non-dispatchable VSCs are taken when absolutely necessary, i.e. when acting on dispatchable VSCs is insufficient to clear the violation.

The tertiary level addresses the optimal and secure operation of the MTDC grid. Its aim is to minimize the losses in the MTDC grid given desired power injections in specified VSCs, while respecting N-1 security constraints. An SCOPF formulation has been proposed based on a non-linear optimization problem. The power limits of the VSCs are included in the formulation through complementarity constraints. The output of the optimization are given as inputs to the secondary level. The effectiveness of the proposed hierarchical control structure for an MTDC grid has been shown on a test system consisting of a five-terminal DC grid, two asynchronous AC areas and an offshore wind farm. Several scenarios have been simulated to demonstrate the effectiveness of the secondary level in alleviating constraints, as well as steering the MTDC grid towards the desired operating point. The coordination of the secondary and tertiary level has been also illustrated considering the outage of a VSC and of an HVDC branch.

The second topic addressed in this thesis has dealt with frequency support among asynchronous AC systems through MDTC grids. Two schemes have been proposed, both inspired of MPC. Frequency support has been considered as emergency control; therefore, both proposed controls are inactive in normal operation. In addition, both schemes rely only on local measurements, readily available to each VSC.

The first scheme aims at changing the power setpoint of the VSC until a pre-defined participation to frequency support is satisfied. The formulation of the MPC includes simplified models for the evolution of frequency and DC voltage in response to the control actions. To prevent causing unacceptable DC voltage deviations, DC voltage constraints are included so that frequency support freezes, if a DC voltage constraint is reached. The second scheme relies on a similar formulation, but addresses the problem of frequency support from a different perspective. Instead of providing a pre-defined participation to frequency support, the controller aims at keeping the frequency above a pre-specified value (or below in case of overfrequency). Specifically, the controller is inactive for normal deviations of frequency, and is only activated when it identifies that the time-varying frequency will reach a threshold. For example, this threshold could be set a little above the triggering value of UFLS relays. Then, the VSC provides as much power as required to prevent (if possible) the frequency from dropping below this threshold, but again without violating any DC voltage constraint. Both methods were tested on a system consisting of two asynchronous AC areas, where it was verified that they can effectively satisfy their objectives, while respecting DC voltage constraints. Their performance has been experimentally validated on a real-life mock-up MTDC grid consisting of physical VSCs and DC cables.

The last topic investigated in this thesis had to do with security assessment of combined AC/DC

grids. The interconnection of multiple asynchronous AC areas through MTDC grids is expected to introduce new challenges to security assessment and coordination between the various TSOs will be required. To this purpose, a generic framework has been proposed in this work. It relies on a centralized entity, the "DC TSO", that has view of the complete AC/DC system and exchanges information regarding control actions and constraints with the AC TSOs.

The proposed framework makes a clear distinction between the way AC and DC contingencies are treated in the security assessment and how corrective controls involving the (fast) VSCs connected to the MTDC grid are calculated. The assessment of AC contingencies is performed by the corresponding AC TSO, which can request corrective actions from the MTDC grid, as long as they satisfy the constraints imposed by the other AC areas. These constraints are collected by the DC TSO and their purpose is to prevent propagation of a disturbance from one AC area to the others.

In contrast, DC contingencies are assessed by the DC TSO. The reason is that such contingencies may impact more than one AC area simultaneously. Therefore, conflicts might arise if these areas request support from the MTDC grid. The use of a centralized entity to handle such cases resolves those conflicts by proposing a single set of actions satisfying the constraints of all AC areas.

7.2 Directions for future work

MTDC grids are still in their infancy, but may become the key infrastructure enabling large power transfers over long distances. Of course, several challenges have yet to be addressed. Some of them are of technological nature, e.g. MTDC grid protection and selective DC fault clearing, while other obstacles are more related to non-technological aspects, such as political willingness and operational issues.

The methods and schemes developed in the context of this work could be further improved or extended along the following directions:

- The MPC-based secondary control of Section 4.2 has been shown to be quite robust. However, its response should be further investigated in presence of communication failures or non-responsiveness of a VSC. In most cases, the closed loop nature of MPC would compensate for such inaccuracies. Nevertheless, a safeguard should be introduced in the form of additional constraints (e.g. maximum range of control actions).
- The tertiary control of Section 4.4 calculates the operating point for a specific power injection of the non-dispatchable VSCs. Therefore, when the powers of the latter change significantly, a new SCOPF should be calculated. Including the response of the secondary

level in the tertiary control would make it possible to calculate a secure operating point for a pre-specified range of the non-dispatchable power and not only for a single operating point.

- It would be of interest to complement the tertiary control with dynamic constraints, e.g. constraints on the maximum overshoot of the DC voltage following the tripping of a VSC. This would require to integrate dynamic simulations (preferably electromagnetic-type ones) to the SCOPF formulation and resort to other (heuristic or meta-heuristic) optimization methods to reach a near-optimal solution.
- The extension of the proposed schemes for frequency support to systems with multiple MTDC grids and/or HVDC point-to-point links operating in parallel should be considered. A way to coordinate these connections should be devised so that inadvertent interactions are avoided.
- The coordination of the frequency control schemes proposed in Chapter 5 with the hierarchical control of an MTDC grid in Chapter 4 should be investigated. Conflicts between local and centralized control should be prevented. One way would be to switch the status of the VSCs where frequency support has been activated from dispatchable to non-dispatchable. In such case, the centralized control would not interfere with frequency support, unless it is deemed necessary in order to preserve the security of the MDTC grid.
- The framework for security assessment proposed in Chapter 6 relies on the determination of constraints on the available MTDC grid actions to be communicated by the AC TSOs to the DC TSO (see Fig. 6.5b). Calculating these limits is a non-trivial task worthy of further investigation.
- The concept of "grid-forming" VSCs is a fast developing and promising field for future investigation. The VSCs considered in this work are of the "grid-feeding" or "grid-following" type, i.e. they synchronize to a system with a sufficient number of synchronous machines. Future plans investigate the feasibility of very low-inertia (or even inertia-less) power systems. Such grids would require several VSCs to act as grid-forming for the rest to synchronize.
- This work has relied on phasor-mode dynamic simulations for the representation of the VSCs and the relatively slow power system dynamics. However, the fast dynamics of the VSCs push the phasor-mode approximation to its limits. EMT simulation remains the reference in terms of validity. Nonetheless, the large computing times associated with such simulations do not make them suitable for dynamic security assessment of large systems. Co-simulation of EMT and phasor models [PAGVC16] can help decrease the computational cost by simulating only a part of the system in EMT mode. Future research should focus on methods to identify the conditions to switch between different types of simulation (i.e. phasor-mode or co-simulation).

Appendix A

VSC and HVDC cable data

The data used for the VSCs are shown in Table A.1:

Table A.1: VSC data

Parameter	Value	Parameter	Value
S_{nom}	1000 MVA	P_{nom}	1000 MW
$V_{g,nom}$	400 kV	V_{nom}	320 kV
R	0.01 pu	L	0.2 pu
H_{dc}	10.24 ms		

Table A.2 provides the data used for the RC-model of the HVDC cables:

Table A.2: HVDC cable data

Parameter	Value	Parameter	Value
r	0.011 Ω/km	c	0.2 μF/km

Appendix B

Derivation of sensitivity matrices $\mathbf{S_p}$, $\mathbf{S_i}$

The power flow equations of an MTDC grid with N DC buses can be written as follows:

$$\boldsymbol{P} = \text{diag}(\boldsymbol{V})\ \boldsymbol{G}\boldsymbol{V} \tag{B.1}$$

where $\boldsymbol{P}_{N\times 1}$ and $\boldsymbol{V}_{N\times 1}$ are the vectors of VSC DC powers and DC voltages, respectively, and $\boldsymbol{G}_{N\times N}$ is the indefinite conductance matrix of the MDTC grid. $\text{diag}(\boldsymbol{X})$ represents a diagonal matrix with the elements of vector $\boldsymbol{X}$ as its diagonal entries. The Jacobian matrix of DC power injections with respect to DC voltages can be derived from (B.1) as follows [Hai12]:

$$\boldsymbol{J}_{dc} = \frac{\partial \boldsymbol{P}}{\partial \boldsymbol{V}} = \text{diag}(\boldsymbol{V})\boldsymbol{G} + \text{diag}(\boldsymbol{G}\boldsymbol{V}) \tag{B.2}$$

Using $\boldsymbol{J}_{dc}$ the relation between power changes $\Delta\boldsymbol{P}$ and DC voltage changes $\Delta\boldsymbol{V}$ can be obtained:

$$\Delta\boldsymbol{P} = \boldsymbol{J}_{dc}\Delta\boldsymbol{V} \tag{B.3}$$

The power of all VSCs are also given by the following equation based on their DC voltage droop characteristics (2.35):

$$\boldsymbol{P} = \boldsymbol{P}^{set} - \boldsymbol{K}_V(\boldsymbol{V} - \boldsymbol{V}^{set}) \tag{B.4}$$

where $\boldsymbol{K}_V = diag\,(K_{V1}\ldots K_{VN})$ is a diagonal matrix with the voltage droop gains as diagonal entries. The linearization of (B.4) yields (assuming that the DC voltage setpoints do not change (i.e. $\Delta\boldsymbol{V}^{set} = 0$)):

$$\Delta\boldsymbol{P} = \Delta\boldsymbol{P}^{set} - \boldsymbol{K}_V\Delta\boldsymbol{V} \tag{B.5}$$

The relation between $\Delta \boldsymbol{P}^{set}$ and $\Delta \boldsymbol{V}$ can now be obtained from (B.3) and (B.5) as follows:

$$\Delta \boldsymbol{P}^{set} = (\boldsymbol{J}_{dc} + \boldsymbol{K}_V)\, \Delta \boldsymbol{V} \tag{B.6}$$

Therefore the sensitivity matrix $\boldsymbol{S}_P$ involved in (4.16) is equal to:

$$\boldsymbol{S}_P = \boldsymbol{J}_{dc} + \boldsymbol{K}_V \tag{B.7}$$

Matrix $\boldsymbol{S}_I$ is derived as follows. If the number of the DC branches is N_{br}, the DC branch currents relate to the DC bus voltages through:

$$\boldsymbol{I} = \boldsymbol{A}\, \boldsymbol{V} \tag{B.8}$$

in which the l-th row of $\boldsymbol{A}_{N_{br} \times N}$ corresponds to the branch between buses i and m and has two nonzero entries:

$$[\boldsymbol{A}]_{li} = g_{im}, \quad [\boldsymbol{A}]_{lm} = -g_{im} \tag{B.9}$$

where g_{im} is the conductance of the branch under concern.

The linearized behavior is obtained from:

$$\Delta \boldsymbol{I} = \boldsymbol{A}\, \Delta \boldsymbol{V} \tag{B.10}$$

which, using (B.6) and (B.7), can be written as:

$$\Delta \boldsymbol{I} = \boldsymbol{A} \boldsymbol{S}_{\boldsymbol{P}}^{-1} \Delta \boldsymbol{P}^{set} \tag{B.11}$$

and hence:

$$\boldsymbol{S}_I = \boldsymbol{A}\, \boldsymbol{S}_P^{-1}. \tag{B.12}$$

Note that the above matrices are small as the number of DC nodes is not expected to be large.

Appendix C

Small-signal stability analysis of VSC connected to weak AC system

C.1 System reduction and linearization

This appendix complements the illustrative example presented in Section 3.4 by investigating the small-signal stability of the system of Fig. 3.16. As before, the focus is on the AC side of the Slave VSC, so the DC voltage dynamics are neglected. In addition, as also shown in Fig. 3.17, this case study considers only the integral gains K_{id} and K_{iq} of the active power and AC voltage loops (i.e. the proportional gains K_{pd} and K_{pq} have been set to 0).

The small-signal analysis is performed by linearizing the system of differential-algebraic equations (2.9), (2.10),(2.13)-(2.24), (2.27)-(2.30), and (3.2)-(3.3).

After algebraic manipulations and variable eliminations, the following differential state vector $\boldsymbol{x}_d$ and algebraic state vector $\boldsymbol{x}_a$ can be chosen:

$$\boldsymbol{x}_d = [i_{gd}\ i_{gq}\ M_d\ M_q\ \theta\ M_\omega\ N_d\ N_q]^T \tag{C.1}$$

$$\boldsymbol{x}_a = [i_{gx}\ i_{gy}\ v_{gx}\ v_{gy}]^T \tag{C.2}$$

which satisfy the equations:

$$\dot{\boldsymbol{x}_d} = \boldsymbol{f}(\boldsymbol{x}_d, \boldsymbol{x}_a) \tag{C.3}$$

$$\mathbf{0} = \boldsymbol{g}(\boldsymbol{x}_d, \boldsymbol{x}_a). \tag{C.4}$$

By linearizing the above nonlinear equations, the system is brought in the form of

$$\begin{bmatrix} \Delta\dot{\boldsymbol{x}}_d \\ 0 \end{bmatrix} = \left[\begin{array}{c|c} \boldsymbol{A} & \boldsymbol{B} \\ \hline \boldsymbol{C} & \boldsymbol{D} \end{array}\right] \begin{bmatrix} \Delta\boldsymbol{x}_d \\ \Delta\boldsymbol{x}_a \end{bmatrix} \tag{C.5}$$

where

$$\boldsymbol{A} = \frac{\partial \boldsymbol{f}}{\partial \boldsymbol{x}_d}, \quad \boldsymbol{B} = \frac{\partial \boldsymbol{f}}{\partial \boldsymbol{x}_a}, \quad \boldsymbol{C} = \frac{\partial \boldsymbol{g}}{\partial \boldsymbol{x}_d}, \quad \boldsymbol{D} = \frac{\partial \boldsymbol{g}}{\partial \boldsymbol{x}_a}. \tag{C.6}$$

The small-signal stability analysis is performed with the eigenvalues of the reduced Jacobian, which is the Schur complement of block $\boldsymbol{D}$:

$$\boldsymbol{J} = \boldsymbol{A} - \boldsymbol{B}\boldsymbol{D}^{-1}\boldsymbol{C}. \tag{C.7}$$

C.2 Parameters and operating point

The small-signal analysis is performed in the weak grid configuration by choosing $X_{eq} = X_w = 2$ pu in (3.2) and (3.3). For simplicity, we take $E = 1$ pu, and we assume that the VSC also keeps its terminal voltage equal to 1 pu. Hence, the static stability limit is $P^{st}_{max} = 0.5$ pu. Since the network resistance has been neglected, the same limit applies for reverse power flow. In this work, the VSC active power is considered positive for inverter operation.

The inner loop controller gains have been tuned to have a response time of 10 ms. In order to have a good time decoupling between the inner and the outer loops, the response time of the latter is chosen ten times slower [RCGN12]. The PLL has been tuned to have a response time of 50 ms.

C.3 Effect of operating point

A total of eight eigenvalues are involved. For instance, for $P^{set} = 0.4$ pu the eigenvalues are the following:

$$s_{1,2} = -196.2 \pm j242.7, \quad s_{3,4} = -203.3 \pm j215.2$$
$$s_{5,6} = -68.2 \pm j18.4, \quad s_{7,8} = -12.4 \pm j29.6$$

Due to the inherent non-linearities in (2.28), (2.30), (2.16), (2.17), the Jacobian $\boldsymbol{J}$ and its eigenvalues change with the operating point. The effect of changing progressively P^{set} on the dominant eigenvalues (i.e. $s_{7,8}$) is shown in Fig. C.1. The eigenvalues are located in the left hand plane

indicating a stable system for low P^{set}. However, as the power increases the eigenvalue moves to the right. The system becomes unstable for P^{set} greater than 0.44 pu.

Note that this limit is smaller than P^{st}_{max}. In fact, the system undergoes a Hopf bifurcation (growing oscillations) for $P^{set} = 0.45$ pu. For $P^{set} = 0.5$ pu, it loses its equilibrium, i.e. it undergoes a saddle-node bifurcation, easily identified by the zero eigenvalue.

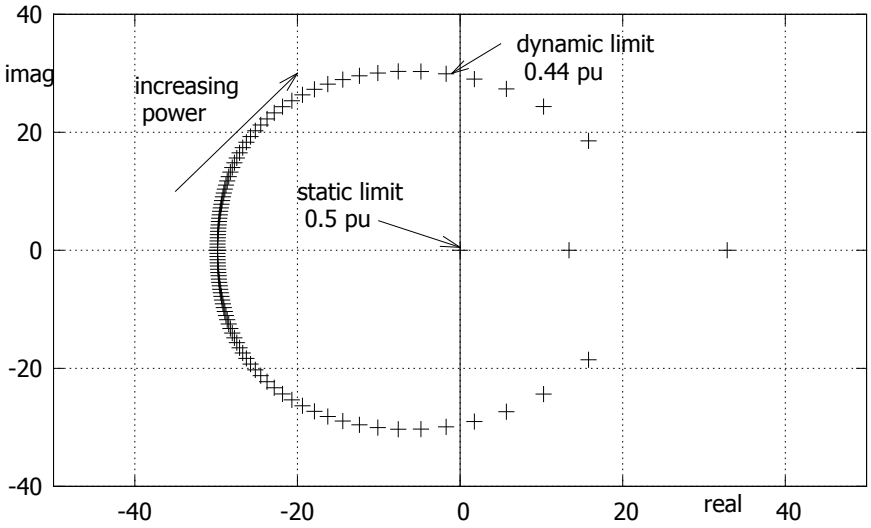

Figure C.1: Dominant eigenvalues when varying the power setpoint P^{set}

C.4 Effect of outer loops tuning

The effect of adjusting the active power and voltage control loops is now discussed. Unless otherwise specified, the response time of the inner loops is 10 ms, of the PLL 50 ms, and of the outer loops 100 ms. The analysis is performed at the first unstable operating point identified in the previous section, i.e. for $P^{set} = 0.45$ pu.

C.4.1 Effect of active power loop

The locus of the dominant eigenvalues when varying the active power loop integral gain K_{id} is depicted in Fig. C.2. It is shown that accelerating the active power control deteriorates stability by moving the eigenvalues towards the right-hand plane.

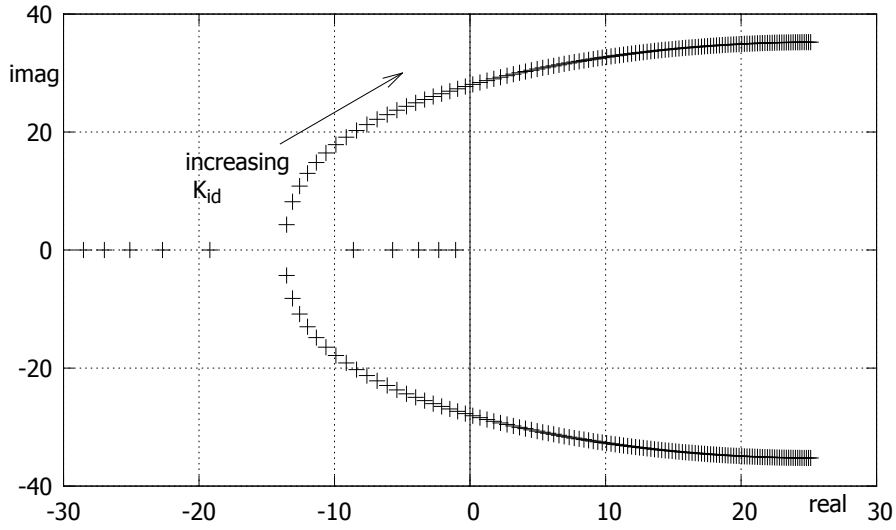

Figure C.2: Dominant eigenvalues when varying K_{id} ($P^{set} = 0.45$ pu)

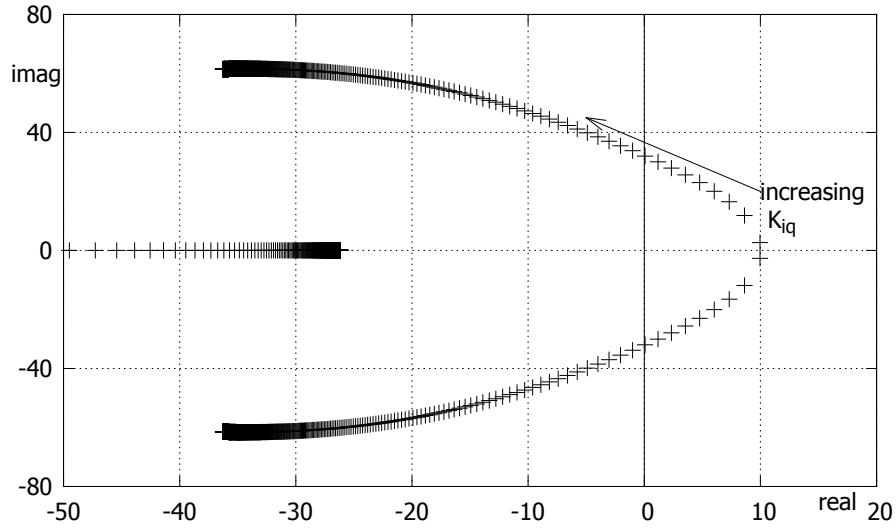

Figure C.3: Dominant eigenvalues when varying K_{iq} ($P^{set} = 0.45$ pu)

C.4.2 Effect of voltage loop

In contrast, when the integral gain K_{iq} is increased, the stability of the system is improved as demonstrated by the locus of the dominant eigenvalues shown in Fig. C.3. For low values of K_{iq} the system is unstable.

The results of Figs. C.2 and C.3 suggest that voltage control should be faster than active power control to increase the range of stable operating points, i.e. to make the dynamic limit approach

the static one (but, of course, never exceed it).

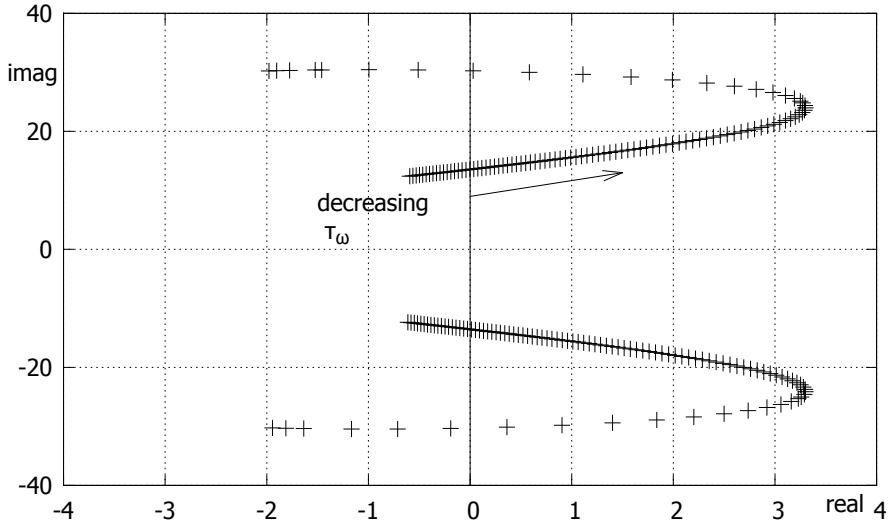

Figure C.4: Dominant eigenvalues when varying τ_ω ($P^{set} = 0.45$ pu)

C.5 Effect of PLL tuning

The effect of adjusting the PLL parameters is shown in Fig. C.4. The gains $K_{p\omega}$ and $K_{i\omega}$ are tuned based on [Chu00] in order to satisfy a desired response time τ_ω as follows:

$$K_{p\omega} = \frac{10}{\tau_\omega} \quad \text{and} \quad K_{i\omega} = \frac{25}{\tau_\omega^2} \tag{C.8}$$

The locus of the dominant eigenvalues when varying τ_ω from 5 ms up to 500 ms is shown in Fig. C.4. It is shown that the system is stable for very slow and very fast PLL response times, whereas it becomes unstable for intermediate values.

It is interesting to note that the small-signal stability analysis of Fig. C.1 is in agreement with the results of Fig. 3.19 (where fault was preceding the line tripping), but not with the ones in Fig. 3.23 (where the line was tripped without a fault). This is mainly due to the active power reduction during the fault and the gradual power restoration after. Hence, in Fig. 3.19 the system was smoothly brought to its final equilibrium point, and the stability limit was not influenced by non-linearities.

Appendix D

Experimental results from application of MPC on a low-scale DC grid mock-up

Before applying the MPC-based control schemes described in Chapter 5 in real-life, some kind of experimental validation is required. This has been performed in the mock-up low-scale MTDC grid developed in University of Lille [ACG+13]. The work for the first option for frequency support described in Section 5.2 has been documented in the paper appended to this thesis.

Several steps had to be performed in order to validate the proposed control on the mock-up MTDC grid. ULiège was involved mainly in the first steps, by providing the necessary code for the implementation of the MPC in MATLAB and validating the results at each step.

The validation for the second method (see Section 5.4) will be reported in a future publication.

Experimental Validation of a Model Predictive Control Strategy on a Three-terminal VSC-HVDC Mock-up

M. M. Belhaouane*, K. Almaksour*, L. Papangelis[††], F. Colas*, T. Prevost[†], X. Guillaud*, T. Van Cutsem [†††]

**Univ. Lille, Arts et Metiers ParisTech, Centrale Lille, HEI, EA 2697 - L2EP - Laboratoire d'Electrotechnique et d'Electronique de Puissance, F-59000.*

[†]Réseau de Transport d'Electricité (RTE), Research and Development Dept. of RTE.

[††] Dept. of Electrical Eng. and Computer Sc., University of Liège, Belgium.

[†††]Fund for Scientific Research (FNRS), University of Liège, Belgium.

Keywords: Model Predictive Control, frequency support, Multi-terminal DC grid, HIL and PHIL, Experimental validation.

Abstract

The subject of this paper is the experimental validation of a recently proposed advanced control scheme for Voltage Source Converters (VSC) based on Model Predictive Control (MPC). The main purpose of the investigated advanced controller is the frequency support from an AC grid to another after significant disturbance through HVDC Grid. The paper reports on the implementation methodology on a small-scale 3-terminal DC mock-up grid consisting of several physical low-scale VSCs, actual DC cables. These components are coupled with real-time simulation tools simulating the adjacent AC grids. The different steps for the validation process of the MPC strategy are illustrated, starting from offline simulation based on a model of the DC grid, up to the actual implementation of the controller in the mock-up of the DC grid.

1 Introduction

High Voltage DC (HVDC) transmission is becoming more and more attractive in the recent years, fuelled by the shift to renewable sources and the need for bulk power transfer over long distance. Most of the HVDC connections in operation today consist of point-to-point links. However, Multi-Terminal DC (MTDC) grids are also envisaged in the future after some challenges have been addressed [1]. Some MTDC grid projects such the European Supergrid [2] and the North Sea Super Grid [3] have already been proposed in Europe.

Unlike AC interconnections, HVDC interconnected areas operate asynchronously, i.e. the speed governors of one area do not respond to frequency deviations of the other areas. Therefore, no frequency support is provided between two AC asynchronous systems linked by HVDC system. This requires the development and integration of dedicated controllers for VSCs, which adjust the power transfer through the MTDC grid in response to frequency deviations.

Frequency support to an AC area through MTDC grid has been the subject of several works in the literature. In the majority of them, a supplementary droop control is added to the control structure of VSC, enabling it to react to frequency deviations [4-7]. For MTDC grids, this results in the so-called dual droop control [8, 9]. However, as shown in [10], the drawback of the simple frequency droop is the strong interaction with its DC voltage droop counterpart, which has been shown to decrease the performances of both control strategies and in the worst case may lead to a DC voltage instability. To achieve the desired participation to frequency support, defined by the Transmission System Operator (TSO), the work in [11] proposes a simple method to retune the frequency droop parameter.

Instead of the dual droop control, the work in [12-14] proposed to use MPC to achieve the desired participation. This allows taking into account the expected effect of DC voltage deviations to the VSC power, as well as respecting DC voltage constraints. The main characteristic of MPC is that it solves a quadratic optimization problem with linear constraints at each sampling time step in order to calculate the control actions [15].

All of the aforementioned schemes have been tested with extensive offline dynamic simulations using simplified models of the VSC and the MTDC grid. However, some kind of experimental validation is required before applying such methods on real systems. Obviously, implementing and testing on real high-scale VSCs is not feasible. To this purpose, the authors of [16] proposed the use of Hardware In the Loop (HIL) and Power Hardware In the Loop (PHIL) simulation with a low-scale mock-up MTDC grid as an intermediate step. Initial results were obtained during the TWENTIES project [17], whereas the work in [18] provided experimental validation of the behaviour of the dual droop control of [11].

This study focuses on the implementation and experimental validation of the MPC-based method proposed in [12]. Compared to conventional linear control schemes (e.g. PI controllers, droop, etc.) this is much more challenging since it requires the formulation and solution of an optimization problem inside the control structure of the VSC. Thus, the main idea of this research work is to illustrate the different steps for the validation process of the MPC strategy, from the offline simulation based on a high-scale power MTDC system to a low-scale power MTDC Mockup. Therefore, a rigorous step-by-step validation method is performed starting from an

offline transient stability simulation software then describing the different stages under SimPowerSystem/Matlab, real time simulation environment, Hardware In the Loop (HIL) simulation and finally Power-Hardware-In-the-Loop (PHIL).
The rest of the paper is organized as follows: Section 2 briefly describes the MPC-based strategy for AC frequency support originally proposed in [12]. Section 3 details the various steps followed for the implementation on the low-scale three-terminal mock-up. The results of the validation are analysed in Section 4. Concluding remarks are provided in Section 5.

2 MPC-based control strategy for AC frequency support

2.1 Description of the studied system

The three-terminal VSC-MTDC system under concern is depicted by the following Fig.1.

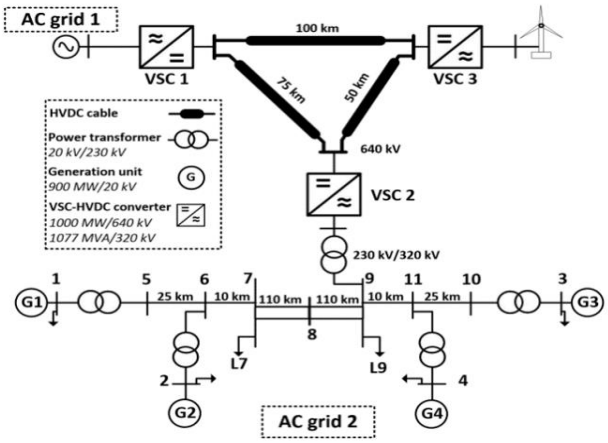

Figure 1: The studied three terminal MTDC System.

It consists of two AC areas (AC grid 1 and 2) and a large offshore wind. The wind farm is assumed to be located 100 km from AC grid 1 and 50 km from AC grid 2. The HVDC cable connecting AC grids 1 and 2 is 75 km. The three VSCs forming the MTDC grid have a nominal DC voltage of 640 kV and a nominal apparent power of 1077 MVA, i.e. a nominal active power of 1000 MW. The VSC 1 and VSC 2 operate in DC voltage droop mode. The offshore wind farm and VSC 3 inject constant power into the MTDC grid, thus not participating to DC voltage control. The AC grid 1 is modelled as an infinite bus. However, the AC grid 2 is based on the hereafter-called Kundur power system, detailed in [19]. It represents two AC areas connected by two long AC lines, whose lengths are shown in Fig. 1. There are four generators, each having a rating of 900 MVA and 20 kV [19, 20]. Then, following the tripping of a generator in this system, the frequency deviates from its nominal value, while the remaining adjust their mechanical power output to restore the equilibrium. The objective of the proposed control strategy is to support frequency when this kind of faults occurs. It is detailed in the next section.

2.2 Studied MPC control strategy

The method for frequency support proposed in [12] is considered as an "emergency" control scheme. For small frequency deviations, the controller is inactive and the VSC power command P^{cmd} is adjusted according to DC voltage deviations following a P-V droop characteristic as follows:

$$P^{cmd} = P^{set} - K_v(V - V^{set}) \quad (1)$$

where K_v the DC voltage droop gain, V the DC voltage of the VSC, V^{set} its corresponding setpoint.
As shown in Fig. 2, P^{cmd}, along with the reactive power command Q^{cmd}, is passed to the current controllers which adjust the signals sent to the modulation strategy of the converter. The VSC 2 is synchronized to the AC grid with a Phase Lock Loop (PLL). When a large enough frequency deviation is sensed through the PLL on the AC side of the VSC, the controller is activated and adjusts the power transfer through the MTDC grid to take advantage of the primary reserves of the other AC areas. The objective of the control is to provide in steady state a predefined participation to frequency support, as defined by a frequency droop gain K_f.
To achieve this, the power setpoint P^{set} of the VSC 2 is adjusted as shown in Fig. 2. First, measurements at time k of the DC voltage, power and frequency $V^m(k), P^m(k)$ and $f^m(k)$ are collected. Then a constrained-optimization problem is solved. The output is the setpoint change $\Delta P^{set}(k)$. The cumulative control changes are then added to the P^{set} of the VSC as shown in Fig. 2.

2.3 Constrained optimization problem

A constrained-optimization problem is the core of the studied MPC-based control. This allows computing a sequence of control changes that minimizes an objective function while satisfying various input and output constraints [15]. This optimization is based on simplified models for the MTDC grid, able to predict the future system evolution. The complete formulation is also included here for convenience. For more information on how the prediction models are computed, as well as definitions of the involved variables, readers are kindly referred to the original reference [12].

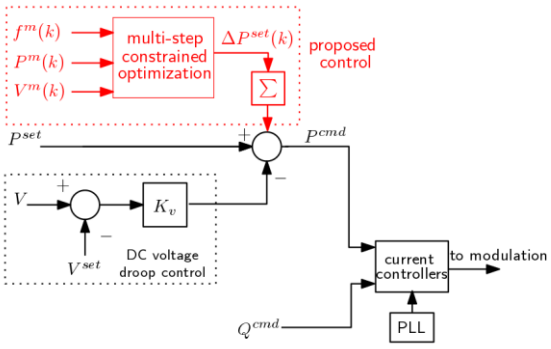

Figure 2: Control structure of VSC including MPC-based frequency support scheme.

The objective function consists of minimizing the deviations of the predicted VSC power from a pre-specified reference trajectory over the control horizon.[1]

$$\min_{P,\epsilon,V,\Delta P^{set}} w \sum_{j=1}^{N_c} [P^{set}(k+j) - P(k+j)]^2 + v \sum_{j=1}^{N_c} [\epsilon(k+j)]^2 \quad (2)$$

where w and v are weighting factors.
The minimization of (2) is subject to the following constraints for $j = 1, \dots, N_c$,:

$$V^{min} - \epsilon(k+j) \le V(k+j) \le V^{max} + \epsilon(k+j) \quad (3)$$

$$P^{min} \le P(k+j) \le P^{max} \quad (4)$$

$$\epsilon(k+j) \ge 0 \quad (5)$$

$$V(k+j) = V(k+j-1) + s_v \Delta P^{set}(k+j-1) \quad (6)$$

$$P(k+j) = P(k+j-1) + \Delta P^{set}(k+j-1) - K_v(V(k+j) - V(k+j-1)) \quad (7)$$

Constraint (3) ensures that the DC voltage will not violate the security minimum and maximum limits V^{min}, V^{max}, respectively, while supporting frequency. Constraint (4) specifies that the VSC minimum and maximum power (P^{min} and P^{max}, respectively) are satisfied. Equality constraints (6)-(7) yield the predicted power and DC voltage in response to the control actions. ϵ is a slack variable to relax output constraint (3) in case of infeasibility. Choosing a high value for the weighting factor v in (2) keeps the value of ϵ as small as possible.
Note that the studied MPC-based control strategy is triggered when frequency exits a deadband (a value of ±100 mHz has been taken) and remains active until frequency is restored inside a narrower deadband (e.g. ±10 mHz).

3 Step-by-step implementation of MPC on low scale three-terminal VSC-HVDC Mockup

The general idea of this section is to explain the proposed methodology that has been developed starting from a High voltage offline simulation and ending in the real-time implementation on a low voltage DC mock up. So, two main steps have been identified such as the integration of the algorithm in C language in a real-time high voltage simulation, and the downscaling of the application to a low voltage MTDC grid.

3.1 Validation of the MPC controller for High Voltage MTDC Grid

The behaviour of the controller has been tested with off-line dynamic simulations in Ramses, a FORTRAN-based dynamic simulation tool developed at University of Liege, which is mandatory for the designed real-time solver [21]. Before moving to the mock-up low-scale DC grid, some steps are required to validate the controller in the tools used by L2EP laboratory, as shown in Fig. 3.

1. The first step consists of the implementation of the whole system and the MPC-based control scheme in the Matlab/SimPowerSystem environment.
2. The second step involves the reformulation of the quadratic optimization control by using only inequality constraints. Then, the updated formulation of MPC-based scheme is implemented and tested under Matlab environment.
3. The last step concerns the implementation of the MPC controller in C language, necessary for implementation in the Digital Signal Processor (DSP) of the VSC. To accelerate the solution of the convex optimization problem, the solver accepts the optimization of the objective function under only inequality constraints.

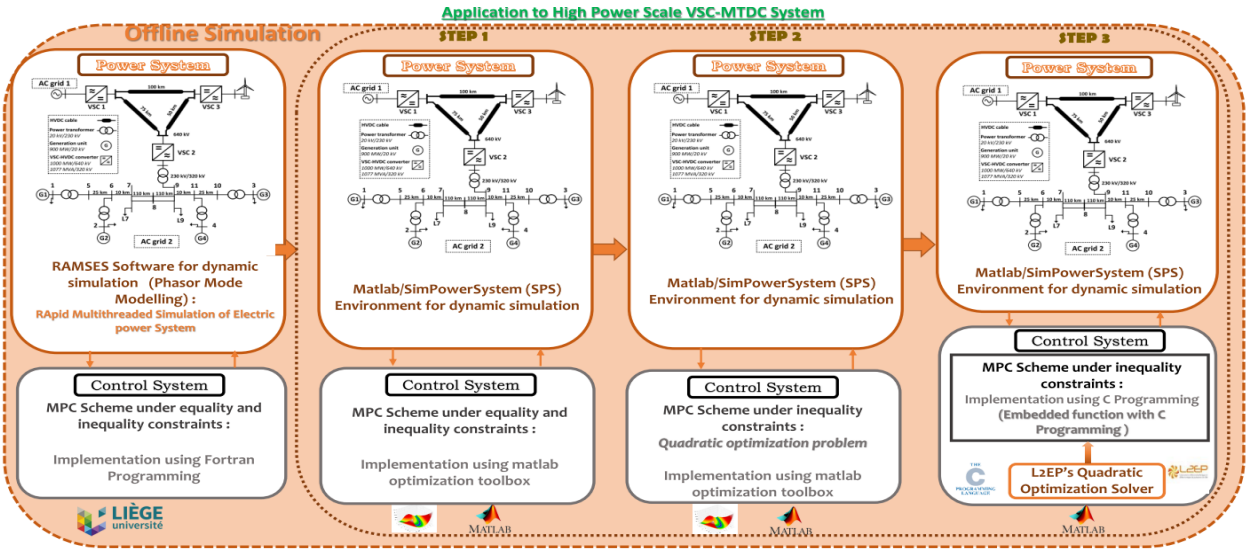

Figure 3: Different steps of MPC validation for high power scale studied system.

[1] here set equal to the prediction horizon

3.2 Validation of the MPC controller on low-scale MTDC mock-up

The next step is the validation of the controller on the low-scale mock-up configuration shown in Fig.4. The mock-up includes two main parts: (i) the physical part (in the middle of the figure below) and (ii) the virtual part implemented in a real-time simulator (highlighted in blue). The interface between the physical devices and the analogue outputs of the real-time simulator is achieved by high-bandwidth AC or DC power amplifiers. The VSC converters are 2-level converters with an LCL filter for mitigating the current harmonics on the AC side, and with a DC capacitor on the DC side. Each one is rated at 3.15 kVA / 200 V - 3 kW / 400 V. Three real DC cables are used to build the DC grid where the lengths are mentioned on the Fig.4. The reader is kindly referred to [16] for more details concerning this system.

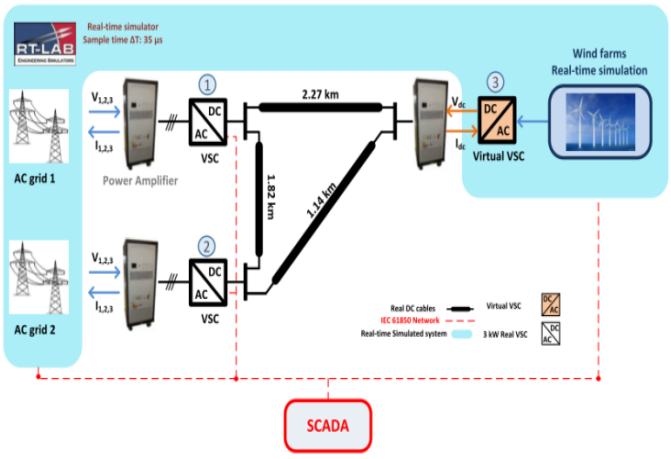

Figure 4: Mock-up general overview.

Four main steps are carried out in order to implement and validate the control on the mock-up:

Step 1: The first step validates the off line simulation of the MPC applied on the down scaled model of the system, As illustrated in Fig.5, the interface between the simulated low-scale DC grid and the high-power Kundur AC grid is performed through a homothetic gain G, equal to the ratio of the base power P_b^{high} of the high-scale system (i.e. the simulated system) over the base power P_b^{low} of the low-scale low scale physical system, i.e.:

$$G = \frac{P_b^{high}}{P_b^{low}} \tag{8}$$

Step 2: Full Real Time Simulation

The second step involves the full real-time simulation performed with a sampling time of 35 µs using OPAL-RT and RTLab tools [22].

Step 3: HIL Simulation

The third step is HIL simulation. The MPC algorithm, as well as the low-level and high-level conventional VSC controllers, is implemented inside the DSP development kit. In this work, the DSP TMS320F28377D (Dual Core Delfino Micro Controller) is used. One core is used to solve the quadratic optimization problem of the MPC, whereas the second for the rest of the VSC controls. It has to be highlighted that the correct operation of the DSP requires good synchronization between both cores. The power part of the system is still simulated in real-time using OPAL-RT. It is important to mention that the CPU of the DSP runs on a 32-bit floating-point precision. The same precision is used for the solution of the MPC. This yields a computational time of 33 ms to solve the quadratic optimization scheme, well below the sampling time of the MPC (set to 250 ms).

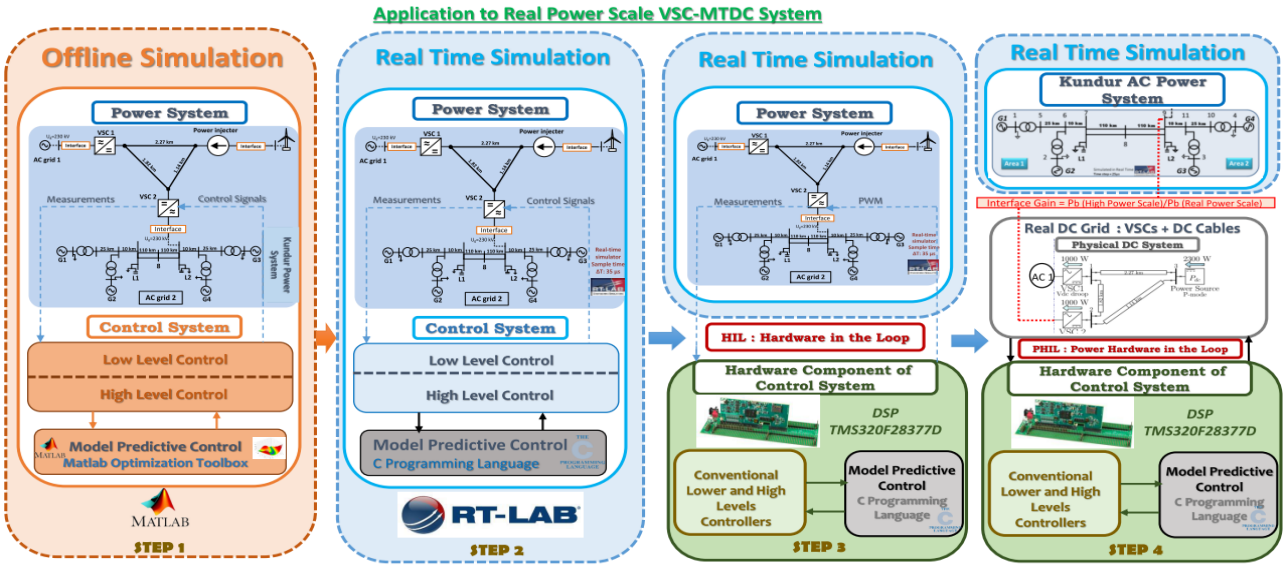

Figure 5: Steps description of MPC application to real power scale of 3 Terminal DC grid.

Step 4: PHIL Simulation. The last step concerns the validation of the controller using PHIL. This consists of using hardware components interacting with the external simulated systems. This last and most important step represents the practical test allowing the experimental validation of the studied advanced control strategy. More technical details concerning the PHIL step are available in [22].

4 Experimental results based on mock-up MTDC grid using PHIL

This section presents the results of the last step i.e. the PHIL simulation depicted by the Fig. 6. The initial operating points for AC grid 2 and the MTDC grid are given in Table 1 and Table 2, respectively. The parameters of the MPC-based controller of VSC2 are given in Table 3. The controller is activated if the frequency measured by VSC2 exceeds a deadband of ±100 mHz.

The experimental results following the tripping of generator G4 are shown in Figs. 7, 8 and 9, which show the frequency of AC grid 2, the DC powers of VSC1 and VSC2, and the MTDC grid DC voltages, respectively. Note that the frequency behaviour corresponds to the speed response of synchronous machine G1. Following the disturbance, the frequency starts decreasing and drops below the frequency deadband (i.e. 49.9 Hz). This activates the frequency support scheme of VSC2, which starts injecting more power in the AC grid. As shown in Fig.7, this support yields good performances in transient and steady state. The power requested by VSC2 is provided through the DC voltage droop mechanism by VSC1, which increases the power it injects into the DC grid, as shown in Fig. 8. It should be highlighted that the frequency support of VSC2 is somewhat "stalled" around 130 s. This is explained due to the DC voltage reaching its threshold V^{min}, hence preventing VSC2 from providing more power. However, following the AC frequency recovery, the power of VSC2 also recovers and settles at the value defined by the selected frequency droop.

Pmin (p.u)	Pmax (p.u)	Vmin (p.u)	Vmax (p.u)	Sv (p.u)	Kv (p.u)	Kf (p.u)
-1	1	0,90	1,1	0,4365	0,82	0,05

Table 3: Control parameters of MPC.

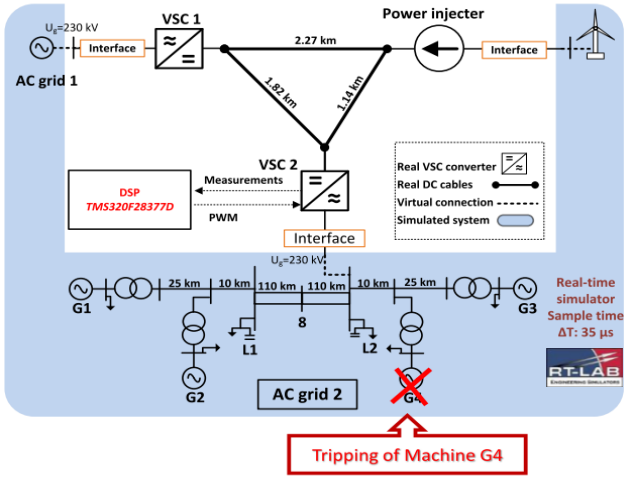

Figure 6: PHIL simulation test with G4 tripping.

Converter	VSC 1	VSC 2	VSC 3
DC Power (W)	1000	1000	-2100
DC Voltage (V)		400	

Table 1: Operating point of DC grid.

	Area 1		Area 2	
Machines	G1	G2	G3	G4
Pn(MW)	900	900	900	900
P (MW)	615	615	615	315
Statism (pu/pu)	----	0,04	0,04	----
Loads (MW)	1463		986	

Table 2: Operating point of AC grid 2.

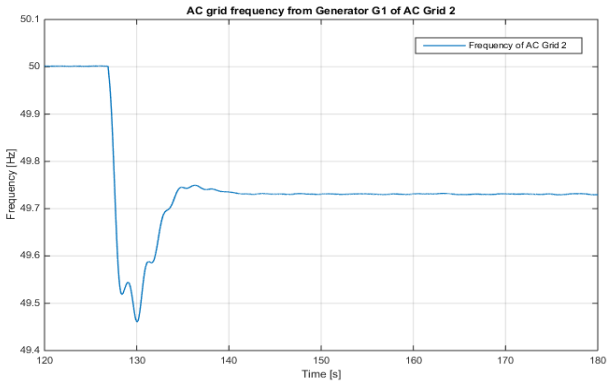

Figure 7: Frequency behaviour of AC grid 2.

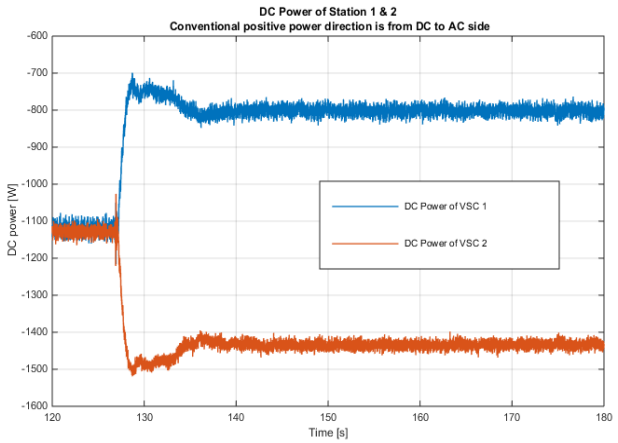

Figure 8: DC Power after losing G4 based on MPC.

5 Conclusion

This paper has presented a step-by-step implementation process of an advanced control strategy inspired of MPC for primary frequency support. A rigorous systematic validation method is performed starting from offline dynamic stability simulations, up to the experimental validation on a physical low-scale mock-up MTDC grid.

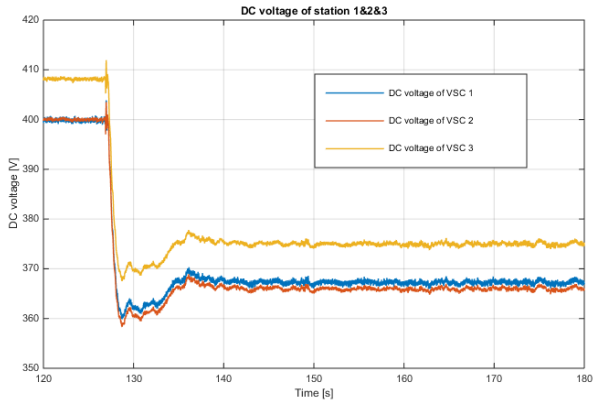

Figure 9: DC voltages after losing G4 based on MPC.

HIL and PHIL simulation methods are employed to reach this purpose. This study has served two purposes. First, it validates the results of the method presented in [12], and demonstrates the agreement between simulation and experimental results. Second, it has demonstrated the feasibility of implementing such advanced control strategies (like MPC), that require the solution of optimization problems. This has been achieved, by using conventional hardware development boards, like the DSP of the VSC, and proves that the use of powerful calculators is not necessary.

Acknowledgement

This research work was supported by the French's TSO, Réseau de Transport d'Electricité (RTE).

References

[1] N.B. Negra, J. Todorovic, T. Ackermann, "Loss evaluation of HVAC and HVDC transmission solutions for large offshore wind farms," Electr. Power Syst. Res. 76 (2006) 916–927.

[2] D. Van Hertem, M. Ghandhari, "Multi-terminal VSC HVDC for the European supergrid: Obstacles", Renewable and Sustainable Energy Reviews 14 (2010) 3156–3163.

[3] T. K. Vrana, "System Design and Balancing Control of the North Sea Super Grid", Ph.D. thesis, Norwegian Univ. of Sc. and Techn., 2013.

[4] T. M. Haileselassie and K. Uhlen, "Primary frequency control of remote grids connected by multi-terminal HVDC," in Proc. 2010 IEEE PES General Meeting.

[5] R. Wiget, G. Andersson, M. Andreasson, D. V. Dimarogonas, and K. H. Johansson, "Dynamic simulation of a combined AC and MTDC grid with decentralized controllers to share primary frequency control reserves," in Proc. 2015 IEEE PES Eindhoven PowerTech.

[6] T. K. Vrana, L. Zeni, and O. B. Fosso, "Active power control with undead-band voltage & frequency droop applied to a meshed DC grid test system," in Proc. 2012 IEEE ENERGYCON.

[7] S. Akkari, J. Dai, M. Petit, and X. Guillaud, "Coupling between the frequency droop and the voltage drop of an AC/DC converter in an MTDC system," in Proc. 2015 IEEE PES Eindhoven PowerTech.

[8] T. M. Haileselassie, T. Undeland, "Multi-Terminal VSC-HVDC System for Integration of Offshore Wind Farms and Green Electrification of Platforms in the North Sea," in: Nord. Workshop Power Ind. Electron., 2008.

[9] A. Sarlette, J. Dai, Y. Phulpin, D. Ernst, "Cooperative frequency control with a multi-terminal high-voltage DC network," Automatica. 48 (2012) 3128–3134.

[10] S. Akkari. Control of a multi-terminal HVDC (MTDC) system and study of the interactions between the MTDC and the AC grids. Phd thesis, Supélec, October 2016.

[11] S. Akkari, J. Dai, M. Petit, X. Guillaud, "Interaction between the voltage-droop and the frequency-droop control for multi-terminal HVDC systems," Transm. Distrib. IET Gener. 10 (2016) 1345–1352.

[12] L. Papangelis, M.-S. Debry, P. Panciatici, and T. Van Cutsem, "A receding horizon approach to incorporate frequency support into the AC/DC converters of a multi-terminal DC grid," Electric Power Systems Research, vol. 148, pp. 1–9, July 2017.

[13] L. Papangelis, M.-S. Debry, T. Van Cutsem, P. Panciatici, "Local control of AC/DC converters for frequency support between asynchronous AC areas", in: Proc. 2017 IEEE Manchester PowerTech.

[14] L. Papangelis, M.-S. Debry, P. Panciatici, and T. Van Cutsem, "Coordinated Supervisory Control of Multi-Terminal HVDC Grids: A Model Predictive Control Approach," IEEE Transactions on Power System, Vol. 32, Issue 6, 2017.

[15] J. M. Maciejowski, Predictive control: with constraints. Pearson education, 2002.

[16] S. A. Amamra, F. Colas, X. Guillaud, P. Rault, S. Nguefeu, "Laboratory Demonstration of a Multi-Terminal VSC-HVDC Power Grid," IEEE Trans. Power Deliv. (2016).

[17] P. Rault. Dynamic Modeling and Control of Multi-Terminal HVDC Grids . Phd thesis, Ecole Centrale de Lille - L2EP, March 2014.

[18] K. Almaksour, S. Akkari, MM. Belhaouane, F. Colas and X. Guillaud, "Power-Hardware-In-the-Loop simulation of VSC-HVDC based three-terminal DC mock-up" The Power Systems Computation Conference, PSCC 2018, Dublin, Ireland.

[19] P. Kundur, N.J. Balu, and M.G. Lauby, Power system stability and control.: McGraw-Hill Professional, 1994.

[20] M. Klein, G. J. Rogers, and P. Kundur, "A fundamental study of inter-area oscillations in power systems," IEEE Transactions on Power Systems, vol. 6, no. 3, pp. 914-921, 1991.

[21] P. Aristidou, L. Papangelis, X. Guillaud, and T. Van Cutsem, "Modular modelling of combined AC and DC systems in dynamic simulations," in Proc. IEEE Eindhoven PowerTech, 2015.

[22] C. Dufour, S. Abourida, and J. Belanger, "Hardware-In-the-Loop Simulation of Power Drives with RT-LAB," in 2005 International Conference on Power Electronics and Drives Systems, 2005, vol. 2, pp. 1646–1651.

Bibliography

[AAB+18] K. Almaksour, S. Akkari, M. M. Belhaouane, F. Colas, and X. Guillaud. Power-Hardware-In-the-Loop simulation of VSC- HVDC based three-terminal DC mock-up. In *Proceedings of IEEE PSCC*, Dublin, 2018.

[ABB17] ABB. ABB achieves breakthrough with world's most powerful hvdc transformer, 2017. Press release: https://new.abb.com/news/detail/2718/.

[ACG+13] S. A. Amamra, F. Colas, X. Guillaud, P. Rault, and S. Nguefeu. Laboratory-based test bed of a three terminals dc networks using power hardware in the loop. In *Proceedings of 15th European Conference on Power Electronics and Applications (EPE)*, Sept 2013.

[ACJ+14] H. Atighechi, S. Chiniforoosh, J. Jatskevich, A. Davoudi, J. A. Martinez, M. O. Faruque, V. Sood, M. Saeedifard, J. M. Cano, J. Mahseredjian, D. C. Aliprantis, and K. Strunz. Dynamic Average-Value Modeling of CIGRE HVDC Benchmark System. *IEEE Transactions on Power Delivery*, 29(5):2046–2054, oct 2014.

[ACML+15] O. D. Adeuyi, M. Cheah-Mane, J. Liang, N. Jenkins, Y. Wu, C. Li, and X. Wu. Frequency support from modular multilevel converter based multi-terminal HVDC schemes. In *Proceedings of IEEE PES General Meeting*, 2015.

[ADF+05] G. Andersson, P. Donalek, R. Farmer, N. Hatziargyriou, I. Kamwa, P. Kundur, N. Martins, J. Paserba, P. Pourbeik, J. Sanchez-Gasca, et al. Causes of the 2003 major grid blackouts in north america and europe, and recommended means to improve system dynamic performance. *IEEE transactions on Power Systems*, 20(4):1922–1928, 2005.

[ADPG15] S. Akkari, J. Dai, M. Petit, and X. Guillaud. Coupling between the frequency droop and the voltage droop of an AC/DC converter in an MTDC system. In *Proceedings of IEEE PES Eindhoven PowerTech*, 2015.

[AEAG14] M. Aragüés-Peñalba, A. Egea-Àlvarez, S. G. Arellano, and O. Gomis-Bellmunt. Droop control for loss minimization in HVDC multi-terminal transmission systems for large offshore wind farms. *Electric Power Systems Research*, 112:48–55, 2014.

[AFV14] P. Aristidou, D. Fabozzi, and T. Van Cutsem. Dynamic Simulation of Large-Scale Power Systems Using a Parallel Schur-Complement-Based Decomposition Method. *IEEE Transactions on Parallel and Distributed Systems*, 25(10):2561–2570, 2014.

[AIT13] S. P. Azad, R. Iravani, and J. E. Tate. Damping inter-area oscillations based on a model predictive control (mpc) hvdc supplementary controller. *IEEE Transactions on Power Systems*, 28(3):3174–3183, 2013.

[Akk16] S. Akkari. *Control of a multi-terminal HVDC (MTDC) system and study of the interactions between the MTDC and the AC grids*. PhD thesis, University Paris-Saclay, France, 2016.

[APGV15] P. Aristidou, L. Papangelis, X. Guillaud, and T. Van Cutsem. Modular modelling of combined AC and DC systems in dynamic simulations. In *Proceedings of IEEE Eindhoven PowerTech*, 2015.

[Ari15] P. Aristidou. *Time-domain simulation of large electric power systems using domain-decomposition and parallel processing methods*. PhD thesis, Université de Liège, Belgium, 2015.

[AS13] B. M. Amaral Silva. *Multi-terminal HVDC Grids : Control Strategies for Ancillary Services Provision in Interconnected Transmission Systems with Offshore Wind Farms*. PhD thesis, University of Porto, Portugal, 2013.

[AWD+15] M. Andreasson, R. Wiget, D. V. Dimarogonas, K. H. Johansson, and G. Andersson. Coordinated Frequency Control through MTDC Transmission Systems. *IFAC-PapersOnLine*, 48(22):106–111, 2015.

[Bah08] M. P. Bahrman. HVDC transmission overview. In *Proceedings of IEEE/PES Transmission and Distribution Conference and Exposition*. IEEE, 2008.

[BCH14] L. Bizumic, R. Cherkaoui, and U. Hger. Ch.17 - interface Protection. In *Monitoring, Control and Protection of Interconnected Power Systems*, pages 333–347. Springer, 2014.

[Bem18] A. Bemporad. Model Predictive Control, 2018. Lecture slides, Available on: http://cse.lab.imtlucca.it/~bemporad/.

[Ber09] A. R. Bergen. *Power systems analysis*. Pearson Education India, 2009.

[BGG+14] J. Beerten, O. Gomis-Bellmunt, X. Guillaud, J. Rimez, A. van der Meer, and D. Van Hertem. Modeling and control of HVDC grids: A key challenge for the future power system. In *Proceedings of IEEE PSCC*, 2014.

[BLM14] B. Berggren, K. Linden, and R. Majumder. DC Grid Control Through the Pilot Voltage Droop Concept - Methods for Establishing Set-Point Tracking. In *Proceedings of IEEE International Energy Conference*, 2014.

[BPR+04] W. Breuer, D. Povh, D. Retzmann, E. Teltsch, and X. Lei. Role of HVDC and FACTS in future power systems. In *Proceedings of CIGRE Symposium, Shanghai*, 2004.

[bri] The BritNed link. Available online: http://www.britned.com/.

[BV15] J. Beerten and D. Van Hertem. Analysis of power redispatch schemes for HVDC grid secondary voltage control. In *Proceedings of IEEE PES General Meeting*, 2015.

[BV18] H. S. Bidgoli and T. Van Cutsem. Combined Local and Centralized Voltage Control in Active Distribution Networks. *IEEE Transactions on Power Systems*, 33(2):1374–1384, mar 2018.

[CB11] S. Cole and R. Belmans. A proposal for standard VSC HVDC dynamic models in power system stability studies. *Electric Power Systems Research*, 81(4):967–973, apr 2011.

[CDBB13] L. Castaing, M.-S. Debry, G. Bareux, and O. Beck. Optimal operation of hvdc links embedded in an ac network. In *Proceedings of Grenoble IEEE PowerTech*, 2013.

[CDW16] J. Cao, W. Du, and H. F. Wang. An Improved Corrective Security Constrained OPF for Meshed AC/DC Grids With Multi-Terminal VSC-HVDC. *IEEE Transactions on Power Systems*, 31(1):485–495, jan 2016.

[CEA13] S. Chatzivasileiadis, D. Ernst, and G. Andersson. The global grid. *Renewable Energy*, 57:372–383, 2013.

[Chu00] S. K. Chung. A phase tracking system for three phase utility interface inverters. *IEEE Transactions on Power Electronics*, 2000.

[CIG07] CIGRE Working Group 601. CIGRE Technical Brochure on REVIEW OF ON-LINE DYNAMIC SECURITY ASSESSMENT. Technical report, 2007.

[CIG14] CIGRE WG B4.57. *Guide for the Development of Models for HVDC Converters in a HVDC Grid*, 2014. CIGRE Technical Brochure 604.

[CMP+11] F. Capitanescu, J. Martinez Ramos, P. Panciatici, D. Kirschen, A. Marano Marcolini, L. Platbrood, and L. Wehenkel. State-of-the-art, challenges, and future trends in security constrained optimal power flow. *Electric Power Systems Research*, 81(8):1731–1741, aug 2011.

[DL74] T. E. Dy Liacco. Real-time computer control of power systems. *Proceedings of the IEEE*, 62(7):884–891, 1974.

[DPD+18] G. Denis, T. Prevost, M.-S. Debry, F. Xavier, X. Guillaud, and A. Menze. The MIGRATE project: the challenges of operating a transmission grid with only inverter-based generation. A grid-forming control improvement with transient current-limiting control. *IET Renewable Power Generation*, 12(5):523–529, apr 2018.

[DSR+12] C. Dierckxsens, K. Srivastava, M. Reza, S. Cole, J. Beerten, and R. Belmans. A distributed DC voltage control method for VSC MTDC systems. *Electric Power Systems Research*, 82(1):54–58, jan 2012.

[DV13] S. De Boeck and D. Van Hertem. Coordination of multiple HVDC links in power systems during alert and emergency situations. In *Proceedings of IEEE PowerTech Grenoble Conference*, 2013.

[EBVG15] A. Egea-Alvarez, J. Beerten, D. Van Hertem, and O. Gomis-Bellmunt. Hierarchical power control of multiterminal HVDC grids. *Electric Power Systems Research*, 121:1–7, apr 2015.

[EE12] ENTSO-E. Load-Frequency Control and Performance, 2012.

[EE14a] ENTSO-E. Draft Network Code on High Voltage Direct Current Connections and DC- connected Power Park Modules, 2014.

[EE14b] ENTSO-E. Technical background for the Low Frequency Demand Disconnection requirements, 2014.

[EFHG15] A. Egea-Alvarez, S. Fekriasl, F. Hassan, and O. Gomis-Bellmunt. Advanced Vector Control for Voltage Source Converters Connected to Weak Grids. *IEEE Transactions on Power Systems*, 2015.

[ENT] ENTSO-E. Regional security coordinators. https://docstore.entsoe.eu/major-projects/RSC/Pages/default.aspx.

[ENT12] ENTSO-e System Protection and Dynamics subgroup. Special Protection Schemes, 2012.

[FC78] L. H. Fink and K. Carlsen. Operating under stress and strain. *IEEE Spectrum;(United States)*, 15(3), 1978.

[FE07] C. Feltes and I. Erlich. Variable Frequency Operation of DFIG based Wind Farms connected to the Grid through VSC-HVDC Link. In *Proceedings of IEEE PES General Meeting*, 2007.

[FGWV09] D. Fabozzi, M. Glavic, L. Wehenkel, and T. Van Cutsem. Security assessment by multiple transmission system operators exchanging sensitivity and tie-line power flow information. In *Proceedings of IEEE Bucharest PowerTech*, 2009.

[FIDM14] A. Fuchs, M. Imhof, T. Demiray, and M. Morari. Stabilization of Large Power Systems Using VSC-HVDC and Model Predictive Control. *IEEE Transactions on Power Delivery*, 29(1):480–488, feb 2014.

[FLB07] X. Feng, Z. Lubosny, and J. W. Bialek. Identification based Dynamic Equivalencing. *Proceedings of IEEE Lausanne PowerTech*, pages 267–272, 2007.

[FPB17] J. Fradley, R. Preece, and M. Barnes. VSC-HVDC for Frequency Support (a review). *13th IET International Conference on AC and DC Power Transmission (ACDC 2017)*, 2, 2017.

[FPS+16] J. Freytes, L. Papangelis, H. Saad, P. Rault, T. V. Cutsem, and X. Guillaud. On the modeling of MMC for use in large scale dynamic simulations. In *Proceedings of Power Systems Computation Conference (PSCC)*, 2016.

[Fre17] J. Freytes. *Small-signal stability analysis of Modular Multilevel Converters and application to MMC-based Multi-Terminal DC grids*. PhD thesis, Ecole Centrale de Lille, 2017.

[GCL+15] C. Gavriluta, I. Candela, A. Luna, A. Gomez-Exposito, and P. Rodriguez. Hierarchical Control of HV-MTDC Systems With Droop-Based Primary and OPF-Based Secondary. *IEEE Transactions on Smart Grid*, 6(3):1502–1510, may 2015.

[GHRVC11] M. Glavic, M. Hajian, W. Rosehart, and T. Van Cutsem. Receding-horizon multi-step optimization to correct nonviable or unstable transmission voltages. *IEEE Transactions on Power Systems*, 26(3):1641–1650, 2011.

[GL15] F. Gonzalez-Longatt. Optimal power flow in MTDC systems based on a DC-independent system operator objective. In *Proceedings of IEEE Eindhoven PowerTech*, 2015.

[Hai12] T. M. Haileselassie. *Control, Dynamics and Operation of Multi-terminal VSC-HVDC Transmission Systems*. PhD thesis, Norwegian University of Science and Technology, 2012.

[HEU15] T. M. Haileselassie, A. G. Endegnanew, and K. Uhlen. Secondary control in multi-terminal VSC-HVDC transmission system. In *Proceedings of IEEE PES General Meeting*, 2015.

[HG06] I. A. Hiskens and B. Gong. Voltage stability enhancement via model predictive control of load. *Intelligent Automation & Soft Computing*, 12(1):117–124, 2006.

[HL17] D. V. Hertem and W. Leterme. D4 . 2 Broad comparison of fault clearing strategies for DC grids. Technical Report 691714, 2017.

[HNA+07] G. Hug-Glanzmann, R. Negenborn, G. Andersson, B. De Schutter, and H. Hellendoorn. Multi-area control of overlapping areas in power systems for FACTS control. In *Proceedings of IEEE Lausanne PowerTech*, 2007.

[HU10] T. M. Haileselassie and K. Uhlen. Primary frequency control of remote grids connected by multi-terminal HVDC. In *Proceedings of IEEE PES General Meeting*, 2010.

[IEE15] IEEE PES Task Force. Test Systems for Voltage Stability Analysis and Security Assessment, 2015. Technical Report PES-TR19, Available online on IEEE PES Resource Center. http://resourcecenter.ieee-pes.org/pes/product/technical-publications/PESTR19.

[IWCA15] E. Iggland, R. Wiget, S. Chatzivasileiadis, and G. Anderson. Multi-Area DC-OPF for HVAC and HVDC Grids. *IEEE Transactions on Power Systems*, 30(5):2450–2459, sep 2015.

[JA15] D. Jovcic and K. Ahmed. *High voltage direct current transmission: converters, systems and DC grids*. John Wiley & Sons, 2015.

[JC15] M. Jimenez Carrizosa. *Hierarchical control scheme for multi-terminal high voltage direct current power networks*. PhD thesis, Universite Paris Sud, 2015.

[JPSE11] D. Jing, Y. Phulpin, A. Sarlette, and D. Ernst. Voltage control in an HVDC system to share primary frequency reserves between non-synchronous areas. In *Proceedings of 17th Power Systems Computation Conference (PSCC)*, 2011.

[KBL94] P. Kundur, N. J. Balu, and M. G. Lauby. *Power system stability and control*, volume 7. McGraw-hill New York, 1994.

[KCV+09] S. Kouro, P. Cortés, R. Vargas, U. Ammann, and J. Rodríguez. Model predictive controla simple and powerful method to control power converters. *IEEE Transactions on industrial electronics*, 56(6):1826–1838, 2009.

[LM03] A. Lesnicar and R. Marquardt. An innovative modular multilevel converter topology suitable for a wide power range. In *Proceedings of IEEE PowerTech Conference, Bologna*, June 2003.

[Mac02] J. M. Maciejowski. *Predictive control: with constraints*. Pearson education, 2002.

[MFM14] S. Mariethoz, A. Fuchs, and M. Morari. A VSC-HVDC Decentralized Model Predictive Control Scheme for Fast Power Tracking. *IEEE Transactions on Power Delivery*, 29(1):462–471, feb 2014.

[MM18] P. McNamara and F. Milano. Model predictive control-based AGC for multi-terminal hvdc-connected ac grids. *IEEE Transactions on Power Systems*, 33(1):1036–1048, 2018.

[MND+16] P. Mc Namara, R. R. Negenborn, B. De Schutter, G. Lightbody, and S. McLoone. Distributed MPC for frequency regulation in multi-terminal HVDC grids. *Control Eng. Practice*, pages 176–187, 2016.

[MS15] I. Martinez-Sanz. *Control of AC / DC Systems for Improved Transient Stability and Frequency Support Provision*. PhD thesis, Imperial College London, 2015.

[MZL+17] K. Meng, W. Zhang, Y. Li, Z. Y. Dong, Z. Xu, K. P. Wong, and Y. Zheng. Hierarchical SCOPF Considering Wind Energy Integration Through Multiterminal VSC-HVDC Grids. *IEEE Transactions on Power Systems*, 32(6):4211–4221, nov 2017.

[Nat13] National Grid Electricity Transmission. The grid code, Dec. 2013.

[NTP16] S. Nanou, O. Tzortzopoulos, and S. Papathanassiou. Evaluation of an enhanced power dispatch control scheme for multi-terminal HVDC grids using Monte-Carlo simulation. *Electric Power Systems Research*, 2016.

[OMGV07] B. Otomega, A. Marinakis, M. Glavic, and T. Van Cutsem. Emergency alleviation of thermal overloads using model predictive control. In *Proceedings of IEEE Lausanne PowerTech*, 2007.

[PAGVC16] F. Plumier, P. Aristidou, C. Geuzaine, and T. Van Cutsem. Co-simulation of electromagnetic transients and phasor models: A relaxation approach. *IEEE Transactions on Power Delivery*, 31(5):2360–2369, 2016.

[PCG12] Y. Pipelzadeh, B. Chaudhuri, and T. C. Green. Inertial response from remote offshore wind farms connected through VSC-HVDC links: A communication-less scheme. In *Proceedings of IEEE PES General Meeting*, 2012.

[PDP+18a] L. Papangelis, M.-S. Debry, T. Prevost, P. Panciatici, and T. Van Cutsem. Decentralized model predictive control of voltage source converters for AC frequency containment. *International Journal of Electrical Power & Energy Systems*, 98:342–349, jun 2018.

[PDP+18b] L. Papangelis, M.-S. Debry, T. Prevost, P. Panciatici, and T. Van Cutsem. Stability of a voltage source converter subject to decrease of short-circuit capacity: a case study. *Proceedings of the 20th PSCC*, 2018.

[PDPV15] L. Papangelis, M.-S. Debry, P. Panciatici, and T. Van Cutsem. A dynamic simulation approach to identify additional reactive reserves against long-term voltage instability. In *Proceedings of IEEE Eindhoven PowerTech*, 2015.

[PDPV17a] L. Papangelis, M.-S. Debry, P. Panciatici, and T. Van Cutsem. A receding horizon approach to incorporate frequency support into the AC/DC converters of a multiterminal DC grid. *Electric Power Systems Research*, 148, jul 2017.

[PDPV17b] L. Papangelis, M.-S. Debry, P. Panciatici, and T. Van Cutsem. Coordinated Supervisory Control of Multi-Terminal HVDC Grids: a Model Predictive Control Approach. *IEEE Transactions on Power Systems*, 2017.

[PDPV17c] L. Papangelis, M.-S. Debry, P. Panciatici, and T. Van Cutsem. Local control of AC/DC converters for frequency support between asynchronous AC areas. In *Proceedings of IEEE Manchester PowerTech*, 2017.

[PGV15] L. Papangelis, X. Guillaud, and T. Van Cutsem. Frequency support among asynchronous AC systems through VSCs emulating power plants. In *Proceedings of IET Intern. Conf. on AC and DC Power Transm.*, 2015.

[Phu12] Y. Phulpin. Communication-Free Inertia and Frequency Control for Wind Generators Connected by an HVDC-Link. *IEEE Transactions on Power Systems*, 27:1136–1137, 2012.

[PWK+17] A. Parisio, C. Wiezorek, T. Kyntaja, J. Elo, K. Strunz, and K. H. Johansson. Cooperative MPC-Based Energy Management for Networked Microgrids. *IEEE Transactions on Smart Grid*, 8(6):3066–3074, nov 2017.

[QB00] S. J. Qin and T. A. Badgwell. An overview of nonlinear model predictive control applications. In *Nonlinear model predictive control*, pages 369–392. Springer, 2000.

[QB03] S. J. Qin and T. A. Badgwell. A survey of industrial model predictive control technology. *Control Eng. Practice*, pages 733–764, 2003.

[Rau14] P. Rault. *Dynamic Modeling and Control of Multi-Terminal HVDC Grids*. PhD thesis, Ecole Centrale de Lille, L2EP, 2014.

[RCGN12] P. Rault, F. Colas, X. Guillaud, and S. Nguefeu. Method for small signal stability analysis of VSC-MTDC grids. In *Proceedings of IEEE Power and Energy Society General Meeting*, 2012.

[RRS05] W. Rosehart, C. Roman, and A. Schellenberg. Optimal Power Flow With Complementarity Constraints. *IEEE Transactions on Power Systems*, 20(2):813–822, may 2005.

[SBGV16] H. Soleimani Bidgoli, M. Glavic, and T. Van Cutsem. Receding-Horizon Control of Distributed Generation to Correct Voltage or Thermal Violations and Track Desired Schedules. In *Proceedings of 19th IEEE Power Systems Computation Conference (PSCC)*, 2016.

[SDM+14] H. Saad, S. Dennetière, J. Mahseredjian, P. Delarue, X. Guillaud, J. Peralta, and S. Nguefeu. Modular multilevel converter models for electromagnetic transients. *IEEE Transactions on Power Delivery*, 29(3):1481–1489, June 2014.

[SGGD15] S. Samimi, F. Gruson, X. Guillaud, and P. Delarue. Control of dc bus voltage with a modular multilevel converter. In *Proceedings of IEEE Eindhoven PowerTech*, 2015.

[SGM+15] H. Saad, X. Guillaud, J. Mahseredjian, S. Dennetière, and S. Nguefeu. MMC Capacitor Voltage Decoupling and Balancing Controls. *IEEE Transactions on Power Delivery*, 30(2):704–712, April 2015.

[SKS17] S. Schilling, M. Kuschke, and K. Strunz. AC-DC optimal power flow implementation: Modeling and application to an HVDC overlay grid. In *Proceedings of IEEE Manchester PowerTech*, 2017.

[SMS+12] B. Silva, C. L. Moreira, L. Seca, Y. Phulpin, and J. Pecas Lopes. Provision of Inertial and Primary Frequency Control Services Using Offshore Multiterminal HVDC Networks. *IEEE Transactions on Sustainable Energy*, 3(4):800–808, oct 2012.

[Sol17] H. Soleimani Bidgoli. *Real-time Corrective Control in Active Distribution Networks*. PhD thesis, University of Liege, 2017.

[SPG13] C. E. Spallarossa, Y. Pipelzadeh, and T. C. Green. Influence of frequency-droop supplementary control on disturbance propagation through VSC HVDC links. In *Proceedings of IEEE PES General Meeting*, 2013.

[TAGS16] R. Teixeira Pinto, M. Aragues-Penalba, O. Gomis-Bellmunt, and A. Sumper. Optimal Operation of DC Networks to Support Power System Outage Management. *IEEE Transactions on Smart Grid*, 7(6):2953–2961, nov 2016.

[TP14] R. Teixeira Pinto. *Multi-Terminal DC Networks System Integration, Dynamics and Control*. PhD thesis, Delft University of Tech., 2014.

[Tri06] F. Trieb. Trans-mediterranean interconnection for concentrating solar power. trans-csp study report, desertec project, 2006.

[VC18] S. G. Vennelaganti and N. R. Chaudhuri. Selective Power Routing in MTDC Grids for Inertial and Primary Frequency Support. *IEEE Transactions on Power Systems*, PP(c):1–1, 2018.

[VCV07] T. Van Cutsem and C. Vournas. *Voltage stability of electric power systems*. Springer Science & Business Media, 2007.

[VDN07] VDN. TransmissionCode 2007. Network and System Rules of the German Transmission System Operators, August 2007.

[VG10] D. Van Hertem and M. Ghandhari. Multi-terminal VSC HVDC for the European supergrid: Obstacles. *Renewable and Sustainable Energy Reviews*, 14(9):3156–3163, dec 2010.

[VHRW08a] A. Venkat, I. Hiskens, J. Rawlings, and S. Wright. Distributed MPC Strategies With Application to Power System Automatic Generation Control. *IEEE Transactions on Control Systems Technology*, 16(6):1192–1206, nov 2008.

[VHRW08b] A. N. Venkat, I. A. Hiskens, J. B. Rawlings, and S. J. Wright. Distributed mpc strategies with application to power system automatic generation control. *IEEE transactions on control systems technology*, 16(6):1192–1206, 2008.

[VR15] D. Van Hertem and R. H. Renner. Ancillary services in electric power systems with HVDC grids. *IET Generation, Transmission & Distribution*, 9(11):1179–1185, 2015.

[Vra13] T. K. Vrana. *System Design and Balancing Control of the North Sea Super Grid*. PhD thesis, Norwegian Univ. of Sc. and Techn., 2013.

[VV13] G. Valverde and T. Van Cutsem. Model Predictive Control of Voltages in Active Distribution Networks. *IEEE Transactions on Smart Grid*, 4(4):2152–2161, 2013.

[WAA+15] R. Wiget, G. Andersson, M. Andreasson, D. V. Dimarogonas, and K. H. Johansson. Dynamic simulation of a combined AC and MTDC grid with decentralized controllers to share primary frequency control reserves. In *Proceedings of IEEE PES Eindhoven PowerTech*, 2015.

[Wei15] B. Weise. Impact of K-factor and active current reduction during fault-ride-through of generating units connected via voltage-sourced converters on power system stability. *IET Renewable Power Generation*, 9(1):25–36, 2015.

[WFGV17] T. Weckesser, V. Franz, E. Grebe, and T. Van Cutsem. A model reduction approach for simulation of long-term voltage and frequency dynamics. In *PowerTech, 2017 IEEE Manchester*, pages 1–6. IEEE, 2017.

[WGE07] L. Wehenkel, M. Glavic, and D. Ernst. A collaborative framework for multi-area dynamic security assessment of large scale systems. In *Proceedings of IEEE Lausanne PowerTech*, 2007.

[WGW11] D. Wang, M. Glavic, and L. Wehenkel. A new MPC scheme for damping wide-area electromechanical oscillations in power systems. In *Proceedings of IEEE Trondheim PowerTech*, 2011.

[Wig15] R. Wiget. *Combined AC and Multi-Terminal HVDC Grids – Optimal Power Flow Formulations and Dynamic Control*. PhD thesis, ETH Zurich, 2015.

[WV17] T. Weckesser and T. Van Cutsem. Equivalent to represent inertial and primary frequency control effects of an external system. *IET Generation, Transmission & Distribution*, 11(14):3467–3474, sep 2017.

[XYS07] L. Xu, L. Yao, and C. Sasse. Grid Integration of Large DFIG-Based Wind Farms Using VSC Transmission. *IEEE Transactions on Power Systems*, 22(3):976–984, aug 2007.

[ZBA+13] J. Zhu, C. D. Booth, G. P. Adam, A. J. Roscoe, and C. G. Bright. Inertia Emulation Control Strategy for VSC-HVDC Transmission Systems. *IEEE Transactions on Power Systems*, 28:1277–1287, 2013.

[ZBAR15] J. Zhu, C. D. Booth, G. P. Adam, and A. J. Roscoe. Coordinated direct current matching control strategy for multi-terminal DC transmission systems with integrated wind farms. *Electric Power Systems Research*, 124:55–64, 2015.

[ZHN10] L. Zhang, L. Harnefors, and H.-P. Nee. Power-Synchronization Control of Grid-Connected Voltage-Source Converters. *IEEE Transactions on Power Systems*, 25(2):809–820, may 2010.